Convention on Long-range Transboundary Air Pollution

emep

Co-operative programme for monitoring and evaluation of the long-range transmission of air pollutants in Europe

STATUS REPORT
2/2023 July 2023

Heavy metals and POPs: Pollution assessment of toxic substances on regional and global scales

Status Report 2/2023

msc-e

EMEP Status Report 2/2023

August 2023

Heavy metals and POPs: Pollution assessment of toxic substances on regional and global scales

METEOROLOGICAL SYNTHESIZING CENTRE - EAST

*Ilia Ilyin, Nadezhda Batrakova, Aleksey Gusev, Olga Rozovskaya, Victor Shatalov, Irina Strizhkina, Nadezhda Vulykh, Oleg Travnikov**

Part I

MCS-E

Meteorological Synthesizing Centre - East

2nd Roshchinsky proezd, 8/4, 115419 Moscow Russia
Phone.: +7 926 292 00 18
E-mail: msce@msceast.org
Internet: www.msceast.org

*now at Jožef Stefan Institute, Ljubljana, Slovenia

EXECUTIVE SUMMARY

This year funding of MSC-E was suspended according to the decision of the CLRTAP Executive Body adopted at 42nd session in December 2022 [ECE/EB.AIR/150]. To support further EMEP activity on assessment of heavy metal and POP pollution, the Government of the Russian Federation decided to pay the assessed contribution to Russia for 2022 and 2023 in accordance with the obligations under 1984 Protocol to the Convention directly to the budget of MSC-E of EMEP (https://unece.org/sites/default/files/2023-08/Item%203%20Letter%20on%20MSC-E%20-%20en.pdf). This allowed MSC-E to resume its work in 2023 and prepare Status report.

General information

Heavy metals and persistent organic pollutants (POPs) are known for their toxicity and harmful effects on human health and the environment. In order to reduce levels of pollutants in the environment UNECE Convention on Long-range Transboundary Air Pollution (hereafter, CLRTAP or the Convention) was established. In the framework of the Convention a number of protocols have been developed. In particular, Protocol on Heavy metals and Protocol on POPs to the Convention, aimed at reduction of emissions of these pollutants to the atmosphere, were adopted in 1998 and amended in 2012 and 2009, respectively. According to the Protocols, the priority heavy metals and POPs are lead (Pb), cadmium (Cd) and mercury (Hg), polychlorinated biphenyls (PCBs), polychlorinated dibenzo(p)dioxins and dibenzofurans (PCDD/Fs), hexachlorobenzene (HCB) and polyaromatic hydrocarbons (PAHs). The considered PAHs comprise benzo(a)pyrene (B(a)P), benzo(b)fluoranthene (B(b)F), benzo(k)fluoranthene (B(k)F), and indeno(1,2,3-cd)pyrene (I(cd)P). According to the amendments made in 2009 a number of Contaminants of Emerging Concern (CECs) were also included to the POP Protocol.

EMEP Programme (Co-operative Programme for Monitoring and Evaluation of Long-range Transmission of Air Pollutants in Europe, www.emep.int) is aimed at scientific support of the implementation of the Protocols. Several EMEP Centres are focused on providing the Parties to the Convention with information on pollution levels and transboundary transport. In particular, information about emissions of heavy metals and POPs in the EMEP region is compiled by Centre on Emission Inventories and Projections (CEIP). Monitoring activity within EMEP is supported by Chemical Coordinating Centre (CCC). Model assessment of pollution levels and transboundary transport of heavy metals and POPs is performed by Meteorological Synthesizing Centre – East (MSC-E). The Working Group on Effects (WGE) is focused on evaluation of adverse impacts of the pollutants on the environment and human health.

Emissions

Emission data sets for modelling for 2021 were produced by MSC-E using the gridded sector data produced by CEIP and derived from CEIP WebDab data base, and additional information on temporal variability, vertical distribution and chemical speciation of emissions. Global-scale gridded emissions for modelling were also prepared by MSC-E using the results of the related research projects and expert estimates.

Monitoring

Information on observed concentrations in air, concentrations in precipitation and precipitation sums is available in the EBAS database coordinated by CCC of EMEP. In 2021 information on Pb and Cd concentrations measured in air was available from 51 stations, and measurements of concentrations in precipitation - from 58 stations. At 47 stations co-located measurements were carried out. Hg concentrations in air and precipitation were available from 10 and 21 stations, respectively. Concentrations of B(a)P, HCB and PCB-153 were measured at 30, 11 and 12 stations, respectively. Available monitoring data were analyzed by MSC-E. Most reliable measurements were further used for evaluation of modelling results against observations.

Status of heavy metal pollution in 2021

Pollution levels of heavy metals (Pb, Cd, Hg) and POPs (PAHs, PCDD/Fs, HCB) in 2021 were assessed for the EMEP region, its sub-regions and particular countries. The highest pollution levels are noted for the Central Europe. This sub-region is characterized by the highest levels of Pb, Cd, Hg, PAHs and HCB compared to the other sub-regions. The lowest pollution levels take place in Northern Europe and Caucasus and Central Asia. Evaluation of changes of pollution levels between 2020 and 2021 induced by meteorological variability shown that the changes in sub-regions of the EMEP domain did not exceed ±15%.

Evaluation of the modelling results against observations was carried out for air concentrations and wet deposition fluxes available from the EMEP monitoring network. For Pb and Cd, at majority of monitoring stations the difference between modelled and observed concentrations in air or wet deposition fluxes lies within a factor of two. The model tends to overpredict concentrations of Pb and Cd in air and wet deposition of Hg, and underpredict wet deposition fluxes of Pb and Cd . The agreement of Hg modeled and measured concentrations in air is within ±6% on average and ±25% for particular EMEP stations. Evaluation of the modelling results against EMEP measurements shows good agreement of modelled and observed concentrations of the sum of 4 PAHs with low bias and high spatial correlation. For about 80% of the monitoring stations, the differences between the modelling results and measured concentrations are within a factor of 2. Modelled PCB-153 air

concentrations are two-fold higher than the measured ones. For most of the stations the differences between modelled and observed HCB air concentrations are lower than a factor 2.

Pollution levels in the EMEP region are formed by three groups of sources such as 1) anthropogenic emissions of the EMEP countries, 2) secondary emissions from the EMEP territory (wind re-suspension, natural and legacy emissions, re-emissions) and 3) emission sources located outside the EMEP countries (non-EMEP sources). Deposition of Pb and Cd are mostly caused by EMEP anthropogenic emissions and secondary sources. Hg is global pollutant and thus its levels are formed basically by non-EMEP sources. In case of PAHs the largest contribution (more than 80%) to deposition is made by the EMEP anthropogenic sources, while other types of emission sources contributed less than 20%. The highest contribution to deposition fluxes of PCDD/Fs, PCB-153 and HCB is made by secondary emission sources of the EMEP domain. The second most important contributors for PCDD/Fs and PCB-153 are the EMEP anthropogenic emissions. For HCB the second most important contributor is the emission outside the EMEP domain boundaries.

MSC-E prepared information on ecosystem-dependent deposition fluxes of heavy metals in 2021. This information could be important for evaluation of critical load exceedances. Besides, exceedances of air quality guidelines for PAHs were assessed. It was shown that about 11% of the population of EMEP countries in 2021 were in areas with exceeded EU target level for annual mean B(a)P air concentrations. The WHO Reference level was exceeded for 63% of population of EMEP countries. In addition to this, atmospheric inputs and source apportionment of heavy metals and POPs for marginal seas (the Baltic, the North, the Mediterranean, the Black and the Caspian Seas) and to the Arctic were assessed. Finally, results of the global-scale simulations aimed at generation of boundary concentrations of the pollutants in the EMEP region were presented.

Research and development

The Eurodelta-Carb intercomparison study of B(a)P models initiated by the TFMM in 2021 in the framework of a broader scientific study on modelling of secondary organic aerosol and black carbon was continued. The main objectives of the Eurodelta-Carb study on B(a)P were to analyze performance of air quality models and uncertainties of their results. Four regional chemistry transport models (CHIMERE, GLEMOS, MINNI and SILAM) were applied to simulate the concentrations of B(a)P in Europe. Participated models have shown high spatial correlation of predicted and observed B(a)P concentrations. Besides, most of the models provided high correlation with observed intra-annual variation of B(a)P concentrations. Furthermore, the model simulations indicated overprediction of observed B(a)P concentrations in Spain and underprediction in Northern Europe (Finland, Latvia, Estonia), which is likely explained by the uncertainties of the reported B(a)P emissions. Further activities within the study can be focused on the sensitivity analyses, an evaluation of the meteorological drivers and an analysis of other model outputs such as B(a)P concentrations in precipitation and deposition fluxes and concentrations of species affecting B(a)P chemical transformations in the atmosphere.

An overview of information on some Contaminants of emerging concern (CECs), such as hexabromocyclododecane (HBCDD), polychlorinated naphthalenes (PCNs) and pentachlorobenzene (PeCB) was prepared. The overview included regulatory activities, their production, usage and emissions, as well as results of monitoring and model assessment of their transport and fate in the environment. It was demonstrated that information on physical-chemical properties of CECs, concentrations in environmental compartments, and levels of emission is not sufficient to perform detailed assessment of their transport and fate in the environment. Additional monitoring data and emission inventories and better understanding of processes governing fate and behavior of CECs are required for modelling of atmospheric pollution levels.

Cooperation

Information on MSC-E research activities in co-operation with TFMM and national experts in the framework of Eurodelta-Carb B(a)P model intercomparison study was presented at the EMEP Task Force on Measurements and Modelling. Updated modelling results on B(a)P of several modelling groups (EMEP/MSC-E, CIEMAT, INERIS, ENEA, FMI) and their evaluation against measurements were presented. Similarities and differences between the annual mean concentrations and intra-annual variations obtained by participated models and observed levels were examined. Further research and cooperation activities within the study are proposed.

MSC-E contributed to the work of the Task Force on Hemispheric Transport of Air Pollution (TF HTAP) aimed at Hg and POP pollution assessment. In particular, the Centre participated in TF HTAP collaborative activities focused on multi-model evaluation and attribution of Hg pollution trends and future scenarios as well as assessment of the impact of wildfires and biomass burning on contamination of the environment by multiple pollutants. Current TF HTAP activities focused on Hg pollution assessment are performed as a part of the Multi-Compartment Hg Modeling and Analysis Project (MCHgMAP). The project is aimed at comprehensive analysis of spatial and temporal trends of Hg pollution levels, source attribution and evaluation of future scenarios to inform effectiveness of the LRTAP Convention and the Minamata Convention on Mercury. MSC-E took part in development of the assessment program and preparation of the position paper at all stages of the project. In particular, it contributed to elaboration of the overall program of the model simulations and analysis, formulation of multi-model experiments and specifications of the output results.

In order to investigate the effect of the wildfires on Hg concentrations, deposition and intercontinental transport, and to improve model estimates of Hg levels, TF HTAP initiated process of development of Hg emissions from wildfires. MSC-E prepared a set of Hg emissions from wildfires for the period from 2010 to 2020. It was shown that the main regions of Hg emission are Southern Africa, South America and South-Eastern Asia, Siberian region of Russia and north-western part of North America. The major contributor to global wildfire emission (around 60% on average) is made by tropical forests followed by. grasslands and savanna (13 – 17%). Seasonal changes of global Hg emissions from wildfires is characterised by spring and autumn peaks. Further activity regarding the effects of wildfires on Hg levels will include comparison of Hg emissions based on different

databases. Besides, model experiments will be undertaken to identify the contribution of wildfires on Hg air concentrations and deposition in different regions of the globe.

MSC-E continued cooperation with international organizations. In particular, MSC-E continued data exchange with the Stockholm Convention on POPs. Evaluation of airborne pollution load of heavy metals and POPs to the Baltic Sea is carried out in the framework of long-term cooperation between EMEP and the Helsinki Commission (HELCOM). The compilation of data on atmospheric emissions and model assessment of atmospheric deposition of cadmium and B(a)P for the period 1990-2020 was prepared and discussed during the third informal consultation session of the HELCOM Pressure Working Group. In accordance with the contract between MSC-E and OSPAR Commission analysis of Pb, Cd and Hg emission sectors in 2020 in the OSPAR Contracting Parties was carried out. Besides, model assessment of atmospheric inputs of Pb, Cd and Hg to the OSPAR regions was performed. Results of the analysis of emission data and model assessment of deposition fluxes to the OSPAR area were presented at the hybrid meeting organized by OSPAR Commission.

Future research

MSC-E is planning to contribute to the research and cooperation activities in the field of assessment of heavy metal and POP pollution levels taking into account priorities of the Long-term Strategy for the Convention for 2020-2030. In particular, detailed analysis of spatial and temporal variations of PAH pollution in the EMEP region and improvement of modelling approach for PAHs will be continued as a part of the TFMM/EuroDelta-Carb multi-model intercomparison study. In order to complete the purposes of TF HTAP Multi-Compartment Hg Modeling and Analysis Project new global Hg multi-model experimental simulations of Hg will be organized. For evaluation of the impact of wildfires on pollution levels and intercontinental transport, TF HTAP is planning to design multi-model multi-pollutant (PM, POPs, metals, ozone) intercomparison study. Preparatory work for the assessment of CECs will be continued collecting information on physical-chemical properties, monitoring of their concentrations in different environmental media, and experimental modelling of their transport and fate. It is planned to continue joint analysis of measurements of heavy metals concentrations in mosses and deposition to various ecosystems in co-operation with ICP Vegetation, ICP Integrated Monitoring, and ICP Forests as well as data exchange with TF Health on PAH pollution levels and exceedances of air quality guidelines. Assessment of atmospheric pollution of the marine environment by heavy metals, POPs and CECs is an important direction of further research and co-operation with HELCOM and OSPAR.

CONTENTS

EXECUTIVE SUMMARY 3

ACKNOWLEDGEMENTS 10

INTRODUCTION 11

Chapter 1. MEASUREMENTS OF HEAVY METALS AND POPs 13

1.1. Monitoring of POPs and heavy metals in 2021 13

Chapter 2. STATUS OF HEAVY METAL AND POP POLLUTION IN 2021 16

2.1. Meteorological conditions of 2021 16

2.2. Model setup 20

2.3. Emission data for modelling 20

2.4. Levels of Heavy Metal and POP pollution 23

2.4.1. Pollution summary 23

2.4.2. Lead 24

2.4.3. Cadmium 30

2.4.4. Mercury 35

2.4.5. PAHs 40

2.4.6. PCDD/Fs, PCBs and HCB 44

2.5. Information for exposure assessment 50

2.5.1. Ecosystem-specific deposition of heavy metals 50

2.5.2. Exceedances of air quality standards for PAHs 52

2.6. Atmospheric loads to the marginal seas 53

2.7. Pollution of the Arctic 56

2.8. Global scale pollution by heavy metals and POPs 59

Chapter 3. RESEARCH ACTIVITIES 63

3.1. Eurodelta-Carb intercomparison of B(a)P models 63

3.2. New substances / Contaminants of emerging concern 68

Chapter 4. COOPERATION 82

4.1. Subsidiary bodies of the Convention 82

4.1.1. Task Force on Measurements and Modelling 82

4.1.2. Task Force on Hemispheric Transport of Air Pollution 83

4.2. International organizations 88

4.2.1. Stockholm Convention 88

4.2.2. Helsinki Commission 88

4.2.3. OSPAR 90

5. MAIN CHALLENGES AND DIRECTIONS OF FUTURE RESEARCH 92

REFERENCES 93

Annex A Supplementary information on heavy metal and POP levels 101

Annex B Update of the assessment results with the new emission reporting data 145

ACKNOWLEDGEMENTS

The EMEP/MSC-E is grateful to the Government of the Russian Federation for the funding of operational and research activities of MSC-E on assessment of heavy metal and POP pollution in the framework of EMEP. This allowed MSC-E to prepare this report.

INTRODUCTION

This year funding of MSC-E was suspended according to the decision of the CLRTAP Executive Body adopted at 42nd session in December 2022 [ECE/EB.AIR/150]. To support further EMEP activity on assessment of heavy metal and POP pollution, the Government of the Russian Federation decided to pay the assessed contribution to Russia for 2022 and 2023 in accordance with the obligations under 1984 Protocol to the Convention directly to the budget of MSC-E of EMEP (https://unece.org/sites/default/files/2023-08/Item%203%20Letter%20on%20MSC-E%20-%20en.pdf). This allowed MSC-E to resume its work in 2023 and prepare Status report.

Heavy metals and persistent organic pollutants (POPs) are known for their toxicity and harmful effects on human health and the environment. In order to reduce levels of pollutants in the environment UNECE Convention on Long-range Transboundary Air Pollution (hereafter, CLRTAP or the Convention) was established. In the framework of the Convention a number of protocols have been developed. In particular, Protocol on Heavy metals and Protocol on POPs to the Convention, aimed at reduction of emissions of these pollutants to the atmosphere, were adopted in 1998 and amended in 2012 and 2009, respectively. According to the Protocols, the priority heavy metals and POPs are lead (Pb), cadmium (Cd) and mercury (Hg), polychlorinated biphenyls (PCBs), polychlorinated dibenzo(p)dioxins and dibenzofurans (PCDD/Fs), hexachlorobenzene (HCB) and polyaromatic hydrocarbons (PAHs). The considered PAHs comprise benzo(a)pyrene (B(a)P), benzo(b)fluoranthene (B(b)F), benzo(k)fluoranthene (B(k)F), and indeno(1,2,3-cd)pyrene (I(cd)P). According to the amendments made in 2009 a number of Contaminants of Emerging Concern (CECs) were also induded to the POP Protocol.

EMEP Programme (Co-operative Programme for Monitoring and Evaluation of Long-range Transmission of Air Pollutants in Europe, www.emep.int) is aimed at scientific support of the implementation of the Protocols. Several EMEP Centres are focused on providing the Parties to the Convention with information on pollution levels and transboundary transport. In particular, information about emissions of heavy metals and POPs in the EMEP region is compiled by Centre on Emission Inventories and Projections (CEIP). Monitoring activity within EMEP is supported by Chemical Coordinating Centre (CCC). Model assessment of pollution levels and transboundary transport of heavy metals and POPs is performed by Meteorological Synthesizing Centre – East (MSC-E). The Working Group on Effects (WGE) is focused on evaluation of adverse impacts of the pollutants on the environment and human health.

The status report summarizes the activity of the EMEP Centres on the assessment of heavy metal and POP pollution in the EMEP region and over the globe in 2021 in accordance with the workplan of the Convention for 2022 – 2023 [ECE/EB.AIR/2021/2]. The major part of the results is presented in Part I of the report. More detailed analysis of the pollution levels will be available in Part II in December, 2023. Chapter 1 overviews the results of monitoring activity in the EMEP domain in 2021. Information on pollution levels, transboundary fluxes, pollution of the Arctic and regional seas, evaluation of human exposure to PAHs as well as global-scale pollution levels are described in Chapter 2. The results presented in Chapter 2 are based on emission data reported for 2020, and meteorological data related to 2021. Updated results obtained using emission data for 2021 are

provided in Annex B. Progress in scientific activity of MSC-E is presented in Chapter 3. Chapter 4 is focused on cooperation of MSC-E with subsidiary bodies to the Convention and international organizations. Finally, the main challenges and proposals for future work are formulated in Chapter 5. Supplementary information about heavy metal and POP pollution levels is provided in Annex A.

More detailed information about results of the model assessment, research and cooperation activities, conducted by MSC-E, is presented in technical reports and the internet. Information about heavy metal pollution levels in the North-West Atlantic and the North Sea is prepared with the support of OSPAR Commission [*Ilyin et al.,* 2023]. Long-term changes of Cd and B(a)P deposition to the Baltic Sea were evaluated in the framework of contract with HELCOM Commission and published in [*Gauss et al.*, 2022]. Finally, the description of the current stable version of the Global EMEP Multi-media Modelling System (GLEMOS) and information on heavy metal and POP pollution of the EMEP region can be found on the MSC-E website (www.msceast.org).

Chapter 1. MEASUREMENTS OF HEAVY METALS AND POPs

1.1. Monitoring of POPs and heavy metals in 2021

Information on observed concentrations in air, concentrations in precipitation and precipitation sums is available in the EBAS database coordinated by CCC of EMEP (https://ebas.nilu.no/). Heavy metals and persistent organic pollutants (POPs) are the part of the EMEP monitoring program since 1999. However, earlier data are available in EBAS. Besides, a number of countries submit their measurement data associated with other monitoring programs (CAMP, HELCOM, AMAP etc.). Coordination of the EMEP monitoring activity is supervised by Chemical Coordinating Centre (CCC) of EMEP.

Monitoring obligations of the EMEP parties are outlined in the EMEP monitoring strategy for 2020 – 2029 [*UNECE,* 2019]. The components required for monitoring by Parties include POPs (PAHs, PCBs, HCB, chlordane, HCHs, DDT/DDE, and preferably congener or isomer specific) and heavy metals (Pb, Cd and Hg as first priority species and As, Ni, Cr, Zn and Cu as second-priority species). Ideally, both concentrations in air and precipitation should be observed. In addition to the list of required pollutants, some countries report measurement data on other metals and POPs.

Information on measured concentrations of Pb and Cd in 2021 is available from 51 EMEP stations. The stations are located mainly in the central, western, northern and south-westerns parts of Europe. In the eastern and south-eastern part no EMEP data is submitted to the EBAS database. Annual mean concentrations of Pb ranged from 0.1 ng/m^3 (IS0091R, Iceland) to 4.5 ng/m^3 (SK0007R, Slovakia) (Fig. 1.1a). Mean value of Pb air concentrations is 1.5 ng/m^3. The lowest and the highest Cd concentrations measured in 2021 were 0.004 ng/m^3 (DK0010G, Denmark, Greenland) and 0.125 ng/m^3 (PL0009R, Poland), respectively (Fig. 1.1b). Mean Cd concentration is 0.044 ng/m^3. The lowest Pb and Cd concentrations were observed in the northern part of Scandinavian Peninsula, Iceland and Greenland. Besides, relatively low values were noted for Spain, France, Denmark, Slovenia, Sweden and Finland. Relatively high concentrations were measured in the south-eastern part of the United Kingdom, Benelux region and Slovakia.

There are several forms of mercury in air observed at the EMEP stations (gaseous oxidized, particulate, elemental, total gaseous). In 2021 information on observed total gaseous or elemental Hg in air was available from 10 stations. These stations are located in Spain, Germany, Finland, Norway, Slovenia and the United Kingdom (Fig. 1.1c). The lowest annual mean concentration was 0.39 ng/m^3 (ES0008R, Spain). However, this value seems too low for atmospheric Hg. The next lowest concentration was 1.15 ng/m^3 measured at station DE0003R (Germany). The highest measured concentration was 1.68 ng/m^3 (GB0048R, the United Kingdom). Mean Hg concentration is 1.34 ng/m^3 (station ES0008R is not included).

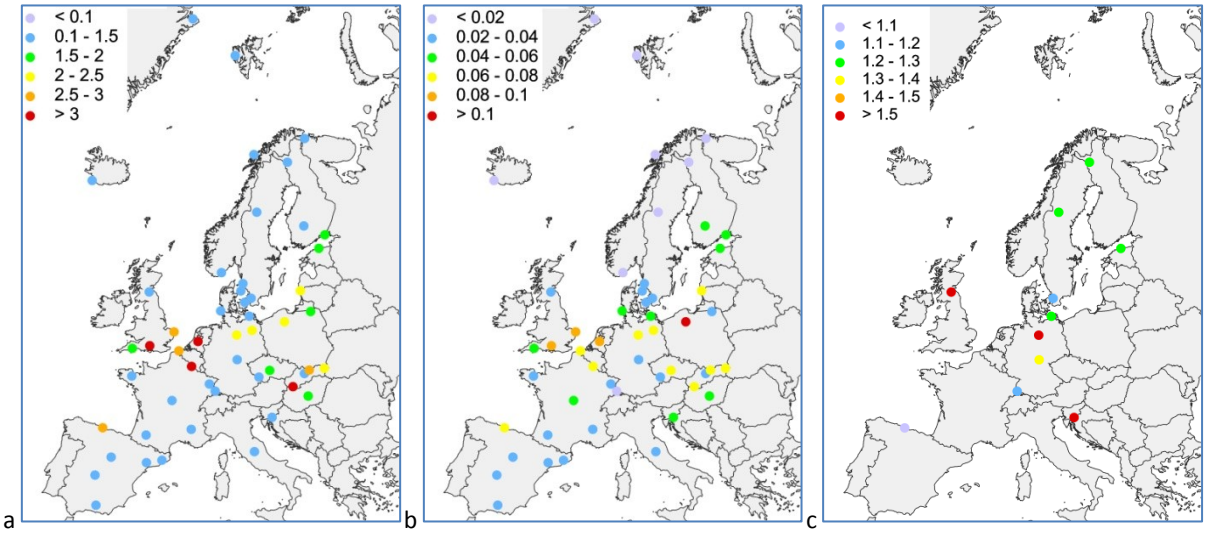

Fig. 1.1. *Annual mean concentrations, ng/m³, of Pb (a), Cd(b) and Hg(c) measured at the EMEP stations in 2021.*

Pb and Cd concentrations in precipitation were measured at 58 stations. Their location is generally the same as that of concentrations in air. At 47 stations both measurements in air and precipitation were carried out. The lowest annual mean concentrations of Pb and Cd in precipitation observed in 2021 were 0.076 µg/L (GB1055R, the United Kingdom) and 0.0012 µg/L (BE0014R, Belgium), respectively (Fig. 1.2a, b). Maximum concentration of Pb was 24.3 µg/L (ES0008R, Spain), and of Cd – 0.09 µg/L (SK0007R, Slovakia). The lowest levels took place in Scandinavian countries. Besides, relatively low Pb concentrations in precipitation were noted in Spain and the southern part of France. Low concentrations of Cd were observed in the United Kingdom.

Laboratories analyzing Cd and Pb concentrations in precipitation took part in regular intercomparison studies organized by CCC [*CCC*, 2022]. At most of laboratories the deviation of observed concentrations from the theoretical value do not exceed ±30%.

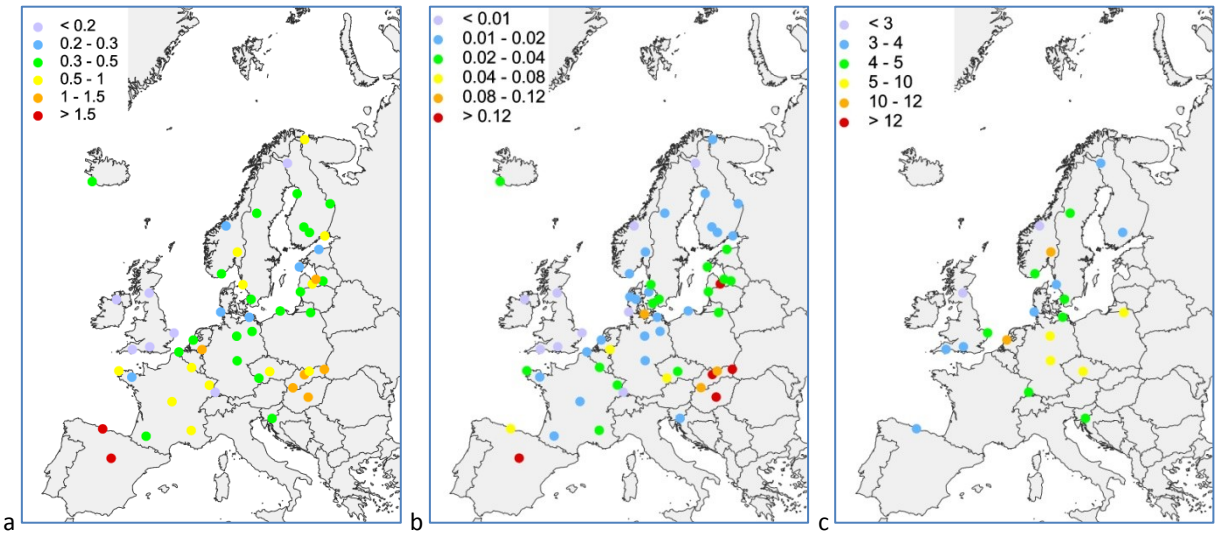

Fig. 1.2. *Annual mean concentrations in precipitation, of Pb (µg/L, a), Cd(µg/L, b) and Hg(ng/L, c) measured at the EMEP stations in 2021.*

Hg concentrations in precipitation in 2021 were available from 21 stations. The stations are located in the central (Germany, Poland, Czechia), western (the United Kingdom), northern (Finland, Sweden, Norway) and southern (Spain, Slovenia) parts of Europe (Fig. 1.2c). The lowest Hg concentration was observed at station GB0048R (the United Kingdom) and equalled to 2.6 ng/L. The highest concentration (11.3 ng/L) was observed at station NO0056R (Norway). Averaged Hg concentration in precipitation was 4.6 ng/L.

Concentrations of B(a)P in 2021 were measured at 30 EMEP stations. The stations are located in the western, south-western, central and northern parts of Europe (Fig. 1.3a). The lowest annual mean concentration was observed at station NO0042G (Norway, Svalbard) and equalled to 0.002 ng/m^3. The highest levels (0.9 ng/m^3) were found at Polish station PL0009R. Mean concentration value was 0.1 ng/m^3. Relatively high B(a)P levels in 2021 were observed in Germany, Poland, Lithuania, Czechia and Slovenia. In Norway, Finland, France, Spain and the United Kingdom the concentrations were typically lower than European mean value.

Eleven stations reported to EBAS data on observed HCB concentrations in air. They are located in Iceland, Germany, Finland, Sweden and Czechia. Minimum, maximum and average values of measured HCB concentrations were 5.3 pg/m^3 (IS0091R, Iceland), 60 pg/m^3 (CZ0003R, Czechia) and 27 pg/m^3, respectively. Relatively high concentrations (compared to the mean value) were observed at stations in Norway. In Sweden, Finland and the southern part of Norway HCB concentrations were relatively low.

Concentrations of PCB-153 were observed at 12 EMEP monitoring stations. The stations are located in Norway, Finland, Sweden, Germany, Iceland and Czechia. The lowest and the highest levels in 2021 were 0.09 pg/m^3 (NO0042G, Norway, Svalbard) and 13 pg/m^3 (CZ0003R, Czechia), respectively. European mean concentration of PCB-153 in 2021 was 1.8 pg/m^3. Scandinavian countries were characterized by relatively low PCB levels, while the concentrations in Germany were relatively high.

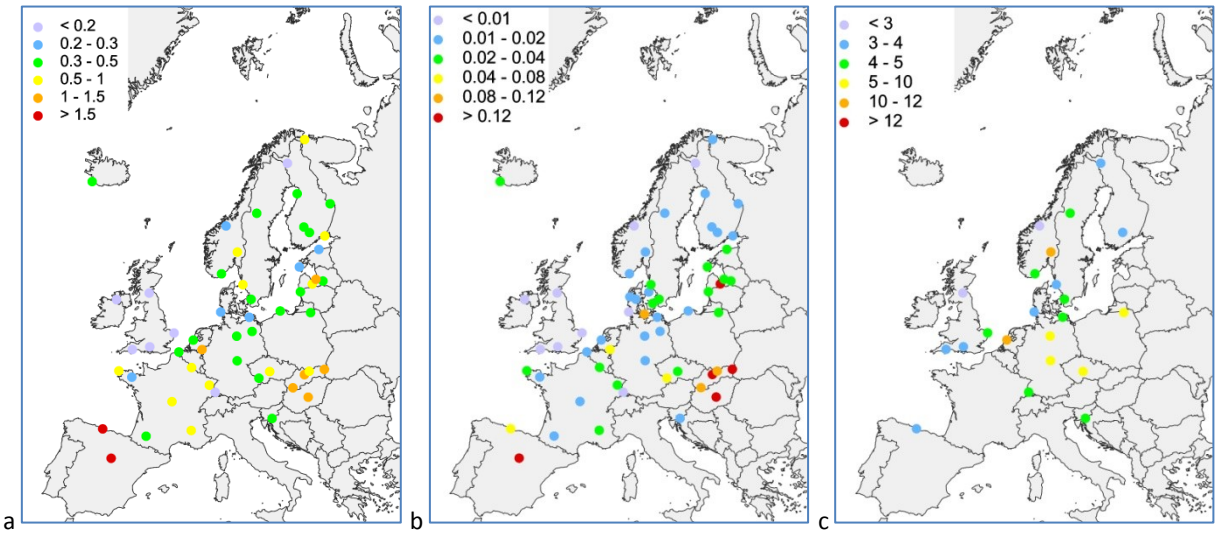

Fig. 1.3. *Annual mean concentrations of B(a)P, ng/m³ (a), HCB, pg/m³(b) and PCB-153, pg/m³(c) measured at the EMEP stations in 2021.*

Chapter 2. STATUS OF HEAVY METAL AND POP POLLUTION IN 2021

2.1. Meteorological conditions of 2021

Atmospheric transport and deposition of heavy metals and POPs are governed by a number of factors, and meteorological conditions is one of them. Wind patterns and turbulent mixing control dispersion of the pollutants in the atmosphere. Deposition fluxes are influenced by precipitation and atmospheric stability. Besides, the rate of pollutants chemical transformations depends on air temperature, humidity and solar radiation.

Meteorological conditions of a particular year may differ from those in other years both due to inter-annual meteorological variability and because of long-term climate change. State of the weather conditions of current (2021) reporting year was analyzed via comparison with the climatic conditions. Besides, meteorological conditions of current year were compared with those of previous (2020) year. Analysis of the differences in key meteorological parameters between two consecutive years helps to explain the changes in pollution levels between 2021 and 2020.

To compare meteorological conditions of the current year with climatic norms, anomalies of air temperatures and precipitation were analyzed. An anomaly is a difference between the value in the current year and the climatic norm. Positive value of the anomaly means that temperature or precipitation sum in this year is higher than the climatic norm, and vice versa. Climatic norm is considered as the average for the period from 1991 to 2020 [*Blunden and Boyer*, 2022]. Information on comparison of current state of meteorological conditions with the climatic norms is based on [*Blunden and Boyer*, 2022].

According to the Global Historical Climate Network (GHCN) v4.0.1 dataset [*Menne et al.*, 2018], 2021 in Europe was 0.2 °C warmer than normal. Over most part of Europe anomalies of temperatures varied within ±1°C (Fig. 2.1a). The Aegean Sea, the eastern part of Türkiye, Transcaucasia and the western part of Kazakhstan were experienced anomaly higher than 1°C. Over the Central Asian region positive anomalies of 1 – 2°C took place. Temperature anomaly demonstrated distinct seasonal variability. In winter anomaly of 1 – 2 °C took place over the major part of Europe and exceeded 3°C over the Balkan region. Besides, anomaly of 3 – 5 °C was observed over Greenland. Negative anomalies occurred over Russia (1 – 4 °C) and the Northern Atlantic (1 – 2 °C). In spring large part of Europe experienced negative anomaly of -1 – -2°C. Positive anomalies took place over the Iberian Peninsula, Russia and Central Asia (1-3°C). In summer and autumn positive anomalies of 1 – 3 °C were observed almost over whole Europe.

Precipitation sums were close to the norm over almost entire Europe. Deficit of precipitation (60-80% of the climatic norm) was noted in the southern part of the Iberian Peninsula, Estonia and the southern part of Norway (Fig. 2.1b). Similar deficit took place in the eastern part of the EMEP domain. Spatial distribution of precipitation anomalies in particular seasons had mosaic character and exhibited considerable temporal variability. In winter significant excess of precipitation (125 – 250% of the norm) occurred in Italy, the Balkan region and the United Kingdom. Main areas of precipitation deficit were Norway, south of Spain, Türkiye, Lithuania, Latvia and Estonia. In spring

precipitation sums in Iceland, Spain, western France, Italy, Greece, Türkiye and Central Asia were below the climatic norm. Precipitation sums above the norm occurred over Romania and the eastern part of Europe. In summer the areas with deficit of precipitation were the eastern part of Europe, Scandinavia, the British Isles and Southern Europe. The central part of Europe, the northern part of France and Türkiye are characterized by the excess of precipitation. In autumn of 2021 precipitation in the Iberian Peninsula, Central Europe, partly in Eastern Europe and Iceland were below the climatic norm.

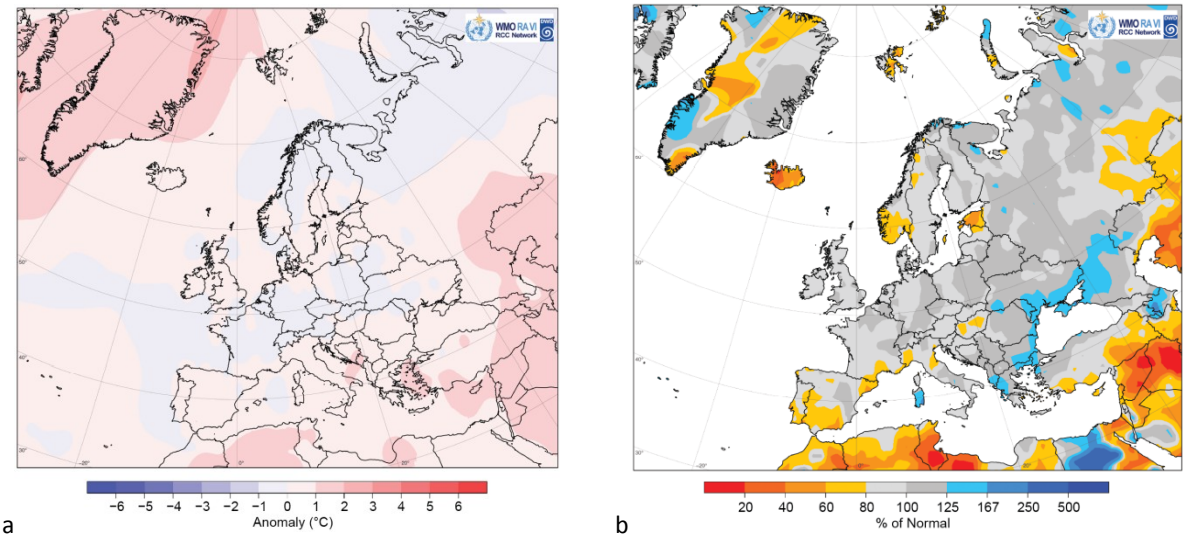

a b

Fig. 2.1. *Anomaly of mean annual air temperature (a) and annual precipitation sum (b) in 2021 [Blunden and Boyer, 2022].*

Changes between precipitation amounts, air temperature and transport patterns between 2020 and 2021 were analyzed. Positive value of change means that a value (e.g., temperature or precipitation sum) in 2021 is higher than that in 2020, and vice versa. Compared to the previous year precipitation sums in 2021 (Fig. 2.2a) increased over most of the EMEP domain (Fig. 2.2b). The most significant increase (> 50%) took place over the Black Sea region, the south-eastern part of Europe, the western coasts of Greece and Türkiye, the western and central parts of the Mediterranean Sea. The decline of precipitation sums occurred in the southern part of Norway, along the western coasts of France, the United Kingdom and Ireland and over most of Central Asia.

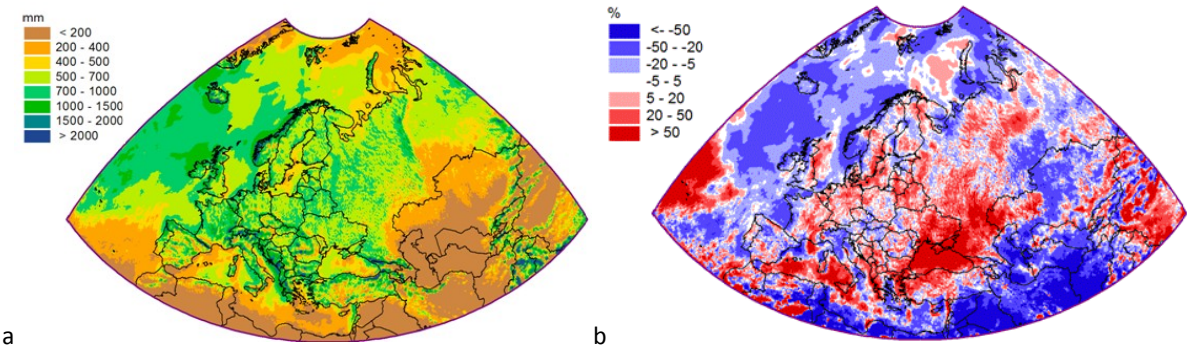

a b

Fig. 2.2. *Annual precipitation sums in 2021 (a) and relative difference between precipitation in 2021 and 2020(b). Positive values mean increase and negative – decrease of precipitation in 2021 relative to 2020.*

Air concentrations of a number of pollutants, e.g., PAHs, undergo substantial seasonal variability with the amplitude between summer minimum and winter maximum reaching an order of magnitude. Smaller seasonal changes are known for air concentrations of heavy metals. Therefore, for the analysis of changes of pollution levels between 2020 and 2021 the changes of air temperature in warm (April-September) and cold (January-March and October-December) seasons are considered separately. Both in warm and cold period boundary layer air temperature in 2021 was lower than that in 2020 over most of the EMEP countries (Fig. 2.3a,b). The difference was up to 1.5°C in warm period and up to 3°C in cold period. In the eastern part of the EMEP domain the difference exceeded 3°C.

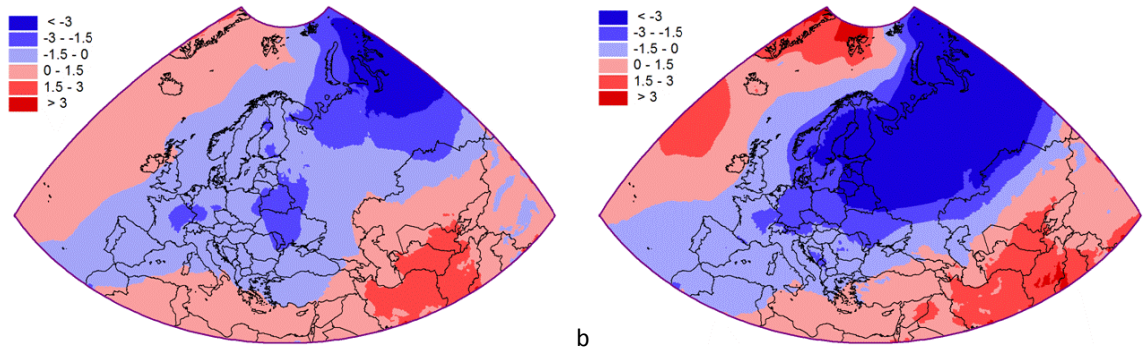

Fig. 2.3. *Difference of warm (a) and cold (b) season mean air temperatures (°C) in the atmospheric boundary layer (~1 km) between 2020 and 2021.*

To analyze the changes between scalar variables like air temperature and precipitation average fields of these parameters can be compared. However, this approach is not applicable for the analysis of changes between vector variables such as wind, because it is important to take into account both the magnitude and direction. For the analysis of changes of atmospheric transport patterns between current and previous years source-receptor matrices of passive tracer were calculated for 2020 and 2021. Since removal processes (wet, dry deposition, chemistry) were switched off, the contribution of countries-sources to a country-receptor is entirely determined by atmospheric transport. The changes between components of source-receptor matrix characterize the changes in atmospheric transport patterns between current and previous year.

Concentration matrices simulated for the EMEP countries were generalized to matrices for the EMEP sub-regions (see Section 2.4.1). Relative changes in atmospheric transport between sub-regions are illustrated in Fig. 2.4. Each sub-region is considered as a source and a receptor of atmospheric pollution. For example, atmospheric transport from Southern Europe sub-region to Central Europe decreased by 13%, while the transport to Caucasus and Central Asia sub-region increased by around 25% (Fig. 2.4). The largest relative changes (50 – 130%) occurred in transport patterns from Eastern Europe, Northern Europe and Caucasus and Central Asia to the Western Europe sub-region. Large relative difference does not always mean large changes in absolute contribution of emissions in one sub-region to pollution in another sub-region. For example, contribution of pollutants emitted by sources of Caucasus and Central Asia to pollution in Western Europe is quite low. Therefore, even large (130%) relative increase of atmospheric transport between these two very remote sub-regions does not mean substantial increase of pollution levels in absolute terms. Transport from Northern

Europe increased to all other sub-regions, especially to the Southern, Western and Central Europe sub-regions (around 40 – 60%). Transport from Eastern European sub-region also increased to almost all other sub-regions. At the same time transport from the Southern to Western and Central Europe sub-regions decreased by 10 – 20%.

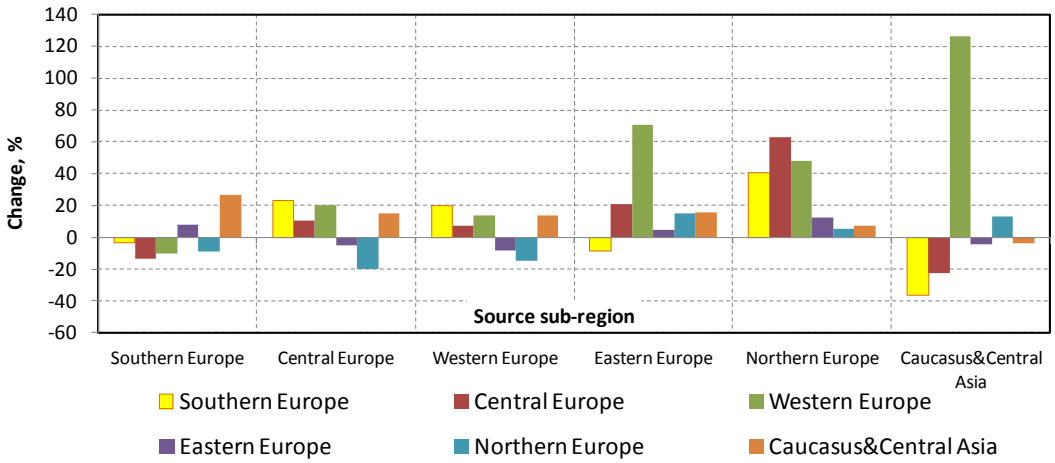

Fig. 2.4. *Relative change (%) of atmospheric transport from the source to receptor sub-regions between 2020 and 2021. Positive value indicates the increase of atmospheric transport from the source to receptor sub-regions, and vice versa. Receptor sub-regions are indicated by colours.*

This approach can be used for analysis of changes in atmospheric transport in particular countries. For example, atmospheric transport from Scandinavian countries to the Netherlands increased by 55 – 150% (Fig. 2.5b). The change of atmospheric transport from other neighbouring countries is relatively low (±15%). Similar tendency is noted for the United Kingdom. Transport from the territory of Finland increased two-fold, and from Sweden by 50% (Fig. 2.5a). The change from other countries was much lower. The changes in atmospheric transport between particular countries could be useful for explaining of the changes between modelled transboundary deposition fluxes in 2020 and 2021.

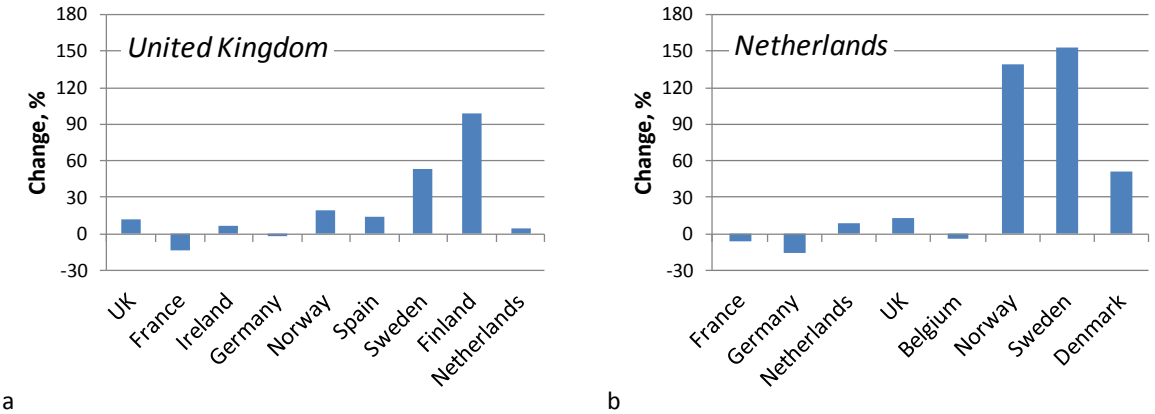

Fig. 2.5. *Relative change (%) of atmospheric transport to the United Kingdom (a)and the Netherlands (b) from main countries-contributors in 2021.*

2.2. Model setup

The operational model assessment of heavy metal and POP pollution in 2021 has been performed using the GLEMOS model, version v2.2.2. Description of the current stable version of the model is available at the MSC-E website (http://msceast.org/index.php/j-stuff/glemos).

Modelling of pollution levels in the EMEP countries as well as estimation of the transboundary transport between them (source-receptor relationships) have been carried out on a regional scale within the EMEP domain (https://www.ceip.at/the-emep-grid). Anthropogenic emission data for modelling of all considered pollutants have been prepared based on the gridded emissions fields provided by CEIP and complemented with additional emission parameters required for model runs (Section 2.3). Natural and secondary Hg emissions from soil and seawater have been estimated depending on Hg concentration in soil and the environmental parameters [*Travnikov and Ilyin*, 2009]. Data on wind re-suspension of particle-bound heavy metals (Pb and Cd) from land and sea surface has been generated using the dust pre-processor [*Gusev et al.*, 2006; 2007].

Meteorological information for the model simulations has been generated from the operational analysis data of the European Centre for Medium Range Weather Forecasts [*ECMWF*, 2023] using the meteorological pre-processor based on the Weather Research and Forecast modelling system (WRF) [*Skamarock et al.,* 2008]. Atmospheric concentrations of chemical reactants and particulate matter, which are required for the description of Hg and POP chemistry, were derived from the GEOS-Chem model simulations.

Boundary conditions for the regional scale simulations of all considered pollutants have been obtained from the GLEMOS model runs on a global scale (Section 2.8). Initial conditions for the evaluation of pollution levels of the long-living POPs (e.g. PCBs, HCB, and PCDD/Fs) in the EMEP region have been extracted from the long-term global model spin-up based on expert estimates of historical emissions.

2.3. Emission data for modelling

Regional emissions

Model assessment of heavy metal and POP pollution in the EMEP domain was made on the basis of gridded emission data with spatial resolution 0.1°x0.1° provided by CEIP (http://www.ceip.at). Pollution levels of heavy metals and POPs in 2021 were evaluated using emission data, reported for the previous year 2020. Detailed description of estimated heavy metal and POP emissions in the EMEP countries, gap-filling methods, and expert estimates, used for preparation of the emission inventory, can be found in the CEIP Technical report 4/2022 [*Poupa*, 2022].

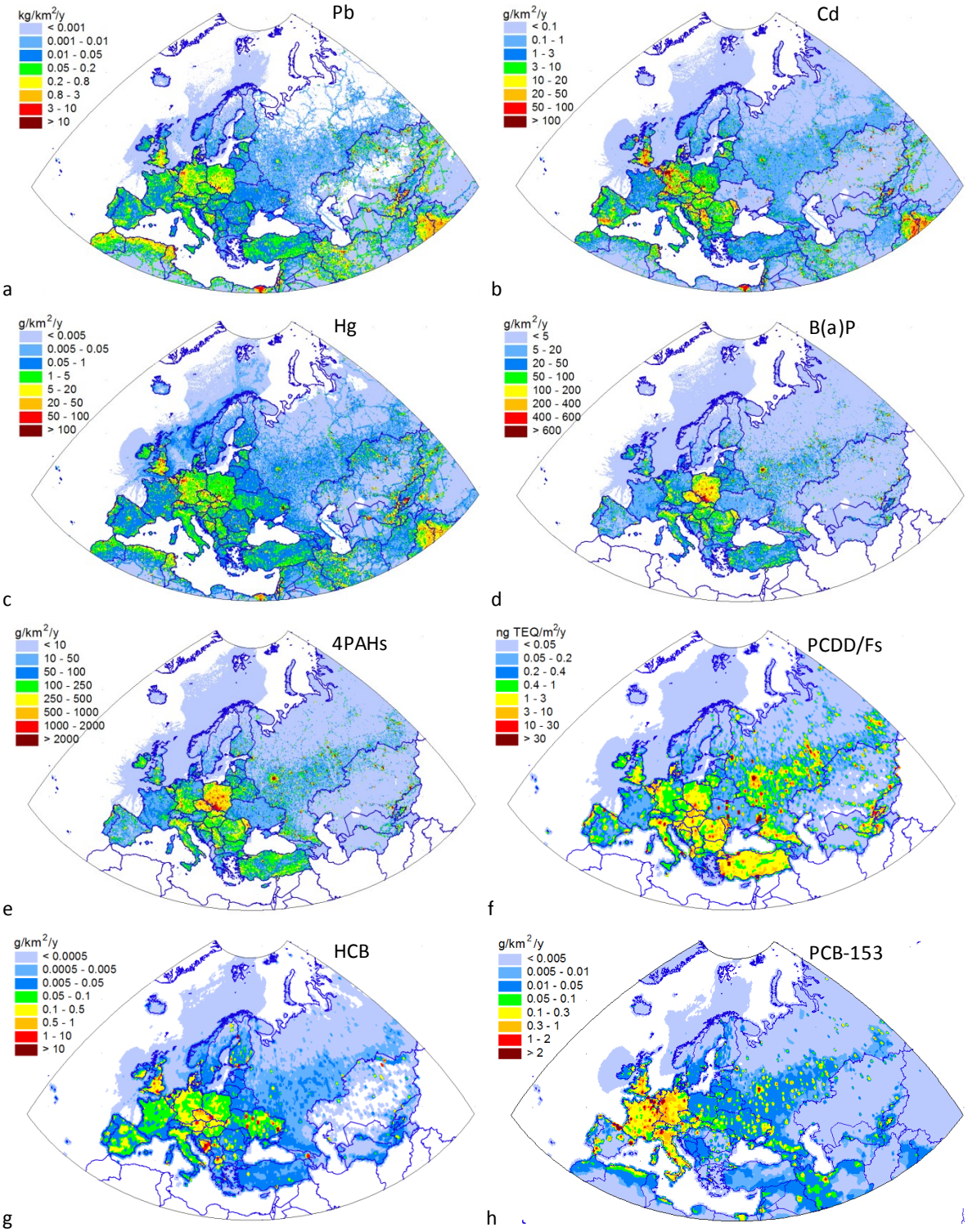

Fig. 2.6. *Spatial distribution of Pb (a), Cd (b), Hg (c), B(a)P (d), sum of 4 PAHs (e), PCDD/Fs (f), HCB (g) and PCB-153 (h) emissions in the EMEP region used in model simulations for 2021.*

Model simulations for Pb, Cd, Hg, PAHs, PCDD/Fs, and HCB were based on the officially reported emission data. For PCBs, a combination of official emission data and expert estimates was applied for modelling. Currently reported PCB emissions provide only total amount of PCBs without specifying particular congener emissions. However, modelling of PCBs requires definition of emissions of particular PCB congeners. Therefore, to evaluate transport and fate of individual PCB congeners, the congener specific emission inventory by *K.Breivik et al.* [2007] was used for modelling.

The indicator congener PCB-153 was selected to characterize transboundary transport and pollution by PCBs. Spatial distribution of PCB-153 emissions was constructed on the base of gridded PCB emissions officially provided by 33 EMEP countries (namely, Austria, Belgium, Bulgaria, Croatia, Cyprus, Czechia, Denmark, Estonia, Finland, France, Georgia, Germany, Greece, Hungary, Ireland, Italy, Latvia, Lithuania, Luxembourg, North Macedonia, Monaco, Netherlands, Norway, Poland, Portugal, Romania, Serbia, Slovakia, Slovenia, Spain, Sweden, Switzerland and the United Kingdom). For other EMEP countries, which did not report gridded emission data, gridded population density was used for spatial allocation of emissions.

Maps illustrating spatial distributions of the pollutants, namely, Pb, Cd, Hg, B(a)P, sum of 4 PAHs, PCDD/Fs, HCB and PCB-153 emission fluxes from anthropogenic sources in the EMEP region, used in the model simulations for 2021, are presented in Fig. 2.6.

Along with gridded emission data, the GLEMOS modelling system requires additional information on heavy metal and POP emissions, including intra-annual variations, distribution of emissions with height and chemical speciation of Hg, PCB, PCDD/F and PAH emissions. Necessary vertical and temporal disaggregation of the emissions was generated using the emission pre-processing tool, developed in MSC-E for the GLEMOS modelling system. More detailed information on the emission pre-processing procedure is presented in the EMEP Status Report [*Ilyin et al.*, 2018].

Global emissions

A number of pollutants, such as mercury and some POPs, are known for their ability to disperse in the atmosphere over the global scale. In order to take into account contribution of intercontinental transport to pollution levels in the EMEP countries and to evaluate boundary and initial conditions required for the regional EMEP modelling, global-scale model simulations are carried out.

Global-scale modelling of Hg is based on gridded emission data produced in the framework of the UNEP Global Mercury Assessment 2018 [*AMAP/UNEP*, 2019] and related to 2015. More detailed information can be found in the EMEP Status Report 2/2021 [*Ilyin et al.*, 2021]. Intercontinental transport of PAHs is simulated based on the inventory, developed by the research group of Peking University [*Shen et al.*, 2013]. Global PAH emission inventories with 0.1°x0.1° spatial resolution were elaborated using a bottom-up approach for the period from 1960 to 2014. For the evaluation of global-scale transport and fate of PCDD/Fs, HCB, and PCBs expert estimates of global emissions were utilized. In particular, global gridded emissions of PCDD/Fs to the atmosphere and soil were prepared using the national emission inventories reported by countries to the Stockholm Convention [*Gusev et al.*, 2014; *Shatalov et al.*, 2014]. Model simulations of HCB global-scale transport were carried out on the basis of experimental emission scenario of historical HCB releases during the period covering several recent decades [*Shatalov et al.*, 2010]. For the PCB-153 modelling, data on global emissions were derived from the inventory of *Breivik et al.* [2007]. Spatial distributions of Hg and PCDD/F emissions, used in the global-scale model simulations for 2021, are shown in Fig. 2.7.

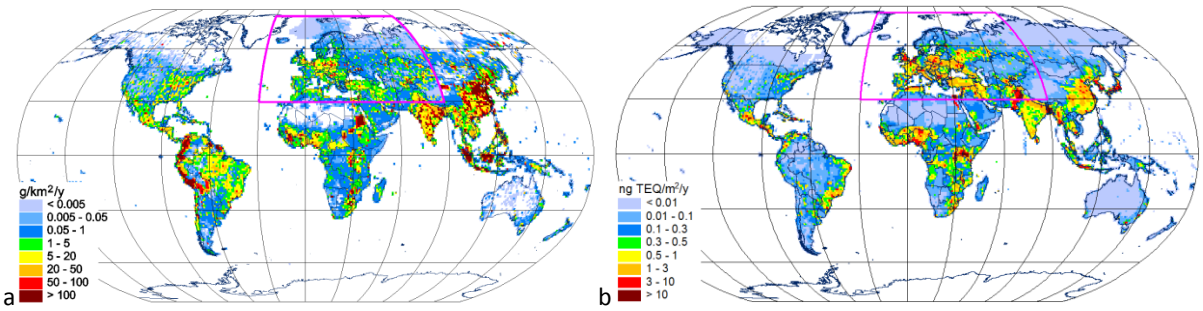

Fig. 2.7*. Spatial distribution of global annual emissions of Hg (a) and PCDD/F (b) with spatial resolution 1°x1°, used in the model simulations for 2021. Pink line depicts boundary of the EMEP region.*

2.4. Levels of Heavy Metal and POP pollution

2.4.1. Pollution summary

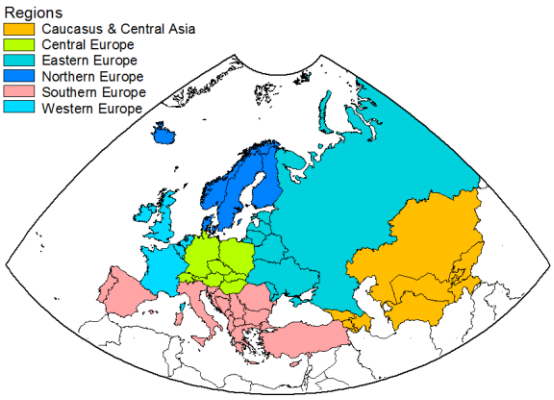

Fig. 2.8*. Definition of sub-regions of the EMEP region used in the report.*

Information on heavy metal and POP pollution levels in 2021 was prepared using EMEP monitoring data and results of transboundary transport modelling. Modelling results are based on emission data for 2020. The data on meteorological conditions, atmospheric reactants and land-cover are related to 2021. Assessment of pollution levels provides information on spatial distributions of concentrations in air and deposition fluxes, source-receptor relationships for the EMEP countries, and changes in the levels between current (2021) and previous (2020) years. More detailed information on pollution levels of each of considered pollutant is available in Sections 2.4.2 – 2.4.6.

This section is aimed at summarizing the information on pollution levels of the considered pollutants (Pb, Cd, Hg, PAHs, PCDD/Fs, HCB) in 2021 in the EMEP region. Mean air concentrations and deposition fluxes are assessed for six sub-regions of the EMEP domain, such as Western Europe, Southern Europe, Northern Europe, Eastern Europe, Central Europe and Caucasus and Central Asia (Fig. 2.8). In order to characterize pollution of the sub-regions in general, deposition fluxes of heavy metals and POPs were normalized using division by mean deposition value and reduced to dimensionless form (Fig. 2.9a). The highest pollution levels are noted for the Central Europe . This sub-region is characterized by the highest levels of Pb, Cd, Hg, PAHs and HCB compared to the other sub-regions. The lowest pollution levels take place in Northern Europe and Caucasus and Central Asia.

The change between pollution level (X) in current and previous year induced by inter-annual variability of meteorological conditions, is calculated as relative difference between 2021 and 2020 according to the following formula:

$$\Delta = \frac{(X_{2021} - X_{2020})}{X_{2020}} \cdot 100\%$$

Positive value of the change indicates the increase of pollution levels from 2020 to 2021, and vice versa. The same approach was applied to characterize changes in air concentrations, deposition and transboundary fluxes of particular pollutants described in Sections 2.4.2 - 2.4.6. Most of the changes range from -10% to 5% (Fig. 2.9b). The highest deposition changes between 2020 and 2021 occurred in Northern Europe . This sub-region is known for the strongest decline of deposition of Pb, Cd and PAHs. In Central Europe sub-region deposition of heavy metals increased by 4 – 11%, while POP deposition slightly declined. In Southern Europe and Caucasus and Central Asia Cd deposition fluxes increased by 8% and 15%, respectively. In Western Europe Pb deposition decreased by 11%.

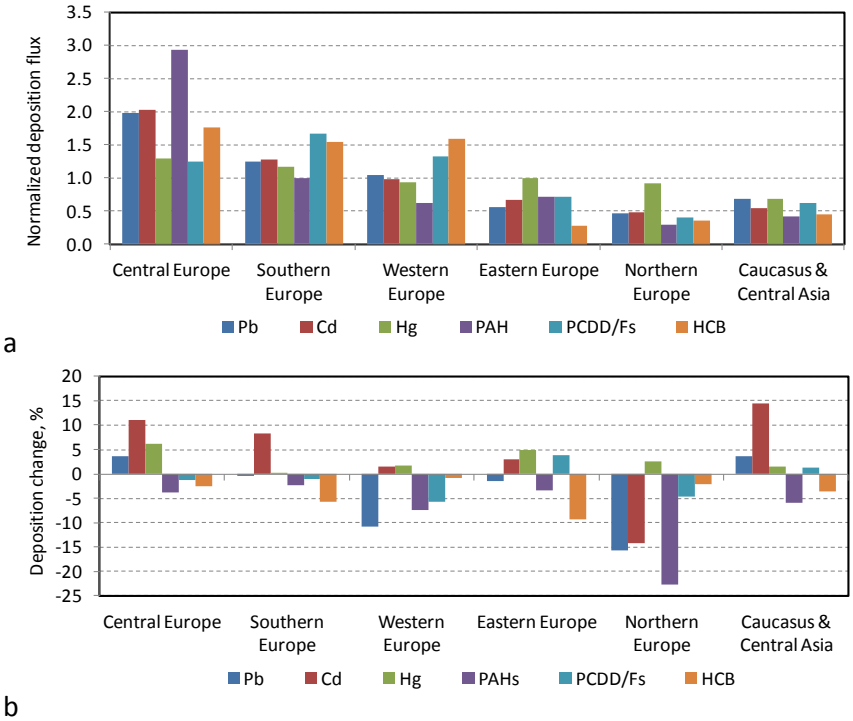

Fig. 2.9. *Normalized mean deposition flux in 2021 (a) and relative changes of heavy metals and POP deposition between 2021 and 2020 (b) in sub-regions of the EMEP region.*

2.4.2. Lead

Lead is found in the atmosphere as a component of aerosol particles. Industry sector is the main anthropogenic emission source of lead in the EMEP region followed by road transport and domestic heating. Lead harmfully affects brain and nervous system of humans, increases risks of high blood pressure and kidney damage, and has adverse impact on fetus (https://www.who.int/news-room/fact-sheets/).

Air concentrations

Over main part of the EMEP domain annual mean concentrations of Pb in air in 2021 varied from 0.3 to 20 ng/m^3 (Fig. 2.10a). Lower levels occurred over the Scandinavian Peninsula, north of Russia and the Arctic regions. In regions affected by significant emissions (e.g., the southern part of Poland, the northern part of Italy) the concentrations exceeded 20 ng/m^3. Central Europe is characterized by the highest spatially mean concentrations (about 3.5 ng/m^3) in 2021 (Fig. 2.10b). The lowest concentrations took place in Northern Europe (around 0.4 ng/m^3) and Eastern Europe (about 0.7 ng/m^3). Relatively low annual mean concentrations in the Eastern Europe sub-region are caused by low concentrations over Russia. In other parts of Eastern Europe the concentrations are comparable with those in other sub-regions.

Modelled annual mean concentrations of Pb generally agree with the levels observed at the EMEP stations. On average, the model slightly (7%) overestimates the observed concentrations. At majority (76%) of stations the difference between modelled and observed levels lies within a factor of two. Spatial correlation coefficient is about 0.7, which means that the model reproduced in general main spatial gradients of Pb air concentrations. However, at particular stations the agreement between modelled and observed Pb concentrations in air may significantly differ from the average value. More detailed information on the evaluation of modelling results against measurements is presented in Annex A.

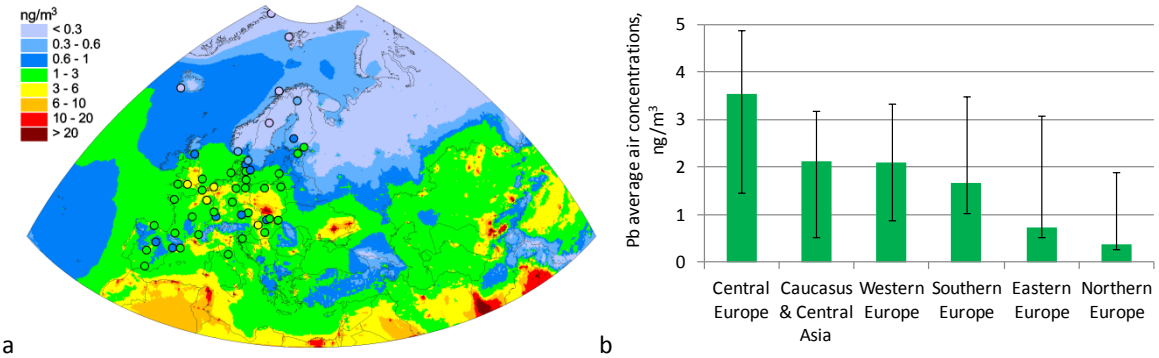

a b

Fig. 2.10. *Annual mean air concentrations of Pb (circles on the map show observed values in the same colour scale) (a) and average air concentrations of Pb in EMEP sub-regions (b) in 2021. Whiskers show the range of concentrations in particular countries of the sub-region.*

Flux of Pb total deposition in 2021 ranged markedly between the least polluted regions (0.1 – 0.2 kg/km^2/y) in the Arctic, over Scandinavia and western part of Central Asia and the most polluted areas (1.5 – 2 kg/km^2/y) in the southern Poland (Fig. 2.11a). The highest spatially mean deposition flux took place in Central Europe (0.55 kg/km^2/y) followed by Southern Europe (0.35 kg/km^2/y) (Fig. 2.11b). Northern Europe and Eastern Europe were the sub-regions with the lowest spatially mean deposition of Pb (0.1 and 0.15 kg/km^2/y, respectively). About three quarters of total deposition are contributed by wet deposition flux, and the remaining share – by dry deposition. However, these ratios may differ markedly across the EMEP domain depending on spatial distribution of atmospheric precipitation and land cover.

The model tends to underestimate Pb wet deposition fluxes. Compared to the observed levels, the modelled wet deposition in 2021 are about 40% lower. Underestimation is noted in Scandinavian region and some countries of Central Europe. Nevertheless, at about 60% of stations the model fits the observations within a factor of two. Results of the model evaluation are described in Annex A in more detail.

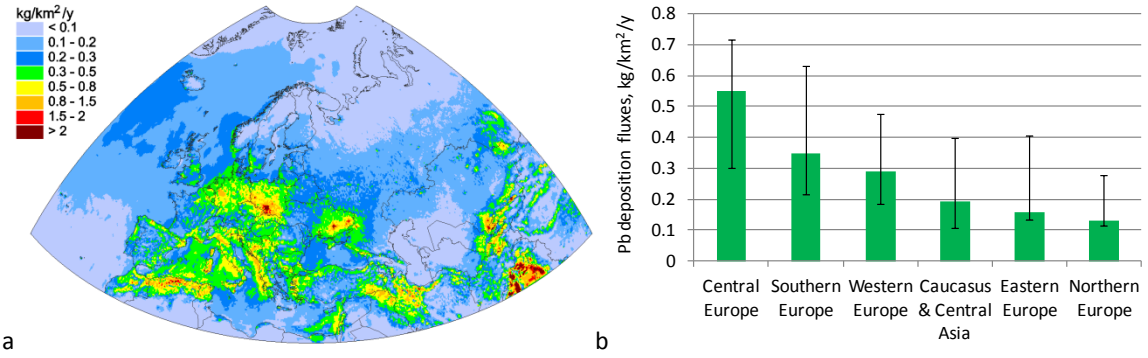

a b

Fig. 2.11. *Annual total deposition flux of Pb (a) and mean total deposition fluxes of Pb to EMEP sub-regions (b) in 2021. Whiskers show the range of country-average concentrations across countries in each sub-region.*

Deposition fluxes depend on a number of factors such as atmospheric precipitation and stability, peculiarities of the underlying surface, spatial distribution and magnitude of emission sources. Three groups of sources are considered: anthropogenic emissions of the EMEP countries, secondary emissions (wind re-suspension of dust particles containing natural and legacy metals) and contribution of sources located outside the EMEP countries (non-EMEP sources).

Spatial distribution of deposition caused by the EMEP anthropogenic emissions correlated with the distribution of locations of emission sources. The highest deposition fluxes were bound to the regions with the most significant anthropogenic emissions, e.g., southern Poland, north-western Germany, some regions in the Balkans, the eastern part of Europe and Central Asia. However, spatial distribution of deposition is smoother than that of emissions (Fig. 2.6a) due to atmospheric dispersion of emitted pollutants. Besides, elevated deposition fluxes are noted for regions with significant atmospheric precipitation (Fig. 2.12), e.g., along the northern coast of Türkiye. The spatially mean contribution of anthropogenic emissions varied from almost 60% in Eastern Europe to 30% in Southern Europe (Fig. 2.12d).

Long-term accumulation of heavy metals, including Pb, led to the enrichment of natural heavy metal levels in soils by legacy component. Wind suspension of soil and dust particles enriched with heavy metals represents one of the sources of atmospheric emissions. Therefore, the highest wind re-suspension occurs in regions with large natural content of heavy metals in soils or in regions of significant anthropogenic emissions and long-term deposition. Therefore, regions of significant deposition from wind re-suspension are large in Central Europe (Germany, Poland), Italy, the southern part of France. In Central Europe deposition flux from secondary sources is the highest (around 0.2 kg/km^2/y). The highest relative contribution of secondary sources (about 60%) was noted in the Northern Europe. It is explained by low anthropogenic emissions and atmospheric transport from neighboring sub-regions, where secondary sources are significant. Noticeable deposition fluxes

(0.1 – 0.2 kg/km^2/y) over the Atlantic are caused by wind suspension of sea spray containing dissolved heavy metals.

Contribution of non-EMEP sources of Pb is relatively low compared to the contributions from anthropogenic and secondary sources, ranging from 6% in Central Europe to almost 30% in Southern Europe (Fig. 2.12d). Relatively high contribution of non-EMEP sources in Southern European sub-region is explained by atmospheric transport of anthropogenic and secondary emissions from North Africa and Asia. Elevated deposition of Pb in the western part of the EMEP domain is explained by intercontinental transport through the western border of the domain.

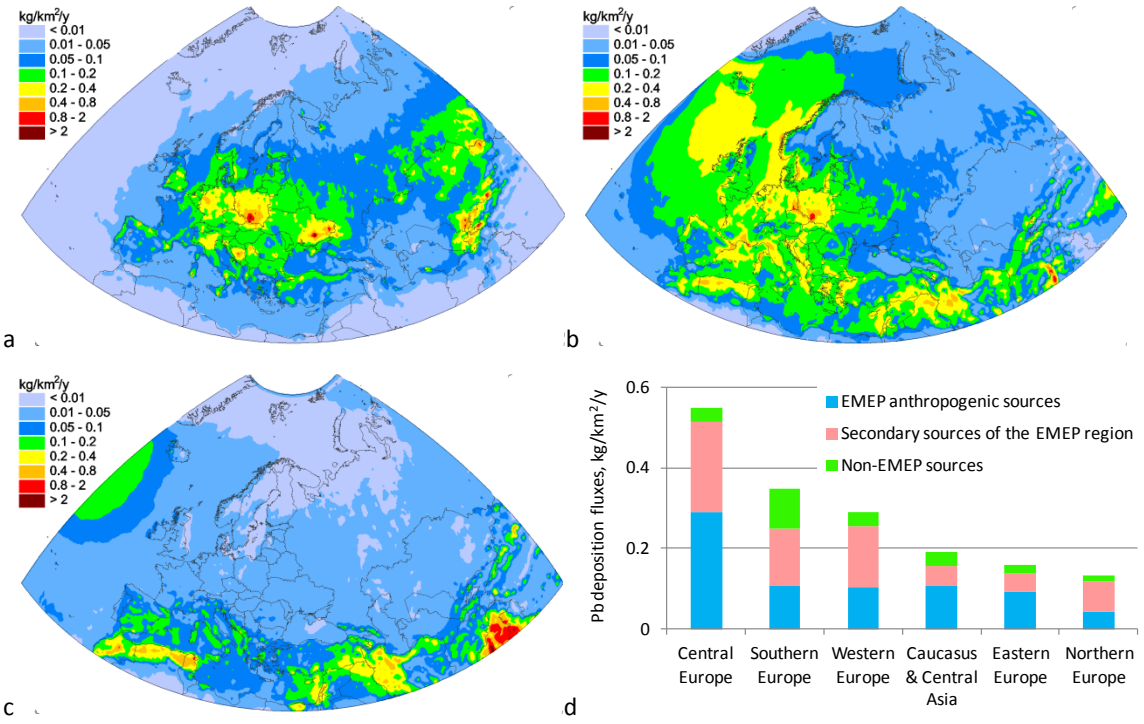

Fig. 2.12. *Annual Pb deposition in 2021 from EMEP anthropogenic sources (a), secondary sources (wind re-suspension) (b) and non-EMEP sources (c), and mean deposition fluxes from these sources to the EMEP sub-regions (d).*

Changes of the pollution levels between 2020 and 2021

Changes in annual mean concentrations in air and total deposition fluxes from 2020 to 2021 are described in this section. Concentrations of Pb decreased in most of the EMEP countries (Fig. 2.13a). Significant decline (20 – 50%) of air concentrations occurred over the southern part of Norway, the central part of France, the eastern part of Germany, over vast areas in the eastern part of Europe. On average, the Western Europe sub-region experienced the largest (almost 20%) decline of Pb air concentrations (Fig. 2.13b). Significant decline was also obtained for Central Europe, Eastern Europe and Northern Europe. Mean concentrations in Caucasus and Central Asia sub-region remained almost the same. In spite of average decline of Pb concentrations in Southern Europe sub-region, in some countries, e.g., Spain, Portugal and Greece, the concentrations increased (Fig. 2.13a).

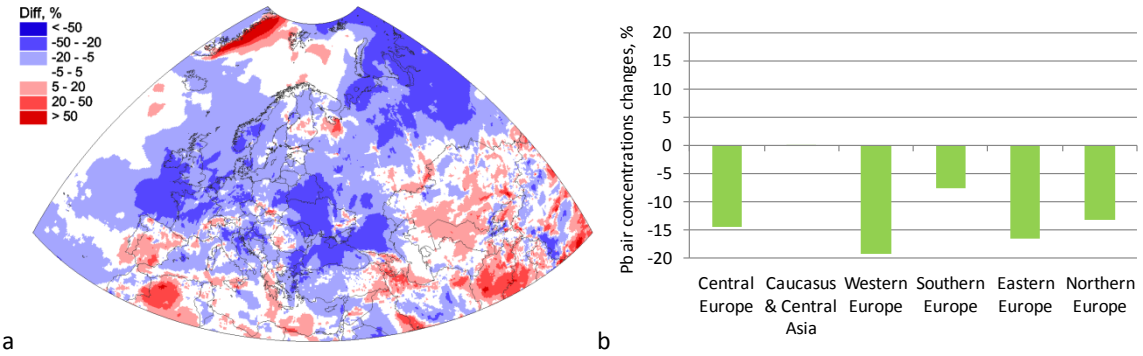

Fig. 2.13. *Relative changes of Pb air concentrations due to the changes in meteorological conditions over the EMEP domain (a), and in the EMEP sub-regions (b) between 2020 and 2021.*

Spatial distribution of deposition changes is characterized by large variability. Decline of deposition flux in 2021 was noted in Ireland, the western parts of France and the United Kingdom, Denmark, the southern parts of the Scandinavian Peninsula, north-eastern part of Poland. Increase of deposition occurred in some regions of the Scandinavian Peninsula, over the central part of Europe and the western and central parts of the Balkan region. Countries of the eastern part of the EMEP region and Central Asia are characterized by intermittent areas of the increase and decline of Pb deposition in 2021. On average, the largest reduction (15%) of deposition took place in the Northern Europe sub-region followed by the Western Europe sub-region (10%) (Fig. 2.14). For other sub-regions the mean changes are within ±5% range.

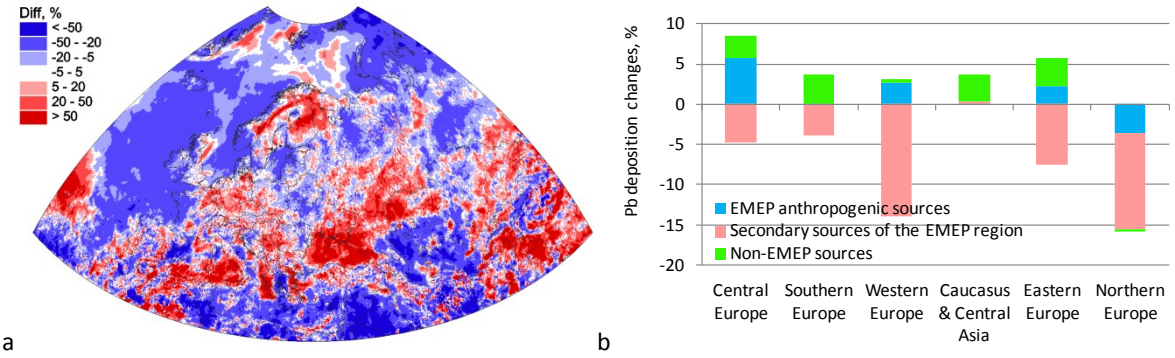

Fig. 2.14. *Relative changes of Pb total deposition due to the changes in meteorological conditions over the EMEP domain (a), and in the EMEP sub-regions (b) between 2020 and 2021.*

Since the calculations for 2021 were carried out using the same emission data as in the calculations for 2020, the changes between the modelling results are explained by the inter-annual variability of meteorological conditions. This variability affects the pollution levels both directly – via changes of precipitation amounts, transport patterns etc., and indirectly – through affecting origin of wind re-suspension.

In Fig. 2.14b the changes of total deposition in the EMEP sub-regions are presented in a form of contributions of the EMEP anthropogenic sources, secondary sources and non-EMEP sources. Only in Northern Europe the negative changes of all three components are occurred. In Caucasus and

Central Asia the contribution of non-EMEP sources increased, while the changes of other components are negligible. In most of sub-regions significant decrease of the re-suspension component is indicated.

Decrease of deposition from secondary sources in Central, Southern, Western and Eastern Europe is caused by the decrease of re-suspension in these sub-regions, which in turn is explained by the increase of precipitation amounts (Fig. 2.12). The increase of annual precipitation sums also led to the increase of deposition from anthropogenic sources in these sub-regions. Decline of re-suspension flux and stronger scavenging of Pb within these sub-regions resulted in lower transport to the Northern Europe sub-region. Therefore, deposition from these two types of sources in Northern Europe decreased. Besides, atmospheric transport patterns favours stronger transport outside Northern Europe in 2021 compared to 2020. While in most part of Europe precipitation increased, in African and Asian parts of the domain (Libya, Iran, Iraq, Afghanistan etc.) significant decrease of precipitation took place. It resulted in the increase of atmospheric transport of Pb emitted in these countries to the EMEP countries that led to increase of deposition from non-EMEP sources in most of the sub-regions.

Transboundary transport

Anthropogenic deposition to the EMEP countries are composed of two components: deposition from national emission sources (own deposition) and deposition caused by foreign countries (transboundary). In 2021, the highest spatially mean flux of Pb deposition from anthropogenic sources is noted for Poland (0.4 kg/km^2/y) followed by Slovakia and Bosnia and Herzegovina (Fig. 2.15a). Contribution of transboundary flux varies widely among the EMEP countries ranging from 17% in the United Kingdom to almost 100% in Monaco and Liechtenstein. In 40 countries of total 51 the contribution of transboundary transport exceeds 50% and in 29 countries it exceeds 75%. Contribution of transboundary transport to deposition in countries depends on a number of factors such as emission on own and neighboring countries, size of the country, prevailing wind patterns.

Changes in meteorological conditions affect transboundary and own deposition fluxes of Pb. Change of anthropogenic deposition between 2020 and 2021 was within ±20% in most of the EMEP countries (Fig. 2.15b). The highest increase (about 30%) of anthropogenic deposition occurred in Belgium. The increase is noted in both own and transboundary components of anthropogenic deposition. The reason for this is increase of precipitation in Belgium accompanied by increase of atmospheric transport from main countries-contributors of transboundary pollution in Belgium such as Germany, France, the Netherlands and the United Kingdom. Substantial decline of anthropogenic deposition took place in Turkmenistan (40%), Cyprus (36%) and Norway (28%). Decline of anthropogenic deposition in Turkmenistan is mainly caused by two-fold decrease of precipitation sums. Decrease of deposition in Cyprus is caused by the combination of two factors such as decline of precipitation and lower transport from Türkiye that was the main contributor of Pb transboundary pollution in Cyprus. Similar combination of the factors was responsible for decrease of anthropogenic deposition of Pb in Norway.

Changes of meteorological conditions between 2020 and 2021 resulted in changes of concentrations, deposition and transboundary fluxes of Pb in countries of the EMEP region. The changes were induced by direct effect of inter-annual variability of meteorological parameters (e.g., precipitation, atmospheric transport patterns) and by influencing wind re-suspension flux. On average the change was about 20%, however spatial variability of the change is significant.

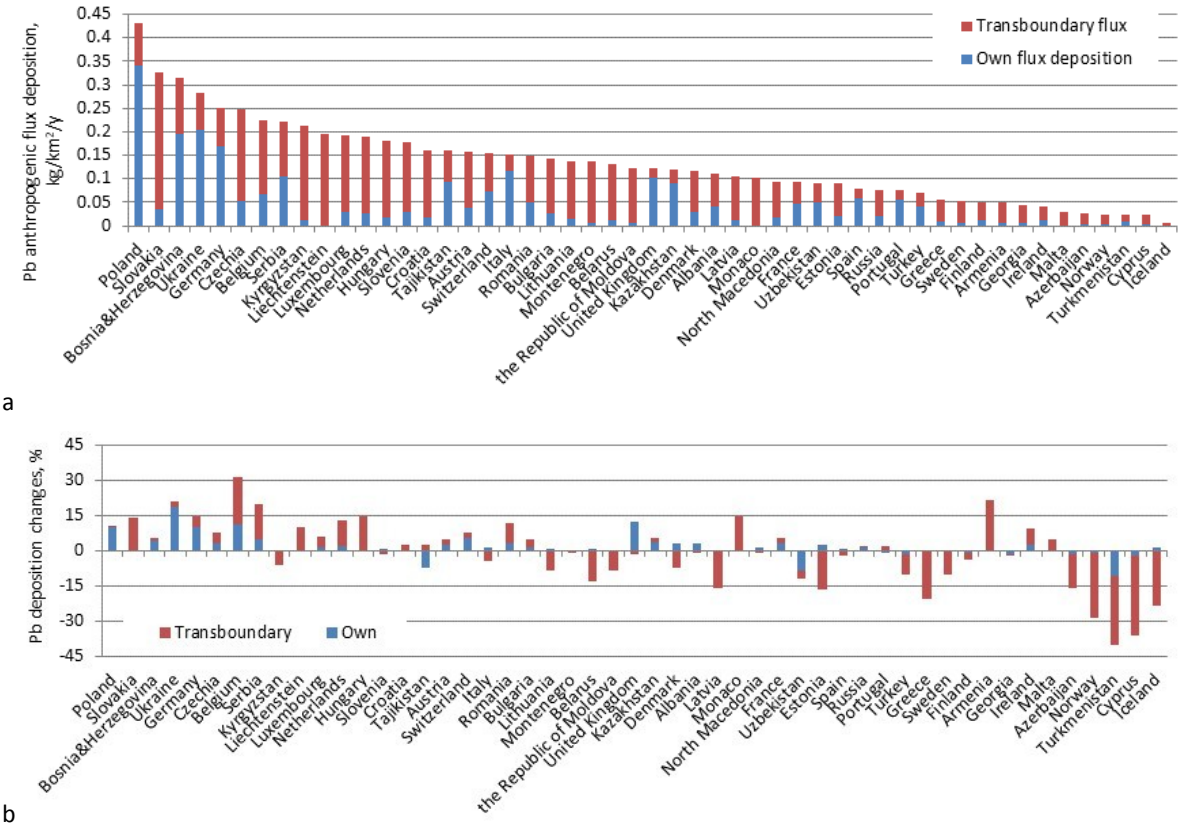

Fig. 2.15. *Spatially averaged deposition flux of Pb in the EMEP countries from national and foreign sources in 2021 (a) and relative change of the deposition fluxes between 2020 and 2021 (b).*

2.4.3. Cadmium

Cadmium in the atmosphere is bound to aerosol particles. The main anthropogenic emission sectors of Cd in the EMEP region are industry, production of electricity and residential combustion. However, in particular countries the contributions of other sectors can also be important. Cadmium is a toxic element known for harmful effects on the kidney, skeletal and respiratory system of humans and is classified as a carcinogen.

Air concentrations

Annual modelled and observed atmospheric concentrations of Cd in 2021 ranged mainly from 0.01 to 0.5 ng/m^3 over the most part of the EMEP countries (Fig. 2.16a). Areas of relatively high Cd concentrations (>0.3 ng/m^3) took place in the north-western part of Germany, the south-western part of Poland, north of Serbia and in a number of locations of the eastern part of Europe and Central

Asia. In general, modelled air concentration are somewhat higher than the observed ones (about 40%). The lowest levels were noted in Iceland, over Scandinavian Peninsula, the Arctic and Siberian regions of Russia, most of Central Asia and Türkiye. Central Europe is characterized by the highest spatially mean air concentrations (0.14 ng/m^3) of Cd in 2021 (Fig. 2.16b). Mean concentration in this sub-region were about two-fold higher than that in the Western Europe and Southern Europe sub-regions. However, it should be noted that the Western Europe sub-region is characterized by the widest variability of country-mean concentrations.

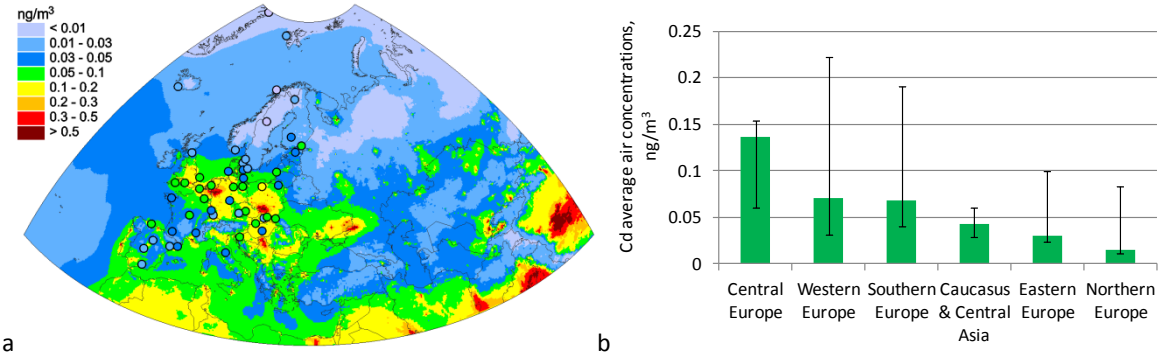

Fig. 2.16*. Annual mean air concentrations of Cd (circles on the map show observed values in the same colour scale) (a) and average air concentrations of Cd in EMEP sub-regions (b) in 2021. Whiskers show the range of country-average concentrations across countries in each sub-region.*

Deposition fluxes

Total deposition fluxes of Cd ranged from 5 to 100 g/km^2/y over a major part of the EMEP countries in 2021. Areas of the most significant (>60 g/km^2/y) Cd deposition included the western part of Germany and the southern part of Poland (Fig. 2.17a). It correlates with the fact that the highest spatially-mean deposition flux (23 g/km^2/y) was calculated for the Central Europe sub-region. Another areas with significant Cd deposition fluxes were the Balkan region (Bosnia and Herzegovina, Serbia, Slovenia), and the eastern part of the EMEP region (Fig. 2.17a). The lowest deposition is noted for the Northern Europe sub-region (around 5 g/km^2/y), in particular, in Nordic countries such as Iceland, Norway, Finland and Sweden. Low deposition also took place over most of Russia and the region of Central Asia.

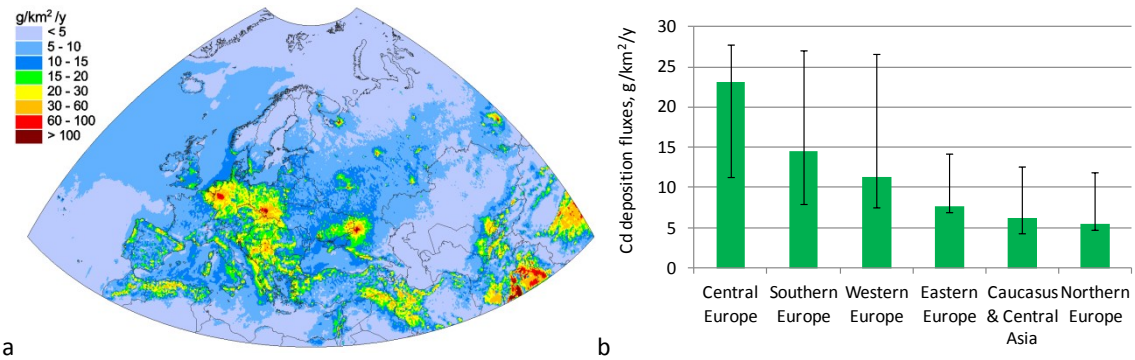

Fig. 2.17*. Annual total deposition flux of Cd (a) and mean total deposition fluxes of Cd to EMEP sub-regions (b) in 2021. Whiskers show the range of country-average concentrations across countries in each sub-region.*

Deposition fluxes of Cd are formed by the EMEP anthropogenic sources, secondary sources and non-EMEP sources. Spatial distribution of deposition from the anthropogenic sources of the EMEP countries (Fig. 2.18a) is correlated with the distribution of anthropogenic emissions (Fig. 2.6b). In particular, significant deposition fluxes from anthropogenic sources in Central Europe, over the Balkans and in countries of Eastern Europe are explained by location of emission sources in these regions. However, due to action of meteorological factors, especially wind patterns and atmospheric precipitation, field of deposition fluxes is smoother compared to that of the emissions. Anthropogenic deposition fluxes over sea areas are mainly caused by the atmospheric transport because the contribution of shipping to emissions of heavy metals is relatively small. The highest contribution of the EMEP anthropogenic sources to total deposition both in relative (almost 80%) and absolute (about 18 g/km^2/y) terms was noted for the Central Europe sub-region (Fig. 2.18d). The lowest (around 40%) relative contribution occurred in the Caucasus and Central Asia sub-region.

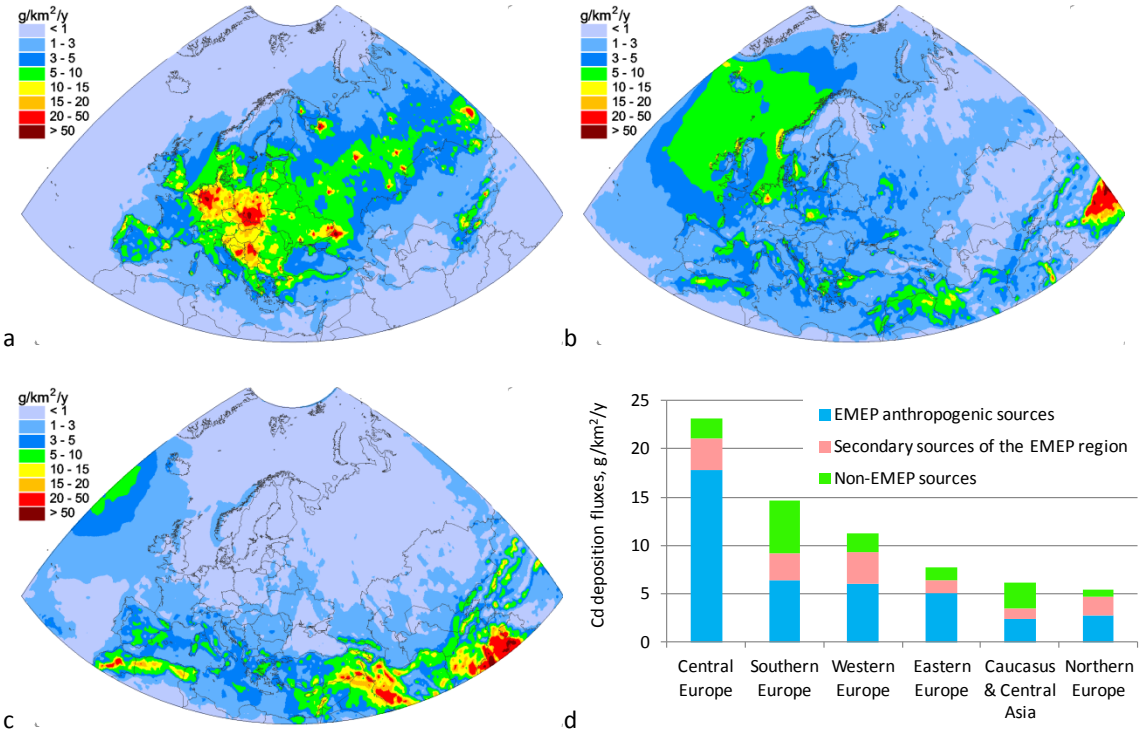

Fig. 2.18. *Annual Cd deposition in 2021 from EMEP anthropogenic sources (a), secondary sources (wind re-suspension) (b) and non-EMEP sources (c), and mean deposition fluxes from these sources to the EMEP sub-regions (d).*

Secondary sources results to re-suspension of soil or dust particles containing cadmium from land surfaces. The highest re-suspension took place in areas where concentration of Cd in soil or dust is significant due to natural reasons or enrichment because of long-term accumulation of anthropogenic deposition. It resulted to relatively high (5-10 g/km^2/y) deposition fluxes from secondary sources in the north-western part of Germany, the south-eastern part of Poland, the southern part of France, in Italy and south-east of Türkiye (Fig. 2.18b). Besides, similar levels of the flux were noted over the North Atlantic. They are caused by re-suspension of Cd with sea spray and consequent scavenging by atmospheric precipitation. Arid climate favours large re-suspension of Cd from desert areas of Central Asia. However, due to low precipitation deposition flux of Cd from

secondary sources in this region is relatively low. The greatest spatially mean deposition flux from secondary sources took place in Western Europe. The highest (roughly 35%) relative contribution of secondary sources was calculated for the Northern Europe sub-region. Since re-suspension in Northern Europe is relatively low, high percentage of secondary sources is caused by atmospheric transport from other sub-regions and by low impact of anthropogenic and non-EMEP sources.

Non-EMEP sources affected mostly southern regions of the EMEP domain. Significant deposition fluxes (5 – 15 g/km^2/y) caused by non-EMEP sources occurred in Spain, Italy, Greece, Bosnia and Herzegovina, Albania, Montenegro, Bulgaria, Türkiye, Tajikistan, the southern parts of Turkmenistan and Kazakhstan (Fig. 2.18c). Even higher levels (15 – 50 g/km^2/y) in south-east of Türkiye are explained by combination of proximity of significant non-EMEP sources and large precipitation amounts. Similar levels of deposition along the Caucasus ridge were caused by high precipitation. Southern Europe and Caucasus and Central Asia are characterized by the highest (about 40%) contribution of non-EMEP sources to Cd total deposition.

Changes of the pollution levels between 2020 and 2021

Changes of annual mean concentrations in the EMEP countries due to meteorological variability between 2020 and 2021 ranged within ±50% (Fig 2.19a). On average, the reduction of air concentrations took place in almost all the EMEP sub-regions except for Caucasus and Central Asia (Fig. 2.19b). The highest decline (14%) took place in the Eastern Europe sub-region. In Western Europe and Northern Europe the mean reduction made up about 7%. Over main part of France, the United Kingdom and Sweden the change in air concentration was from -5% to -20%. In Finland the concentrations decreased in southern part of the country and increased in the central part. In other sub-regions the change is within ±5%. Nevertheless, in particular countries the changes could be wider than these limits.

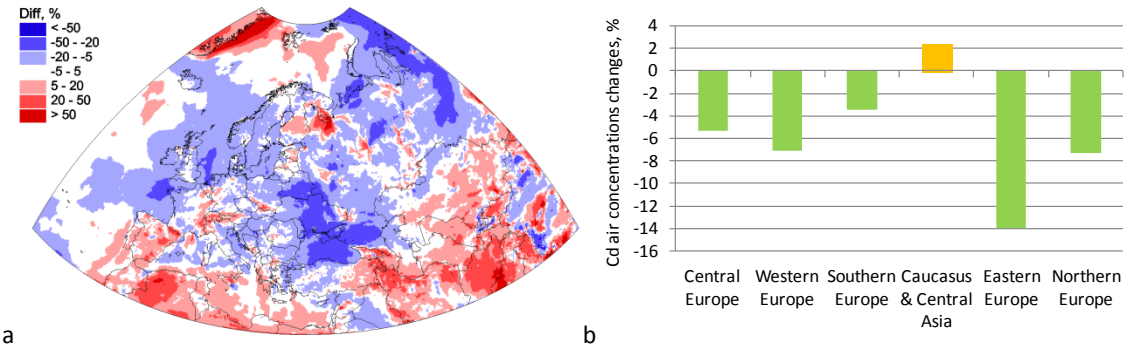

a b

Fig. 2.19. *Relative changes of Cd air concentrations due to the changes in meteorological conditions over the EMEP domain (a), and in the EMEP sub-regions (b) between 2020 and 2021.*

Deposition of Cd in 2021 increased in most of the EMEP countries and sub-regions (Fig. 2.20). Over most part of the EMEP country's area the changes in Cd deposition varied from -50% to 50% (Fig. 2.20a). Deposition fluxes increased in a number of countries of central Europe, such as Germany, Poland, Czechia and Slovakia. Spatially mean increase of deposition in Central Europe made up around 10% (Fig. 2.20b). Another sub-region with significant (15%) increase of deposition is Caucasus

and Central Asia. In this sub-region most marked increase took place in Georgia, Tajikistan, most of Kazakhstan and the southern part of Uzbekistan. At the same time, deposition declined in the south-western part of Kazakhstan, northern Uzbekistan and most part of Turkmenistan. Northern Europe is characterized by general decline of deposition by almost 15%. The decrease is pronounced in Iceland, Denmark, the southern parts of Norway, Sweden and Finland. However, in the central and northern parts of Finland and in the northern part of Norway deposition of Cd increased up to 50%.

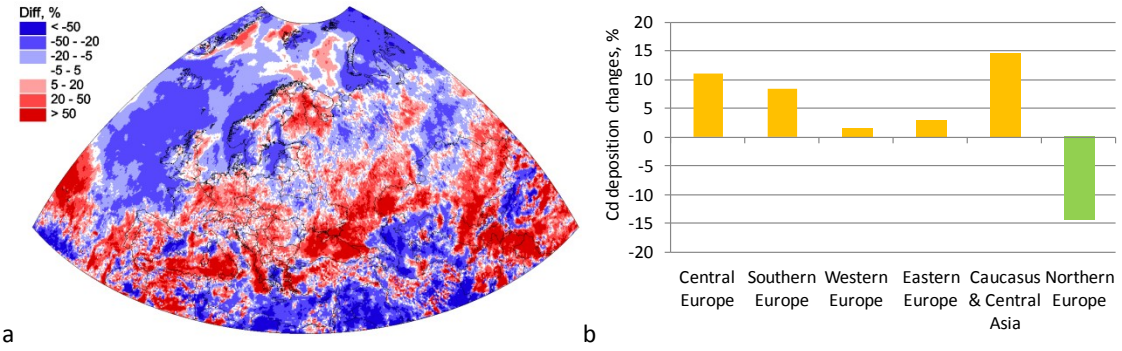

a b

Fig. 2.20. *Relative changes of Cd total deposition due to the changes in meteorological conditions over the EMEP domain (a), and in the EMEP sub-regions (b) between 2020 and 2021.*

Transboundary transport

Spatially mean Cd deposition flux to the EMEP countries caused by the EMEP anthropogenic sources ranged from 0.2 g/km^2/y (Iceland) to around 20 g/km^2/y (Serbia, Poland, Slovakia) (Fig. 2.21a). This flux consists of two components, such as deposition from national emission sources (own deposition flux) and deposition from foreign emission sources (transboundary flux). Contribution of transboundary transport to Cd anthropogenic deposition in 2021 ranged from about 20% (the United Kingdom, Spain, Portugal) to almost 100% (Monaco, Lichtenstein, Iceland). In 39 countries of 51 the contribution of transboundary transport to pollution from anthropogenic sources exceeded 50%, and in 15 countries it exceeded 75%. Due to inter-annual variability of meteorological conditions own and transboundary deposition in the EMEP countries changed. The largest increase was noted for Belgium (around 40%) followed by Armenia and Luxembourg (about 15% each). The highest decline occurred in Turkmenistan (32%), Norway and Iceland (26% each), and Cyprus (25%). The reasons of the changes are similar to those of Pb (Section 2.4.2).

Due to the inter-annual variability of meteorological conditions between 2020 and 2021 pollution levels of Cd in the EMEP region changed. On average, the changes in particular countries were within ±15%. However, regional differences in concentrations, deposition and transboundary fluxes between 2020 and 2021 could be much larger.

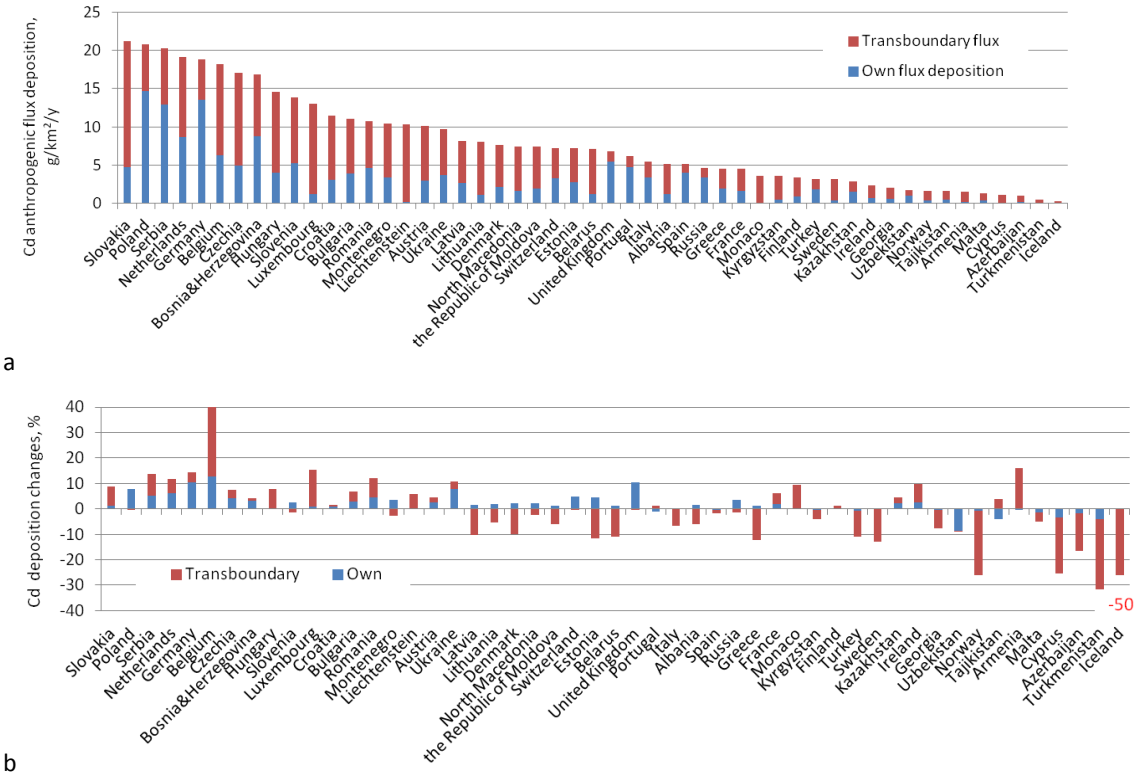

a

b

Fig. 2.21. *Spatially averaged deposition flux of Cd in the EMEP countries from national and foreign sources in 2021 (a) and relative change of the deposition fluxes between 2020 and 2021 (b).*

2.4.4. Mercury

Mercury is a toxic pollutant capable of long-range transport, bioaccumulation in ecosystems and leading to adverse effects on human health and biota. Mercury mainly occurs in the free and lower troposphere in the gaseous elemental form (Hg^0) with a small contribution of oxidized forms (Hg^{II}). Besides, mercury deposition is determined by Hg^{II}, which is directly emitted from anthropogenic sources and formed chemically in the atmosphere from Hg^0, as well as by air-vegetation exchange of Hg^0. Thus, Hg deposition depends on a number of factors including spatial patterns of anthropogenic and natural emission, chemical composition of the atmosphere as well as meteorological conditions.

Air concentrations

Over most of the EMEP domain concentrations of Hg^0 in the surface layer varied from 1.4 to 3 ng/m^3 (Fig. 2.22a). Compared to other considered pollutants, this variability is low. It is explained by long atmospheric life time of Hg favouring well mixing in the global atmosphere. Concentrations exceeding 1.6 ng/m^3 took place in the southern and eastern parts of the region, i.e., in Spain, Italy, Bosnia and Herzegovina, Greece, Serbia, Bulgaria and some other countries. Besides, levels exceeding 1.6 ng/m^3 took place over the Caspian Sea. Levels of 1.5 – 1.6 ng/m^3 occurred over the southern part of the North Sea, Belgium, the Netherlands and south-west of Poland. Central and Southern Europe were characterized by the highest spatial-mean Hg concentrations, while the lowest

levels were noted for Northern Europe (Fig. 2.22b). Modelled concentrations of Hg in air fit the observed levels with mean bias 6%. The difference between modelled and observed air concentrations for individual stations does not exceed 25%.

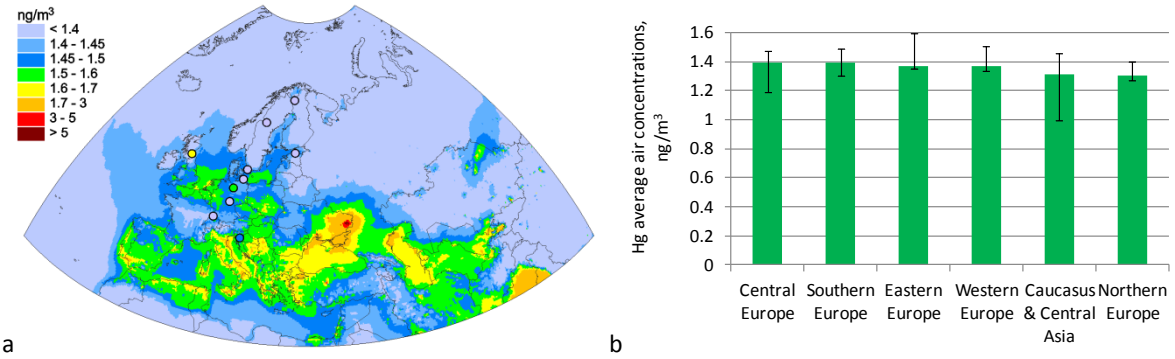

a b

Fig. 2.22. *Annual mean air concentrations of Hg (circles on the map show observed values in the same colour scale) (a) and mean air concentrations of Hg in EMEP sub-regions (b) in 2021. Whiskers show the range of country-average concentrations across countries in each sub-region.*

Deposition fluxes

Annual deposition fluxes of Hg exhibited much larger spatial variability compared to air concentrations. Relatively low fluxes (below 7 g/km^2/y) took place in the central part of Norway, the Baltic Sea, over the most part of Central Asia (Fig. 2.23a). Relatively high fluxes (> 16 g/km^2/y) occurred in most countries of Central and Southern Europe, in the northern part of Norway, in the Balkan region, southern part of Türkiye and in the eastern European countries of the EMEP domain (Fig. 2.23b). Unlike concentrations in air, represented mainly by long-lived elemental Hg^0, deposition fluxes are formed by short-lived oxidized forms of Hg. It results in higher spatial variability of Hg deposition compared to Hg concentrations in air. Relatively high deposition fluxes (10-20 g/km^2/y) occurred over the Arctic waters of the Atlantic Ocean and the Barents Sea were caused by intensive oxidation of Hg^0 during the Atmospheric Mercury Depletion Events (AMDEs). However, it is worth mentioning that large part of Hg deposited due to AMDEs tends to re-vaporize back to the atmosphere. The highest spatially averaged deposition flux is noted for Central Europe sub-region followed by Southern Europe sub-region (Fig. 2.23b). However, Southern and Eastern Europe sub-regions were characterized by the largest variability of deposition fluxes averaged over country's territories. The lowest deposition was simulated for the Caucasus and Central Asia sub-region. This sub-region is characterized by relatively low emissions (on average) and low annual sums of atmospheric precipitation. The agreement between the modelled and observed Hg wet deposition fluxes is within factor of 2. The more detailed information on evaluation of modeling results against observations is presented in Annex A.

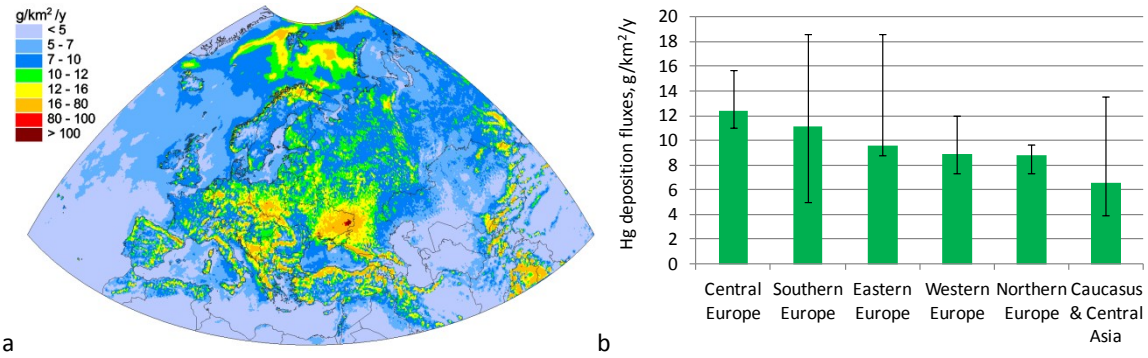

Fig. 2.23. *Annual total deposition flux of Hg (a) and mean total deposition fluxes of Hg to EMEP sub-regions (b) in 2021. Whiskers show the range of country-average concentrations across countries in each sub-region.*

Fig. 2.24 depicts spatial distributions of Hg deposition from anthropogenic, secondary and non-EMEP sources. The highest deposition flux from anthropogenic sources took place in regions with the highest emissions, e.g., in south-western Poland, north-western Germany, the Balkan countries, certain areas in the eastern part of Europe (Fig. 2.24a). Central Europe sub-region is characterized by the largest average deposition flux from the EMEP anthropogenic sources (Fig. 2.24d).

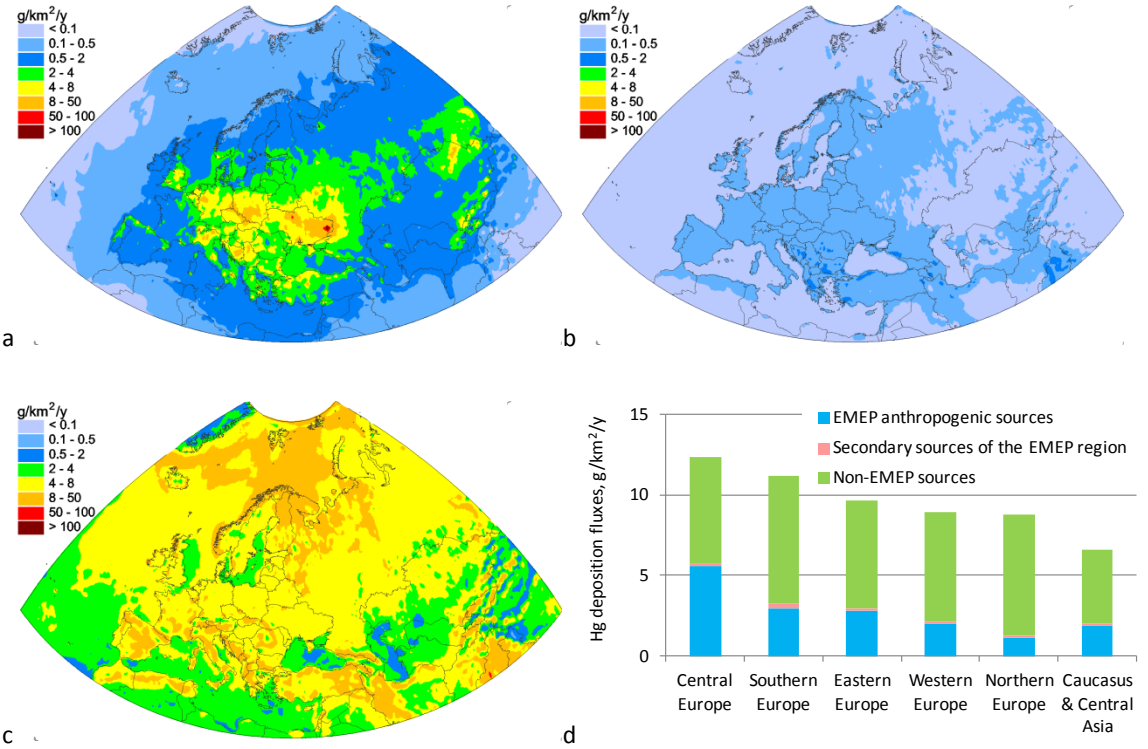

Fig. 2.24. *Annual Hg deposition in 2021 from EMEP anthropogenic sources (a), EMEP secondary sources (natural and re-emission) (b) and non-EMEP sources (c), and mean deposition fluxes from these sources to the EMEP sub-regions (d)*

Contribution of non-EMEP sources is more uniform compared to that of anthropogenic deposition. It is explained by long residence time of Hg in the atmosphere. Elemental mercury originated from the sources located outside the EMEP counties enters the EMEP domain being well mixed in the

troposphere. Then Hg^0 is oxidized and deposited to the surface with precipitation (wet deposition) or due to interactions with the underlying surface (dry deposition). Hence, spatial distribution of Hg deposition from non-EMEP sources reflects the distribution of chemical reactants, atmospheric precipitation and peculiarities of the underlying surface. The largest regional-mean deposition from non-EMEP sources was noted for the Southern Europe sub-region due to higher oxidation, followed by the Northern Europe sub-region where high precipitation occurred. The fraction of non-EMEP sources ranged from 54% to 86%. However, it should be noted that due to the long-time residence of Hg in the atmosphere, non-EMEP sources might contain some fraction of the mercury input from the EMEP anthropogenic sources that was transported out through the boundaries of the region, mixed with inputs from other anthropogenic sources, and transported back into the region in composition of the non-EMEP sources. Natural or legacy Hg is released to the atmosphere as long-lived Hg^0. Therefore, after emission it quickly leaves the EMEP domain and, hence, the contribution of secondary Hg sources to the EMEP countries is weak (1-3%).

Changes of the pollution levels between 2020 and 2021

Changes of Hg concentrations in air due to inter-annual variability of meteorological conditions between 2020 and 2021 were within ±3% limits over most of the EMEP countries (Fig. 2.25a). The increase of concentrations took place in Finland, some regions of France, Germany, Czechia, Poland and over large areas of the Eastern Europe. Decreased concentrations were noted over Scandinavian Peninsula, the Balkan region, the Mediterranean, Black Seas and the Arctic. Spatially averaged changes of concentrations in sun-regions of the EMEP were below ±1% (Fig. 2.25b).

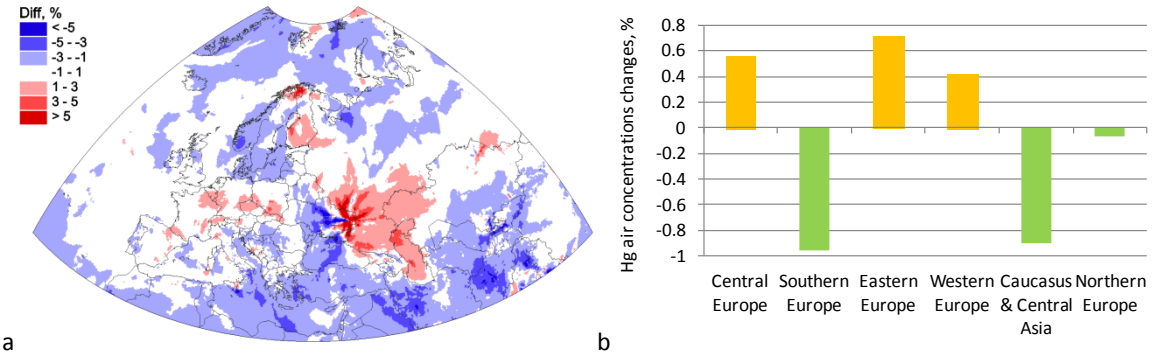

a b

Fig. 2.25. *Relative changes of Hg air concentrations due to the changes in meteorological conditions over the EMEP domain (a) and in the EMEP sub-regions (b) between 2020 and 2021.*

Significant (20-50%) increase of total deposition of Hg was noted for Scandinavian Peninsula, large areas of the Eastern Europe, the southern coasts of the Adriatic Sea and the central part of the Mediterranean Sea (Fig. 2.26). The decrease was indicated for the north-western part of Russia, a number of areas in Central Asia, Caspian and Aegean Seas. In all sub-regions spatially mean deposition fluxes in 2021 increased. The increase ranged from 0.3% (Southern Europe) to about 6% (Central Europe). The main reason of Hg deposition increase was the increase of precipitation amounts (see Section 2.1).

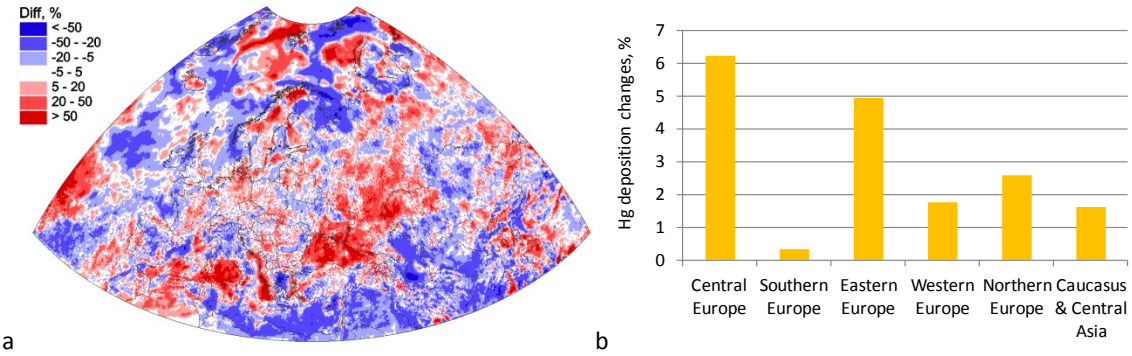

a b

Fig. 2.26. *Relative changes of Hg total deposition due to the changes in meteorological conditions over the EMEP domain (a) and in the EMEP sub-regions (b) between 2020 and 2021.*

Transboundary transport

In 2021 contribution of national sources exceeded the contribution of transboundary transport to Hg anthropogenic deposition in the EMEP countries in 10 countries. These are countries characterized by significant national emissions or by remote location from main emission sources. In 41 countries the contribution of transboundary transport exceeds 50%, and in 26 exceeds 75% to anthropogenic deposition of Hg. In 11 countries total anthropogenic deposition in 2021 decreased, and in 40 countries – increased compared to that in 2020. In majority of EMEP countries these changes are mostly caused by the changes in transboundary component of deposition (Fig. 2.27b).

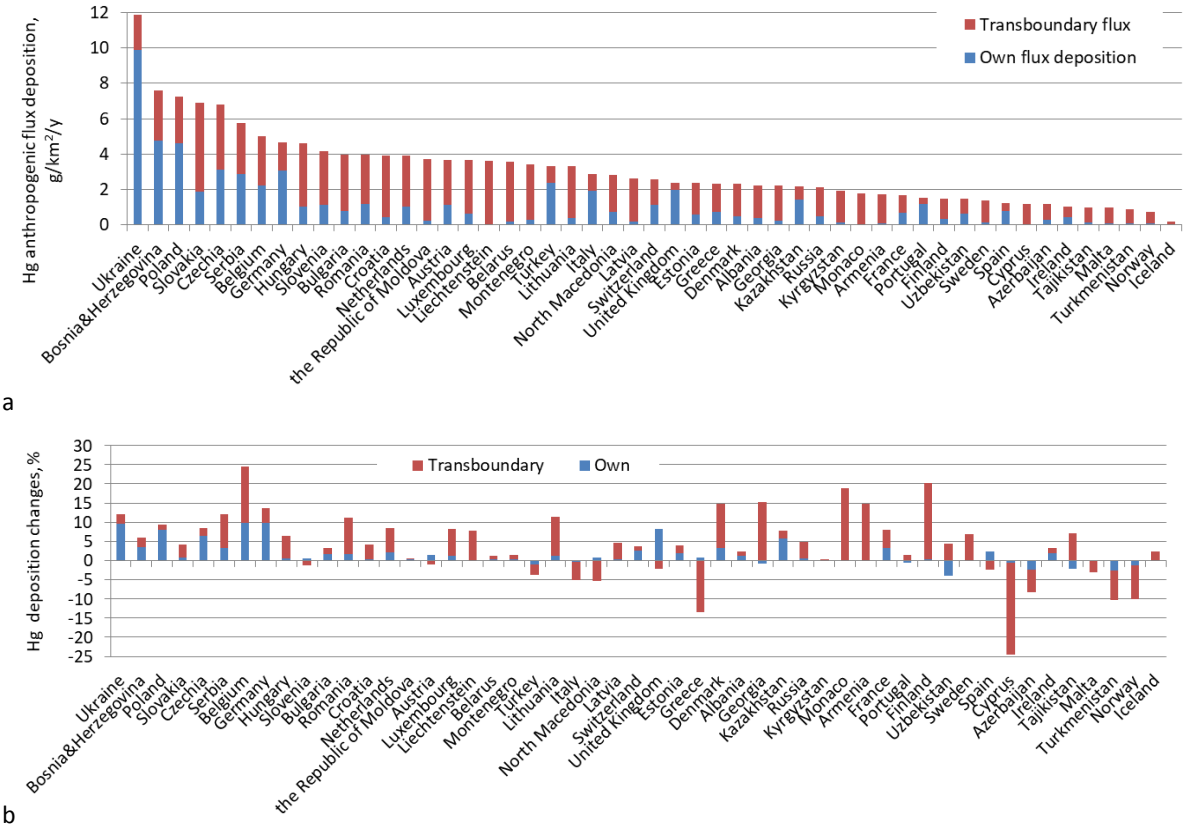

a

b

Fig. 2.27. *Spatially averaged deposition flux of Hg in the EMEP countries from national and foreign sources in 2021 (a) and relative change of the deposition fluxes between 2020 and 2021 (b).*

2.4.5. Polycyclic Aromatic Hydrocarbons (PAHs)

Polycyclic Aromatic Hydrocarbons comprise a large group of organic chemicals that are released to the environment from natural and anthropogenic emission sources. The most significant part of anthropogenic PAH emissions originates from incomplete combustion of various types of fossil fuels and biomass burning. PAHs belong to semi-volatile compounds that are presented in the atmosphere in gaseous and particulate phase and undergo chemical reactions. Entering the atmosphere PAHs can be transported over long distances. Some of the PAHs have carcinogenic, mutagenic, and teratogenic properties and can pose serious risk to human health [*Keyte et al.*, 2013; *Kim et al.*, 2013].

Assessment of PAH pollution levels and exceedances of air quality guidelines is made for the 4 PAH compounds, targeted by the LRTAP Protocol on POPs (namely benzo(a)pyrene, benzo(b)fluoranthene, benzo(k)fluoranthene, and indeno(1,2,3-cd)pyrene). In this section overview of PAH pollution levels and long-range transport in the EMEP region is presented based on the results of monitoring and model simulations for 2021. Information on exceedances of air quality guidelines for 4 PAHs is given in Section 2.5.2. More detailed results of modelling and monitoring of PAH pollution levels can be found in Annex A.

Air concentrations

Annual mean air concentrations of the sum of 4 PAHs in 2021 are illustrated in Fig. 2.28a. PAH concentrations in air in the EMEP region vary from less than 0.1 ng/m^3 up to about 5 ng/m^3. The highest average atmospheric concentrations (about 2 ng/m^3) are estimated for the countries of Central Europe followed by Southern and Eastern Europe (about 0.5 ng/m^3) (Fig. 2.28b). Other areas of the EMEP region are characterized by relatively low air concentrations of 4 PAHs (0.1 – 0.3 ng/m^3) with the lowest levels (below 0.1 ng/m^3) in Northern Europe (Fig. 2.28b).

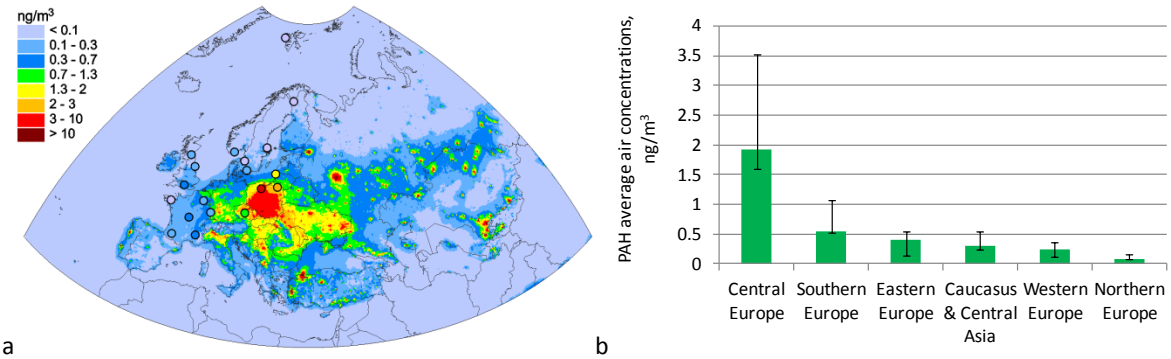

a b

Fig. 2.28. *Annual mean air concentrations of the sum of 4 PAHs (circles on the map show observed values in the same color scale) (a) and average air concentrations of the sum of 4 PAHs in the EMEP sub -regions (b) in 2021. Whiskers show the range of concentrations in particular countries of the sub -region.*

The model simulations indicate high levels of pollution (above 1.5 ng/m^3) in particular countries, e.g. in Poland, Czechia, Slovakia, and Hungary. High level of concentrations is also noted for certain areas of Italy, Croatia, Serbia, Romania, and a number of regions of the eastern part of Europe. In some of

these countries pollution levels exceeded air quality guidelines established for B(a)P by the EU and WHO (Section 2.5.2).

Monitoring of 4 PAHs in 2021 was carried out at 33 monitoring sites in 14 EMEP countries. Evaluation of the modelling results against EMEP measurements shows good agreement of modelled and observed concentrations of the sum of 4 PAHs with low bias (-3%) and high spatial correlation (0.91). For about 80% of the monitoring stations, the differences between the modelling results and measured concentrations are within a factor of 2. Evaluation of modelling results for individual 4 PAH compounds against the EMEP measurements indicates -26%, 9%, -18%, -22% bias for B(a)P, B(b)F, B(k)F and I(cd)P, respectively. The model satisfactory reproduced the spatial distribution of observed 4 PAH air concentrations with correlation coefficients about 0.81-0.96.

Deposition fluxes

Spatial distribution of the sum of 4 PAHs deposition fluxes in the EMEP region in 2021 is shown in Fig. 2.29a. Deposition flux of PAHs depends on a number of factors that include distribution of emission sources, atmospheric transport, properties of underlying surface and precipitation amount. The highest deposition fluxes (200-700 g/km^2/y and higher) are estimated for some countries of Central and Eastern Europe. Moderate levels of deposition (30-200 g/km^2/y) take place in countries of Western and Southern Europe. Similar to air concentrations, the highest spatially averaged deposition fluxes of 4 PAHs (about 180 g/km^2/y) are noted for Central Europe, and the lowest ones for Northern Europe (about 15 g/km^2/y) (Fig. 2.29b).

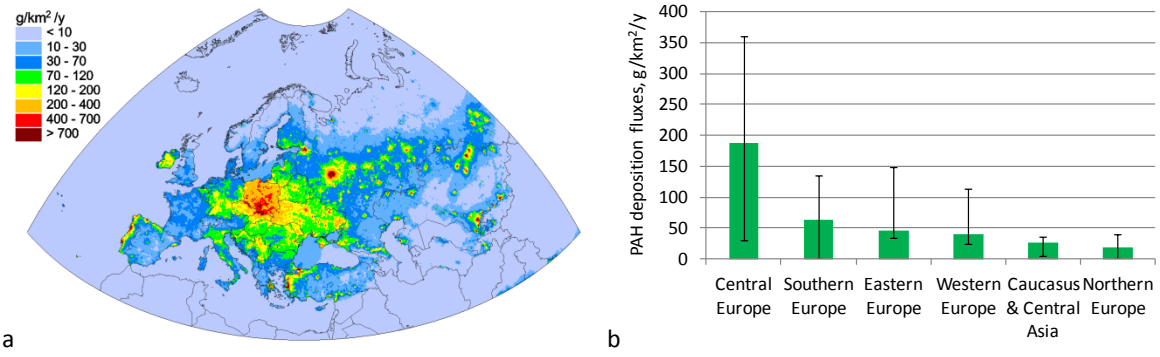

a b

Fig. 2.29. *Annual total deposition flux of the sum of 4 PAHs (a) and average total deposition fluxes of the sum of 4 PAHs to the EMEP sub-regions (b) in 2021. Whiskers show the range of deposition fluxes in particular countries of the sub-region.*

Three groups of emission sources of PAH deposition are considered in the model simulations, namely, EMEP anthropogenic sources, secondary sources (re-volatilization from surface compartments) in the EMEP domain and emission sources located outside the EMEP countries (non-EMEP sources). The largest contribution (more than 80%) is made by the EMEP anthropogenic sources, while other types of emission sources contributed less than 20%.

Changes of pollution levels between 2020 and 2021

Relative changes of PAH air concentrations between 2020 and 2021 due to meteorological variability are shown for the whole EMEP domain (Fig. 2.30a), and as spatially averaged air concentrations in six sub-regions (Fig. 2.30b). Over the most part of the EMEP countries the differences of air concentrations between two years varied within ±20%. The largest increase of spatially averaged air concentrations is estimated for Western Europe (about 8%). Smaller increase is calculated for Central (3%) and Southern Europe (1%). The largest decrease of PAH concentrations (about -4%) is calculated for Northern Europe. Less significant decline is noted for Eastern Europe (-2%) and Caucasus and Central Asia (-1%).

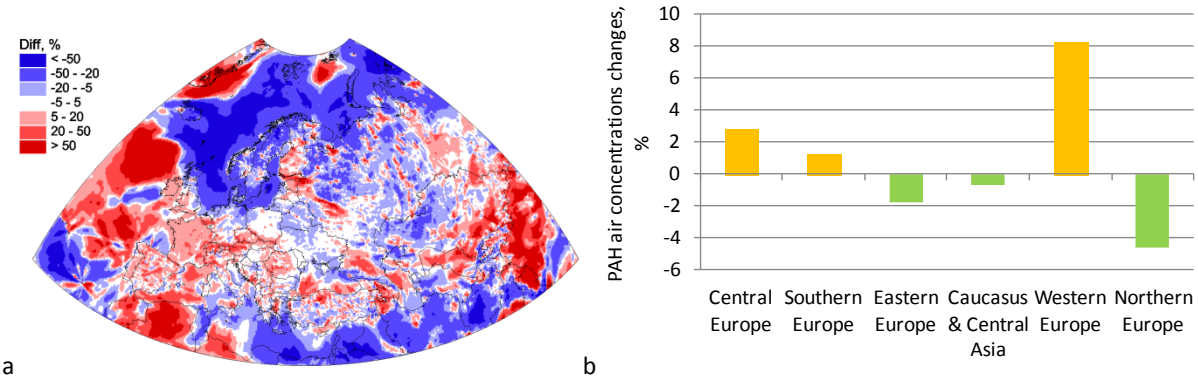

a b

Fig. 2.30. *Relative changes of the sum of 4 PAHs air concentrations between 2020 and 2021 over the EMEP domain due to meteorological conditions (a). The bar chart (b) shows relative changes of concentrations of the sum of 4 PAHs in EMEP sub-regions.*

Relative changes of total deposition fluxes of 4 PAHs from 2020 to 2021 are illustrated in Fig. 2.31a. Similar to air concentrations, in most of the EMEP countries changes of deposition fluxes varied within the range of ±20%. In all the sub-regions spatially averaged PAH deposition fluxes tended to decrease from 2020 to 2021. The largest decline of spatially averaged deposition fluxes is estimated for Northern Europe (-22%). In other sub-regions less significant changes are noted, in particular, in Western Europe, Caucasus and Central Asia, Central Europe, Eastern Europe, and Southern Europe by -7%, -6%, -4%, -3%, and 2%, respectively. Similar to air concentrations, more significant relative decrease of deposition fluxes is estimated for some areas of the Atlantic Ocean and the Mediterranean and Black Seas. Estimated changes in PAH concentrations and deposition fluxes from 2020 to 2021 can be attributed to inter-annual variations of meteorological conditions, namely, temperature and atmospheric circulation patterns, described in Section 2.1.

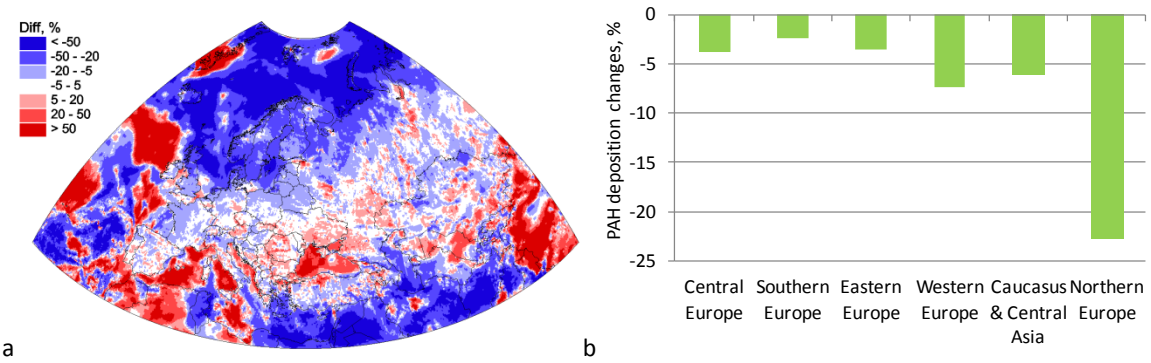

a b

Fig. 2.31. *Relative changes of the sum of 4 PAHs deposition between 2020 and 2021 over the EMEP domain due to meteorological conditions (a). The bar chart (b) shows relative changes of deposition fluxes of the sum of 4 PAHs in the EMEP sub-regions.*

Transboundary transport

Modelling of PAH long-range transport and country-to-country deposition fluxes permit to characterize relative contributions of national and foreign emission sources to total PAH deposition in particular countries. Spatially averaged deposition fluxes of the sum of 4 PAHs to EMEP countries are shown in Fig. 2.32a. The highest deposition flux is estimated for Poland (300 g/km^2/y) followed by Slovakia (200 g/km^2/y) and Czechia (180 g/km^2/y), while the lowest one is calculated for Iceland and Malta (below 1 g/km^2/y). PAH deposition from transboundary transport exceeds deposition from national sources in 16 EMEP countries (e.g. Slovakia, Lithuania, and Luxembourg). The highest contribution of transboundary transport (about 97 – 99%) is noted for Liechtenstein, Monaco and Montenegro due to their relatively small territory or low national emissions. The lowest contribution of transboundary transport (below 10%) is estimated for Ireland, Portugal, and Italy due to their relative remoteness from major foreign emission sources.

Changes of PAH deposition to each EMEP country from national and foreign emission sources between 2020 and 2021 are shown in Fig. 2.32b.

For most of the countries difference between PAH deposition fluxes in 2020 and 2021 ranges between 5% and -15%. A few exceptions include Monaco, Iceland, Norway, Norway, Sweden, and Denmark. Changes of transboundary fluxes were more significant compared to the changes of deposition fluxes from national sources. In some countries (e.g. Bulgaria, Slovakia) deposition from national emission sources decreased in 2021 while deposition from foreign emission sources increased. Difference in estimates of PAH pollution levels for 2020 and 2021 is explained by the effect of inter-annual variability of meteorological parameters.

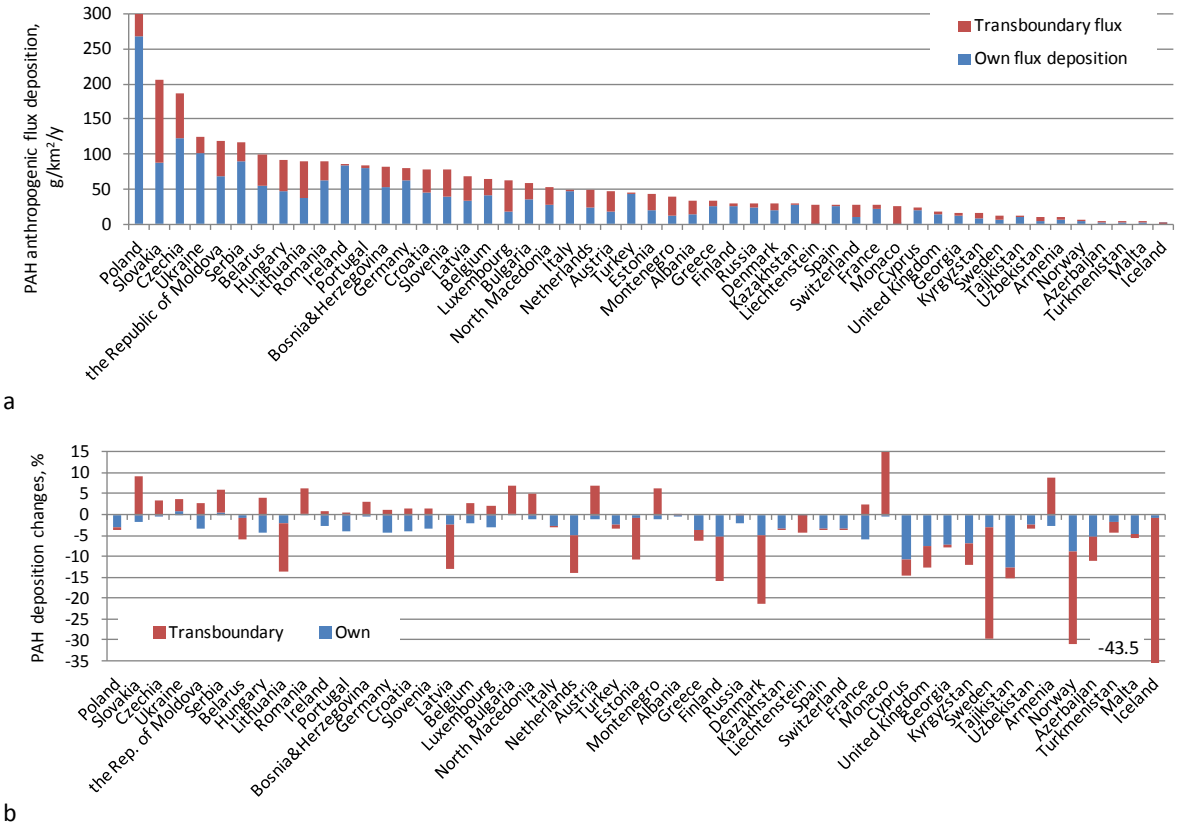

Fig. 2.32. *Spatially averaged deposition flux of the sum of 4 PAHs in the EMEP countries from national (national flux) and foreign (transboundary flux) anthropogenic emission sources in 2021 (a) and relative change of the deposition fluxes between 2020 and 2021 due to meteorological variability (b).*

2.4.6. PCDD/Fs, PCBs and HCB

This section summarizes observed and modelled pollution levels of PCDD/Fs, PCBs, and HCB in 2021 in the EMEP region. These are semi-volatile persistent pollutants widely dispersed in the environment. Studies of their adverse effects indicate that they pose risk to human health and biota [*WHO*, 2000; 2003; *Starek-Świechowicz et al.,* 2017]. PCDD/Fs, PCBs, and HCB are formed as unintentional by-products during various anthropogenic activities (e.g. combustion of fossil fuels, chemical manufacture processes, waste incineration) and can be released into the atmosphere and other environmental compartments. Long-term accumulation in the terrestrial and aquatic compartments can lead to their secondary emissions (re-volatilization) to the atmosphere making significant contribution to the pollution levels.

Air concentrations

Annual mean modelled PCDD/Fs, PCB-153 and HCB air concentrations in the EMEP domain simulated for 2021 are presented in Figs. 2.33a,c,e. Model predictions of PCDD/Fs and PCB-153 concentrations in the EMEP countries vary in a wider range compared to HCB concentrations. Relatively homogeneous distribution of HCB can be attributed to its more significant persistence in the atmosphere. Along with the modelling results annual mean concentrations, measured at the EMEP monitoring stations in 2021, are shown on the maps.

Averaged air concentrations for six sub-regions of the EMEP region are given in Figs. 2.33b,d,f. The highest concentrations of PCDD/Fs are estimated for Southern Europe (4.5 fg TEQ/m^3), of PCB-153 for Western, Central and Southern Europe (3-4 pg/m^3), and for HCB for Eastern and Central Europe (35-40 pg/m^3). The lowest pollution levels are noted for countries in Northern Europe.

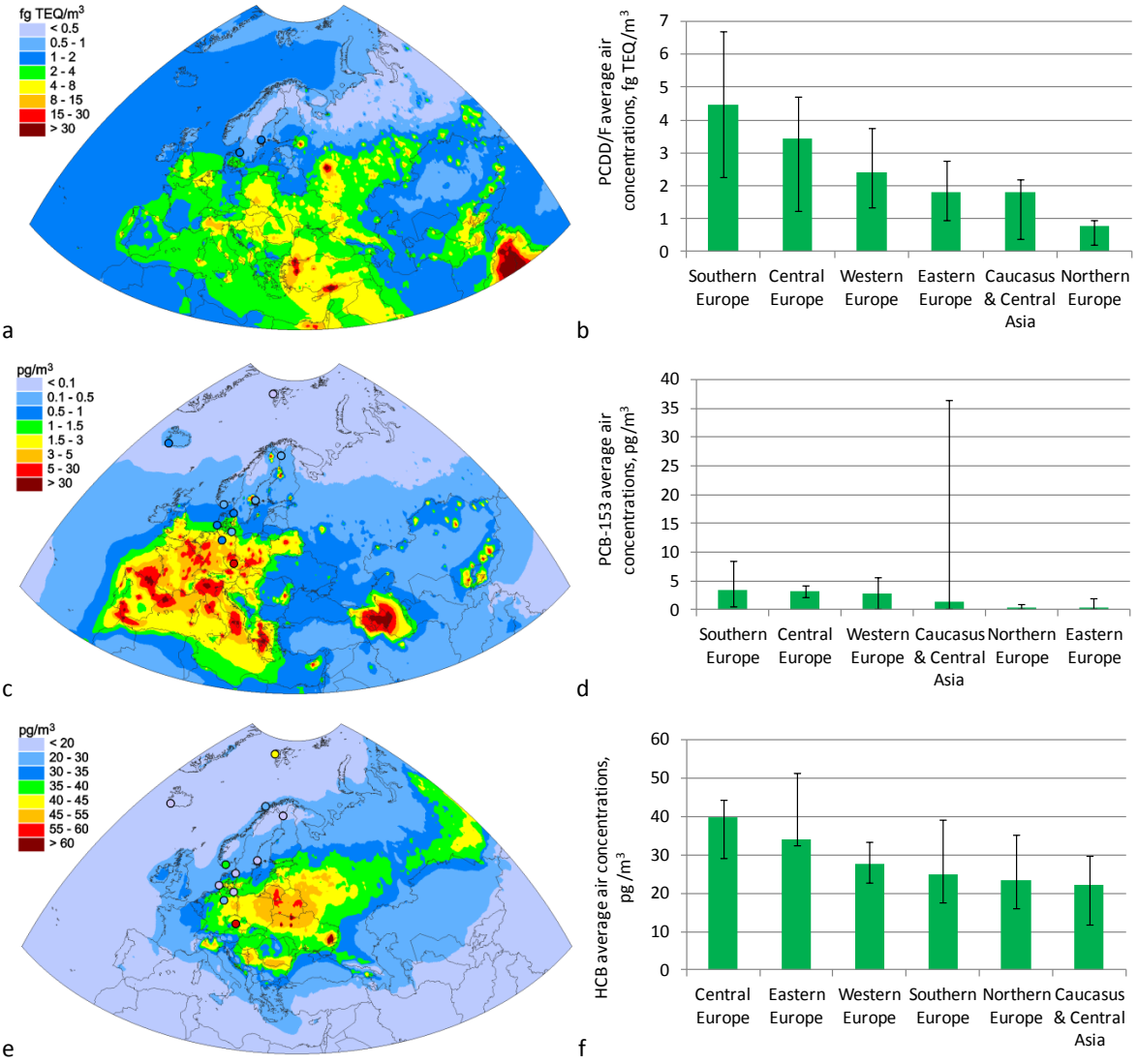

Fig. 2.33. *Annual mean modelled and observed air concentrations of PCDD/Fs (a), PCB-153 (c), and HCB (e) (circles on the map show observed values in the same color scale) and averaged air concentrations of PCDD/Fs (b), PCB-153 (d), and HCB (f) in the EMEP sub-regions in 2021. Whiskers show the range of concentrations in particular countries of the sub-regions.*

Modelling results for 2021 were compared with observed PCB-153 and HCB concentrations at the EMEP monitoring network. Modelled PCB-153 air concentrations are two-fold higher than the measured ones. The highest differences (more than a factor of 2) are found for the stations CZ0003R, DE0002R, DE0008R, DE0009R, and IS0091R. Modelled HCB air concentrations are slightly higher than measurements (by 13%). For most of the stations differences between modelled and observed values are lower than a factor 2.

Deposition fluxes

Modelled PCDD/Fs, PCB-153 and HCB annual deposition fluxes in the EMEP domain for 2021 are demonstrated in Fig. 2.34a,c,e. Deposition of these pollutants depend on a number of factors, including location of main emission sources, precipitation amounts, properties of underlying surface and contribution of secondary emissions.

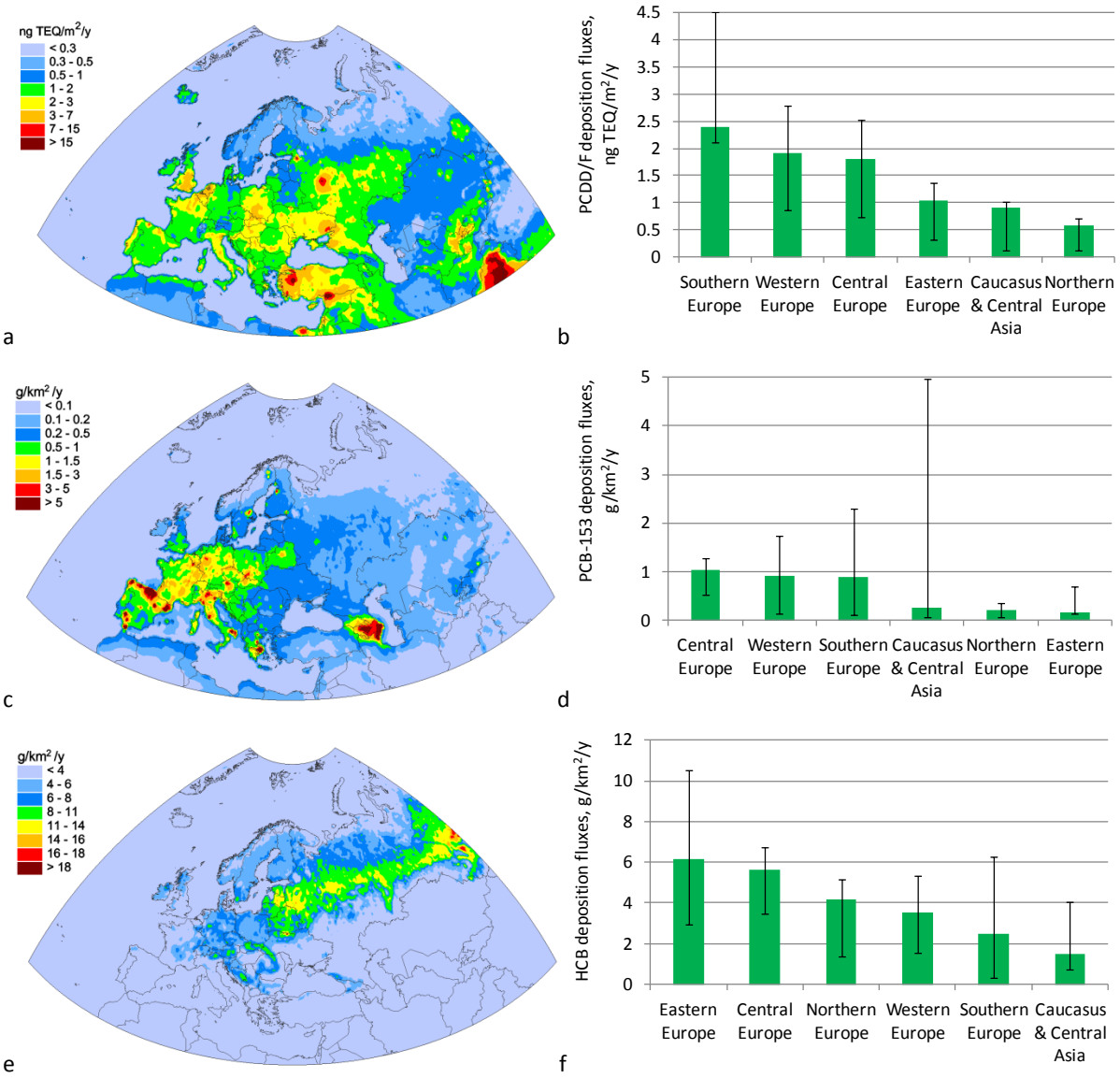

Fig. 2.34. *Annual modelled deposition fluxes of PCDD/Fs (a), PCB-153 (c), and HCB (e) and averaged deposition fluxes of PCDD/Fs (b), PCB-153 (d), and HCB (f) in the EMEP sub-regions in 2021. Whiskers show the range of deposition fluxes in particular countries of the sub-regions.*

Spatial distributions of PCDD/Fs, PCB-153 and HCB deposition fluxes in 2021 generally follow the distribution of air concentrations of these pollutants. In particular, maximum values of PCDD/Fs and PCB-153 deposition fluxes are estimated for countries in Western, Central and Southern Europe. For HCB relatively high deposition fluxes are indicated for Eastern, Central and Northern Europe.

Average annual total deposition fluxes of PCDD/Fs, PCB-153 and HCB for different EMEP sub-regions are illustrated in Fig. 2.34b,d,f. The highest average annual deposition fluxes take place in Southern Europe for PCDD/Fs, in Central Europe for PCB-153 and in Eastern Europe for HCB. The lowest pollution levels are estimated for Northern Europe in case of PCDD/Fs, for Eastern Europe in case of PCB-153, and for Caucasus and Central Asia in case of HCB.

Three groups of emission sources were considered in the model simulations, namely, EMEP anthropogenic sources, secondary sources (re-volatilization) in the EMEP domain and emission sources located outside the consolidated area of all EMEP countries (non-EMEP sources). The contributions of these three groups of sources to average annual deposition fluxes in six sub-regions of EMEP domain are shown in Fig. 2.35.

Modelling results show that the highest contribution to deposition fluxes is made by secondary emission sources of the EMEP domain. The second most important contributors for PCDD/Fs and PCB-153 are the EMEP anthropogenic emissions. For HCB the second most important contributor is the emission outside the EMEP domain boundaries while the EMEP anthropogenic emissions contributed much less.

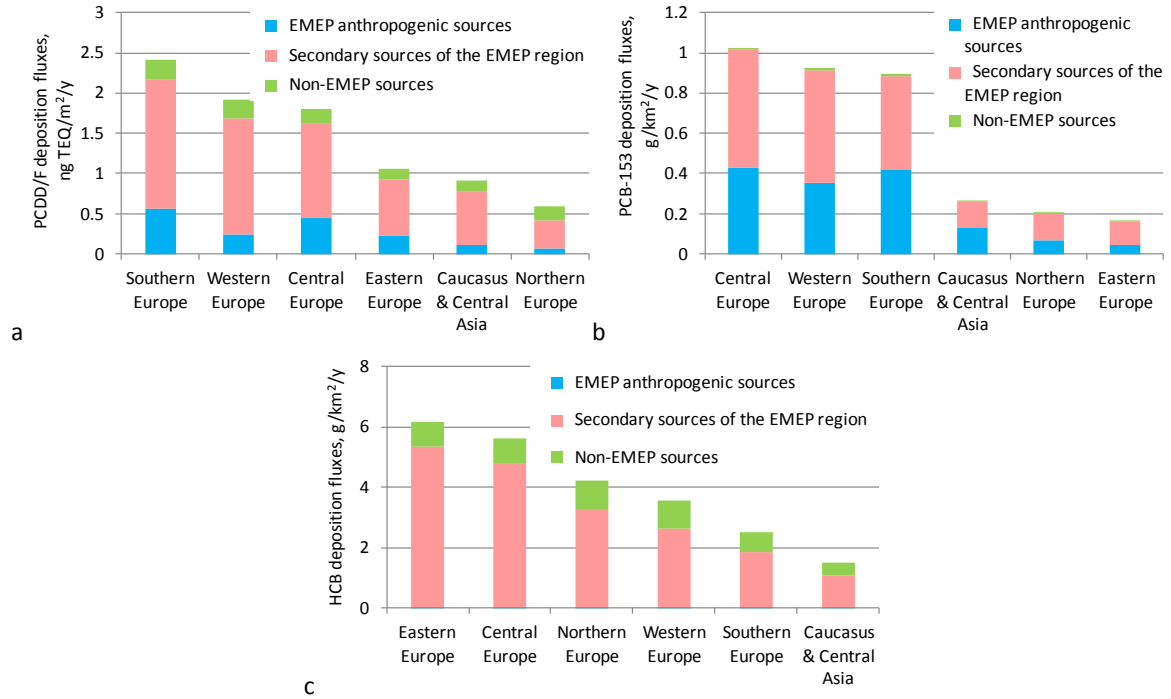

Fig. 3.35. *Annual average deposition fluxes of PCDD/Fs (a), PCB-153 (b) and HCB (c) to EMEP sub-regions in 2021 from the EMEP anthropogenic sources, secondary sources (re-volatilization) and non-EMEP sources.*

Changes of the pollution levels between 2020 and 2021

This section describes inter-annual changes of pollution levels between 2020 and 2021 due to variability of meteorological conditions. To evaluate the effect of changes of meteorological parameters, two model simulations were carried out using meteorological data for 2020 and 2021 and the same emission dataset for 2020. Examples of modelling results are given for PCDD/Fs and HCB.

Relative changes of PCDD/Fs and HCB annual mean air concentrations from 2020 to 2021 are shown in Fig. 2.36. For most of sub-regions PCDD/F air concentrations increased by 2-8% with the exception of Southern Europe for which small decline was estimated. The largest increase is estimated for Eastern Europe (about 8%) followed by Central Europe (about 6%). HCB air concentrations declined in all sub-regions. The largest change is estimated for Eastern Europe (-11%). The lowest change is noted for Western Europe (-2%).

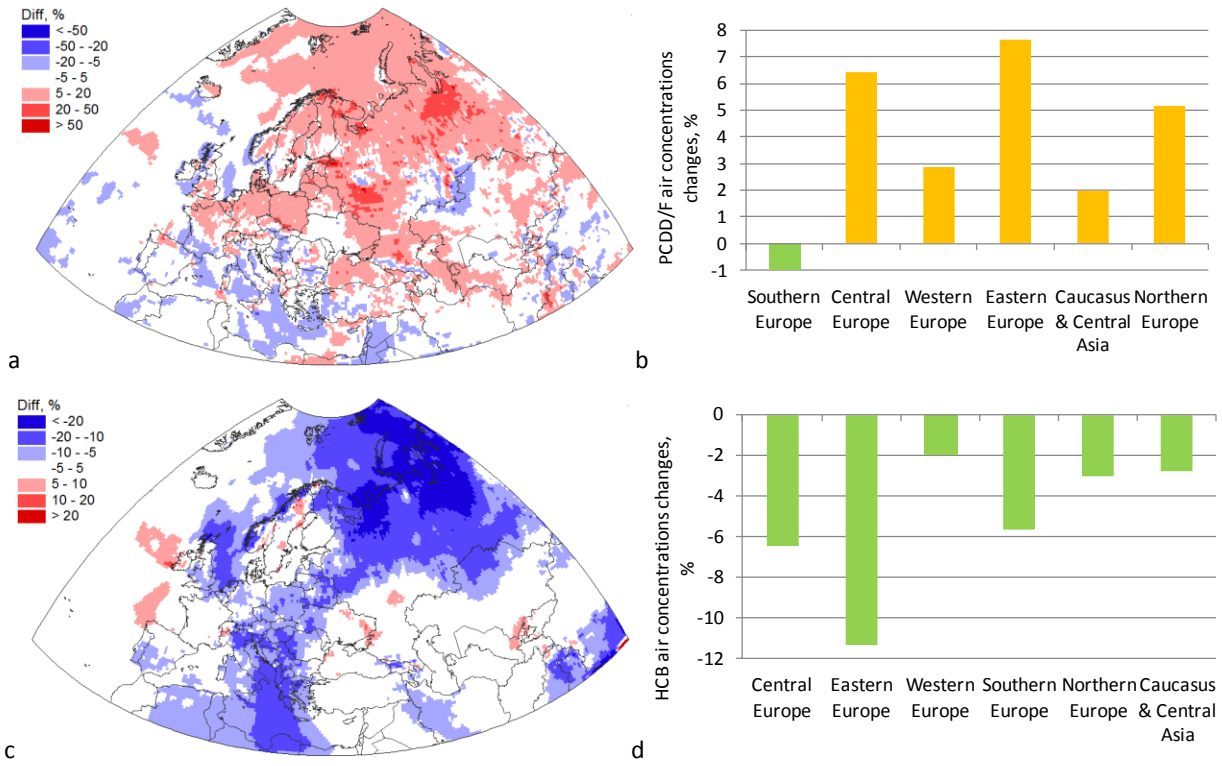

Fig. 2.36. *Relative changes of PCDD/Fs and HCB air concentrations between 2020 and 2021 in the EMEP domain (a,c) and in its six sub-regions (b,d).*

Relative changes of PCDD/Fs and HCB annual deposition fluxes from 2020 to 2021 are demonstrated in Fig. 2.37. Deposition of PCDD/Fs increased in Eastern Europe (by 4%) and Caucasus and Central Asia (by 1%). In Western, Northern, Central, and Southern Europe deposition fluxes declined by 5%, 5%, 1%, and 1%, respectively. Similar to air concentrations, deposition fluxes of HCB decreased in all the sub-regions. The largest change is estimated for Eastern Europe (about -9%) followed by Southern Europe (about -6%). Inter-annual changes of air concentrations and deposition fluxes described above can be attributed to the changes of air temperature, precipitation amount and pathways of atmospheric circulation.

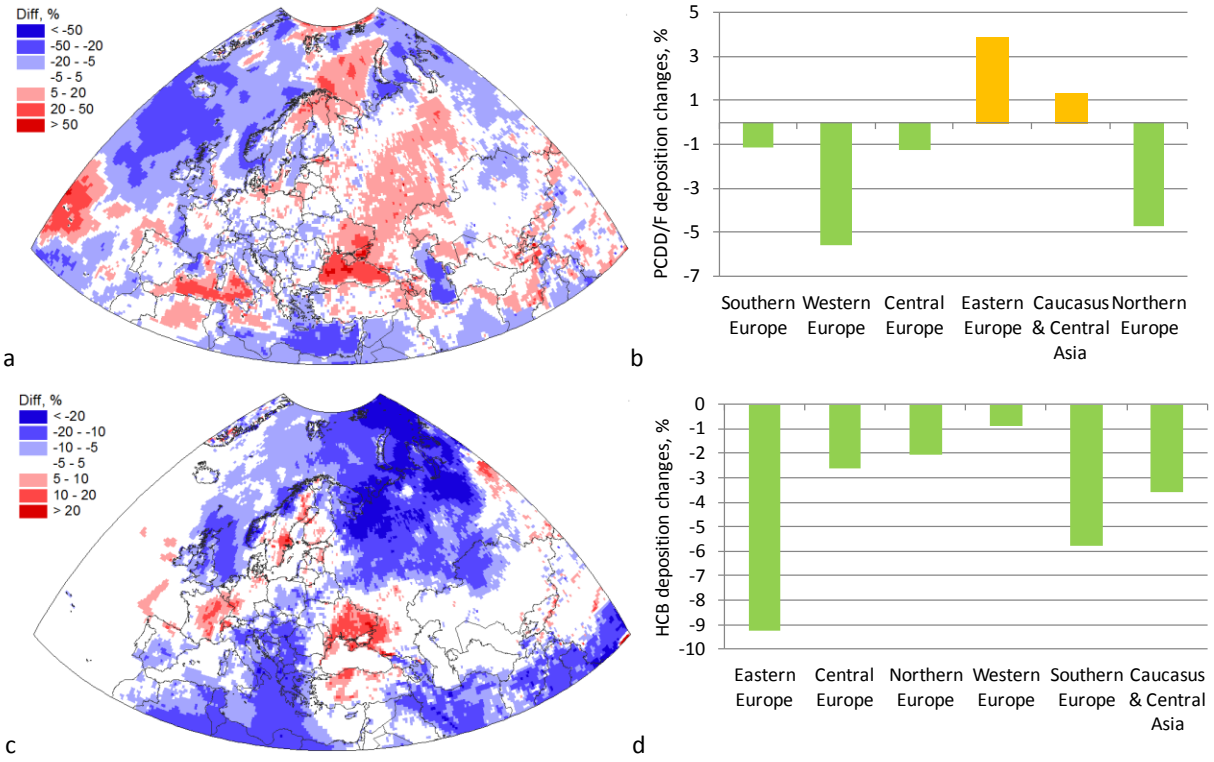

Fig. 2.37. *Relative changes of PCDD/Fs and HCB deposition fluxes between 2020 and 2021 in the EMEP domain (a,c) and in its six sub-regions (b,d).*

Transboundary transport

Anthropogenic component of deposition to the EMEP countries can be split into two parts: deposition caused by national emission sources and deposition caused by transboundary atmospheric transport from the sources of other EMEP countries (foreign sources). The example of modelling results, evaluating contributions of national and foreign sources to PCDD/F deposition, is presented in Fig. 2.38. The largest deposition fluxes were estimated for Türkiye, Slovakia and Albania, while the lowest ones for Finland, Norway and Iceland.

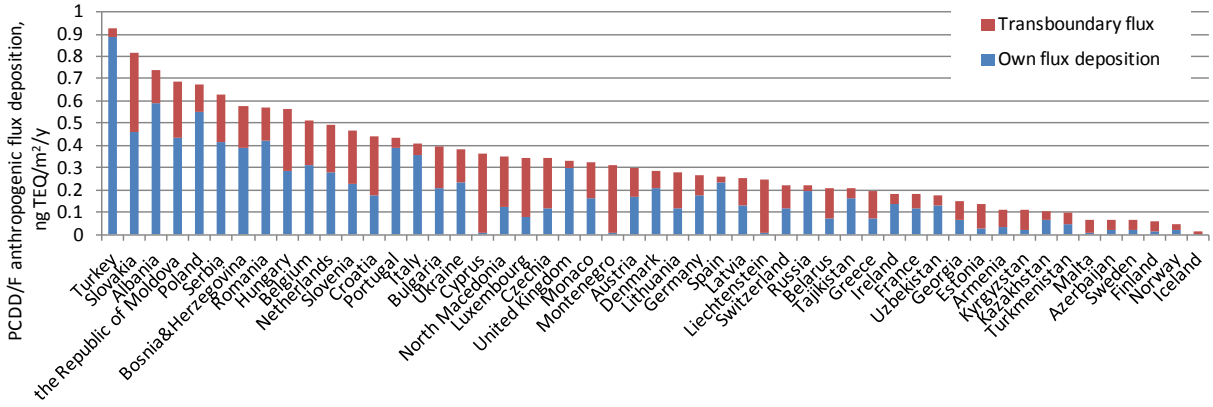

Fig. 2.38. *Spatially averaged deposition flux of PCDD/Fs over EMEP countries from national and foreign sources in 2021.*

Model simulations indicate that transboundary atmospheric transport of POPs plays important role in the pollution of EMEP countries. The highest contribution of transboundary transport is noted for the countries with small territory and/or low national emissions (e.g. in Liechtenstein, Cyprus, Montenegro). The lowest contribution of transboundary transport is estimated for the countries with substantial national emissions and relatively large territory (e.g. in Poland, the United Kingdom, Italy). Furthermore, significant influence of national sources is noted for the countries located in the western part of the EMEP region due to predominant westerly atmospheric transport and relative remoteness from major foreign emission sources.

According to the modelling results, variability of meteorological conditions between 2020 and 2021 led to changes of PCDD/Fs deposition fluxes from -10% to 10% in the majority of EMEP countries (Fig. 2.39). The largest increase of deposition is estimated for Armenia (by 12%), while the largest decrease of deposition (by 26%) for Iceland. In most of the countries estimated changes of PCDD/F deposition fluxes were caused by the changes of transboundary contributions. Some of the countries are characterized by the changes of national and transboundary components of deposition in opposite directions (e.g. Slovakia, Hungary).

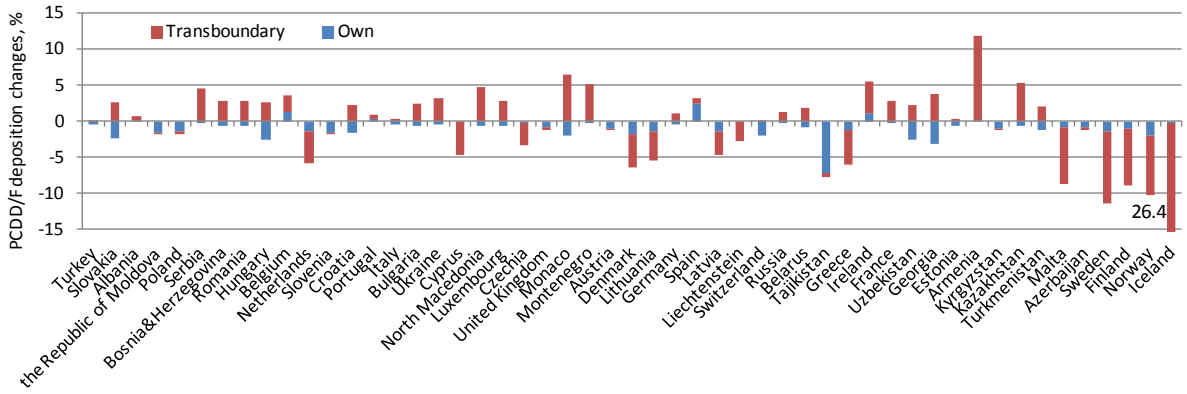

Fig. 2.39. *Relative changes of the deposition fluxes of PCDD/Fs contribution from 2020 to 2021.*

2.5. Information for exposure assessment

2.5.1. Ecosystem-specific deposition of heavy metals

Deposition of heavy metals to different land-cover categories (ecosystems) are regularly calculated by MSC-E. The purpose of these calculations is to provide WGE with important information for assessment of exceedances of critical loads. The calculations were carried out for 17 types of land cover (forests, arable land, urban area, water surface etc.). Modelled ecosystem-specific deposition fluxes in 2021 are available on the MSC-E website (https://msceast.org/pollution-assessment/emep-domain-menu/land-use-menu).

Deposition fluxes to various ecosystems differ significantly due to different dry deposition velocities and spatial distribution of emissions. In particular, dry deposition velocities to areas covered by high vegetation (forests, shrubs) are higher than those in low-vegetation ecosystems (grasslands, agricultural lands). For example, Hg deposition fluxes to different types of forests are considerably

higher than the fluxes to wetlands (Fig. 2.40a,b). Deposition flux of Hg to wetlands mostly varied from 7 to 15 g/km^2/y, while the flux to forests mostly ranged from 10 to 30 g/km^2/y. Similar results were obtained for other heavy metals (Pb, Cd).

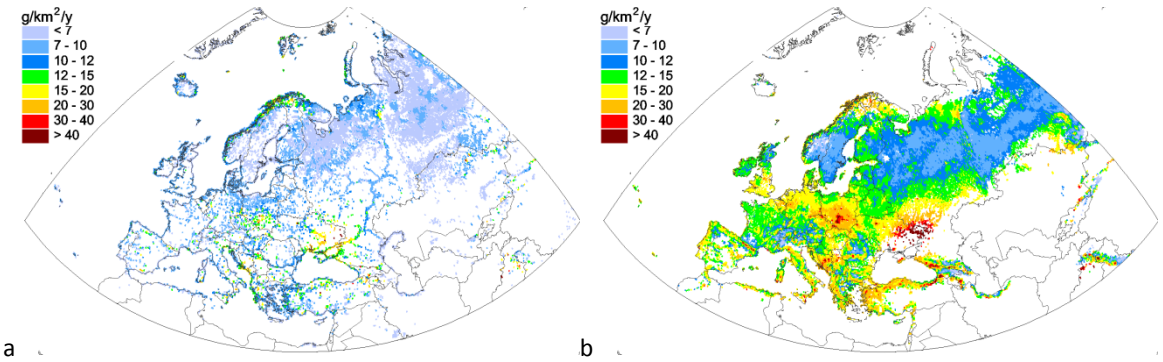

Fig. 2.40. *Annual deposition flux of Hg to wetlands (a) and forests (b) in 2021.*

Mean Hg deposition fluxes to different types of ecosystems in 2021 are shown in Fig. 2.41. Relatively high fluxes were noted for forests (10 – 17 g/km^2/y) and urban areas (15 g/km^2/y). For comparison, mean deposition flux to low-vegetation ecosystems varied from 7 to 10 g/km^2/y, and the lowest mean deposition took place in bare lands (around 5 g/km^2/y). Country-mean deposition to urban areas were characterized by the largest ranged between minimum and maximum values.

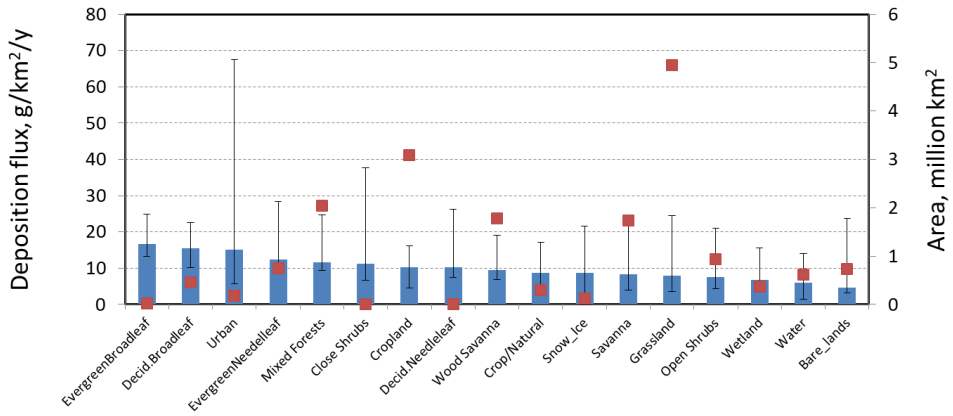

Fig. 2.41*. Deposition flux of Hg to various ecosystem types within the EMEP domain in 2021. Bars show average value for all EMEP countries; whiskers show range of deposition flux variation (minimum and maximum values) among the EMEP countries. Red squares show areas occupied by land-cover types within the EMEP domain.*

The most recent estimates of critical load exceedances of heavy metal deposition are related to 2010 [*de Wit et al.*, 2015]. In order to evaluate up-to-date effect of heavy metal deposition on human health and biota new estimates of the exceedances are needed.

2.5.2. Exceedances of air quality guidelines for PAHs

Modelling results and measurements of PAH pollution levels in 2021 within the EMEP domain were used to evaluate population exposure to high levels of concentrations exceeding air quality guidelines. Several threshold values were established in European Union for B(a)P as an indicator compound (European Directive 2004/107/EC). The threshold values include target value of B(a)P air concentration equal to 1 ng/m^3 as well as the upper and lower assessment thresholds (UAT and LAT) equal to 0.6 and 0.4 ng/m^3 respectively. Along with this, the reference level of 0.12 ng/m^3 for B(a)P has been defined by World Health Organization (WHO) as a level of air concentrations corresponding to the excess lifetime cancer risk level of 10^{-5} [*WHO*, 2017].

Modelled annual mean B(a)P air concentrations for 2021 are shown in Fig. 2.42a. Based on these data amount of population in the areas, where levels of concentrations exceeded air quality guidelines, was estimated (Fig. 2.42b). Data on gridded distribution of urban and rural areas have been adapted from the outcome of the project GRUMP1 [*SEDAC*, 2011].

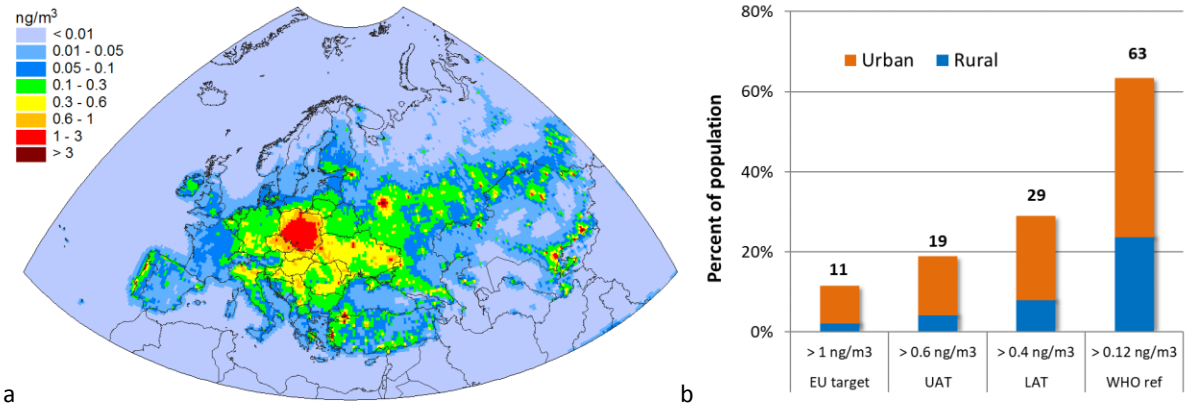

Fig. 2.42. *Spatial distribution of annual mean B(a)P air concentrations for 2021 (a) and percentage of urban and rural population of the EMEP countries in the areas with annual mean B(a)P air concentrations in 2021 exceeding the EU limit values and WHO reference level (b).*

Model estimates show that about 11% of the population of EMEP countries in 2021 were in areas with exceeded EU target level for annual mean B(a)P air concentrations. The upper assessment thresholds (UAT) and lower assessment thresholds (LAT) values were exceeded in the areas with about 19% and 29% of population, respectively. The WHO Reference level was exceeded for 63% of population of EMEP countries.

To evaluate population exposure to mixture of 4 PAHs the approach based on toxic equivalency factors was used [*Liu et al.*, 2019]. Information on toxic properties is available for some of the PAH compounds that allows to define specific toxic equivalence factors (TEF) for them to characterize their potent toxicity relative to that of B(a)P [*ALS*, 2013]. The TEFs can be applied to characterize the carcinogenic potency of each considered PAH and calculate B(a)P equivalent concentration of PAH mixture. Distribution of equivalent B(a)P concentration of the 4 PAHs (namely, B(a)P, B(b)F, B(k)F, I(cd)P in the EMEP domain calculated for 2021 is shown in Fig. 2.43a. B(a)P equivalent concentrations

are calculated as the sum of concentrations of individual PAHs multiplied by corresponding values of TEFs. It is seen that the model estimates of B(a)P equivalent concentrations show higher percentage of population in the areas of exceeded EU target value and WHO reference level, namely, 15% and 71%, respectively.

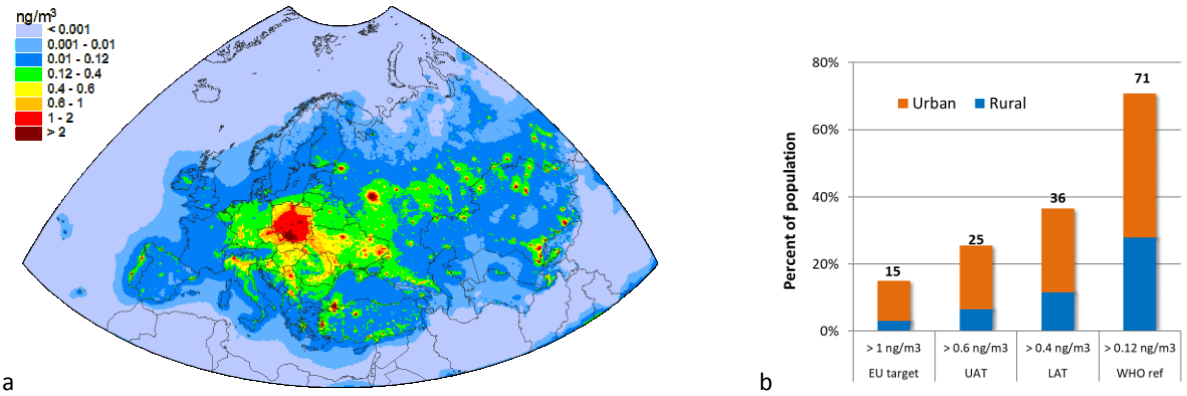

***Fig. 2.43**. Calculated B(a)P equivalent concentrations of the sum of 4 PAHs in the EMEP region for 2021 (a) and percentage of urban and rural population of the EMEP countries in the areas with equivalent B(a)P air concentrations exceeding the EU limit values and WHO reference level in 2021 (b).*

The information on exceedances of the EU and WHO air quality guidelines for B(a)P as well as data on B(a)P equivalent air concentrations of PAHs can be used to support activities of the Task Force on Health and Working Group on Effects with regard to the analysis of population exposure to toxic substances and their impacts on human health.

2.6. Atmospheric loads to the marginal seas

Pollution of marine ecosystems by hazardous contaminants is one of environmental problems acknowledged at national and international level. In particular, international agreements, such as HELCOM, OSPAR, Barcelona Convention, Bucharest Convention, and Tehran Convention, were developed to protect the environment of the Baltic, North, Mediterranean, Black and Caspian Seas, respectively. Besides, protection of waters around Europe is the aim of Marine Strategy Framework Directive.

Information on atmospheric deposition of heavy metals and POPs to marginal seas (the Baltic, North, Mediterranean, Black and Caspian Seas) is calculated regularly on annual basis. In this report information on spatially mean deposition fluxes is exemplified by Pb, Hg, HCB and PCDD/Fs. More detailed information on these and other metals and POPs is available on request. In addition to this, the results on assessment of atmospheric pollution of the Baltic Sea and the North Sea obtained in cooperation with HELCOM and OSPAR commissions, are presented in Sections 4.2.2 and 4.2.3, respectively.

The highest spatially mean Pb deposition fluxes in 2021 were noted for the Mediterranean Sea, followed by the North Sea and the Black Sea (Fig. 2.44a). The lowest deposition flux was calculated for the Caspian Sea. Due to long-term reduction of Pb anthropogenic emissions the contribution of the EMEP anthropogenic emission sources has significantly declined for the recent decades. Therefore, relative contribution of other emission types such as secondary (re-suspension) sources became comparable with the contribution from the anthropogenic sources or even exceeded them. Besides, substantial contribution (about 30%) of the non-EMEP sources is noted for Mediterranean and Caspian Seas. Atmospheric deposition to these seas is strongly impacted by emission sources located in non-EMEP countries of Africa and Asia.

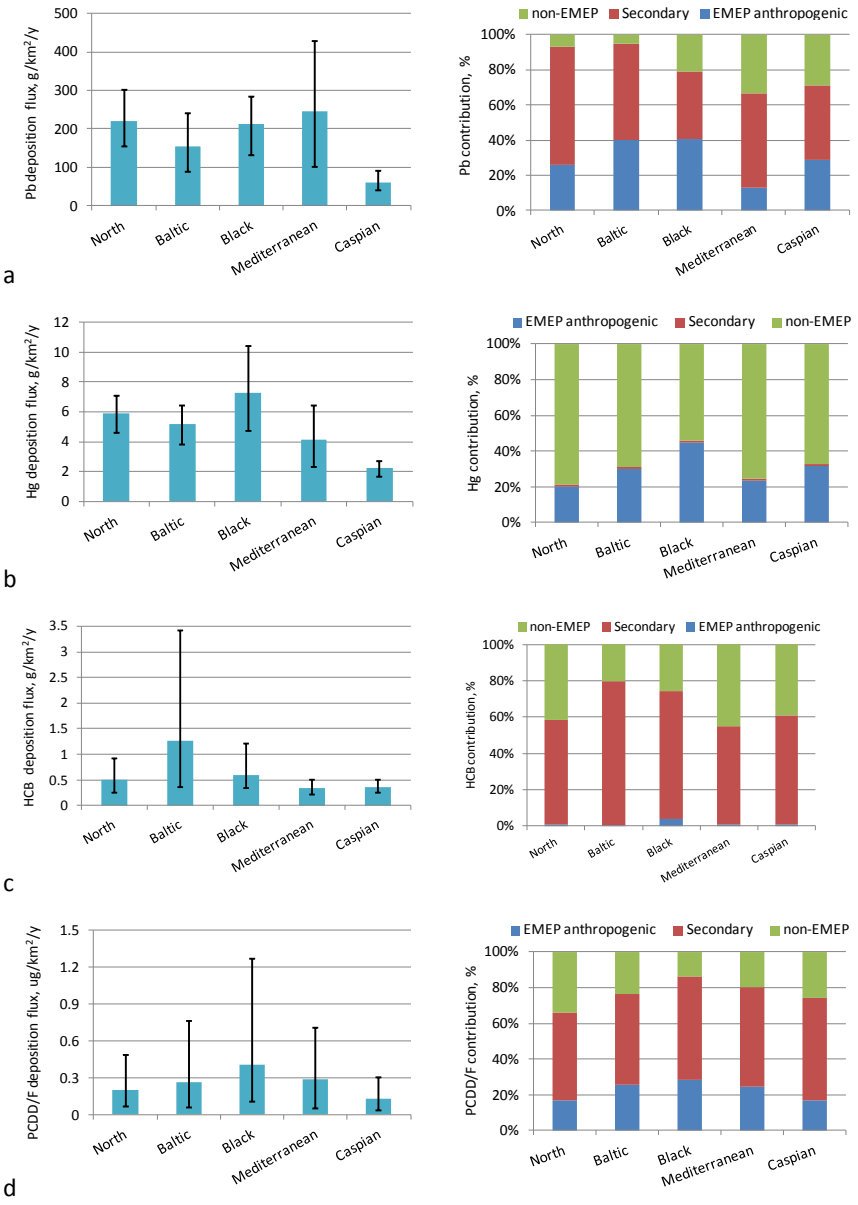

Fig. 2.44. Mean deposition fluxes (left) and relative contribution of various source types to deposition (right) of Pb(a), Hg(b), HCB(c) and PCDD/Fs(d) to the marginal seas of the EMEP region in 2021. The whiskers indicate the range between 10th and 90th percentiles of gridded deposition fluxes.

The highest Hg deposition flux is noted for the Black Sea, and the lowest – to the Caspian Sea (Fig. 2.44b). Unlike aerosol-bound heavy metals, Hg in the atmosphere is presented mostly by the gaseous elemental form capable of transporting over global distances. Hence, the major contributor to Hg deposition to the marginal seas is non-EMEP sources. Its contribution varied from about 50% (the Black Sea) to almost 80% (the North Sea) . Other important contributor is the EMEP anthropogenic emission sources, while re-emission of Hg from the EMEP countries contributes around 1%.

The Baltic Sea is characterized by the highest HCB mean deposition flux (about 1.3 g/km^2/y). The fluxes to other seas are much lower varying from 0.3 to 0.6 g/km^2/y (Fig. 2.44c). Unlike other considered pollutants, contribution of the EMEP anthropogenic sources is only few per cent. Due to strong restrictions on usage of HCB, anthropogenic emissions in the EMEP region significantly declined, and the main source of HCB is re-emission from soils, where it was accumulated over the previous decades. Deposition of HCB re-emitted from the territories of the EMEP countries ranges from 50 to 80%, and atmospheric transport from non-EMEP sources adds up 20-40% to total deposition.

The highest deposition flux of PCDD/Fs takes place in the Black Sea, and the lowest – in the Caspian Sea (Fig. 2.44d). The main source of atmospheric deposition to the marginal seas is re-emission. Its contribution ranges from 50% (the North Sea) to almost 60% (the Caspian Sea). The largest anthropogenic fraction of deposition is noted for the Black Sea (28%) followed by the Baltic and the Mediterranean Seas. The remaining part of deposition is caused by atmospheric transport from non-EMEP emission sources.

Figures 2.44a-d characterize mean deposition flux to the area of marginal seas. However, in different parts of the seas the fluxes may differ markedly from the mean value. Spatial distribution of Cd deposition flux to the North Sea in 2021 is exemplified in Fig. 2.45a. The highest fluxes (12 – 15 g/km^2/y) are noted for the south-eastern coast of the sea. This part of the sea is impacted by emission sources of Germany, Belgium, the Netherlands and Denmark. Besides, similar deposition fluxes occur near the southern and western coasts of Norway. The reason for this is high annual precipitation sums in this part of the sea. The lowest levels took place in the north-western part of the North Sea due to relatively precipitation sums and low emissions in the northern part of the United Kingdom.

Distinct gradient of deposition fluxes is noted for B(a)P (Fig. 2.45b). Deposition of B(a)P depends on precipitation to much less extent compared to Cd. Hence, spatial gradients of B(a)P deposition fluxes mainly reflect atmospheric transport patterns and distance from main emission sources. The highest deposition fluxes (1.5 – 3 g/km^2/y) took place along the southern coast of the North Sea, and the lowest fluxes occur in its northern part (0.1 – 0.2 g/km^2/y).

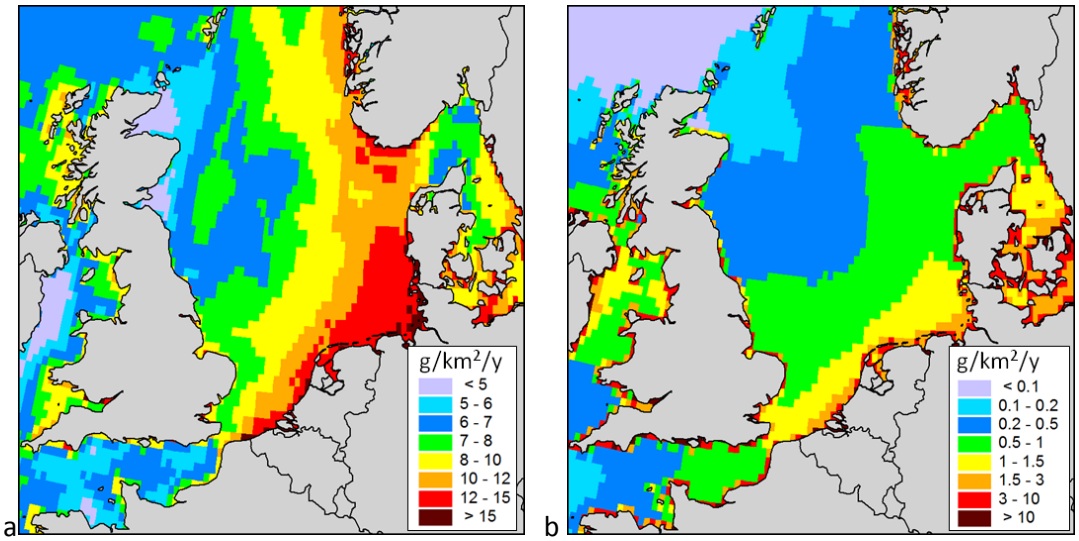

Fig. 2.45. *Deposition flux of Cd (a) and B(a)P(b) to the North Sea in 2021.*

2.7. Pollution of the Arctic

This section is focused on information on pollution of the Arctic by heavy metals (Pb, Cd, Hg) and POPs (PAHs, PCDD/Fs, HCB, PCBs) in 2021. In particular, spatial distribution of deposition fields based on global-scale simulations is described. In order to account for quick re-emission of Hg from snow surface during Atmospheric Mercury Depletion Events (AMDEs) [*Dastoor et al.*, 2022] net flux is considered instead of deposition. Besides, source apportionment of heavy metal and POP deposition is presented for the EMEP sector of the Arctic region. The borders of the Arctic area are defined according to the AMAP formulation.

The Arctic region is remote from the main atmospheric emission sources of heavy metals and POPs. Therefore, pollution levels in the Arctic are generally lower than those in other parts of the EMEP region. Besides, annual precipitation sums in the Arctic are lower than that in the temperate zone, which also favours decreasing of atmospheric deposition. The highest (50-100 g/km^2/y) deposition flux of Pb in the Arctic land areas in 2021 is found in Kola Peninsula, the eastern coast of Russia and the south-western part of Alaska (Fig. 2.46a). Higher levels (up to 300 g/km^2/y) are noted over the sea areas, such as Bering Sea and the eastern part of the Labrador Sea. The lowest levels of Pb deposition (below 10 g/km^2/y) took place over central parts of Russian Siberia, Canada and the Arctic Ocean. Deposition fluxes of Cd are characterized by similar spatial distribution. Besides, some spots of relatively high Cd fluxes are noted in the eastern part of the Russian Arctic (Fig. 2.46b). The most significant Hg net deposition flux (up to 20 g/km^2/y) is noted for the northern part of Atlantic (the Barents and Norwegian Seas) and over the Bering Sea in the northern part of the Pacific (Fig. 2.46c). These high deposition fluxes are explained by the effect of ADMEs. For the comparison, over the most of other Arctic area the net Hg flux ranges from 1 to 4 g/km^2/y.

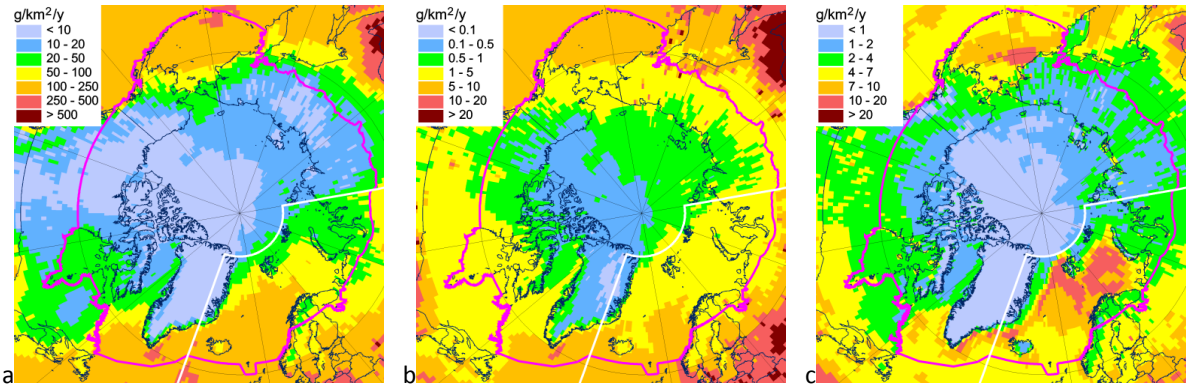

Fig. 2.46. *Total deposition fluxes of Pb (a) and Cd (b) and net deposition flux of Hg (c) to the Arctic in 2021. Purple line denotes the border of the Arctic region adopted by AMAP, and white line denotes a border of the EMEP domain.*

Similar to heavy metals, deposition of POPs in the Arctic are substantially lower than that in the temperate latitudes. Over major part of the Arctic deposition flux of B(a)P is below 0.5 g/km^2/y (Fig. 2.47a). Higher deposition (15 – 50 g/km^2/y or even more) took place in Canada and in the eastern part of Russia, which can be explained by the presence of significant emission sources in these regions. Most significant deposition fluxes of PCDD/Fs were obtained for Iceland (0.5 – 3 ng TEQ/m^2/y), as well as for northern part of Scandinavian Peninsula and Kola Peninsula (0.3 – 0.5 ng TEQ/m^2/y) (Fig. 2.47b). Similar distribution takes place for PCB-153 deposition (Fig. 2.47c).

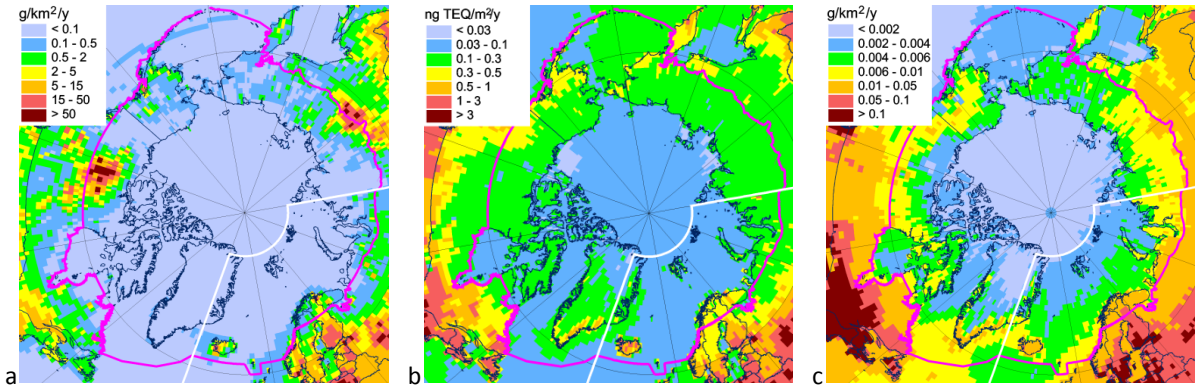

Fig. 2.47. *Total deposition fluxes of B(a)P (a), PCDD/Fs (b) and PCB-153 (c) to the Arctic in 2021. Purple line denotes the border of the Arctic region adopted by AMAP, and white line denotes a border of the EMEP domain.*

Similar to the analysis of pollution levels in the EMEP countries, contributions of three groups of emission sources to deposition to the land areas of the Arctic within EMEP domain were considered. These groups include anthropogenic emissions from the EMEP countries, secondary emissions and non-EMEP sources. The main contributor (around 55%) to Pb deposition to the Arctic is secondary emission sources (Fig. 2.48). It is explained by the significant re-suspension of sea spray aerosol containing dissolved trace metals, in particular, Pb. Due to the same reason contribution of re-suspension to Cd deposition is also considerable (about 30%). About 50% of Cd deposition is caused by the EMEP anthropogenic sources. Mercury is a global-scale pollutant. Hence, most of Hg

deposition to the Arctic is caused by non-EMEP sources. However, it should be noted that this contribution includes also some fraction of Hg emitted by the EMEP sources which left the EMEP domain and then returned as non-EMEP Hg. Major input (around 75%) of B(a)P to the Arctic is caused by the EMEP anthropogenic sources, and around 25% are explained by re-emission. Contribution of non-EMEP sources to B(a)P deposition in the Arctic is negligible. Re-emission is the main contributor to deposition of PCDD/Fs, HCB and PCB-153. In case of PCDD/Fs, the contributions of re-emission and non-EMEP sources are comparable while the EMEP anthropogenic sources provide 7% to the deposition. Since HCB emissions in the EMEP domain ceased almost completely, the main sources to deposition in the Arctic are re-emission from the EMEP region (around 70%) and non-EMEP sources (about 30%). Contributions of re-emission and anthropogenic sources of PCB-153 are comparable (46% and 42%, respectively), and the remaining part is non-EMEP sources.

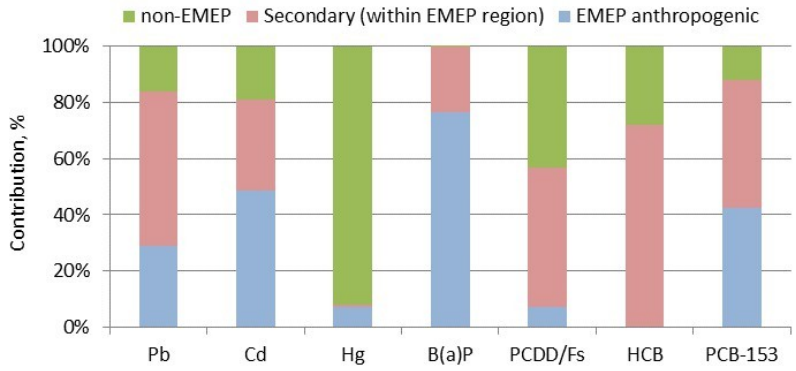

Fig. 2.48. *Relative contributions of the EMEP anthropogenic, secondary and non-EMEP sources to deposition in the Arctic (within the EMEP domain) in 2021.*

Contribution of particular countries to anthropogenic deposition to the land areas of the Arctic was estimated. This contribution depends on a number of factors such as magnitude of emissions, distance of the main sources from the Arctic, prevailing patterns of atmospheric transport etc. For majority of the considered pollutants Russia is the main contributor of transboundary pollution, mainly because of the location of Russian sources in or close to the Arctic. For example, Pb anthropogenic deposition is explained by sources of Russia by 41% (Fig. 2.49a). The second contributor is Kazakhstan. Although this country is located far from the Arctic region, its national Pb emission makes up about a quarter of the total EMEP emission. Similar situation takes place for PCDD/Fs (Fig. 2.49b). The main contributors to the Arctic pollution levels, except for Russia, are Türkiye, Norway and Poland. In spite of remoteness of Türkiye and Poland from the Arctic, their national emissions are large enough to provide 3-4% contribution to the PCDDFs pollution in the Arctic. In case of B(a)P, the main contributors to the Arctic pollution are Russia and Finland (Fig. 2.49c).

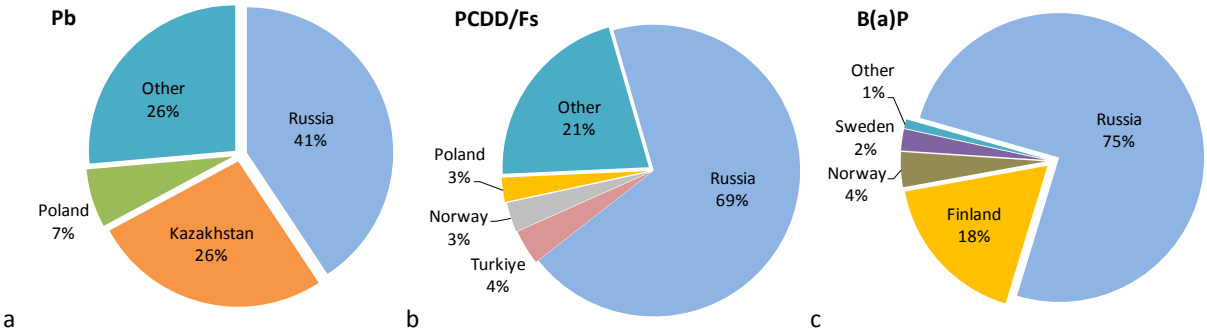

***Fig. 2.49**. Source apportionment of heavy metal and POP anthropogenic deposition to the Arctic (within the EMEP domain) in 2021.*

2.8. Global-scale pollution by heavy metals and POPs

Pollution levels within EMEP countries are caused by emission sources located both within and outside the EMEP domain. Intercontinental transport substantially contributes to concentrations and deposition fluxes of pollutants with long atmospheric residence time, e.g., Hg and some POPs in the EMEP countries (see Section 2.4). Countries in the southern and eastern parts of the EMEP region are influenced by non-EMEP sources of pollutants with shorter lifetime, such as Pb, Cd and PAHs. In order to account for the effect of emission sources located outside the EMEP countries global-scale modelling is performed. Global-scale model simulations were used to produce boundary concentrations of heavy metals and POPs. Besides, global-scale modelling results were used to characterize pollution levels outside the EMEP countries (e.g., most part of Arctic, North Atlantic, or other continents).

The highest air concentrations of Pb in 2021 took place in the south-eastern (China) and southern (India) parts of Asia. Annual mean concentrations in these regions exceed 15 ng/m^3 (Fig. 2.50a). Concentrations of 2-4 ng/m^3 were noted for the northern part of Africa and the western part of Asia, in the central part of Europe and in countries of Central Asia. These levels are explained by contribution of both anthropogenic emissions and wind re-suspension. In North America, most part of South America and vast areas of Asia the concentrations are relatively low (0.2 – 2 ng/m^3).

In case of Cd, China was one of the regions with relatively high concentrations in air ranging from 0.5 to 2 ng/m^3 or even exceeding 2 ng/m^3 in some regions (Fig. 2.50b). These levels were mainly caused by significant emissions of Cd. However, similar levels of air concentrations were also noted for the western part of South America (Chile, Peru, Ecuador, Columbia) and several regions in Africa (Ghana, Burkina Faso, South Africa). These elevated levels are caused by uncertainties of Cd emission data in these regions (see Section 2.4.3). In Europe, the southern and central parts of Asia the concentrations mainly ranged from 0.05 to 0.2 ng/m^3. Main Cd emission sources of North America are located in Mexico and the eastern part of the USA, which led to relatively high concentrations in these regions.

Compared to Cd and Pb, concentrations of Hg^0 in 2021 were distributed more uniformly over the globe. Over most part of the Northern Hemisphere the concentrations of Hg ranged from 1.2 to 1.8

ng/m^3 (Fig. 2.50c). In the Southern Hemisphere the concentrations were lower (about 1 ng/m^3). The contrast between the hemispheres is explained by stronger anthropogenic emission sources in the Northern Hemisphere and limited air mixing between the hemispheres. Industrial activity resulted to increased concentrations of Hg in China up to 3 ng/m^3 or even higher. Relatively high Hg levels were also noted for a number of regions of South America and South-Eastern Asia because of artisanal and small-scale gold mining activities responsible for significant emissions of Hg. Elevated Hg levels along the western coast of North America are caused by the emissions from soils naturally enriched with Hg.

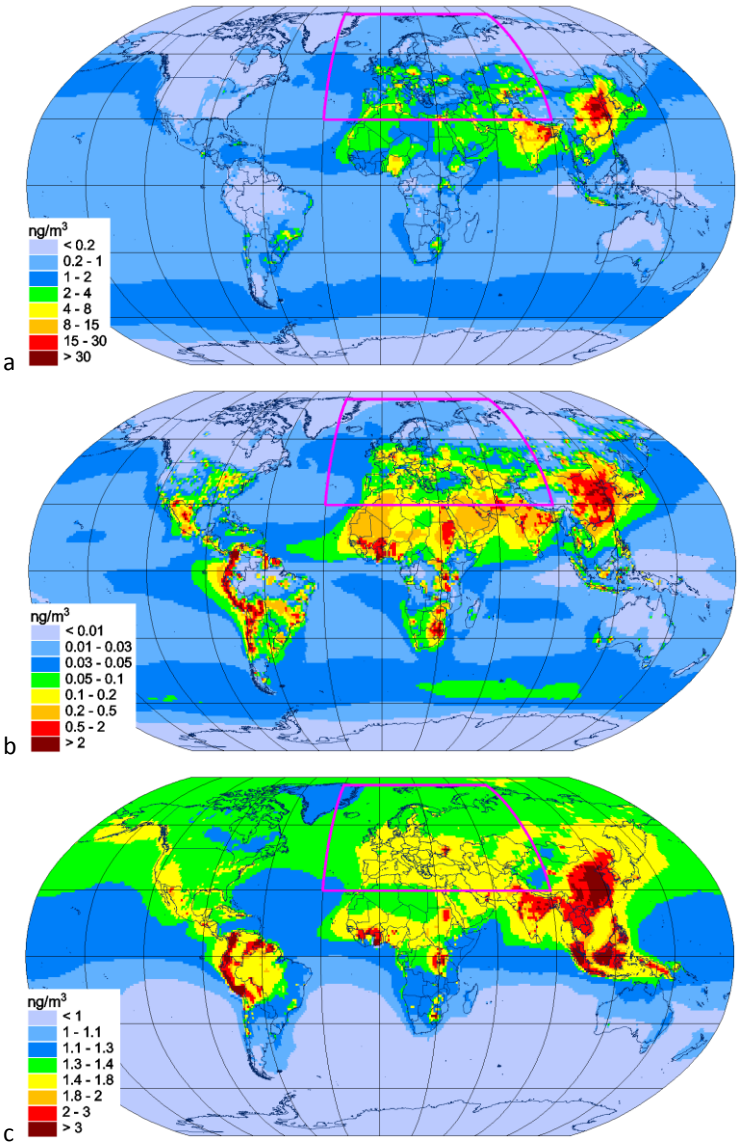

Fig. 2.50. *Global distributions of annual mean air concentration of Pb (a), Cd (b) and Hg^0 (c) in 2021. Red line depicts boundary of the EMEP region.*

Air concentrations of B(a)P demonstrated the highest spatial variability compared to other considered pollutants. In regions with high emissions, such as Central and Western Europe, Southern and South-Eastern Asia, Central Africa the concentrations varied from 0.1 to 2 ng/m^3 (Fig. 2.51a). In some countries, e.g., China, India, Bangladesh, the concentrations even exceeded 2 ng/m^3. In North and South America the concentrations mostly ranged from 0.002 to 0.1 ng/m^3. Since main emission

sources of B(a)P are land-based, the concentrations over oceans were much lower (0.0002 – 0.02 ng/m^3). However, relatively higher concentrations took place in areas of intensive marine traffic and along sea coasts.

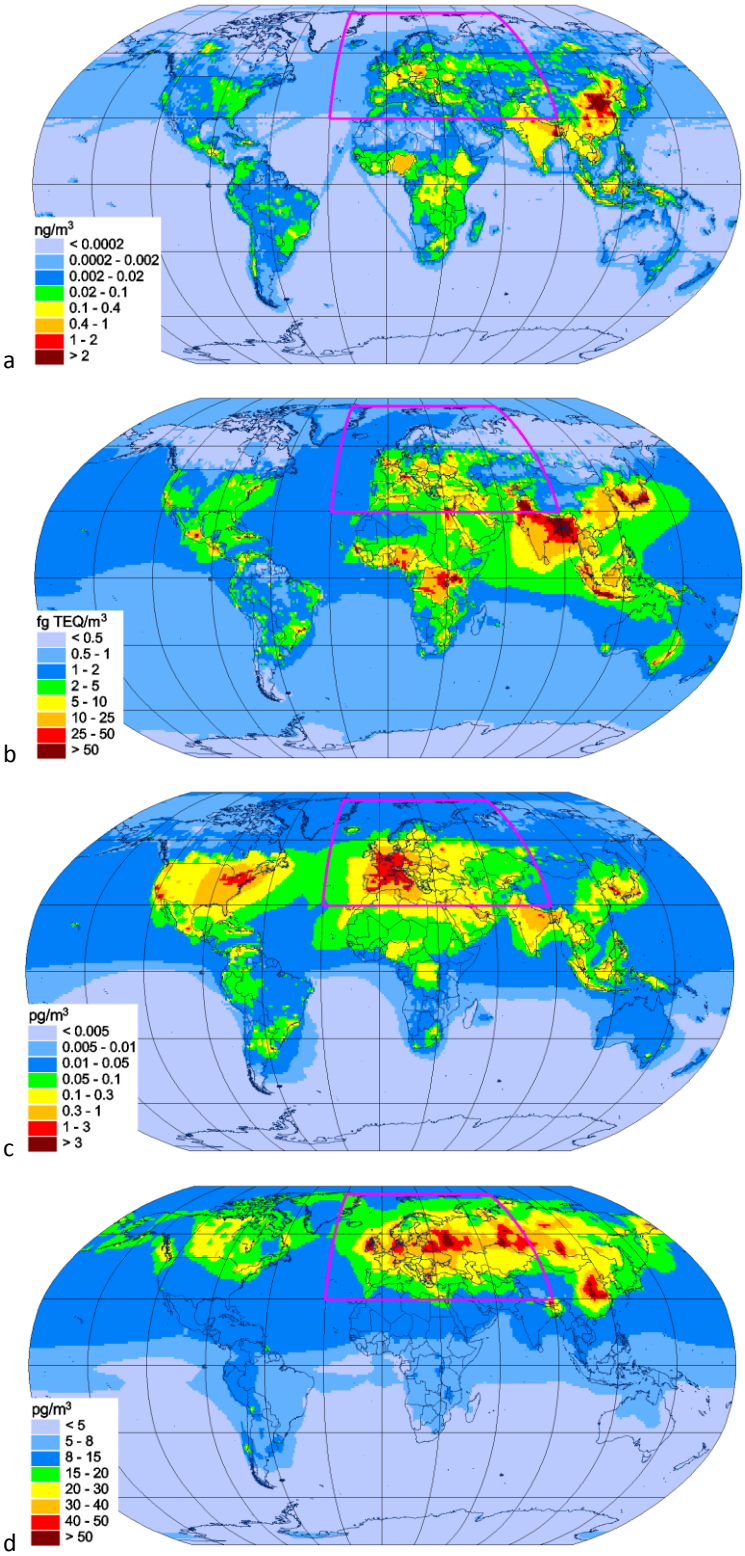

Fig. 2.51. *Global distribution of annual mean air concentration of B(a)P (a), PCDD/Fs (b), PCB-153(c), and HCB (d) in 2021.Red line depicts boundary of the EMEP region.*

Annual mean concentrations of PCDD/Fs in air varied from 1 to 25 fg TEQ/m^3 over most part of the globe (Fig. 2.51b). Higher levels were noted for the regions with significant anthropogenic emissions such as Bangladesh, the eastern and northern parts of India, Japan, the southern islands of Indonesia, Korean Peninsula and the central part of Africa. Relatively low levels (below 0.5 fg TEQ/m^3) occurred over Canada, Alaska, Russian Siberia and large part of the Scandinavian Peninsula. These low concentrations could be explained by several factors. First of all, emissions in these regions are lower compared to other parts of the globe. Besides, net deposition flux from air to soil and vegetation is much stronger than that to sea surface. The final possible reason is peculiarities of atmospheric circulation. In winter predominant anticyclonic systems over Canada and Siberia prevent transport of PCDD/Fs from regions with high emissions. The contrast between PCDD/Fs concentrations over Canada, Siberia and regions with significant emissions in winter is substantially higher than that in summer.

Annual mean concentrations of PCB-153 ranged from 0.05 to 1 pg/m^3 over most of land areas of the Northern Hemisphere (Fig. 2.51c). The most significant concentrations (>1 pg/m^3) took place in Europe, the eastern part of the USA and in Eastern Asia (South Korea, Japan). These regions are characterized by the most significant anthropogenic emissions. Vast areas of elevated concentrations over the North Atlantic indicated potential of PCB-153 to long-range atmospheric transport. Concentrations over oceans in Southern Hemisphere were much lower than those in Northern Hemisphere. The reason of this gradient is higher emissions in Northern Hemisphere and limited exchange of air masses between the hemispheres.

Unlike other considered pollutants, current atmospheric releases of HCB are almost entirely represented by re-emission of legacy HCB rather than anthropogenic emissions. Therefore, spatial distribution of annual mean air concentrations of HCB in 2021 poorly correlated with the distribution of current anthropogenic emissions (Fig. 2.51d). Besides, the concentrations were strongly affected by the processes of exchange between air and surface compartments. The highest air concentrations of HCB (30-50 pg/m^3) took place in Europe, the eastern part of Russia and China. In other parts of the Eurasian continent and North America the concentrations mostly ranged from 8 to 30 pg/m^3. Similar to Hg and PCB-153, there was distinct gradient of air concentrations between Northern and Southern Hemispheres.

Concentrations of heavy metals and POPs strongly depend on quality of emission data. Currently no official global-scale emission data are available, and the model calculations are based on emission expert estimates. In order to improve global scale model estimates of heavy metal and POP pollution cooperation with international organizations (UN Environment, Stockholm Convention, Minamata Convention, etc.) is needed to develop up-to-date global emission inventories.

Chapter 3. RESEARCH ACTIVITIES

3.1. Eurodelta-Carb intercomparison of B(a)P models

The Eurodelta-Carb intercomparison of B(a)P models was initiated by the TFMM in 2021 in the framework of a broader scientific study on modelling of secondary organic aerosol and black carbon. The main objectives of the Eurodelta-Carb study on B(a)P were to analyze performance of air quality models and uncertainties of their results. Besides, the study was aimed to contribute to the refinement of B(a)P emissions from the combustion of fossil fuel and biomass burning and to further improve available B(a)P modelling approaches. Four regional chemistry transport models were applied to simulate the concentrations of B(a)P in Europe. The modelling results were compared with the observed B(a)P concentrations provided by the EMEP monitoring network. Evaluation of the modelled concentrations was performed in close cooperation with national experts in B(a)P modelling.

Model simulations setup and input data

The Eurodelta-Carb B(a)P modelling exercise is focused on the time period from the beginning of December 2017 to the end of 2018. Simulations of B(a)P were performed using four chemistry transport models: CHIMERE, GLEMOS, MINNI and SILAM. These models are being developed by the modelling teams of INERIS (France), CIEMAT (Spain), MSC-E (EMEP), ENEA (Italy), and FMI (Finland) to study air pollution levels on regional and national scales. All the models use prescribed modelling domain and gridded B(a)P annual emissions data for 2018, generated by CEIP. Other input data and parameterizations, such as meteorological input, intra-annual variations of B(a)P emissions, emissions of other pollutants, boundary conditions, model parameterizations, are specific to each model.

The participating models have different approaches to B(a)P modelling. In particular, CHIMERE, GLEMOS, and MINNI consider B(a)P as a reactive semi-volatile substance that undergoes gas-particle partitioning and degradation in the atmosphere due to chemical reactions with OH in the gaseous form. Also, GLEMOS and MINNI include the chemical reaction of B(a)P with ozone in particulate form. All three models consider deposition of gaseous and particulate B(a)P from the atmosphere. In the case of SILAM, the model simulations were carried out assuming that B(a)P is an inert substance emitted to the atmosphere in the gaseous phase and subject only to degradation process depending on the temperature variation.

The program of model simulations includes a model run for the specified time period with the prescribed B(a)P emission data using independently defined model setups. Preliminary results were published in the previous EMEP status report [*Ilyin et al.*, 2022] and were presented at the HARMO21 conference [*Gusev et al.*, 2022].

In 2023 the B(a)P model intercomparison study was continued. In particular, modelling results of CHIMERE and SILAM were updated. In addition, an analysis of factors affecting differences between

the models output on B(a)P was discussed and initiated (e.g. emission temporal profiles, parametrizations of B(a)P degradation in particulate phase, dry and wet deposition, gas-particle partitioning). In this section updated modelling results and their analysis is described.

Modelling results and analysis

Spatial distributions of annual mean total B(a)P air concentrations, simulated by CHIMERE, GLEMOS MINNI and SILAM for 2018, are shown in Figure 3.1. The largest concentrations were estimated by all the models for the countries in Central Europe as well as for Northern Italy and some areas in Eastern Europe. The lowest concentrations were predicted for the countries of Northern Europe and remote areas. In general, relatively higher concentrations were simulated by CHIMERE followed by GLEMOS, MINNI, and SILAM. The differences between the simulated B(a)P concentrations may be attributed to the effect of different model parameterizations applied (e.g. for gas-particle partitioning, degradation, and deposition processes) as well as the different meteorological inputs. Additional contributions could also have been made by different emission temporal profiles and concentrations of reactants used in the models to estimate B(a)P chemical transformations.

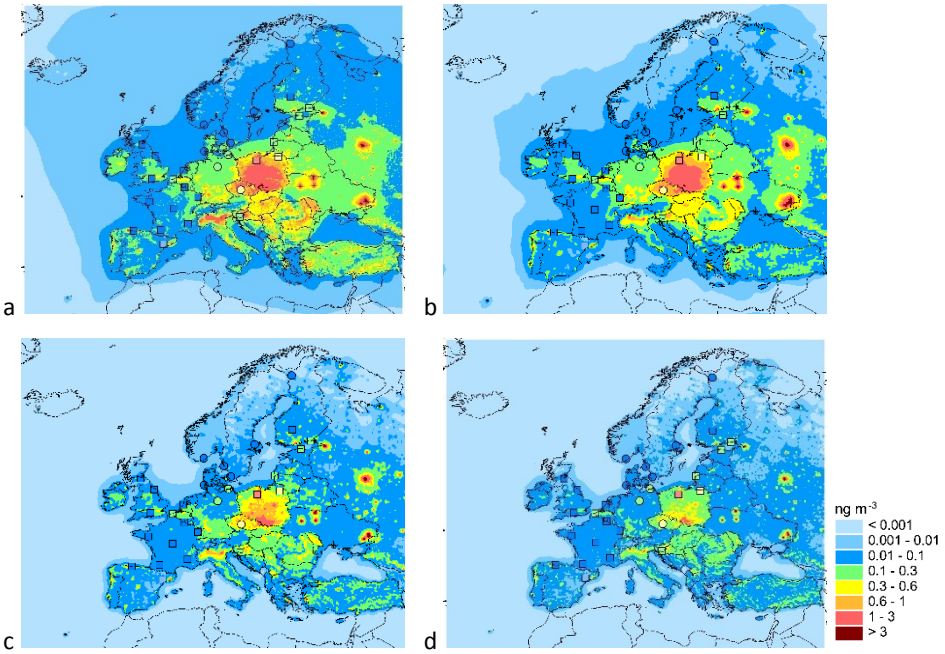

Fig. 3.1. *Maps of annual mean modelled total (gaseous + particulate phase) B(a)P atmospheric concentrations in 2018 simulated by CHIMERE (a), GLEMOS (b), and MINNI (c) and SILAM (d) for the base case model run. For the comparison, observed total and particulate phase B(a)P concentrations, reported by the EMEP monitoring stations, are shown as colored circles and squares, respectively, on the same scale as the modelled values.*

Evaluation of the model output against measurements for the 2018 was carried out using the data of 29 EMEP monitoring stations. Of these, 9 stations located in Central and Northern Europe measured total B(a)P concentrations, whilst B(a)P concentrations in particulate phase were measured at 20 stations covering a wider geographical area (Fig. 3.1).

For the model-measurement comparison, the daily mean modelled total or particulate phase concentrations, depending on the type of measurement, were extracted from the model output files for the station locations. Modelled values were then averaged to the temporal resolution and periods of the observations (e.g. daily or weekly). A summary of the statistical analysis of the modelled and observed annual mean B(a)P concentrations is presented in Table 3.1. All the models reproduced the spatial pattern of observed total and particulate B(a)P concentrations well with correlation coefficients (R) of 0.72-0.96. CHIMERE and GLEMOS tended to slightly overestimate observed total B(a)P levels with a mean bias of about 4%, whereas MINNI underestimated the measured values with a mean bias of -53%. For the particulate B(a)P concentrations, CHIMERE overestimated concentrations with a mean bias about 0.3%, while GLEMOS and MINNI underestimate the observed concentrations with mean biases of -19% and -52%, respectively. Estimated total B(a)P concentrations were within a factor of 2 of the measured values for 89%, 78%, 11%, and 0% of monitoring stations for CHIMERE, GLEMOS, MINNI, and SILAM respectively, whereas for B(a)P in particulate phase they were within a factor of 2 for 80%, 70%, 40%, and 20% of monitoring stations. The fraction of model values that were within a factor of 3 from measurements is larger. In particular, for 100%, 100%, 22%, and 11% of stations, measured total B(a)P concentrations and for 90%, 85%, 70%, and 35% of stations, measured particulate B(a)P concentrations, respectively.

Table 3.1. *Summary of statistical metrics, calculated on the basis of annual mean total and particulate phase B(a)P air concentrations for 2018, observed at EMEP monitoring stations and estimated by CHIMERE, GLEMOS and MINNI in the base case model run.*

Models	Mean ($ng\ m^{-3}$)	NMB[a] (%)	R[a]	RMSE[a] ($ng\ m^{-3}$)	F2[a] (%)	F3[a] (%)
Total B(a)P concentrations (9 stations), mean observed 0.116 ng m^{-3}						
CHIMERE	0.120	3.8	0.93	0.057	89	100
GLEMOS	0.121	4.3	0.91	0.087	78	100
MINNI	0.054	-53.3	0.86	0.090	11	22
SILAM	0.026	-77.5	0.86	0.124	0	11
Particulate B(a)P concentrations (20 stations), mean observed 0.156 ng m^{-3}						
CHIMERE	0.157	0.3	0.88	0.116	80	90
GLEMOS	0.126	-19.3	0.96	0.095	70	85
MINNI	0.075	-52.1	0.93	0.168	40	70
SILAM	0.047	-69.9	0.72	0.226	20	35

[a] *NMB is normalized mean bias; R is the spatial correlation between modelled and observed concentrations; RMSE is the root mean square error; F2 and F3 represent fractions of sites for which the modelled value is within a factor of 2 and 3, respectively, of the observed value.*

The evaluation of annual mean modelled B(a)P concentrations against the measurements of total and particulate B(a)P concentrations from individual EMEP monitoring stations is shown in the scatter plots in Fig. 3.2. An overestimation of observed particulate B(a)P concentrations was found for two Spanish stations ES8 and ES14 for all the models. For other stations, different kinds of discrepancies were obtained. In particular, for CHIMERE, an overestimation about a factor of 2 was found for the stations GB48, GB1055, and NL91 that measured particulate B(a)P. In the case of GLEMOS, the largest underestimation (more than a factor of 3) was found for total B(a)P observed at

DE9 and FI36, and for particulate B(a)P at FR23 and FR25. In case of MINNI, the greatest deviations (underestimation by more than a factor of 5) were found for the stations DE1, DE9, and FI36 that measured total B(a)P, and for LV10 and FR23 that measured particulate B(a)P. In case of SILAM, for most of the stations measured B(a)P concentrations were underestimated by the model.

The scatter plots indicate that CHIMERE modelling results have the highest regression slope value (0.81) followed by GLEMOS (0.77), MINNI (0.44), and SILAM (0.28). The scattering of modelled-observed pairs is best for GLEMOS (coefficient of determination 0.88) compared with MINNI, CHIMERE, and SILAM (0.83, 0.80, and 0.67, respectively).

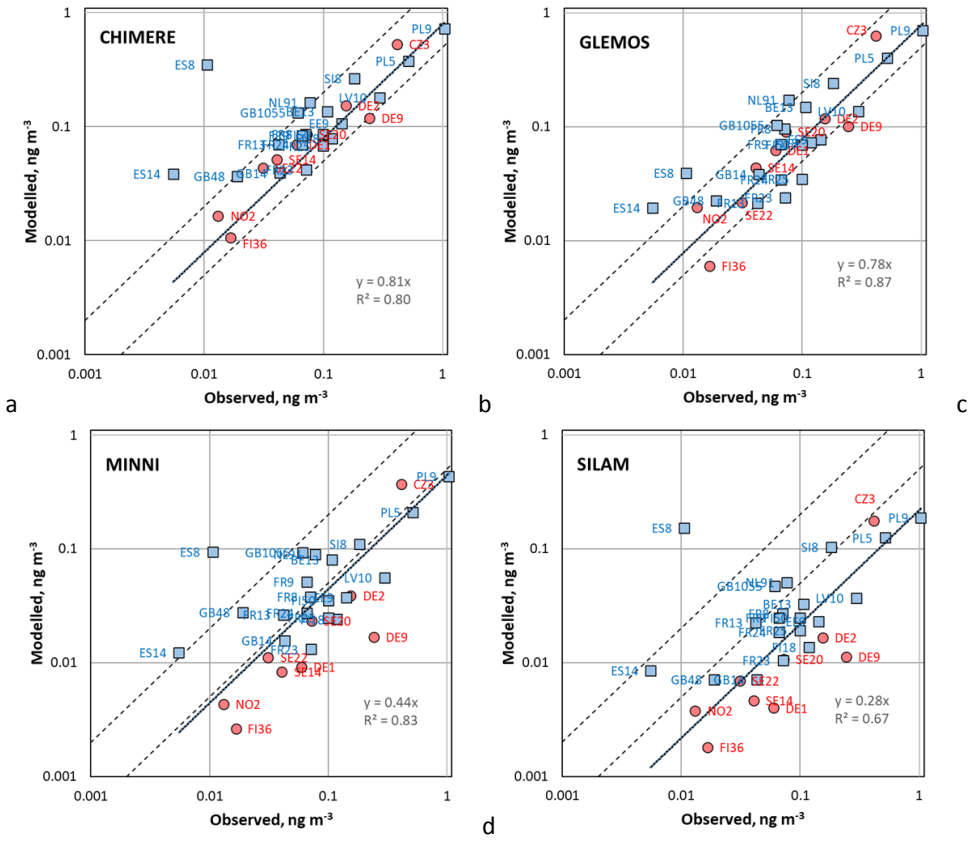

Fig. 3.2. *Scatter plots on a log-log scale of the comparison of modelled B(a)P air concentrations (total and particulate) simulated by CHIMERE (a), GLEMOS (b), MINNI (c) and SILAM (d) with measurements of EMEP monitoring stations in 2018. The region between the dashed lines indicates the model estimates within a factor of two of the measured values and the solid line is the linear regression of all data points. Total B(a)P concentrations are shown as red circles and particulate B(a)P concentrations are shown as blue squares.*

Figure 3.3 shows examples of modelled and observed B(a)P time series for two EMEP monitoring stations, namely, CZ0003R and PL0009R that measured total and particulate B(a)P concentrations, respectively. For these stations, the comparison of modelled and observed concentrations for CHIMERE, GLEMOS, and MINNI shows, in general, a good level of agreement. Model estimates capture high levels of observed concentrations in the cold season, and low concentrations in the warm season, as well as peak concentrations. However, in some of the episodes, especially in winter months, the models underestimate measured concentrations. In case of SILAM, modelled

concentrations show noticeable underestimation of measured B(a)P in cold season compared to other three models. Differences between the modelled and measured intra-annual variations of B(a)P concentrations may be explained both by an underestimation of emissions and by the uncertainties in the temporal disaggregation of B(a)P emissions that were applied in the model simulations.

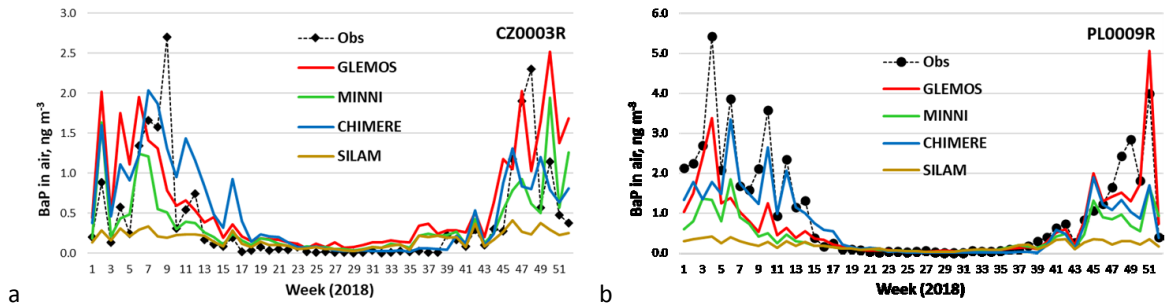

a b

Fig. 3.3. *Intra-annual variations of total B(a)P air concentrations, observed at the EMEP station CZ0003R (a), and particulate B(a)P concentrations, observed at the station PL0009R (b), and the total and particulate B(a)P concentrations simulated by CHIMERE, GLEMOS, MINNI, and SILAM for 2018.*

In Figure 3.4 the the model estimates of B(a)P particulate to total ratio are shown for CHIMERE, GLEMOS, and MINNI. The highest ratio of particulate to total (gaseous + particulate) B(a)P concentration for the locations of 29 EMEP stations is obtained by MINNI (about 0.95) followed by CHIMERE (about 0.88) and GLEMOS (about 0.75) (Fig. 3.4a). In case of B(a)P concentrations in the whole modelling domain (Fig. 3.5b), MINNI similarly provided the highest ratio of B(a)P in particulate phase (about 0.9). At the same time, CHIMERE and GLEMOS showed more comparable results and slightly lower mean ratio of B(a)P in particulate phase of about 0.55. Differences in modelled particulate and total B(a)P concentrations can be explained by different parameterizations of gas-particle partitioning and degradation processes applied in the models.

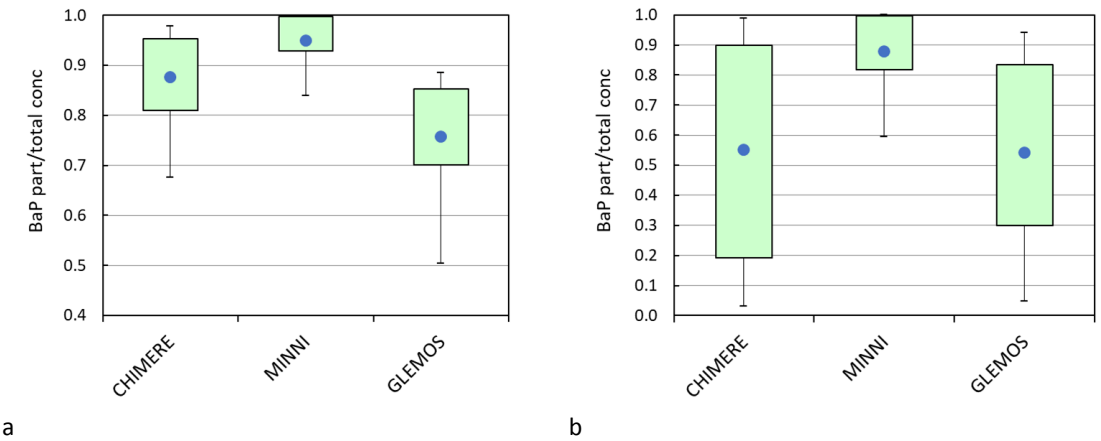

a b

Fig. 3.4. *Average ratio of annual mean particulate to total B(a)P concentrations and its variability estimated by CHIMERE, GLEMOS, and MINNI for 2018 for the locations of 29 EMEP stations (a) and for the whole modelling domain (b). On the diagrams dots represent median ratio, colored boxes – 25% and 75% percentiles, and whiskers - 5% and 95% percentiles.*

Participated models have shown high spatial correlation of predicted and observed B(a)P concentrations. Besides, most of the models provided high correlation with observed intra-annual variation of B(a)P concentrations. Furthermore, the model simulations indicated overprediction of observed B(a)P concentrations in Spain and underprediction in Northern Europe (Finland, Latvia, Estonia), which is likely explained by the uncertainties of the reported B(a)P emissions.

Significant difference between the modelling results of four participated models is noted. Thus, more detailed analysis is required to explore the reasons of the differences and substantial over- and underestimates of observed B(a)P concentrations for some of the stations. Further activities within the study can be focused on the sensitivity analyses, an evaluation of the meteorological drivers and an analysis of other model outputs such as B(a)P concentrations in precipitation and deposition fluxes and concentrations of species affecting B(a)P chemical transformations in the atmosphere.

3.2. New substances/Contaminants of emerging concern

Contaminants of emerging concern (CECs) comprise a wide range of substances having potential to adversely affect wildlife and human health. CECs are characterized by a wide range of physical-chemical properties and different behavior in the environment. Many of CECs are being used in consumer and personal care products and in building materials. CECs include both new POPs, recently started to be regulated and characterized by limited data on their pollution levels, fate and effects, and substances, which are currently unregulated due to the properties falling partly outside existed criteria to be considered as POPs. In spite of limited knowledge, significant attention is paid to the CECs in recent and ongoing research activities including monitoring and assessment of their distribution in the environment and potential risks.

Selected CECs were added to the CLRTAP POP Protocol for regulation of their production and use, in particular, hexachlorobutadiene (HCBD), octabromodiphenyl ether (octa-BDE), pentachlorobenzene (PeCB), pentabromodiphenyl ethers (PBDEs), perfluorooctane sulfonates (PFOS), polychlorinated naphthalenes (PCNs) and short-chain chlorinated paraffins (SCCPs). Besides CECs are included in the annexes of the Stockholm Convention and are listed by AMAP, HELCOM, OSPAR for the analysis of their pollution levels, exposure assessment, and regulatory activities.

Ambient concentrations of CECs (e.g. of hexabromocyclododecane (HBCDD), PCNs, and PeCB are being monitored at EMEP monitoring stations in Northern Europe in accordance with the new EMEP monitoring strategy [ECE/EB.AIR/144/Add.1]. Besides, national monitoring networks carry out measurements of selected CECs in mosses in the framework of ICP-Vegetation Programme activities. Furthermore, preparatory work for evaluation of CEC pollution levels, transport and fate in the environment is performed in accordance with the EMEP work plan for 2022-2023. As a part of this activity, a workshop on CEC monitoring and model assessment is planned to be organized in 2023 in co-operation with TFMM, TF HTAP and CCC.

In the framework of co-operation with HELCOM, MSC-E carries out compilation of information on CECs with the focus on the Baltic Sea area. In this section an overview of information on HBCDD,

PCNs, and PeCB is presented, which includes regulatory activities, their production, usage and emissions, as well as results of monitoring and model assessment of their transport and fate in the environment. More detailed information can be found in the Joint reports of the EMEP Centres for HELCOM [*Gauss et al.*, 2022].

Hexabromocyclododecane (HCBDD)

Hexabromocyclododecane (HBCDD[1]) is one of the most commonly used brominated flame retardants. It has been primarily applied as a fire protection additive to synthetic materials (e.g. expanded (EPS) and extruded (XPS) polystyrene foams), which have been used in the construction of buildings (e.g. as thermal insulation materials), in furniture, vehicle textiles, packaging materials and electrical and electronic equipment. Releases of HBCDD to the atmosphere and other environmental compartments can take place at all stages of the HBCDD products life cycle including production, transportation, usage and disposal [*Schrenk et al.*, 2021].

HBCDD is a persistent, bioaccumulative, toxic compound that has low solubility in water, high affinity to particulate matter and potential to long-range transport in the environment. HBCDD is known to have adverse effects for terrestrial and aquatic organisms, and pose risks to human health. The toxicological effects of HBCDD include reproductive and developmental toxicity. In addition, HBCDD is suspected of causing neurobehavioral effects and endocrine disruption [*WHO*, 2013; *European Commission*, 2014; *Feiteiro et al.*, 2021].

Regulation

Due to physical-chemical properties and adverse effects, HBCDD was included in the lists of hazardous pollutants by various national and international organizations for the restriction of production and use. In 2007, HBCDD was included in the HELCOM Baltic Sea Action Plan as one of the substances of specific concern to the Baltic Sea [*HELCOM*, 2007]. HELCOM Contracting Parties agreed on severe restrictions of the use of hazardous substances, including HBCDD, in the entire catchment area of the Baltic Sea. HBCDD was also included in list of chemicals for priority action of OSPAR Convention [*OSPAR*, 2009].

In 2009, HBCDD was considered as a candidate for the inclusion into the Protocol on POPs to the Convention on Long-Range Transboundary Air Pollution. Two options were identified for possible inclusion of HBCDD to the Protocol, namely, listing in Annex I to the Protocol to eliminate production and use, and in Annex II to the Protocol to restrict certain uses [*UNECE*, 2010]. In 2013, HBCDD was added to Annex A of the Stockholm Convention on Persistent Organic Pollutants as the chemical which production and use should be eliminated. HBCDD is one of the chemicals of emerging Arctic concern which is considered in AMAP Assessment [*AMAP*, 2016].

[1]HBCDD is a standardized abbreviation (in a singular form) of a group of HBCDD stereoisomers commonly used in scientific literature. Other possible abbreviations include HBCD, however HBCDD is preferable to avoid confusion with hexabromocyclodecane [*AMAP*, 2016]

HBCDD is considered as priority substance in the EU Water Framework Directive [*EU*, 2013]. In accordance with the EU REACH[2] and CLP Regulation[3], HBCDD is classified as a chemical suspected to be toxic to reproduction and causing harm to breast-fed children. Besides, this chemical is considered by ECHA also as very toxic to aquatic life with long lasting effects[4]. The European Chemical Agency included HBCDD in the Candidate list of substances of very high concern and in the Authorization List as persistent, bioaccumulative, and toxic substance (PBT). HBCDD is listed in the Annexes I and IV of the EU Regulation 2019/1021 on persistent organic pollutants[5]. In accordance with the Article 3 of the Regulation, manufacturing, placing on the market and use of HBCDD shall be restricted. In accordance with the Article 7, specific waste management provisions are to be applied for HBCDD.

In 2019, HBCDD was listed in Annex III of Rotterdam Convention, where banned or severely restricted chemicals were listed [*Rotterdam Convention*, 2019]. Following this decision, the export of HBCDD is only possible with the prior consent of the recipient countries, which should be properly informed about the associated health and environmental risks.

Production, use, and emissions

HBCDD is an industrial chemical which belongs to the group of brominated flame retardants. It is used as an additive in polymer applications, providing fire protection during the service life of vehicles, buildings, articles, as well as protection while stored. HBCDD is applied in four principal polymer product types, which are expandable polystyrene (EPS), extruded polystyrene (XPS), high impact polystyrene (HIPS) and in polymer dispersions for textiles.

HBCDD has been produced for the world market since the late 1960s. It was mainly manufactured in China, Europe, Japan and the United States of America [*UNEP*, 2017]. According to industry information, global consumption of HBCDD in 2001 was 16,700 t y^{-1} with approximately 57% in Europe, 23% in Asia-Pacific region, 17% in North America and 5% in other regions [*Nordic Council of Ministers*, 2007]. From 2001 to 2011 the global production of HBCDD increased to 31,000 t y^{-1} that included about 13,000 t y^{-1} in the EU and the United States, and 18,000 t y^{-1} in China [*UNEP*, 2017].

Commercially produced HBCDD products contained a mixture of several stereoisomers with the most significant fraction of α-HBCDD (72-90%) followed by β-HBCDD (9-13%) and γ-HBCDD (<0.5-12%) [*Schrenk et al.*, 2021]. HBCDD stereoisomers are characterized by unique physical-chemical properties, which lead to different distribution and behavior in the environment, including

[2] Regulation (EC) No 1907/2006 of the European Parliament and of the Council of 18 December 2006 concerning the Registration, Evaluation, Authorization and Restriction of Chemicals (REACH), establishing a European Chemicals Agency, amending Directive 1999/45/EC and repealing Council Regulation (EEC) No 793/93 and Commission Regulation (EC) No 1488/94 as well as Council Directive 76/769/EEC and Commission Directives 91/155/EEC, 93/67/EEC, 93/105/EC and 2000/21/EC

[3] Regulation (EC) No 1272/2008 of the European Parliament and of the Council of 16 December 2008 on classification, labelling and packaging of substances and mixtures, amending and repealing Directives 67/548/EEC and 1999/45/EC, and amending Regulation (EC) No 1907/2006

[4] Source: European Chemical Agency, https://echa.europa.eu/registration-dossier/-/registered-dossier/15003/2/1

[5] Regulation (EU) 2019/1021 of the European Parliament and of the Council of 20 June 2019 on persistent organic pollutants. Source: http://data.europa.eu/eli/reg/2019/1021/oj

accumulation in biota. HBCDD stereoisomers are widely dispersed in the environment including biota and humans with predominant concentrations of α-HBCDD [*WHO*, 2013; *Schrenk et al.*, 2021].

HBCDD stereoisomers are not chemically bound to the produced polymers. Therefore, their releases into the environment may occur at any stage during the life-cycle of products (during production, manufacturing, processing, transportation, use, handling, storage, and disposal) [*Schrenk et al.*, 2021]. The emissions of HBCDD during production and use are estimated to be small compared to the releases from waste [*ECHA*, 2009]. Due to long lifetime of XPS and EPS information on the historical use of materials containing HBCDD is of importance. Under the Stockholm Convention, the guidance on preparing inventories of HBCDD production, uses and disposal has been developed to help parties to implement measures on HBCDD elimination [*UNEP*, 2021].

In the EU the annual HBCDD emissions into air, surface water and waste water in 2006 were estimated to 649, 924 and 1553 kg y^{-1}, respectively [*ECHA*, 2009]. The releases to water were the largest in the EU, while for Japan the largest releases were estimated to air (571 kg y^{-1} to air and 41 kg y^{-1} to water) [*Managaki et al.*, 2009].

Monitoring

HBCDD is included in the monitoring campaigns of several countries as a persistent organic pollutant of emerging concern. In particular, measurements of HBCDD air concentrations are available from monitoring sites in Norway, Sweden and Finland. Due to low vapor pressure and affinity to particulate matter HBCDD stereoisomers were mainly found in particulate phase in the atmosphere. In Northern Europe HBCDD levels in air have been measured since 1990s [*de Wit*, 2002]. In particular, in 1990-1991 observed air concentrations of HBCDD at two monitoring sites in the Baltic Sea (at southern tip of Gotland) were 5.3 and 6.1 pg m^{-3}.

At monitoring sites Birkenes and Zeppelin in Norway, measurements of three HBCDD stereoisomers (α-HBCDD, β-HBCDD and γ-HBCDD) in air have been made since 2006. Measured concentrations showed significant decrease of HBCDD levels after 2006, however a lot of observed values (especially in period 2008-2020) were below the detection limit [*NILU*, 2021].

In 2020, at Zeppelin all HBCDD stereoisomers were detected in >50% of the samples. On the contrary, at Birkenes only α-HBCDD concentrations were above the detection limit [*NILU*, 2021]. The measurement results for HBCDD stereoisomers at Zeppelin monitoring site obtained in 2019 and 2020 are shown in Figure 3.5. It can be seen that α-HBCDD is predominant in the atmosphere. In the previous periods of observations at the Norwegian monitoring sites, seasonal fluctuations in HBCDD air concentrations were not detected [*NILU* 2018, 2019]. However, in March 2019 and March and April 2020 at the Zeppelin, the concentrations of all HBCDD stereoisomers demonstrated maximum values. Besides, annual mean observed HBCDD concentrations (0.418 pg m^{-3}) in 2020 appeared to be higher than that in 2019 (0.16 pg m^{-3}) [*NILU*, 2021].

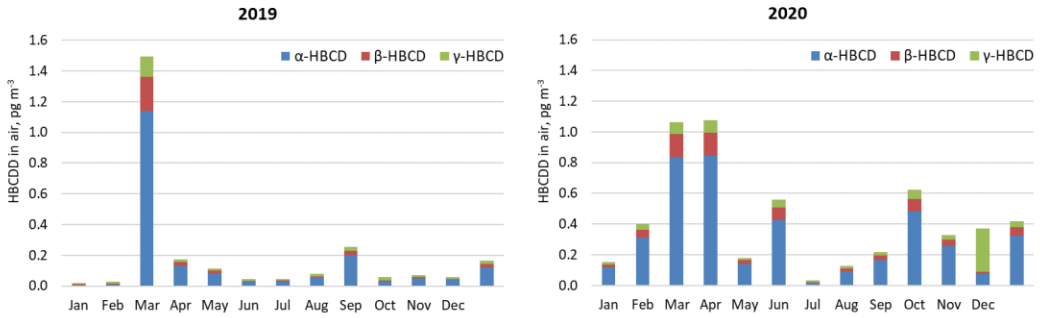

Fig. 3.5. *Air concentrations of α-, β- and γ-HBCDD measured at Zeppelin monitoring site in 2019 and 2020.*

In 2016-2019, at background monitoring sites Pallas and Raö measured atmospheric concentrations of the sum of three HBCDD stereoisomers were at the same level as in Norway below 0.1 pg m^{-3} (0.020-0.064 pg m^{-3} in Rao and <0.004-0.092 pg m^{-3} in Pallas) [*Fredricsson et al.*, 2021]. These levels are in good agreement with the passive sampling of HBCDD performed during 2014 at the Global Atmospheric Passive Sampling (GAPS) Network. Most of the observed concentrations in the background areas in Central Europe (Košetice, the Czech Republic), Canada (Alert), USA (Barrow) were also below 0.09 pg m^{-3} [*Rauert et al.*, 2018].

In the Arctic, temporal trend studies on HBCDD reviewed in the AMAP Assessment of Chemicals of Emerging Arctic Concern showed increasing or inconclusive trends for air, ice core, and biota until 2005–2010. At the same time, data after 2010 demonstrated relatively stable or declining concentrations [*AMAP*, 2016].

HBCDD concentrations are significantly higher in urban air. For instance, in 2014, concentrations of α-HBCDD in Paris ranged from 11 to 40 pg m^{-3}, while concentrations of β-HBCDD and γ-HBCDD were 1.7–6.8 and 3.0–12.0 pg m^{-3}, respectively [*Rauert et al.*, 2018]. Values of observed HBCDD concentrations in urban areas of China were even higher, ranging from 3.21 to 123 pg m^{-3} in Shanghai (2006), from 20 to 1800 pg m^{-3} in Beijing (2008–2009), and from 3.9 to 6700 pg m^{-3} in Harbin (2008–2013) [*Li et al.*, 2012; *Hu et al.*, 2011; *Li et al.*, 2016].

Modelling

A number of studies were recently performed to evaluate levels of HBCDD concentrations in the environment using available modelling approaches. In particular, modelling study of HBCDD diastereomer profiles in global environment [*Li and Wania*, 2018] was carried out using BETR-Global model [*MacLeod et al.*, 2011] coupled to dynamic substance flow model, named Chemicals in Products - Comprehensive Anthropospheric Fate Estimation model (CiP-CAFE) [*Li and Wania*, 2016], which took into account pathways and releases of HBCDD during production, use and waste disposal stages. Modelling results for 2015 indicated that 340–1000 tonnes of HBCDD were emitted globally, with 50–65% of γ-HBCDD and 30–50% of α-HBCDD. It was shown that α-HBCDD dominated in the contamination of the air in populated areas, whereas γ-HBCDD dominated in remote background areas and in the regions with HCBDD production and processing facilities. It was also noted that the

relative abundance of α-HBCDD was expected to increase after the production of HBCDD was eliminated.

Mass balance box models and spatially resolved multicompartment models were applied to evaluate long-range transport potential (LRTP) and overall persistence (Pov) of HBCDD [*Arnot et al.*, 2009; *Vulykh et al.*, 2009]. In particular, long-range atmospheric transport and persistence of HBCDD were evaluated using the MSCE-POP multicompartment hemispheric transport model [*Vulykh et al.*, 2009]. The model predicted the residence time of HBCDD mixture in the atmosphere about 3 days and the transport distance about 1800 km.

Polychlorinated naphthalenes (PCNs)

Polychlorinated naphthalenes (PCNs) is a group of dioxin-like chemicals that includes 75 theoretical congeners with from one to eight chlorine atoms substituting the hydrogen atoms of the naphthalene ring [*Falandysz et al.*, 2014]. PCNs were among the first commercially produced synthetic industrial chemicals. They are characterized by dielectric, water-repellent, flame retardant, and fungus-resistant properties. PCNs were mainly applied in the electrical industry as separators in storage batteries, capacitor impregnates, as binders for electrical grade ceramics, and in cable covering compositions [*Jakobsson and Asplund*, 2000]. Also, they were used as additives in cutting and engine oils, in die casting, and as wood and paper preservatives [*Yamashita et al.*, 2000]. Their large-scale production was started in 1920s in the United States and Europe and was discontinued in 1980s. Along with the industrial production, PCNs can also be unintentionally formed during waste incineration, metallurgical and chlor-alkali processes. Besides, they were found as impurities in the commercial PCB mixtures [*Yamashita et al.*, 2000]. Main sources of their releases into environment are the diffusion during production, use, and disposal of PCN mixtures.

PCNs were identified as persistent, toxic substances capable to long-range transport in the environment and bioaccumulation in biota [*UNEP*, 2012]. Some of PCN congeners cause toxicological effects similar to those of dioxin-like compounds [*Hanberg et al.*, 1990, *Blankenship et al.*, 1999; *Villeneuve et al.*, 2000; *Blankenship et al.*, 2000; *Kilanowicz et al.*, 2011; *Zacs et al.*, 2021; *Kilanowicz et al.*, 2019a, 2019b]. Some of the studies concluded that a number of PCNs may be characterized as carcinogenic contaminants, however they are not currently listed by the International Agency for Reasearch on Cancer (IARC) [*Li et al.*, 2021; *Zacs et al.*, 2021; *IARC*, 2022].

Toxicity of PCN mixture can be estimated using Relative Potency Factors (RPFs) which have been suggested for a number of PCN congeners [*Blankenship et al.*, 2000; *Falandysz et al.*, 2014]. Hexa-CNs and hepta-CNs are considered to be the most toxic among PCN congeners, followed by penta-CNs and tetra-CNs. The highest values of RPFs were estimated for PCN-63, PCN-64, PCN-66, PCN-67, PCN-68, PCN-69, PCN-70, PCN-73 [*Fang et al.*, 2019; *Falandysz et al.*, 2014].

Regulation

PCNs are listed in the regulatory documents of national and international organizations with the aim to collect information on their environmental levels and trends as well as for the development of measures for the restriction of their usage and reduction of emissions.

In 2009 PCNs were added to the Annex I to the Protocol on Persistent Organic Pollutants to the Convention on Long-Range Transboundary Air Pollution among the new POPs for prohibition of production and use [*UNECE*, 2009]. Later on in 2015, PCNs were added to the Annexes A (elimination) and C (unintentional production) of the Stockholm Convention on Persistent Organic Pollutants with specific exemptions for the use in the production of polyfluorinated naphthalenes, including octafluoronaphthalene [*UNEP*, 2015]. It should be noted that mono-CNs are not listed in the Stockholm Convention. PCNs are also listed in the Annex VIII of the Basel Convention on the control of transboundary movements of hazardous wastes and their disposal.

PCNs are considered as POPs under EU Regulation 2019/1021[6] and are listed in the Annexes I, III and IV of the Regulation[7]. In accordance with the Article 3 of the Regulation, manufacturing, placing on the market and use of PCNs shall be restricted. A specific exemption for PCNs is the possibility of placing on the market and use of the products containing PCNs that were already in use before or on 10 July 2012. The Article 7 of the Regulation establishes specific waste management provisions for PCNs. Release reduction provisions and requirements for PCNs are described in the Article 6. PCNs are also listed in the Annex V (List of Banned or Restricted Chemicals) of EU Regulation 649/2012 concerning the export and import of hazardous chemicals. In according with the Article 15, the export of PCNs is not possible.

PCNs are listed in Part C of the OSPAR List of Chemicals for Priority Action as a group of substances which are not currently produced or used in the OSPAR states. However, Contracting Parties should inform OSPAR if they would find any evidence that these substances are being produced, used or discharged.

Production, use, and emissions

PCNs were used mainly in the electrical industry as separators in storage batteries, capacitor impregnates, as binders for electrical grade ceramics and sintered metals, and in cable insulation. Other applications of PCNs included impregnation of wood, paper and textiles to attain waterproofness, flame resistance and protection against insects, molds and fungi. Furthermore, PCNs have been used as an additive in engine oils, electroplating masking compounds, feedstock for dye productions, dye carriers, capacitors and refracting index oils [*Jakobsson and Asplund*, 2000; *ESWI*, 2011].

PCNs production was initiated around 1910 in both Europe and the United States. According to *van de Plassche and Schwegler* [2002], most part of PCNs was produced from the 1920s to the 1950s, with the majority occurring in the USA. Total global production of PCNs is estimated at 150,000–400,000 tonnes in the period 1920–1965 [*UNEP*, 2012]. Until 1970s PCNs remained high volume production chemicals.

[6] Regulation (EU) 2019/1021 of the European Parliament and of the Council of 20 June 2019 on persistent organic pollutants

[7] In the Regulation (EU) 2019/1021 "polychlorinated naphthalenes means chemical compounds based on the naphthalene ring system, where one or more hydrogen atoms have been replaced by chlorine atoms".

The annual total world production of PCNs was about 9000 tonnes in the 1920s. In the United States, 3200 tonnes were produced in 1956 which had decreased to 320 tonnes in 1978 due to the replacement of PCNs by a variety of substitutes. Production of PCNs was stopped in 1980 [*Jakobsson and Asplund*, 2000]. Small amounts of PCNs around 15 tonnes were imported into the USA in 1981, which were mainly used in refractive index testing oils and capacitor dielectrics [*US EPA*, 1983]. In Japan, about 4000 tonnes of PCNs were produced between 1940 and 1976. In 1979 the production and use were banned [*Yamamoto et al.*, 2016].

In the UK the production was stopped in the mid-1960s, although it was reported that in 1970 small amounts of PCNs were still produced. In Germany about 100-300 tonnes of PCNs per year were produced in 1980-1984 for the use as dye intermediates [*UNECE*, 2007]. *Popp et al.* [1997] reported that PCNs were used in a German plant producing models and tools for car manufacturing and mining until 1989. Production of PCNs in Germany was stopped in 1989.

PCNs can be formed unintentionally during uncontrolled waste combustion, waste incineration (e.g. municipal, clinical and industrial waste) and other thermal (domestic and industrial) processes. This includes coking processes, different metal processing steps such as secondary copper production, secondary aluminum production, magnesium production as well as iron sintering and electrical arc furnace processes for iron production, industrial solvent production, and cement industry processes which can be considered as emission sources [*ESWI*, 2011].

Although PCNs are included in the Protocol on POPs to CLRTAP, no official emission data are being collected currently. Besides, the Air Pollutant Emission Inventory Guidebook does not provide information on the emission factors for PCNs [*EEA*, 2019]. At the same time, under the Stockholm Convention, the guidance on preparing inventories of PCN production, uses and disposal has been developed to help parties to implement measures on PCN elimination [*UNEP*, 2021].

Inventory of PCN emissions in Europe was developed for the year 2000 by TNO. The total annual emission of PCNs to the atmosphere was estimated to 1.03 tonnes [*Denier van der Gon et al.*, 2005]. The inventory was based on the data reported by countries and expert estimates where detailed data were missing. Waste incineration contributed 74% to total PCN emissions in 2000. Industrial combustion and processes accounted for 11%, followed by residential, commercial and other combustion with 10% of total PCN emissions. The remaining part was divided between the public power and heat production, as well as solvent production and use [*Denier van der Gon et al.*, 2007].

PCN emission inventory was prepared by the United Kingdom as part of the National Implementation Plan for the Stockholm Convention on Persistent Organic Pollutants. PCN emissions to air and land were estimated for the period 1990-2014. Estimates of PCN releases to the environment in the UK in 2014 were around 104 kg to air and 98 kg to land [*UK DEFRA*, 2017].

Monitoring

Monitoring of PCNs in various environmental compartments and biota was performed in Sweden [*Haglund et al.*, 2011]. Atmospheric concentrations of different PCN homologue groups were measured at two monitoring sites Raö and Pallas in 2010 (Fig. 3.6). Less halogenated di-CNs and tri-CNs were found to make the highest proportion to the total PCN concentrations. Concentrations of ΣPCNs at Raö were about 1.5 pg m^{-3} in August and 2.5 pg m^{-3} in November, while at Pallas they were about 0.5 and 1.5 pg m^{-3}, respectively. Monitoring of PCN concentrations in the vicinity of various types of emission sources showed generally higher levels for municipal solid waste incinerators and metal industries. At the same time, importance of long-range atmospheric transport of PCNs was also noted [*Haglund et al.*, 2011].

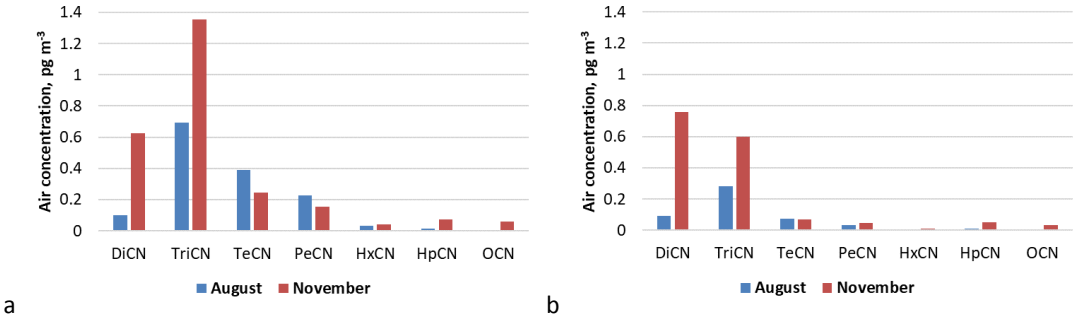

Fig. 3.6. *Atmospheric concentrations of the PCN congeners observed in August and November 2010 at stations Raö (a) and Pallas (b).*

Although PCNs are considered as organic pollutants of emerging concern and are listed in the POP Protocol to LRTAP Convention, they are not currently included in the EMEP monitoring strategy for regular monitoring [ECE/EB.AIR/144/Add.1].

PCNs were measured in the Arctic and sub-Arctic areas in 1993-2005. Total measured atmospheric concentrations ranged from 0.16 to 40 pg m^{-3} [*Bidleman et al.*, 2010]. It was shown that PCNs were widespread in the Arctic, and the European Arctic is characterized by higher levels of ΣPCNs. Besides, it was noted that ΣPCN concentrations were comparable to the concentrations of ΣPCBs. Atmospheric concentrations of ΣPCNs at monitoring sites in Norway in 2001-2003 ranged from 27 to 48 pg m^{-3} (with mean value 35 pg m^{-3}) at Ny-Ålesund and from 9 to 47 pg m^{-3} (with mean value 25 pg m^{-3}) at Tromsø [*Herbert et al.*, 2005]. For both sites, the contribution of tri-CNs was the most significant among PCN homologue groups (65–71%), followed by tetra-CNs (24–31%). The contribution of penta-CNs was lower (<4%) [*Herbert et al.*, 2005].

Atmospheric concentrations of PCNs were measured in 2000-2001 at two rural/semirural sites in the United Kingdom and one remote site on the west coast of Ireland [*Lee et al.*, 2005]. In Ireland, ΣPCN concentrations ranged from 1.7 to 55 pg m^{-3} (with mean value 15 pg m^{-3}). In the northwest part of the United Kingdom, ΣPCN concentrations ranged from 31 to 310 pg m^{-3} (with mean 110 pg m^{-3}), in southwest part of the country observed values ranged from 31 to 180 pg m^{-3} (with mean value 85 pg m^{-3}). It was noted that the observed concentrations of ΣPCNs were close to or exceeded the concentrations of ΣPCBs for all the sites.

Modelling

A number of studies have been recently carried out to evaluate physical-chemical properties and levels of PCNs in the environment using available modelling approaches. In particular, partition coefficients, Henry's Law constants, and water solubilities of 75 PCNs were estimated using QSPR models in the studies [*Puzyn and Falandysz*, 2007; *Puzyn et al.*, 2009]. Partition coefficients and water solubility were also predicted using QSPR model in the study of *Chayawan and Vikas* [2015] and were recommended for the use in the model assessment of PCN pollution. The half-live values for all PCN congeners due to reaction with the OH radical in the atmosphere were calculated applying QSPR approach [*Puzyn et al.*, 2008]. It was shown that the average half-lives for PCNs of different homologue groups ranged from 2 days for mono-CNs up to 343 days for octa-CNs. The quantum mechanical descriptors and QSPR were also applied to predict supercooled liquid vapor pressure of PCNs [*Sosnovska et al.*, 2014; *Vikas and Chayawan*, 2015].

The long-range atmospheric transport and overall persistence of PCN-47 congener were estimated using the MSCE-POP multicompartment hemispheric transport model [*Vulykh et al.*, 2005b]. The model predicted the residence time of PCN-47 in the environment of about 3.2 months and the atmospheric transport distance of about 2300 km that indicated significant long-range transport potential of this compound.

Pentachlorobenzene (PeCB)

Pentachlorobenzene (PeCB or PeCBz[8]) is a chlorinated aromatic hydrocarbon consisting of a benzene ring with 5 chlorine atoms substituting hydrogen atoms. PeCB occurs as white crystalline solids at room temperatures. Being characterized by relatively high subcooled liquid-vapour pressure [*Mackay et al.*, 2006], PeCB presents in the atmosphere mostly in the gaseous phase. It has a very low solubility in water. At the same time, it has high octanol water partition coefficient. PeCB has been found in air, rain, surface water, sediment and biota samples collected from various locations around the world, including remote regions [*UNEP*, 2007].

Intentionally produced PeCB was used in PCB products, for the production of quintozene and in dye carriers. Other applications include also its use as a pesticide and as a flame retardant [*UNEP*, 2007]. As unintentional by-product, PeCB can occur as an impurity in solvents or pesticides. It also can be formed during various combustion, thermal and industrial processes, including waste incineration. It should be noted that combustion of PeCB may result in the formation of other toxic compounds such as polychlorinated dibenzodioxins and polychlorinated dibenzofurans.

PeCB is considered as persistent and bioaccumulative substance, which has hazardous effects to human health and wildlife, especially for aquatic life. Monitoring of environmental levels suggests that PeCB has significant potential for long-range atmospheric transport. It has long residence time in the atmosphere and is characterized by high persistence under anaerobic conditions in sediments and soils [*Canada Communication Group*, 1993].

[8] Both PeCB and PeCBz abbreviations are used in the scientific literature for pentachlorobenzene.

Regulation

PeCB is included in a number of programs of various national and international activities, aimed at collection of data on its environmental levels and their trends. Besides, measures have been developed for the restriction of its usage and reduction of emissions to the environment.

PeCB is one the new POPs that were added in 2009 to the Annex I (prohibition of production and use) to the POP Protocol of the Convention on Long-Range Transboundary Air Pollution [*UNECE*, 2009]. However, inventories of PeCB emissions are not currently officially reported under the Convention [*UNECE*, 2015] and emission factors for PeCB are not present in the Air Pollutant Emission Inventory Guidebook [*EEA*, 2019].

Risk management evaluations, made under the Stockholm Convention [*UNEP*, 2007, 2008a, 2008b], indicate that PeCB has significant long-range transport potential and can cause significant adverse human health and environment effects. In 2009, PeCB was listed under Annex A (elimination) and Annex C (unintentional production) of the Stockholm Convention on Persistent Organic Pollutants without specific exemptions [*UNEP*, 2009]. PeCB is listed in the OSPAR 1998 List of Candidate Substances [*UNEP*, 2007].

In accordance with the EU REACH[9] and CLP Regulation[10], PeCB is classified as very toxic for aquatic species with long lasting effects[11]. PeCB is listed in the Annexes I, III and IV of the EU Regulation 2019/1021 on POPs[12]. Article 3 of the Regulation requires a prohibition of manufacturing, placing on the market and use of PeCB. In according with the Article 7 and Annex IV of the Regulation, specific waste management provisions are applied to PeCB. Release reduction provisions and requirements for PeCB are described in Article 6. Besides, PeCB is listed in Part B of Annex III, which however does not require mandatory monitoring of this substance in the environment. PeCB is considered as a priority substance in the EU Water Framework Directive[13] .

Production, use, and emissions

PeCB was intentionally produced in the past as a component of PCB products for the electrical equipment. Besides, it was used as an intermediate chemical for the production of fungicide quintozene. Other applications of PeCB included the use in dyestuff carriers, as a pesticide, and as a flame retardant. The major European and American producers of quintozene have changed their manufacturing processes to eliminate the use of PeCB. It also can present at low levels in herbicides, pesticides and fungicides as an impurity and product of degradation. There is no quantitative information on historic production and use of PeCB [*UNEP*, 2007a; *UNEP*, 2008].

---

[9] Regulation (EC) No 1907/2006 of the European Parliament and of the Council of 18 December 2006 concerning the Registration, Evaluation, Authorisation and Restriction of Chemicals (REACH), establishing a European Chemicals Agency, amending Directive 1999/45/EC and repealing Council Regulation (EEC) No 793/93 and Commission Regulation (EC) No 1488/94 as well as Council Directive 76/769/EEC and Commission Directives 91/155/EEC, 93/67/EEC, 93/105/EC and 2000/21/EC.

[10] Regulation (EC) No 1272/2008 of the European Parliament and of the Council of 16 December 2008 on classification, labelling and packaging of substances and mixtures, amending and repealing Directives 67/548/EEC and 1999/45/EC, and amending Regulation (EC) No 1907/2006.

[11] https://echa.europa.eu/information-on-chemicals/cl-inventory-database/-/discli/details/62913.

[12] Regulation (EU) 2019/1021 of the European Parliament and of the Council of 20 June 2019 on persistent organic pollutants.

[13] Directive 2000/60/EC of the European Parliament and of the Council of 23 October 2000 establishing a framework for Community action in the field of water policy.

At present the most relevant sources of PeCB releases to the environment can be unintentional formation of PeCB during various industrial processes (e.g. combustion of fossil fuels, production of steel and iron, and waste incineration). Further, waste water treatment, which leads to the generation of sewage sludge containing PeCB, has been considered as relevant emission source [*ESWI*, 2011].

The European Pollutant Release and Transfer Register (E-PRTR) contains specifications for the reporting of PeCB release to the environmental compartments. A small number of EU Member States report emissions of PeCB to air and water (Belgium, Finland, France, Italy, Luxembourg, Portugal, Spain and the United Kingdom).

Within the E-PRTR dataset only a limited number of sites across Europe reported the PeCB emissions to air for the period 2008–2011. According to these data main contribution belonged to manufacturing of pig iron and steel. The other reported minor sources were waste water treatment plants, and plants for the processing of vegetable and animal matter. Reported releases of PeCB to air from iron and steel manufacturing sector ranged from 348 to 1779 kg y^{-1} (based on three metal facilities reporting for 2008 to 2010, and two for 2011).

PeCB releases to water, reported in the E-PRTR (2007-2020), illustrate a small number of sources. Organic chemicals manufacture, waste water treatment works, petroleum refineries, and hazardous waste treatment reported emissions almost every year. According to E-PRTR, releases of PeCB to water from manufacturing of organic chemicals ranged from 11 to 44 kg y^{-1}, with an average of 30 kg y^{-1}, and from waste water treatment works ranged from 14 and 84 kg y^{-1}, with an average of 40 kg y^{-1}. Petroleum refineries contributed between 2 and 121 kg y^{-1} with an average of 30 kg y^{-1}.

According to expert estimates [*Bailey*, 2007], global emissions of PeCB around the year 2000 amounted to 85 t y^{-1}. The largest contributions were made by the combustion of biomass, coal, and solid wastes. However, it was noted that there was a considerable uncertainty in these estimates of PeCB emissions (up to an order of magnitude potentially). Updating of these estimates resulted in higher total annual emissions about 121 t y^{-1} [*Bailey et al.*, 2009], where more importance was given to pesticide use and degradation of chemicals.

Several national inventories of PeCB emissions were made by particular countries. The total release of PeCB around the year 2003, provided by Environment Canada in the risk management strategy, was 41.9 kg y^{-1} [*Environment Canada*, 2005]. The most significant sources in the Canadian risk management report were barrel burning of household waste, municipal solid waste incineration and hazardous waste incineration.

According to US EPA Toxics Release Inventory annual emissions of PeCB in the USA varied from 763 to 1512 kg y^{-1} in period 2000-2004. The inventory included atmospheric emissions, surface water discharges, underground injection, on site releases to land and transfers off-site for disposal. Atmospheric emissions were about 74 - 100 kg y^{-1} [*UNEP*, 2007a;b].

Overall discharges of PeCB in Europe in 2010 were estimated to 2632 kg y^{-1} using mass flow approach [*ESWI*, 2011]. About 88% of this were released to the atmosphere and soil and only approximately 12% end up as waste. PeCB emissions were dominated by the power production from coal (79%).

An inventory of PeCB emissions in the United Kingdom and Ireland was prepared as part of the National Implementation Plan for the Stockholm Convention on Persistent Organic Pollutants [*UK DEFRA*, 2017; *Ireland EPA*, 2018]. PeCB emissions to the atmosphere, water and land were estimated for the period 1990-2014 in the United Kingdom and up to 2015 in Ireland. Estimates of PeCB releases to the environment in the United Kingdom in 2014 were around 33 kg to the atmosphere, 3 kg to water and 9 kg to land [*UK DEFRA*, 2017]. In Ireland, emissions of PeCB to the atmosphere, water and land in 2015 were estimated to 14 kg, 0.15 kg and 0.002 kg, respectively [*Ireland EPA*, 2018].

Monitoring

Atmospheric concentrations of PeCB were measured at two EMEP monitoring stations in Norway and the Czech Republic, Zeppelin (NO0042R) and Kosetice (CZ0003R), respectively. In 2004-2006, concentrations of PeCB in air at the Zeppelin station varied from 7.5 to 105 pg m^{-3} with annual mean concentrations 19.5 pg m^{-3} in 2004 and 23.9 pg m^{-3} in 2006. Measurements of PeCB air concentrations at the Kosetice station were performed for longer period starting from 2001 up to the present time. In 2001-2005, annual mean PeCB air concentrations varied from 13 to 55 pg m^{-3} with minimum concentrations 0.5 pg m^{-3} and maximum concentration 441 pg m^{-3} [*Dvorska et al.*, 2008]. In 2011-2020, almost similar levels of annual mean PeCB air concentrations were observed equal to 6.2-11.6 pg m^{-3}, with the exception of 2020, when maximum annual mean concentration 15.5 pg m^{-3} was observed (Fig. 3.7a). Seasonal changes of PeCB concentrations showed minimum values in summer period of the year, while maximum values were measured in winter period (Fig. 3.7b).

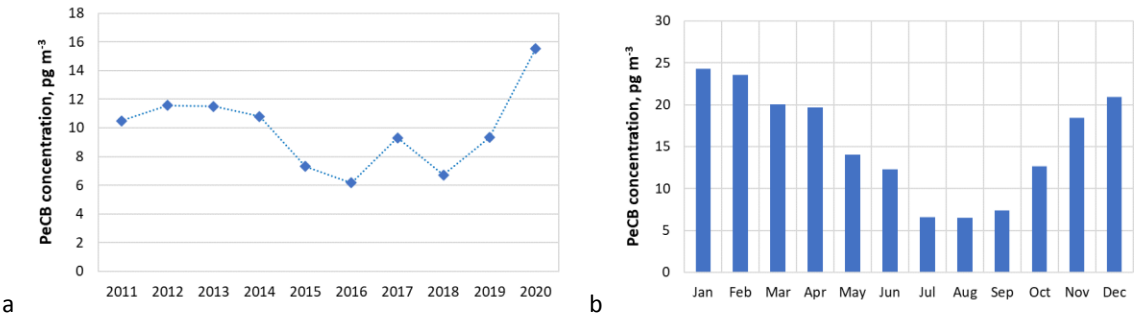

Fig. 3.7. *Annual mean concentrations of PeCB in air measured at monitoring site Kosetice (CZ0003R) in period 2011-2020 (a) and seasonal variations of observed PeCB air concentrations in 2020 (b).*

Spatial distribution of PeCB air concentrations in Norway was analyzed based on the measurements made using passive air sampling [*Halvorsen et al.*, 2021]. PeCB concentrations were measured at 97 locations across Norway in summer 2016. Observed concentrations varied from 16 to 38 pg m^{-3} with mean concentration equal to 22 pg m^{-3}. The ratio of maximum and minimum observed PeCB concentrations was about 2 times indicating low spatial variability of concentrations and potentially significant role of long-range transport of pollution.

Modelling

Modelling approaches were applied to evaluate physical-chemical properties, expert estimates of emissions and pollution levels of PeCB on global and regional scales. In particular, a complete set of physical-chemical properties (e.g. octanol-water partition coefficient K_{OW}, vapor pressure P, Henry's law constant H, octanol-air partition coefficient K_{OA}) and their temperature dependence, necessary for model assessment, was derived in the study [*Shen and Wania*, 2005]. The approach is based on the compiling and evaluating measured data from the literature, selecting literature-derived values through averaging or linear regression and making estimates of the uncertainty of these values.

Spatial distribution and long-range transport of PeCB was evaluated in the study [*Shen et al.,* 2005] based on monitoring data of 40 passive air sampling stations across North America. Measurements were performed for the whole year 2000 to obtain annually averaged concentrations. Empirical travel distance for PeCB estimated using monitoring data was about 13000 km. Model predictions of characteristic travel distance, made by the models TaPL3 and ELPOS, showed higher values about 84000 km.

Accuracy of global PeCB emission estimates [*Bailey et al.*, 2007] was evaluated in the study [*Bailey et al.*, 2009] using Globo-POP environmental model [*Wania and Mackay*, 1995]. The model was run with constant PeCB emission rate of 100000 kg y^{-1} using physical-chemical properties from [*Shen and Wania*, 2005]. In spite of considerable uncertainties in model parameterization and properties of PeCB used in these simulations, the model predictions for PeCB were close to the observed atmospheric concentrations of PeCB. It was shown that decline of pollution levels of PeCB would depend on the rate of PeCB degradation in soil, sediments and water. Besides, PeCB concentrations would be observed for a period of years after emissions would be completely stopped. Current PeCB concentrations are likely supported to some extent by re-emission from soil exposed in the past.

The long-range atmospheric transport and overall persistence of PeCB were evaluated in the study [*Vulykh et al.*, 2005a] using the MSCE-POP multicompartment hemispheric transport model. The model predicted the atmospheric transport distance of PeCB about 8300 km using conventional point emission source. The half-life of PeCB in the environment was estimated to approximately 6 months indicating significant long-range transport potential of this contaminant.

Concluding remarks and further activities

Literature overview on HBCDD, PCNs, and PeCB has indicated that information on physical-chemical properties of CECs, concentrations in environmental compartments, and levels of emission is not sufficient to perform detailed assessment of their transport and fate in the environment. Model assessment of pollution by these substances requires additional monitoring data on their concentrations in the environment and temporal trends as well as elaboration of emission inventories. Besides, improvement of understanding of processes governing their fate is of importance for the assessment of pollution levels (e.g. of gas-particle partitioning in the atmosphere, air-surface exchange, degradation in media).

Chapter 4. COOPERATION

4.1. Subsidiary bodies of the Convention

4.1.1. Task Force on Measurements and Modelling

The EMEP Task Force on Measurements and Modelling (TFMM) held its 24th meeting in Warsaw in May 2023. During the meeting participants were provided with the information on research activities performed by the Centre in co-operation with TFMM and national experts in the framework of Eurodelta-Carb B(a)P model intercomparison study.

Updated modelling results on B(a)P of several modelling groups (EMEP/MSC-E, CIEMAT, INERIS, ENEA, FMI) and their evaluation against measurements were presented. Similarities and differences between the annual mean concentrations and intra-annual variations obtained by participated models and observed levels were examined. Preliminary analysis of modelling results demonstrates generally reasonable level of agreement of the model predictions with observed B(a)P concentrations. At the same time, for some of the stations modelled concentrations significantly deviated from the observed values indicating possible effect of uncertainties in emission estimates, modelling approaches, and measurements. In particular, the model simulations indicated overprediction of observed B(a)P concentrations in Spain and underprediction in Northern Europe (Finland, Latvia, Estonia), which is likely explained by the uncertainties of the reported B(a)P emissions. Significant difference between the modelling results of four participated models is also noted that requires further analysis of the differences and substantial over- and underestimates of observed B(a)P concentrations for some of the stations. Further research and cooperation activities within the study are proposed. They include sensitivity analyses, an evaluation of the meteorological drivers and an analysis of other model outputs such as B(a)P concentrations in precipitation and deposition fluxes and concentrations of species affecting B(a)P chemical transformations in the atmosphere.

In addition to this, national experts from Spain (CIEMAT) presented the results of the case study on B(a)P emissions in Spain. The study explored the effect of spatial redistribution of annual B(a)P emissions from the Residential combustion sector. The procedure applied to produce officially reported emissions, leads to concentration of B(a)P emissions from this sector in the large cities where the use of biomass burning is likely not a common practice as in the rural areas. This results in an overestimation of residential combustion emissions in urban areas and in an underestimation in rural areas. Proposed approach for spatial redistribution of B(a)P emissions permits to improve the agreement of model estimates of B(a)P pollution levels and measurements in Spain.

4.1.2. Task Force on Hemispheric Transport of Air Pollution

MSC-E contributed to the work of the Task Force on Hemispheric Transport of Air Pollution (TF HTAP) aimed at Hg and POP pollution assessment. In particular, the Centre participated in TF HTAP collaborative activities focused on multi-model evaluation and attribution of Hg pollution trends and future scenarios as well as assessment of the impact of wildfires and biomass burning on contamination of the environment by multiple pollutants.

Multi-Compartment Hg Modeling and Analysis Project (MCHgMAP)

Current TF HTAP activities focused on Hg pollution assessment are performed as a part of the Multi-Compartment Hg Modeling and Analysis Project (MCHgMAP). The project is aimed at comprehensive analysis of spatial and temporal trends of Hg pollution levels, source attribution and evaluation of future scenarios to inform effectiveness of the LRTAP Convention and the Minamata Convention on Mercury. It includes collection of available monitoring and emissions data as well as multi-model estimates of Hg dispersion in the atmosphere and the ocean. To direct and facilitate the assessment activities an international expert group has elaborated a long-term action plan in a form of position paper, which will be published soon and presented to both Conventions. The paper contains all relevant information on the set-up and coordination of the assessment including review, scientific rationale and recommendations of using and further improvement of anthropogenic and geogenic emission inventories, observational data on Hg levels in air and seawater, and air-surface exchange fluxes, characteristics of available chemical transport models for Hg, and detailed plan of the model simulations and analysis of the assessment results. The position paper has the following structure:

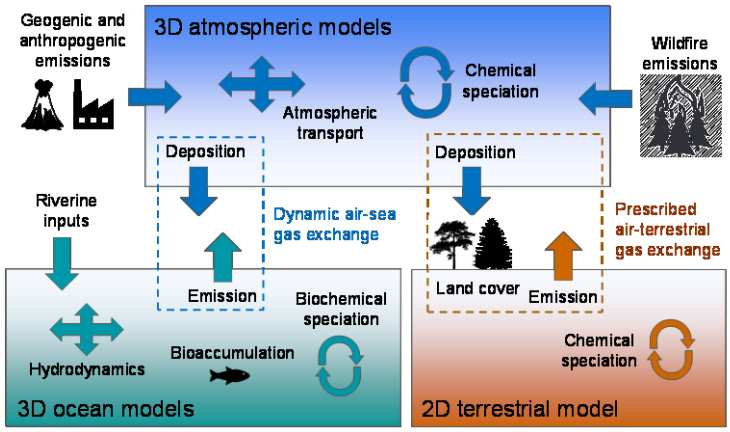

Fig. 4.1. *Conceptual design of Hg multi-model simulations within MCHgMAP.*

- *Scope of the project;*
- *Multi-model ensemble (selection and characteristics of available atmospheric, oceanic, mass balance and exposure models);*
- *Emission sources* (anthropogenic and geogenic emissions, wildfire emissions, and future emission scenarios);
- *Observational data* (measurements of Hg concentrations in air and seawater, wet deposition and air-surface exchange, environmental archives);

- *Multi-model simulations design* (co-ordination of multi-media simulations of atmospheric, ocean, terrestrial, and mass-balance models) (Fig. 4.1);
- *Model evaluation* (methodology of modelling results evaluation vs. observations);
- *Model analysis and products design* (analysis of spatial patterns, historical trends, source attribution);
- *Future scenarios* (model-based projections and analysis of future Hg levels);
- *Uncertainty analysis.*

MSC-E took part in development of the assessment program and preparation of the position paper at all stages of the project. In particular, it contributed to elaboration of the overall program of the model simulations and analysis, formulation of multi-model experiments and specifications of the output results. It also elaborated a harmonized approach to estimates of Hg exchange between the atmosphere and the ocean for consistent use within the project. In addition, it developed a global inventory of Hg emissions from wildfires (Section 4.1.2). The Centre participated in numerous technical meetings of the MCHgMAP expert group and in the annual TF HTAP meeting on global Hg emissions and modelling (online, April 19, 2023, https://htap.org/event/global-mercury-emissions-and-modeling/).

Mercury emissions from wildfires

Wildfires are significant source of numerous atmospheric pollutants including mercury [*Andreae and Merlet*, 2001; *Urbanski et al*., 2009; *De Simone et al*., 2015; *Kumar and Wu*, 2019; *van der Werf et al*., 2017; *Friedli et al*., 2003a,b]. In order to investigate the effect of the wildfires on Hg concentrations, deposition and intercontinental transport, and to improve model estimates of Hg levels, TF HTAP initiated process of development of Hg emissions from wildfires. Initial MSC-E results of the Hg emissions from wildfires at different spatial scales were presented at TF HTAP meeting held in November, 2022. This section presents further steps in the development of wildfire emission approach.

The approach to estimate Hg release to the atmosphere from the wildfires is based on the assumption that Hg emission is proportional to biomass burnt during the fire. Coefficient of proportionality is called emission factor. Information on burnt biomass is derived from the available databases on wildfires. Brief overview of the available global-scale wildfire databases is presented in Table 4.1. TF HTAP experts involved in the MCHgMAP project decided to prepare two sets of Hg wildfire emission data basing on GFED4 and FINN (version 2.5) data sets. In particular, MSC-E was responsible for preparation of Hg emissions from FINN data.

Table 4.1. *Global biomass burning emission datasets.*

Data set	Spatial resolution	Time range and temporal resolution	Data products
GFED(*)	0.25°x0.25°	2000-2020; 3-h, daily, monthly	Burned area; Burnt mass; Emission factors, incl. PM2.5
FINN(**)	1x1 km^2	2002-2021; Daily	Burned area; Burnt mass; Emissions of species, incl. PM2.5
GFAS(***)	0.1°x0.1°	2003-present; Daily	Combustion rate; Burnt mass; Emission of species incl. PM2.5; Injection height
QFED(****)	0.1°x0.1°	2000-present; daily, monthly	Emission of species incl. PM2.5

(*)-Global Fire Emissions Database; http://www.globalfiredata.org

(**) - Fire INventory from NCAR; https://www2.acom.ucar.edu/modeling/finn-fire-inventory-ncar

(***) - Global Fire Assimilation System; http://modis-fire.umd.edu

(****) - Quick Fire Emissions Dataset; https://portal.nccs.nasa.gov/datashare/iesa/aerosol/emissions/QFED/v2.4r6/

Detailed description of FINN data base (version 2.5) is available in [*Wiedinmyer et al.*, 2023]. These data are derived from MODIS satellite measurements of fire activity. Besides, VIIRS (Visible Infrared Imaging Radiometer Suite) instrument allows identifying small wildfires. Wildfires from several land cover types (grasslands and savanna, wood savanna and shrubs, tropical forests, temperate forests, boreal forests, temperate evergreen forests, and croplands) are distinguished. For each of the land-cover type specific emission factor was set. The values of the emission factors (Fig. 4.2) were derived from [*Anderae*, 2019; *McLagan et al.*, 2021 and *Desservettaz et al.*, 2017]. Spatial distribution of Hg wildfire emissions was prepared on global-scale grid with spatial resolution of 0.25°x0.25°. Example of Hg emissions in 2015 is shown in Fig. 4.3. Main regions of Hg emission are Southern Africa, South America and South-Eastern Asia. Besides, some areas of significant wildfire emissions are noted for the Siberian region of Russia and north-western part of North America. In Europe emissions from wildfires are relatively low. Although spatial distribution of Hg wildfire emissions may vary from year to year, the main regions of the emissions remain the same.

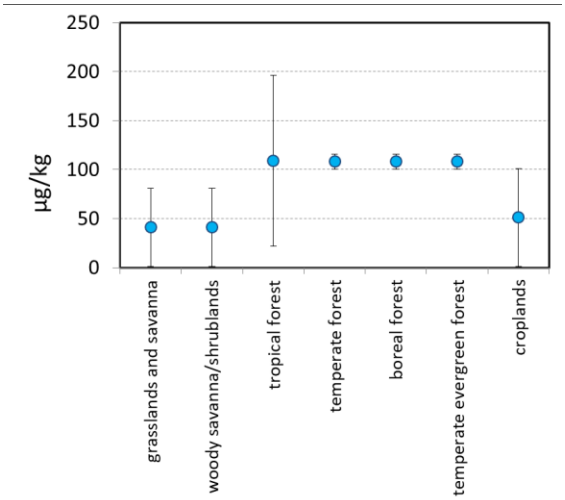

Fig. 4.2. *Emission factors for different land cover types. Whiskers indicate uncertainty range.*

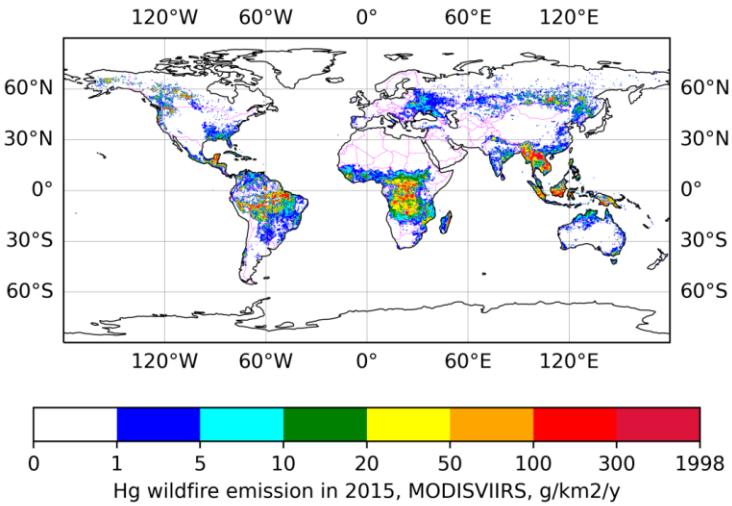

***Fig. 4.3**. Emissions of Hg from wildfires in 2015 based on FINNv2.5 data with spatial resolution 0.25°x0.25°.*

In 2010-2020, total Hg emission from wildfires varies from 714 t/y (2010) to about 500 t/y (2018), and its mean value is about 600 t/y (Fig. 4.4). Main TF HTAP regions responsible for most of Hg emissions from wildfires are Southern Africa, South America and South-Eastern Asia. Their mean contributions are 33%, 22% and 20%, respectively. Wildfires in North America contribute on average 3% and fires in Siberia contribute 5% of Hg on average.

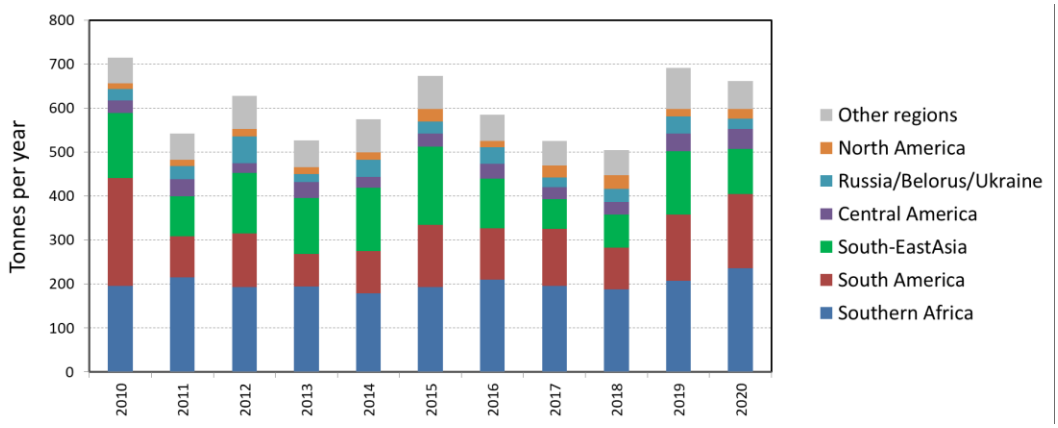

***Fig. 4.4**. Contribution of different TH HTAP regions to global Hg wildfire emissions in 2010 – 2020.*

Among seven land-cover types where wildfires exist the major contributor (around 60% on average) is made by tropical forests (Fig. 4.5). The second in importance contributor is grasslands and savanna varying from 13 to 17%. Contribution of over land-cover types to global Hg emission from wildfires is typically below 10%.

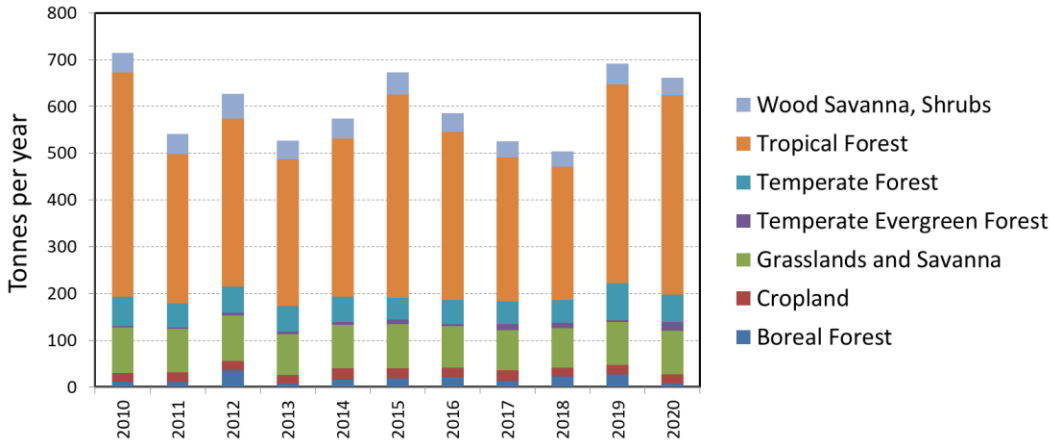

Fig. 4.5. *Contributions land-cover types to global Hg wildfire emissions in 2010 – 2020.*

Seasonal changes of global Hg emissions from wildfires demonstrate two maximums. The first peak occurs in March or April , and the second – in August or September (Fig. 4.6). Fires in South-East Asia are responsible for the spring peak, while the peak in summer/autumn is caused mostly by fires in South America. Peaks in both in spring and summer/autumn occur in Southern Africa.

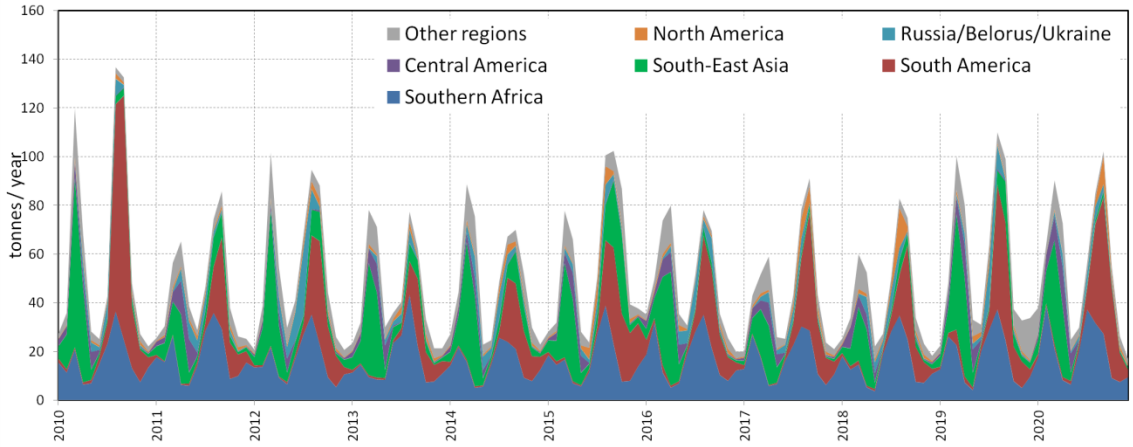

Fig. 4.6. *Monthly values of global Hg emissions from wildfires in 2010 – 2020.*

Global annual emission of mercury from anthropogenic sources is around 2200 tonnes [*AMAP/UNEP*, 2019], which is around 3.5 times higher than the mean Hg emissions from wildfires. Nevertheless, in certain regions and in particular periods of time contribution of wildfires to total Hg emissions can be significant. Further activity regarding the effects of wildfires on Hg levels will include comparison of Hg emissions based on FINN and GFED databases. Besides, model experiments will be undertaken to identify the contribution of wildfires on Hg air concentrations and deposition in different regions of the globe.

4.2. Cooperation with international organizations

4.2.1. Stockholm Convention

MSC-E continued co-operation and data exchange with the Stockholm Convention on POPs. Collection and refinement of national POP emission inventories under the Stockholm Convention provides additional information for the evaluation of emissions of the EMEP countries. Besides, national emissions inventories are used for the updating of the scenarios of global emission for global scale modelling and estimation of EMEP region boundary conditions. Furthermore, updated monitoring data on POP concentrations, collected in the Global Monitoring Plan Data Warehouse (GMP DWH), is applied for the analysis of global POP transport.

4.2.2. Helsinki Commission

Evaluation of airborne pollution load of heavy metals and POPs to the Baltic Sea is carried out in the framework of long-term cooperation between EMEP and the Helsinki Commission (HELCOM). In 2022 MSC-E continued collaborating with HELCOM and evaluating pollution levels and trends for extended list of heavy metals and POPs that includes metals of the first and the second priority as well as legacy POPs and chemicals of emerging concern.

In accordance with the contract, the compilation of data on atmospheric emissions and model assessment of atmospheric deposition of cadmium and B(a)P for the period 1990-2020 is presented in the Joint report of the EMEP Centres for HELCOM [*Gauss et al.*, 2022]. In addition, a review of information on regulation, emissions, monitoring, and model assessment of HBCDD, PCNs and PeCB is included in the report. Besides, information on emissions and modelling results on cadmium and B(a)P is also summarized in the Baltic Environment Fact Sheets, published on the HELCOM website (http://www.helcom.fi). This information is based on the results presented to the 8th Joint session of the Working Group on Effects and the Steering Body to EMEP, which took place on 12-16 September 2022. In this section a brief outline of MSC-E contribution to the Joint EMEP report for HELCOM is provided.

Anthropogenic emissions of Cd and B(a)P in the HELCOM countries reduced from 1990 to 2020 by 66% and 23%, respectively (Fig. 4.7a). The most substantial decline of the emissions took place in period 1990-2000, while in subsequent period the rate of emission reduction slowed down. In 2020 the main contributions to Cd and B(a)P emissions among the HELCOM countries were made by Russia, Poland and Germany. Their emissions in total contributed more than 90% to total emissions of the HELCOM countries.

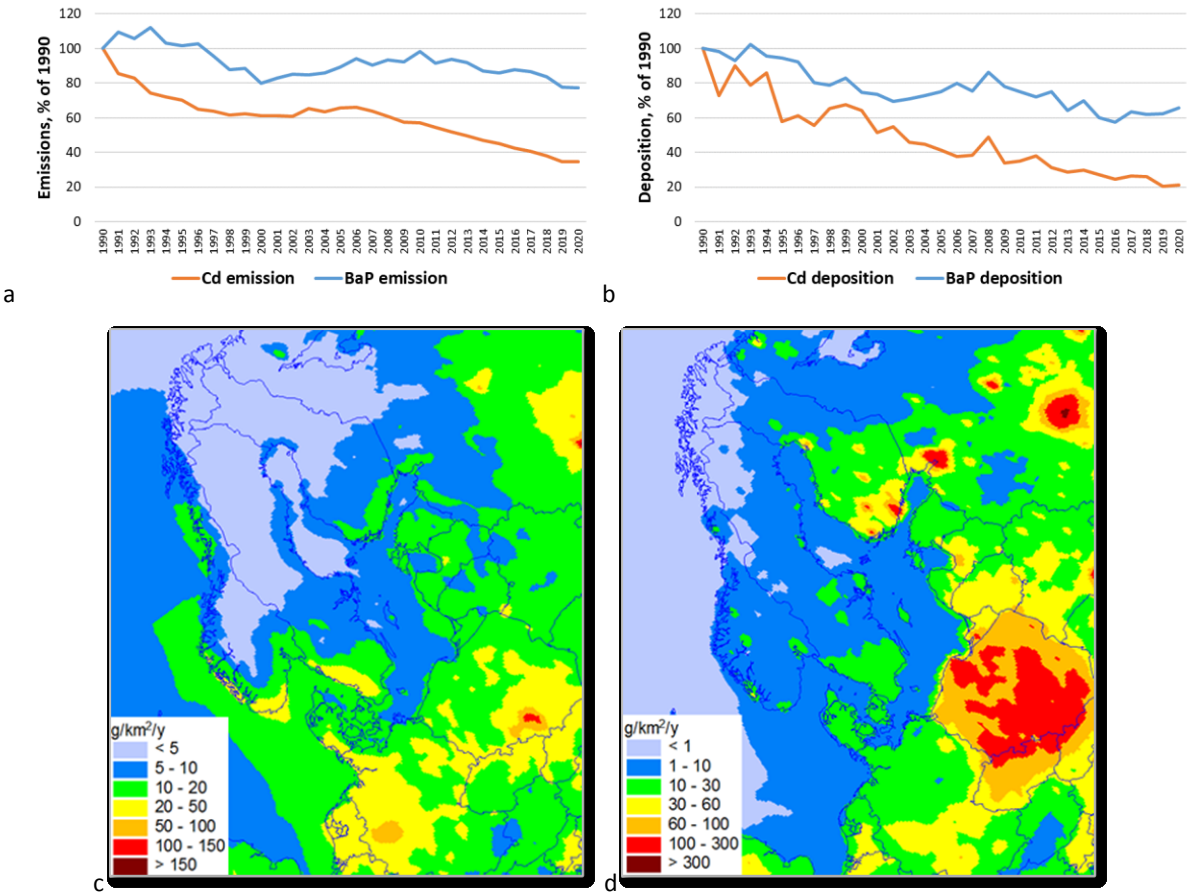

Fig. 4.7. *Relative changes of annual total emissions of HELCOM countries (a) and annual atmospheric Cd and B(a)P deposition (b) to the Baltic Sea in the period 1990-2020. Total annual deposition fluxes of Cd (c) and B(a)P (d) estimated for 2020.*

The model simulations showed large decline of Cd deposition to the Baltic Sea from 1990 to 2020 by 79%, whereas B(a)P deposition declined only by 34% (Fig. 4.7b). Significant inter-annual variability of atmospheric Cd and B(a)P deposition is noted due to changes in meteorological conditions (precipitation amount, atmospheric transport patterns) from year to year. Decline of calculated deposition varied among the different sub-basins of the Baltic Sea. Particularly, the highest reduction of Cd deposition is noted for the Sound and the Gulf of Finland sub-basins (about 80%). In case of B(a)P the highest decline is estimated for the Sound and Western Baltic sub-basins (around 50%). The highest total Cd deposition fluxes over the Baltic Sea in 2020, exceeding 10 g/km^2/y, are estimated for the Sound and the Western Baltic sub-basins (Fig. 4.7c). In case of B(a)P, the highest deposition fluxes, about 15-20 g/km^2/y, are estimated for the Gulf of Finland and Sound sub-basins (Fig. 4.7d).

Anthropogenic emission sources of the HELCOM countries contributed 43% and 76% to deposition to the Baltic Sea for Cd and B(a)P, respectively. Cd emissions of Poland and Germany were the main contributors to anthropogenic deposition of heavy metals. Main anthropogenic sources of B(a)P deposition were Poland and Finland.

The information on airborne input of Cd and B(a)P to the Baltic Sea was presented and discussed during the third informal consultation session of the HELCOM Pressure Working Group (IC PRESSURE 3-2022) held in October 2022.

4.2.3. OSPAR

Cooperation between MSC-E of EMEP and the Convention for the Protection of the Marine Environment of the North-East Atlantic (OSPAR) continued. In accordance with the contract between MSC-E and OSPAR Commission analysis of Pb, Cd and Hg emission sectors in 2020 in the OSPAR Contracting Parties (Norway, Sweden, Finland, Denmark, Germany, the Netherlands, Belgium, Luxemburg, France, Spain, Portugal, the United Kingdom, Ireland, Iceland and Switzerland) was carried out. Besides, model assessment of atmospheric inputs of Pb, Cd and Hg to the OSPAR regions (Fig. 4.8) was performed. The data for 2020 allowed updating long-term trends calculated previously for 1990-2020 (ref.). Detailed description of the results prepared for the OSPAR Commission are presented in [*Ilyin et al.*, 2023].Emission data covering the period from 1990 to 2020 used in the model assessment are prepared by the EMEP Centre on Emission Inventories and Projections (CEIP) (http://www.ceip.at/). Emissions for 2020 are based on the EMEP reporting of emissions data in 2022. Sectoral emission data in the OSPAR Contracting Parties are prepared for the following gridded NFR (Nomenclature For Reporting) emission sectors (A_PublicPower; B_Industry; C_OtherStatComb; D_Fugitive; E_Solvents; F_RoadTransport; G_Shipping; H_Aviation; I_Offroad; J_Waste; L_AgriOther and M_Other) used in the model assessments within the EMEP programme. Emission of each gridded NFR (GNFR) sector is a result of aggregation of particular NFR sectors.

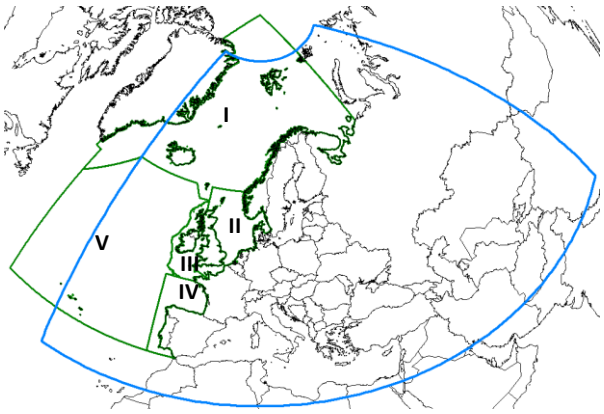

Fig. 4.8. *Borders of the EMEP domain (blue line) and OSPAR maritime area (green line) with indication of the OSPAR regions (I - V).*

Total Pb, Cd and Hg emission in the OSPAR Contracting Parties as a whole in 2020 amounted to 483, 32 and 20 tonnes, respectively. The highest emission values of these metals in 2020 were noted for Germany. German emissions of Pb, Cd and Hg in 2020 made up 143, 11, and 6 tonnes, respectively. Other major OSPAR countries-emitters were the United Kingdom, Spain and France. Contribution of these four countries to total OSPAR emission was 80% for Pb and 74% for Cd and Hg. The lowest heavy metal emissions took place in Iceland and Luxembourg.

The main emission sectors contributing to Pb emissions in the OSPAR countries were B_Industry (45%), F_RoadTransport (32%) and C_OtherStatComb (10%). The main contribution to Cd emissions in the OSPAR Contracting Parties was made by the sector B_Industry (58%), followed by C_OtherStatComb (14%) and E_Solvents (11%). In case of Hg the sectors B_Industry (46%), A_PublicPower (29%) and J_Waste (8%) were the main contributors to total emission of the OSPAR countries.

Spatial distribution of heavy metal deposition fluxes to the North-Eastern Atlantic is non-uniform. The highest deposition fluxes of Pb and Cd in 2020 are noted for the east of the North Sea (Fig. 4.9). The main reason for this is the impact of emission sources in countries surrounding the North Sea.

Besides, relatively high levels take place along the Scandinavian coast and the western coasts of the United Kingdom and Ireland, over the northern part of Wider Atlantic region and Danish Strait that is explained by high annual precipitation sums.

Distribution of Hg deposition to the OSPAR maritime area differs from that of Pb and Cd. The highest fluxes occur over the Arctic part of the OSPAR area. The reason for this is the effect of springtime Arctic Mercury Depletion Events (AMDEs) [*Steffen et al.*, 2008].Long-term deposition fluxes to the OSPAR regions were calculated for the period from 1990 to 2020. Existence of long-term declining deposition trends was confirmed by Mann-Kendall test at 0.001 level of significance. The highest decline of Pb, Cd and Hg deposition took place in Region II (Greater North Sea) and amounted to 87%, 81% and almost 50%, respectively. The lowest decline of deposition is noted for Region I (Arctic Waters) and Region V (Wider Atlantic), amounting to about 55% for Pb, about 35% - 40% for Cd and around 20% for Hg.

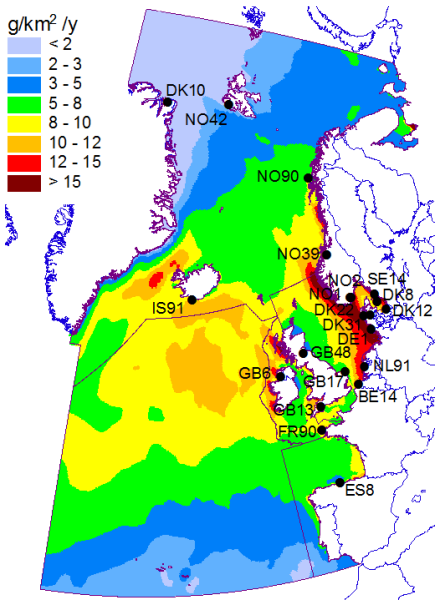

Fig. 4.9. *Spatial distribution of annual Cd deposition flux to the OSPAR maritime area in 2020. Purple lines depict borders of the OSPAR regions.*

Results of the analysis of emission data and model assessment of deposition fluxes to the OSPAR area were presented at the hybrid meeting organized by OSPAR Commission. Contribution of the emission sectors, deposition fluxes and their trends as well as comparison of modelled and observed deposition fluxes were overviewed. The results were described in the technical report submitted to OSPAR secretariat.

5. MAIN CHALLENGES AND DIRECTIONS OF FUTURE RESEARCH

The Status Report summarizes main results of the EMEP activities on heavy metal and POP pollution assessment in 2023. The report presents the information on emissions, measured and modelled pollution levels for 2021 as well as model estimates of transboundary pollution of the EMEP countries. The assessment was performed in co-operation with national experts, Subsidiary Bodies of the Convention, and international organizations. Main challenges of the pollution assessment and directions of future research are outlined below.

- PAH pollution levels are still high and exceed air quality guidelines in some of the EMEP countries indicating the need of further scientific research and reduction of population exposure to this group of pollutants. Detailed analysis of spatial and temporal variations of PAH pollution in the EMEP region and improvement of modelling approach for PAHs will be continued as a part of the TFMM/EuroDelta-Carb multi-model intercomparison study.
- Current TF HTAP activities focused on Hg pollution assessment are performed as a part of the Multi-Compartment Hg Modeling and Analysis Project (MCHgMAP). The project is aimed at comprehensive analysis of spatial and temporal trends of Hg pollution levels, source attribution and evaluation of future scenarios to inform on effectiveness of the LRTAP and the Minamata Conventions. In order to reach the goals of the project new global Hg multi-model experimental simulations of Hg will be organized.
- Wildfires are considered as a potentially significant source of emissions of a wide range of pollutants, including mercury, other heavy metals and POPs. In order to evaluate the impact of wildfires on pollution levels and intercontinental transport, TF HTAP is planning to design multi-model multi-pollutant (PM, POPs, metals, ozone) intercomparison study.
- Contaminants of emerging concern (CECs) comprise a large group of environmental pollutants that pose risk for human health and environment. Assessment of CECs pollution is subject of significant challenges that include insufficient knowledge of their sources, properties, trends in observed pollution levels, transport and fate in the environment. Preparatory work for the assessment of CECs will be continued collecting information on physical-chemical properties, monitoring of their concentrations in different environmental media, and experimental modelling of their transport and fate.
- Evaluation of adverse effects of heavy metal and POP pollution on human health and ecosystems is an important activity within the Convention coordinated by WGE. It is planned to continue joint analysis of measurements of heavy metals concentrations in mosses and deposition to various ecosystems in co-operation with ICP Vegetation, ICP Integrated Monitoring, and ICP Forests. Besides, data exchange with TF Health on PAH pollution levels and exceedances of air quality guidelines is of importance.
- Toxic pollutants such as heavy metals of first and second priority, some of POPs and CECs are known to adversely affect marine ecosystems and biota. Assessment of atmospheric pollution of the marine environment by heavy metals, POPs and CECs, including model evaluation of long-term trends and source apportionment of atmospheric load, is an important direction of further research and co-operation with HELCOM and OSPAR.

References

ALS [2013] Benzo(a)pyrene toxic equivalence quotient (TEQ) and aggregate organochlorine pesticides parameters, *EnviroMail* No. 59 Re-Release, July, 2013.

AMAP [2016] AMAP Assessment 2016: Chemicals of Emerging Arctic Concern. Arctic Monitoring and Assessment Programme (AMAP), Oslo, Norway. xvi+353pp. ISBN – 978-82-7971-104-9

AMAP/UNEP [2019] Technical Background Report for the Global Mercury Assessment 2018. Arctic Monitoring and Assessment Programme, Oslo, Norway/UN Environment Programme, Chemicals and Health Branch, Geneva, Switzerland. viii + 426 pp including E-Annexes.

Andreae M.O. and Merlet P. [2001] Emission of trace gases and aerosols from biomass burning. *Global Biogeochemical cycles*, Vol. 15, 4, 955-966.

Andreae M.O. [2019] Emission of trace gases and aerosols from biomass burning – an updated assessment. *Atmos. Chem. Phys.*, 19, 8523–8546, 2019. https://doi.org/10.5194/acp-19-8523-2019.

Arnot Jon.,Lynn McCarty, James Armitage, Liisa Toose-Reid, Frank Wania, Ian Cousins [2009] An evaluation of hexabromocyclododecane (HBCD) for Persistent Organic Pollutant (POP) properties and the potential for adverse effects in the environment. Submitted to: European Brominated Flame Retardant Industry Panel (EBFRIP). https://unece.org/fileadmin/DAM/env/documents/2009/EB/wg5/wgsr45/Informal%20docs/An%20evaluation%20of%20hexabromocyclododecane_Final%20report.pdf

Bailey R.E. [2007] Pentachlorobenzene – Sources, environmental fate and risk characterization. Euro Chlor Science Dossier, July 2007.

Bailey R.E., Van Wijk D. and P.C.Thomas [2009] Sources and prevalence of pentachlorobenzene in the environment. *Chemosphere*, 75, 555-564, 2009. DOI: 10.1016/j.chemosphere.2009.01.038.

Bidleman T. F.; P. A. Helm; B. M. Braune; G. W. Gabrielsen [2010] Polychlorinated naphthalenes in polar environments — A review. *Science of the Total Environment*, 408(15), 2919–2935. DOI:10.1016/j.scitotenv.2009.09.013.

Blankenship A., Kannan K., Villalobos S., Villeneuve D., Falandyz J., Imagawa T., Jakobsson E., Giesy J. [1999] Relative potenties of halowax mixtures and individual polychlorinated naphthalenes (PCNs) to induce Ah receptor-mediated responses in the rat hepatoma H4IIE-Luc cell bioassay, *Organohalogen Compounds*, vol.42, pp. 217-220.

Blankenship A., Kannan K., Villalobos S., Villeneuve D., Falandyz J., Imagawa T., Jakobsson E., Giesy J. [2000] Relative potencies of individual polychlorinated naphthalenes and Halowax mixtures to induce Ah receptor-mediated responses, *Environ. Sci. Technol.*, vol.34, pp. 3153-3158. DOI: 10.1021/es9914339.

Blunden, J. and T. Boyer, Eds. [2022] "State of the Climate in 2021". Bull. Amer. Meteor. Soc., 103 (8), Si–S465, https://doi.org/10.1175/2022BAMSStateoftheClimate.1.

Breivik K., Sweetman A., Pacyna J.M. and K.C.Jones [2007] Towards a global historical emission inventory for selected PCB congeners - A mass balance approach-3. An update. *Science of the Total Environment*, 377, 296-307.

Canada Communication Group [1993] Pentachlorobenzene (Priority substances list assessment report). Canadian Environmental Protection Act. Minister of Supply and Services Canada 1993. Canada Communication Group – Publishing Ottawa, Canada K1A 0S9, Cat. No. En40-215/26E, ISBN 0-662-21064-6

CCC [2022] EMEP laboratory intercomparison. Heavy metals in precipitation 2021 - % deviation from expected value. https://projects.nilu.no/ccc/intercomparison/index.html. Site visited 10.08.2023

Chayawan and Vikas [2015] Externally predictive single-descriptor based QSPRs for physico-chemical properties of polychlorinatednaphthalenes: Exploring relationships of log SW, log K-OA, and log K-OW with electron-correlation. Journal of Hazardous Materials, 296:68-81. DOI: 10.1016/j.jhazmat.2015.04.028

Dastoor A, Angot H,, Bieser J., Christensen J.H., Douglas T.A., Heimb rger-Boavida L-E., Jiskra M., Mason R.P, McLagan D.S., Obrist D. Outridge P.M., Petrova M.V., Ryjkov A., St. Pierre K.A., Schartup A.T., Soerensen A.L., Toyota K. Travnikov O., Wilson S.J.and Zdanowicz C. [2022]. Arctic mercury cycling. https://doi.org/10.1038/s43017-022-00269- w.

De Simone F., Cinnirella S., Gencarelli C.N., Yang X., Hedgecock I.M., and Pirrone N. [2015]. Model Study of Global Mercury Deposition from Biomass Burning. *Environ. Sci. Technol*. 2015, 49, 6712−672. DOI: 10.1021/acs.est.5b00969.

De Wit C. [2002] An overview of brominated flame retardants in the environment. *Chemosphere*, 46, 583–624. DOI: 10.1016/S0045-6535(01)00225-9.

De Wit H.A., Hettelingh J-P., and Harmens H. [2015] Trends in ecosystem and health responses to long-range transported atmospheric pollutants . Norwegian Institute for Water Research, 92p.

Denier van der Gon H.A.C., van het Bolscher M., Visschedijk A.J.H. and P.Y.J.Zandveld [2005] Study to the effectiveness of the UNECE persistent organic pollutants protocol and costs of possible additional measures phase I: estimation of emission reduction resulting from the implementation of the POP protocol. TNO Report B&O-A R 2005/194.

Denier van der Gon H.A.C., van het Bolscher M., Visschedijk A.J.H. and P.Y.J. Zandveld [2007] Emissions of persistent organic pollutants and eight candidate POPs from UNECE–Europe in 2000, 2010 and 2020 and the emission reduction resulting from the implementation of the UNECE POP protocol. *Atmospheric Environment* 41, 9245–9261.

Desservettaz M., Paton-Walsh C., Griffith D.W.T., Kettlewell G., Keywood M.D., Vanderschoot M.V., Ward J., Mallet M.D., Milic A., Miljevic B., Ristovski Z.D., Howard D., Edwards G.C., and Atkinson B. [2017] Emission factors of trace gases and particles from tropicalsavanna fires in Australia. *J. Geophys.Res. Atmos*.,122, 6059–6074,doi:10.1002/2016JD025925.

Dvorska A., G. Lammel, J. Klanova, I. Holoubek [2008] Kosetice, Czech Republic – ten years of air pollution monitoring and four years of evaluating the origin of persistent organic pollutants. DOI: 10.1016/j.envpol.2008.01.034.

ECHA[2009] Data on manufacture, import, export, uses and releases of HBCDD as well as information on potential alternatives to its use. ECHA_2008_2_SR04_HBCDD_report_12_01_2009.doc

ECMWF [2023] Operational archive. https://www.ecmwf.int/en/forecasts/dataset/operational-archive. Accessed 11.01.2023.

EEA [2019] EMEP/EEA air pollutant emission inventory guidebook 2019. Technical guidance to prepare national emission inventories, EEA Report No 13/2019.

Environment Canada [2005] Environment Canada, Risk Management Strategy for Pentachlorobenzene (QCB) and Tetrachlorobenzenes (TeCBs), Chemicals Control Branch, Environmental Protection Service, June 2005.

ESWI [2011] Study on waste related issues of newly listed POPs and candidate POPs. Final Report. Expert Team to Support Waste Implementation (ESWI). Source: https://ec.europa.eu/environment/pdf/waste/studies/POP_Waste_2010.pdf.

ESWI [2011] Study on waste related issues of newly listed POPs and candidate POPs. Service request under the framework contract No ENV.G.4/FRA/2007/0066. Final report of 13 April 2011.

EU [2013] Directive 2013/39/EU of the European Parliament and of the Council of 12 August 2013 amending Directives 2000/60/EC and 2008/105/EC as regards priority substances in the field of water policy. Official Journal of the European Union L 226/1, 24 August 2013.

European Commission [2014] 2014/118/EU: Commission Recommendation of 3 March 2014 on the monitoring of traces of brominated flame retardants in food Text with EEA relevance (OJ L 65 05.03.2014, p. 39, CELEX: https://eur-lex.europa.eu/legal-content/EN/TXT/?uri=CELEX:32014H0118)

Falandysz J., A. Fernandes, E. Gregoraszczuk and M. Rose [2014] The toxicological effects of halogenated naphthalenes: A review of aryl hydrocarbon receptor-mediated (dioxin-like) relative potency factors. *Journal of Environmental Science and Health* C, 32:239-272.

Fang Y., Z. Nie, J. Yang, Q. Die, J. He, H. Yu, Q. Zhou, Q. Huang [2019] Polychlorinated naphthalene emissions to the atmosphere from typical secondary aluminum smelting plants in southwestern China: concentrations, characterization, and risk evaluation. *Environmental Science and Pollution Research*, DOI:10.1007/s11356-019-04744-8.

Feiteiro J., Mariana M., Cairrão E. [2021] Health toxicity effects of brominated flame retardants: From environmental to human exposure. Environmental Pollution, 285, 117-475. DOI: 10.1016/j.envpol.2021.117475.

Fredricsson, M., Danielsson, H., Hansson, K., Pihl Karlsson, G., Nerentorp, M., Potter, A., and Leung, W. [2021] Nationellluftövervakning Sakrapport med data frånövervakninginom ProgramområdeLuftt.o.m 2019.

Friedli H. R., Radke L. F., Prescott R., Hobbs V. and P. Sinha [2003a]. Mercury emissions from the August 2001 wildfires in Washington State and an agricultural waste fire in Oregon and atmospheric mercury budget estimates. GLOBAL *BIOGEOCHEMICAL CYCLES*, VOL. 17, NO. 2, 1039, doi:10.1029/2002GB001972.

Friedli H.R., Radke L.F., Lu J.Y., Banic C.M., Leaitch W.R. and MacPherson J.I. [2003b]. Mercury emissions from burning of biomass from temperate North American forests: laboratory and airborne measurements. *Atmospheric Environment*, Volume 37, Issue 2, January 2003, Pages 253-267.

Gauss M., A. Gusev, W. Aas, V. Shatalov, I. Ilyin, O. Rozovskaya, H. Klein, A. Nyiri, N. Batrakova, N. Vulyh [2022] Atmospheric Supply of Nitrogen, Cadmium, B(a)P, HBCDD, PCNs and PeCB to the Baltic Sea in 2020 EMEP Centres Joint Report for HELCOM. MSC-W Technical Report 1/2022.

Gusev A., Ilyin I., Mantseva L., Rozovskaya O., Shatalov V. and Travnikov O. [2006]. Progress in further development of MSCE-HM and MSCE-POP models (implementation of the model review recommendations). EMEP/MSC-E Technical Report 4/2006.

Gusev A., M. G. Vivanco, M. R. Theobald, J. L. Garrido, V. Gil, F. Couvidat, A. Collette, M. Mircea, M. Adani4, I. D'Elia, R. D. Kouznetsov, E. V. Kadantsev [2022] EURODELTA-Carb exercise: Intercomparison of modelled estimates of benzo(a)pyrene (BaP) in Europe. Proceedings of HARMO21 conference.

Gusev A., O.Rozovskaya, V. Shatalov [2007] Modelling POP long-range transport and contamination levels by MSCE-POP model . EMEP/MSC-E Technical Report 1/2007.

Gusev A., O.Rozovskaya, V.Shatalov, W. Aas, P. NizzettoGusev et al., [2014] Persistent Organic Pollutants in the Environment. EMEP Status Report 3/2014.

Haglund P., L. Kaj, E. Brorström-Lundén [2011] Results from the Swedish National Screening Programme 2010. Subreport 1 Polychlorinated Naphthalenes (PCNs). Organization: Umeå University (UmU), IVL Swedish Environmental Research Institute Ltd. IVL Report B2002.

Halvorsen H. L., P. Bohlin-Nizzetto, S. Eckhardt, A. Gusev, I. S. Krogseth, C. Moeckel, V. Shatalov, L. P. Skogeng. K. Breivik [2021] Main sources controlling atmospheric burdens of persistent organic pollutants on a national scale . Ecotoxicology and Environmental Safety, DOI: 10.1016/j.ecoenv.2021.112172.

Hanberg A. , Wern F., Asplund L., Haglund E., Safe S. [1990] Swedish Dioxin Survey: Determination of 2,3,7,8 – TCDD Toxic Equivalent Factors for Some Polychlorinated Biphenyls and Naphthalenes using Biological tests. Chemosphere, vol. 20, No. 7 – 9, pp. 1161 – 1164.

HELCOM [2007] HELCOM Baltic Sea Action Plan. Adopted on 15 November 2007 in Krakow, Poland by the HELCOM Extraordinary Ministerial Meeting https://www.helcom.fi/wp-content/uploads/2019/08/BSAP_Final.pdf

Herbert B.M.J., Halsall C.J., Villa S., Fitzpatrick L., Jones K.C.,. Lee R.G.M , Kallenborn R. [2005] Polychlorinated naphthalenes in air and snow in the Norwegian Arctic: a local source or an Eastern Arctic phenomenon? *Science of the Total Environment vol*. 342, p. 145–160.

Hu J., Jin J., Wang Y., Ma Z., and Zheng, W. [2011] Levels of polybrominated diphenyl ethers and hexabromocyclododecane in the atmosphere and tree bark from Beijing, China. Chemosphere, 84(3), 355–360. DOI: 10.1016/j.chemosphere.2011.04.002.

IARC [2022] https://monographs.iarc.who.int/agents-classified-by-the-iarc/

Ilyin I., Rozovskaya O., Travnikov O., Aas W. and K.A.Pfaffhuber [2018] Assessment of heavy metal transboundary pollution on global, regional and national scales. EMEP Status Report 2/2018.

Ilyin I., N.Batrakova, A.Gusev, M.Kleimenov, O.Rozovskaya, V.Shatalov, I.Strizhkina, O.Travnikov, K.Breivik, H.L.Halvorsen, P.B.Nizzetto, K.A.Pfaffuffer, W.Aas, K.Mareckova, S.Poupa, R.Wankmueller, B.Ullrich, A.Degorska [2021]. Heavy metals and POPs: Pollution assessment of toxic substances on regional and global scales. EMEP Status Report 2/2021, 148 p. (https://msceast.org/reports/2_2022.pdf).

Ilyin I, Travnikov O. and Rozovskaya O.et al.,[2023] Assessment of Pb, Cd and Hg atmospheric pollution of OSPAR maritime area in 2020. EMEP/MSC-E Technical Report 1/2023. 47 p.

Ilyin I., N.Batrakova, A.Gusev, M.Kleimenov, O.Rozovskaya, V.Shatalov, I.Strizhkina, O.Travnikov, K.Breivik, P.B.Nizzetto, K.A.Pfaffuffer, W.Aas, S.Poupa, R.Wankmueller, B.Ullrich, M. Bank, Q. T. Ho, M. G. Vivanco, M. R. Theobald , J. L. Garrido, V. Gil, F. Couvidat, A. Collette, M. Mircea, M. Adani4, I. D'Elia, R. D. Kouznetsov, E. V. Kadantsev [2022] Assessment of heavy metal and POP pollution on global, regional and national scales. EMEP Status report 2/2022. July 2022.

Ireland EPA [2018] Ireland's Update of National Implementation Plan for the Stockholm Convention on Persistent Organic Pollutants. EPA Ireland, 2018

Jakobsson E. and L. Asplund [2000] Polychlorinated Naphthalenes (PCNs). The Handbook of Environmental Chemistry Vol. 3 Part K. New Types of Persistent Halogenated Compounds, Chapter 5, 2000.

Keyte I., R Harrison, G. Lammel [2013] Chemical reactivity and long-range transport potential of polycyclic aromatic hydrocarbons – a review. http://dx.doi.org/10.1039/c3cs60147a.

Kilanowicz, A., Markowicz, M., Klimczak, M., Stragierowicz, J., Sikora, J. [2019a] Hexachloronaphthalene as a hemostasis disturbing factor in female Wistar rats e a pilot study. *Chemosphere* 228, 577-585. DOI:10.1016/ j.chemosphere.2019.04.147.

Kilanowicz, A., Sitarek, K., Stragierowicz, J., Klimczak, M., Bruchajzer, E. [2019b] Prenatal toxicity and maternal-fetal distribution of 1,3,5,8- tetrachloronaphthalene (1,3,5,8-TeCN) in Wistar rats. *Chemosphere* 226, 75-84. DOI:10.1016/j.chemosphere.2019.03.107.

Kilanowicz, A.; K. Sitarek; M. Skrzypinska-Gawrysiak; A. Sapota [2011] Prenatal developmental toxicity of polychlorinated naphthalenes (PCNs) in the rat. DOI:10.1016/j.ecoenv.2010.08.025.

Kim K., S.A. Jahan, E. Kabir E., R.J.C. Brown [2013] A review of airborne polycyclic aromatic hydrocarbons (PAHs) and their human health effects. http://dx.doi.org/10.1016/j.envint.2013.07.019.

Kumar A. and Wu S. [2019]. Mercury Pollution in the Arctic from Wildfires: Source Attribution for the 2000s. *Environ. Sci. Technol*. 2019, 53, 11269−11275. DOI: 10.1021/acs.est.9b01773.

Lee, Robert G. M.; Thomas, Gareth O.; Jones, Kevin C. [2005] Detailed Study of Factors Controlling Atmospheric Concentrations of PCNs. *Environmental Science & Technology*, 39(13), 4729–4738. DOI:10.1021/es048156c.

Li H., Mo L., Yu Z., Sheng G., and Fu J. [2012] Levels, isomer profiles and chiral signatures of particle-bound hexabromocyclododecanes in ambient air around Shanghai, China. *Environmental Pollution*, 165, 140–146. DOI: 10.1016/j.envpol.2012.02.015.

Li L., and F. Wania [2016] Tracking chemicals in products around the world: introduction of a dynamic substance flow analysis model and application to PCBs, Environment International, 94, 674-686. DOI: 10.1016/j.envint.2016.07.005.

Li L., and F. Wania [2018] Elucidating the Variability in the Hexabromocyclododecane Diastereomer Profile in the Global Environment. *Environ. Sci. Technol*. 2018, 52, 18, 10532–10542. DOI: 10.1021/acs.est.8b03443.

Li W.-L., Huo C.-Y., Liu L.-Y., Song W.-W., Zhang Z.-F., Ma W.-L., and Li Y.-F. [2016] Multi-year air monitoring of legacy and current-use brominated flame retardants in an urban center in northeastern China. *Science of the Total Environment,* 571, 633–642. DOI: 10.1016/j.scitotenv.2016.07.031.

Li, C., Li, J., Lyu, B., Wu, Y., Yang, L., Zheng, M., Liu, G. [2021] Burden and Risk of Polychlorinated Naphthalenes in Chinese Human Milk and a Global Comparison of Human Exposure. *Environmental Science and Technology*, 55(10), 6804–6813. DOI:10.1021/acs.est.1c00605.

Liu K., Wang X., Wei N., Song Z., Li D. [2019] Accurate quantification and transport estimation of suspended atmospheric microplastics in megacities: Implications for human health. *Environment International* 132, 105127. https://doi.org/10.1016/j.envint.2019.105127.

Mackay D, Shiu W-Y, Ma K-C, Lee SC [2006] Physical-chemical properties and environmental fate for organic chemicals. 2nd ed. Boca Raton, FL, U.S.A.: CRC Press, Taylor & Francis Group. 4182 pp.

MacLeod M., H. von Waldow, P. Tay, J. M. Armitage, H. Wöhrnschimmel, W. J. Riley, T. E. McKone, K. Hungerbuhler [2011] BETR global – A geographically-explicit global-scale multimedia contaminant fate model. *Environmental Pollution* 159, 1442 – 1445.

Managaki S., Miyake Y., Yokoyama Y., Hondo H., Masunaga S., Nakai S., Kobayashi T., Kameya T., Kimura A., Nakarai T., Oka Y., Otani H. and A. Miyake [2009] Emission load of hexabromocyclododecane in Japan based on the substance flow analysis. *Organohalogen Compounds*, 71, pp.2471–2476.

McLagan D.S., Stupple G.W. , Darlington A. , Hayden K. , and Steffen A. [2021]. Where there is smoke there is mercury: Assessing boreal forest fire mercury emissions using aircraft and highlighting uncertainties associated with upscaling emissions estimates. Atmos. Chem. Phys., 21, 5635–5653, 2021 https://doi.org/10.5194/acp-21-5635-2021.

Menne, M. J., C. N. Williams, B.E. Gleason, J. J Rennie, and J. H. Lawrimore [2018] The Global Historical Climatology Network Monthly Temperature Dataset, Version 4. J. Climate, in press. doi:10.1175/JCLI-D-18-0094.1.

NILU [2018]Monitoring of environmental contaminants in air and precipitation. Annual report 2018. Author(s): Pernilla Bohlin-Nizzetto, Wenche Aas and Vladimir Nikiforov. NILU report 11/2019

NILU [2019] Monitoring of environmental contaminants in air and precipitation. Annual report 2019. Author(s): Pernilla Bohlin-Nizzetto, Wenche Aas and Vladimir Nikiforov. NILU report 06/2020.

NILU, [2021] Monitoring of environmental contaminants in air and precipitation. Annual report 2020. Author(s): Pernilla Bohlin Nizzetto, Wenche Aas, Helene Lunder Halvorsen, Vladimir Nikiforov and Katrine Aspmo Pfaffhuber. NILU report 12/2021

Nordic Council of Ministers [2007] Hexabromocyclododecane as a possible global POP. TemaNord 2008:520. Copenhagen 2007. Source: http://chm.pops.int/portals/0/repository/hbcdd/unep-pops-poprc-hbcdd-08-nor-a1.english.pdf.

OSPAR [2009] OSPAR Background Document on Certain Brominated Flame Retardants. Hazardous Substances Series. Publication Number 394/2009.

Popp W., Norpoth K., Vahrenholz C., Hamm S., Balfanz E. and J.Theisen [1997] Polychlorinated naphthalene exposures and liver function changes. *American journal of industrial medicine*, 32(4), 413–416.

Poupa S. [2022] Methodologies applied to the CEIP GNFR gap-filling 2022. Part II: Heavy Metals (Cd, Hg, Pb) and Persistent Organic Pollutants (Benzo(a)pyrene, Benzo(b)fluoranthene, Benzo(k)fluoranthene, Indeno(1,2,3-cd)pyrene, Total polycyclic aromatic hydrocarbons, Dioxin and Furan, Hexachlorobenzene, Polychlorinated biphenyls) of the year 2020. Technical report CEIP 04/2022.

Puzyn, T. and J. Falandysz [2007] QSPR Modeling of partition coefficients and Henry's law constants for 75 chloronaphthalene congeners by means of six chemometric approaches – a comparative study. Journal of Physical and Chemical Reference Data, 36:203-214. DOI: 10.1063/1.2432888.

Puzyn T., A. Mostrag, J. Falandysz, Y. Kholod and J. Leszczynski [2009] Predicting water solubility of congeners: Chloronaphthalenes—A case study. Journal of Hazardous Materials, 170, 1014–1022. DOI: 10.1016/j.jhazmat.2009.05.079.

Puzyn T., A. Mostrag, N. Suzuki and J. Falandysz [2008] QSPR-based estimation of the atmospheric persistence for chloronaphthalene congeners. Atmospheric Environment, 42:6627-6636. DOI: 10.1016/j.atmosenv.2008.04.048.

Rauert C., J. K. Schuster, A. Eng, and T. Harner [2018] Global Atmospheric Concentrations of Brominated and Chlorinated Flame Retardants and Organophosphate Esters, *Environ. Sci. Technol*. 2018, 52, 2777-2789.

Rotterdam Convention [2019] Rotterdam Convention on the prior informed consent procedure for certain hazardous chemicals and pesticides in international trade. Text and annexes. Revised in 2019. UNEP-FAO-RC-CONVTEXT-2019.English.pdf

Schrenk D., Bignami M., Bodin L., Chipman J.K., del Mazo J., Grasl-Kraupp B., Hogstrand C., Hoogenboom L., Leblanc J.-C., Nebbia C.S., Nielsen E., Ntzani E., Petersen A., Sand S., Schwerdtle T., Wallace H., Benford D., Furst P., Rose M., Ioannidou S., Nikolic M., Bordajandi L.R. and Vleminckx C. [2021] Update of the risk assessment of hexabromocyclododecanes (HBCDDs) in food. EFSA Panel on Contaminants in the Food Chain (CONTAM). EFSA Journal 2021,19(3):6421, 130 pp. doi: 10.2903/j.efsa.2021.6421.

SEDAC [2011] Global Rural-Urban Mapping Project, Version 1 (GRUMPv1): Urban Extents Grid (Africa). Palisades, NY: NASA Socioeconomic Data and Applications Center (SEDAC). Center for International Earth Science Information Network - CIESIN - Columbia University, International Food Policy Research Institute - IFPRI, The World Bank, and Centro Internacional de Agricultura Tropical - CIAT. 2011. (https://sedac.ciesin.columbia.edu/data/set/grump-v1-urbanextents/maps).

Shatalov V., Gusev A., Dutchak S., Rozovskaya O., Sokovykh V. and N.Vulykh [2010] Persistent Organic Pollutants in the Environment. EMEP Status Report 3/2010.

Shatalov V., Ilyin I., Gusev A., Rozovskaya O. and O.Travnikov [2014] Heavy Metals and Persistent Organic Pollutants: Model Assessment of Pollution and Research Activities. EMEP/MSC-E Technical report 4/2014.

Shen H., Huang Y., Wang R., Zhu D., Li W., Shen G., Wang B., Zhang Y., Chen Y., Lu Y., Chen H., Li T., Sun K., Li B., Liu W., Liu J. and S.Tao [2013] Global atmospheric emissions of polycyclic aromatic hydrocarbons from 1960 to 2008 and future predictions. *Environ Sci Technol*., 2013, 47, 12, 6415-6424.

Shen, L., Wania, F. [2005] Compilation, evaluation, and selection of physical–chemical property data for organochlorine pesticides. *J. Chem. Eng. Data* 50, 742–768. DOI: 10.1021/je049693f.

Shen, L., Wania, F., Lei, Y.D., Teixeira, C., Muir, D.C.G., Bidleman, T.F. [2005] Atmospheric distribution and long-range transport behavior of organochlorine pesticides in North America. *Environ. Sci. Technol*. 39, 409–420. DOI: 10.1021/es049489c.

Skamarock W.C., Klemp J.B., Dudhia J., Gill D.O., Barker D.M., Duda M.G., Huang X-Y., Wang W. and Powers J.G. [2008]. A Description of the Advanced Research WRF Version 3. NCAR/TN–475+STRNCAR TECHNICAL NOTE.

Sosnowska, A., M. Barycki, K. Jagiello, M. Haranczyk, A. Gajewicz, T. Kawai, N. Suzuki and T. Puzyn [2014] Predicting enthalpy of vaporization for persistent organic pollutants with Quantitative Structure–Property Relationship (QSPR) incorporating the influence of temperature on volatility. *Atmospheric Environment*, 87:10-18. DOI: 10.1016/j.atmosenv.2013.12.036.

Starek-Świechowicz, B., Budziszewska, B., & Starek, A. [2017] Hexachlorobenzene as a persistent organic pollutant: Toxicity and molecular mechanism of action. Pharmacological Reports, 69(6), 1232–1239. doi:10.1016/j.pharep.2017.06.013.

Steffen A. et al. [2008] A synthesis of atmospheric mercury depletion event chemistry in the atmosphere and snow. Atmos. Chem. Phys. 8, 1445-1482.

Travnikov O., Ilyin I. [2009] The EMEP/MSC-E mercury modeling system. In Mercury Fate and Transport in the Global Atmosphere, R. Mason, N. Pirrone, Eds. Springer, Boston, MA, pp. 571–587.

UK DEFRA [2017] National Implementation Plan for the Stockholm Convention on Persistent Organic Pollutants. United Kingdom of Great Britain and Northern Ireland. Department for Environment Food & Rural Affairs, 2017.

UNECE [2007] Exploration of management options for Polychlorinated Naphthalenes (PCN). Paper for the 6th meeting of the UNECE CLRTAP Task Force on Persistent Organic Pollutants, Vienna, 4-6 June 2007. Final. / By André Peeters Weem, The Netherlands.

UNECE [2009] Decision 2009/2. Listing of short-chain chlorinated paraffins and polychlorinated naphtalenes in annexes I and II to the 1998 Protocol on Persistent Organic Pollutants. ECE/EB.AIR/99/ADD.1. https://unece.org/DAM/env/documents/2009/EB/eb/EB%20Decisions/Decision%202009%202.e.pdf

UNECE [2010] OPTIONS FOR ADDING NEW SUBSTANCES TO THE PROTOCOL ON PERSISTENT ORGANIC POLLUTANTS. Source: https://unece.org/DAM/env/documents/2010/eb/wg5/wg47/ECE.EB.AIR.WG.5.2010.8_e.pdf.

UNECE [2015] ECE/EB.AIR/128 United Nations Economic Commission For Europe. Guidelines for Reporting Emissions and Projections Data under the Convention on Long-Range Transboundary Air Pollution. https://unece.org/fileadmin/DAM/env/documents/2015/AIR/EB/English.pdf.

UNECE [2019] Monitoring strategy for the Cooperative Programme for Monitoring and Evaluation of the Long-range Transmission of Air Pollutants in Europe for the period 2020–2029. EB Decision 2019/1, ECE/EB.AIR/144/Add.1. URL: http://www.unece.org/fileadmin/DAM/env/documents/2019/AIR/EB_Decisions/Decision_2019_1.pdf.

UNEP [2007] Report of the Persistent Organic Pollutants Review Committee on the work of its third meeting. Risk profile on pentachlorobenzene. UNEP/POPS/POPRC.3/20/Add.7 http://chm.pops.int/Portals/0/download.aspx?d=UNEP-POPS-POPRC.3-20-Add.7.English.pdf.

UNEP [2007a] Report of the Persistent Organic Pollutants Review Committee on the work of its third meeting: Addendum. Risk profile on pentachlorobenzene. UNEP/POPS/POPRC.3/20/Add.7.

UNEP [2007b] Other information provided by the intersessional working group on pentachlorobenzene. UNEP/POPS/POPRC.3/INF/21.

UNEP [2008] Report of the Persistent Organic Pollutants Review Committee on the work of its fourth meeting: Addendum. Risk management evaluation for pentachlorobenzene. UNEP/POPS/POPRC.4/15/Add.2.

UNEP [2008a] Report of the Persistent Organic Pollutants Review Committee on the work of its fourth meeting . Addendum to the risk profile for pentachlorobenzene UNEP/POPS/POPRC.4/15/Add.5 http://chm.pops.int/Portals/0/download.aspx?d=UNEP-POPS-POPRC.4-15-Add.5.English.pdf.

UNEP [2008b] Report of the Persistent Organic Pollutants Review Committee on the work of its fourth meeting. Risk management evaluation for pentachlorobenzene. UNEP/POPS/POPRC.4/15/Add.2 http://chm.pops.int/Portals/0/download.aspx?d=UNEP-POPS-POPRC.4-15-Add.2.English.pdf

UNEP [2009] SC-4/16: Listing of pentachlorobenzene. http://www.pops.int/Portals/0/download.aspx?d=UNEP-POPS-COP.4-SC-4-16.English.pdf.

UNEP [2010a]. Final review of scientific information on lead. UNITED NATIONS ENVIRONMENT PROGRAMME. Chemicals Branch, DTIE. 255 p. +annexes.

UNEP [2010b]. Final review of scientific information on cadmium. UNITED NATIONS ENVIRONMENT PROGRAMME. Chemicals Branch, DTIE. 201 p.+ annexes.

UNEP [2012] Risk profile on Chlorinated Naphthalenes. Addendum Report of the Persistent Organic Pollutants Review Committee on the work of its eighth meeting. UNEP/POPS/POPRC.8/16/Add.1.

UNEP [2015] SC-7/14: Listing of polychlorinated naphthalenes http://chm.pops.int/Portals/0/download.aspx?d=UNEP-POPS-COP.7-SC-7-14.English.pdf.

UNEP [2017] Guidance for inventory of hexabromocyclododecane (HBCD). Stockholm Convention. Draft document. Source: http://chm.pops.int/Portals/0/download.aspx?d=UNEP-POPS-NIP-GUID-InventoryAndSubstitution-HBCD-201703.En.pdf.

UNEP [2021] Guidance on preparing inventories of hexabromocyclododecane (HBCD). Secretariat of the Basel, Rotterdam and Stockholm Conventions. United Nations Environment Programme. Source: http://chm.pops.int/Implementation/NationalImplementationPlans/Guidance/tabid/7730/Default.aspx.

Urbanski S.P., Hao W.M. and Baker S. [2009] Chemical composition of wildland fire emission. In: Bytnerowicz A., Arbaugh M., Riebau A. and Andersen C. (Editors). *Developments in Environmental Science*, Volume 8. pp 79 – 107.

US EPA [1983] Category of chemical substances known as chlorinated naphthalenes: proposed determination of significant new uses. Federal register, 48(89):20668–20679.

van de Plassche E. and A. Schwegler [2002] Polychlorinated naphthalenes. Preliminary risk profile. Report L0002.A0/R0010/EVDP/TL. Ministry VROM/DGM, the Netherlands.

van der Werf G.R, Randerson J.T., Giglio L., van Leeuwen T.T., Chen Y., Rogers B.M., Mu M., van Marle M. J. E., Morton D.C., Collatz G.J, Yokelson R.J., and Kasibhatla P.S. [2017]. Global fire emissions estimates during 1997–2016. Earth Syst. Sci. Data, 9, 697–720, 2017. https://doi.org/10.5194/essd-9-697-2017.

Vikas and Chayawan [2014] Externally predictive quantitative modeling of supercooled liquid vapor pressure of polychlorinated-naphthalenes through electron-correlation based quantum-mechanical descriptors. *Chemosphere*, 95:448-454. DOI: 10.1016/j.chemosphere.2013.09.093.

Villeneuve D.L., Kannan K., Khim J.S., Falandyz J., Nikiforov V.A., Blankenshio A.L., Giesy J.P. [2000] Relative Potencies of Individual Polychlorinated Naphthalenes to Induce Dioxin-Like Responses in Fish and Mammalian In Vitro Bioassays, *Arch. Environ. Contam. Toxicol*., vol.39, pp. 273-281.

Vulykh N., O. Rozovskaya, V. Shatalov [2009] Model assessment of potential for long-range transboundary atmospheric transport and persistence of hexabromocyclododecane (HBCDD), EMEP MSC-E Information Note 4/2009.

Vulykh N., S. Dutchak, E. Mantseva, V. Shatalov [2005a] EMEP CONTRIBUTION TO THE PREPARATORY WORK FOR THE REVIEW OF THE CLRTAP PROTOCOL ON PERSISTENT ORGANIC POLLUTANTS. NEW SUBSTANCES: Model assessment of potential for long-range transboundary atmospheric transport and persistence of Pentachlorobenzene. EMEP/MSC-E Information Note 15/2005 https://en.msceast.org/reports/15_2005.pdf.

Vulykh, N., E. Mantseva, and V. Shatalov [2005b] EMEP Contribution to the Preparatory Work for the Review of the CLRTAP Protocol on POPs. New Substances: Model Assessment of Potential for Long-range Transboundary Atmospheric Transport and Persistence of Polychlorinated Naphthalene. EMEP/MSC-E Information Note 16/2005.

Wania, F., Mackay, D. [1995] A global distribution model for persistent organic chemicals. *Sci. Total Environ*. 160–161, 211–232.

WHO [2013] State of the science of endocrine disrupting chemicals 2012. Edited by Å. Bergman, J. J. Heindel, S. Jobling, K. A. Kidd and R. T. Zoeller. ISBN: 978-92-807-3274-0 (UNEP) and 978 92 4 150503 1 (WHO).

WHO [2000] Air Quality Guidelines - Second Edition. Chapter 5.11 Polychlorinated dibenzodioxins and dibenzofurans. https://www.euro.who.int/__data/assets/pdf_file/0017/123065/AQG2ndEd_5_11PCDDPCDF.pdf?ua=1.

WHO [2003] Concise International Chemical Assessment Document 55. Polychlorinated biphenyls: human health aspects. ISBN 92 4 153055 3; ISSN 1020-6167. https://www.who.int/ipcs/publications/cicad/en/cicad55.pdf?ua=1.

WHO [2017] Evolution of WHO air quality guidelines: past, present and future. Copenhagen. WHO Regional Office for Europe. (http://www.euro.who.int/__data/assets/pdf_file/0019/331660/Evolution-air-quality.pdf).

Wiedinmyer, C., Kimura, Y., McDonald-Buller, E. C., Emmons, L. K., Buchholz, R. R., Tang, W., Seto, K., Joseph, M. B., Barsanti, K. C., Carlton, A. G., and Yokelson, R. [2023]. The Fire Inventory from NCAR version 2.5: an updated global fire emissions model for climate and chemistry applications, EGUsphere [preprint], https://doi.org/10.5194/egusphere-2023-124, 2023.

Yamamoto T., Noma Y. and S.Sakai [2016] Thermal destruction of wastes containing polychlorinated naphthalenes in an industrial waste incinerator. *Environ Sci Pollut* Res. DOI 10.1007/s11356-016-7100-8.

Yamashita N., K. Kannan, T. Imagawa, A. Miyazaki, and J.P. Giesy [2000] Concentrations and Profiles of Polychlorinated Naphthalene Congeners in Eighteen Technical Polychlorinated Biphenyl Preparations. *Environ. Sci. Technol*. 2000, 34, 4236-4241. DOI: 10.1021/es001122u.

Zacs D.; Perkons I.; Pasecnaja E.; Bartkevics V. [2021]. Polychlorinated naphthalenes (PCNs) in food products in Latvia: Congener-specific analysis, occurrence, and dietary exposure of the general population. *Chemosphere*, 264, DOI:10.1016/j.chemosphere.2020.128460.

Annex A

Supplementary information on heavy metal and POP levels

A.1. EVALUATION OF MODELLING RESULTS VS. OBSERVATIONS FOR HMs

In order to verify modelling results comparison of modelled concentrations and wet deposition fluxes with the observed parameters was carried out. Observed values were measured at the EMEP monitoring stations and derived from the EBAS database (https://ebas.nilu.no/). Modelled and observed Pb, Cd and Hg annual mean concentrations in air and annual sums of wet deposition fluxes for each monitoring station are summarized in Tables A.1.2-A.1.7. The corresponding bar charts and time series for monthly values (Fig. A.1.2-4.1.12) are demonstrated for visualization purposes. Statistical indicators of the comparison are presented in Table A.1.

Some of the stations were not used in the comparison. First, the data from station NO0098R were not considered because of location of this station close to large emission source. Latvian stations LV2000U, LV5000U and LV6000U are urban stations and are not representative for verification of modelled regional-scale pollution levels. At station CZ0005R annual sums of precipitation are suspiciously low (about 2mm), which results to too low wet deposition fluxes of Pb and Cd. Therefore, wet deposition data observed at this station were also not used in the comparison. Measured Hg concentration in air (0.4 ng/m^3) was not used in the comparison since this value is quite low compared to other measured Hg concentrations and the mean global value of around 1.5 ng/m^3.

At some of the stations the difference between modelled and observed values exceeds a factor of three. These are DK0005R, EE0011R, FR0008R, FR0009R, FR0090R, HU0002R, SK0004R, SK0006R, SK0007R (Cd wet deposition), NO0056R (Pb wet deposition) and EE0009R, ES0008R, ES0009R, GB0048R, GB1055R, FR0008R, and SK0002R (Pb and Cd wet deposition). The uncertainty of the modelled deposition derived from the results of the model intercomparisons [*UNEP*, 2010a,b] is estimated at a value of a factor of two. Uncertainty on analytical methods regularly, evaluated by annual intercomparison tests under CCC supervision, is within ±30% for majority of laboratories [*CCC*, 2022]. However, this uncertainty characterizes only analytical part of monitoring, and does not take into account uncertainties associated with sampling, shipping, storage etc. Therefore, high differences between modelled and observed values are caused not only by the model uncertainties, but by other factors like uncertainties of measurement or emission data. The measured values from these stations were not used in calculations of statistical indicators (Table A.1). Nevertheless, modelled and measured values at these stations are presented in Tables A.1.2-A.7 and the corresponding bar charts (Fig. A.1, A.3, A.5, A.7, A.9, A.11).

Information from 49 stations were used in comparison of modelled and observed concentrations of Pb in air. Mean relative bias is 7% (Table A.1) indicating close agreement between modelled and observed air concentrations for the set of stations as a whole. Pearson's correlation coefficient is 0.7 indicating that spatial gradients are generally reproduced by the model. For most of the stations the difference between modelled and observed concentrations is within a factor of two. Relatively good (±50%) match between modelled and observed Pb air concentrations is noted for most of stations in

Czechia, Germany, Spain, France, the United Kingdom, Italy, the Netherlands, Norway, Poland and Slovakia.

Data from 43 stations were used in comparison of modelled and observed wet deposition fluxes of Pb. Mean relative bias is around -40% that indicates general tendency to underestimate the observed fluxes. For about half of the stations the agreement between modelled and observed values is within a factor of two. Nevertheless, spatial gradients were reproduced by the model taking into account correlation coefficient of 0.65. Reasonable (within ±50%) agreement between modelled and observed fluxes occurred for most of stations in Germany, Belgium, Poland, Sweden and Slovakia. Significant (50 – 70%) underestimation of Pb wet deposition is noted for stations in Finland, Norway, Czechia and Hungary. For stations in the United Kingdom the model tends to overestimate observed wet deposition fluxes.

Concentrations of Cd measured at 46 EMEP stations were used in the model verification. The model tends to overestimate concentrations of Cd in air, which is confirmed by mean relative bias of around 40%. Correlation coefficient is 0.65, and about 70% of model-measurement pairs fit factor of two criterion. Discrepancies between modelled and observed concentrations differ between countries and particular stations. In most stations of France, the United Kingdom, Iceland, Poland and Slovakia the model matches the observations within ±50% range. At the same time, significant overestimation of the observed levels is noted for station in Belgium, the Netherlands, a number of German, Swedish, Danish and Spanish stations.

There are 37 stations measured Cd wet deposition fluxes used in comparison of modelled and observed values. The model tends to underestimate the observed wet deposition of Cd by almost 40% on average (Table A.1). For most of stations the difference between modelled and observed wet deposition fluxes lie within a factor of two. At most stations in Germany, Belgium, Denmark, the United Kingdom, the Netherlands, Sweden and Slovenia the model agrees with observations within ±50% limits. At the same time, underestimation is noted for most of stations in Czechia, Finland, France, Iceland and Norway.

There are 11 stations which report measured concentrations of elemental or total gaseous Hg in air. The data from station ES0008R were not used in comparison because of suspiciously low measured levels. Besides, the data from station DE0002R cover only four months of year 2021. They do not characterize annual situation and therefore are not included into annual statistics. Mean relative bias is 6% that indicated good reproduction of mean observed Hg levels. Due to smooth spatial distribution of Hg in air correlation coefficient is not high. For particular stations the difference between modelled and observed Hg concentrations is better than ±25%.

Wet deposition fluxes of Hg were measured at 22 EMEP stations. The model overestimates the observed wet deposition (MRB = 58%). Most of model-observation pairs match the factor of two criterion. Overestimation of the observed Hg levels can be caused by uncertainties of mercury atmospheric chemistry and insufficient information on speciation of Hg in the anthropogenic emissions.

Table A.1. *Statistical indices of comparison of modelled and observed mean annual concentrations in air and wet deposition fluxes in 2021.*

Substance	Parameter	N	MRB, %	Rc	F2(%)
Pb	Air conc.	49	7	0.7	76
	Wet dep.	40	-39	0.65	58
Cd	Air conc.	46	38	0.65	72
	Wet dep.	37	-37	0.6	65
Hg	Air conc.	9	6	-0.4	100
	Wet dep.	22	58	0.4	55

A.1.1. Lead

Air concentrations

Table A.2. *Annual mean modelled and observed Pb air concentrations, ng/m³, temporal correlation coefficient (Rc) and relative bias (Bias) at EMEP stations in 2021.*

Station name	Code	Longitude	Latitude	Observed	Modelled	Rc	Bias
Koksijde	BE0014R	2.66	51.12	2.97	5.18	0.57	74.69
Kosetice (NOAK)	CZ0003R	15.08	49.57	1.86	2.26	0.51	21.76
Churanov	CZ0005R	13.60	49.07	0.67	0.93	0.45	38.25
Westerland	DE0001R	8.31	54.93	1.33	1.72	0.72	29.37
Waldhof	DE0002R	10.76	52.80	2.38	2.30	0.84	-3.08
Schauinsland	DE0003R	7.91	47.91	0.81	1.75	0.24	115.53
Neuglobsow	DE0007R	13.03	53.17	2.20	2.01	0.76	-8.68
Schmucke	DE0008R	10.77	50.65	1.15	1.61	0.24	39.70
Zingst	DE0009R	12.72	54.44	1.48	1.92	0.82	29.31
Anholt	DK0008R	11.52	56.72	0.88	1.24	0.51	40.07
Station-Nord	DK0010G	-16.67	81.60	0.15	0.04	0.13	-71.72
Riscoe	DK0012R	12.09	55.69	1.01	2.93	0.80	190.14
Lahemaa	EE0009R	25.90	59.50	1.58	0.61	0.44	-61.40
San Pablo de los Montes	ES0001R	-4.35	39.55	1.14	1.10	0.38	-3.38
Viznar	ES0007R	-3.53	37.24	1.32	1.42	0.08	8.23
Niembro	ES0008R	-4.85	43.44	2.79	1.90	-0.53	-31.91
Campisabalos	ES0009R	-3.14	41.27	0.99	1.02	0.78	3.30
ElTorms	ES0014R	0.73	41.39	0.97	1.72	0.74	77.07
Montseny	ES1778R	2.35	41.77	1.21	3.33	-0.46	175.86
Virolahti III	FI0018R	27.67	60.53	1.79	0.49	0.69	-72.47
Pallas (Matorova)	FI0036R	24.24	68.00	0.38	0.18	0.22	-51.49
Hyytiälä	FI0050R	24.28	61.85	0.93	0.24	0.48	-73.90
Donon	FR0008R	7.13	48.50	1.35	1.40	0.63	3.94
Revin	FR0009R	4.63	49.90	3.62	1.70	0.66	-52.99
Peyrusse Vieille	FR0013R	0.18	43.62	1.40	1.10	0.61	-21.58
Saint-Nazaire-le-Desert	FR0023R	5.28	44.57	1.23	1.02	0.72	-17.36
Verneuil	FR0025R	2.61	46.81	1.45	1.15	0.74	-20.66
Kergoff	FR0028R	-2.94	48.26	1.10	1.46	0.48	32.32
Yarner Wood	GB0013R	-3.71	50.60	1.66	1.73	0.75	4.52
Heigham Holmes	GB0017R	1.62	52.72	2.87	2.94	0.61	2.39
Auchencorth Moss	GB0048R	-3.24	55.79	0.72	1.26	-0.58	74.14
Chilbolton Observatory	GB1055R	-1.44	51.15	3.03	2.65	0.88	-12.31
K-puszta	HU0002R	19.58	46.97	1.84	3.58	0.82	94.97
Vestmannaeyjar	IS0091R	-20.29	63.40	0.10	0.68	-0.41	558.78
Momte-Martano	IT0019R	12.57	42.81	1.37	1.84	0.27	33.95
Rucava	LV0010R	21.17	56.16	2.22	1.12	0.38	-49.73
Bilthoven	NL0008R	5.20	52.12	3.60	3.15	0.74	-12.51
Birkenes II	NO0002R	8.25	58.39	0.42	0.43	0.53	2.07
Zeppelin mountain (Ny-Alesund)	NO0042G	11.89	78.91	0.16	0.20	-0.21	20.74
Alomar	NO0090R	16.01	69.28	0.14	0.42	-0.06	190.58
Diabla Gora	PL0005R	22.07	54.15	1.81	1.64	0.60	-9.34
Zielonka	PL0009R	17.93	53.66	2.50	2.61	0.36	4.65
Bredkälen	SE0005R	15.33	63.85	0.18	0.16	-0.04	-10.58
Råö	SE0014R	11.91	57.39	0.59	0.93	0.63	57.53
Hallahus	SE0020R	13.15	56.04	0.74	1.55	-0.09	111.14
Iskrba	SI0008R	14.87	45.57	1.13	1.05	0.31	-6.93
Chopok	SK0002R	19.58	48.93	0.76	1.58	0.20	107.94
Stara Lesna	SK0004R	20.28	49.15	2.52	2.18	-0.06	-13.60
Starina	SK0006R	22.27	49.05	2.01	1.66	0.41	-17.27
Topolniky	SK0007R	17.86	47.96	4.46	3.64	0.79	-18.51

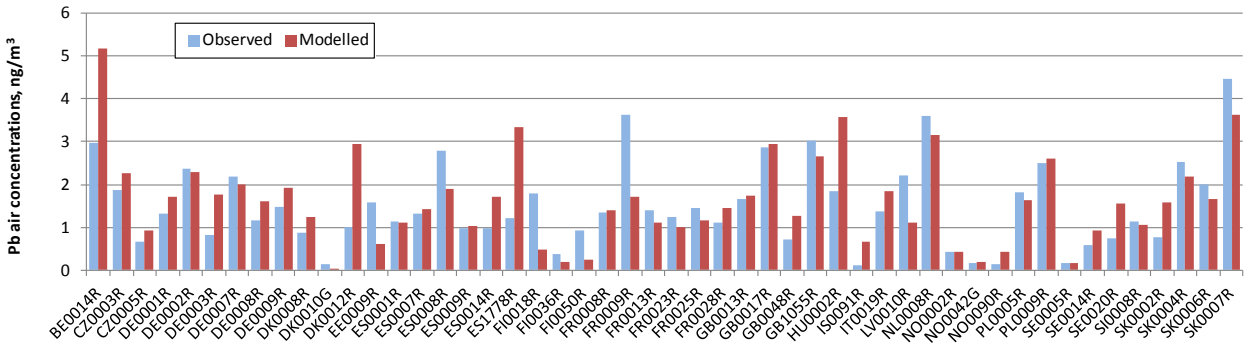

Fig. A.1. *Modelled and observed annual mean concentrations of Pb in air at the EMEP stations in 2021.*

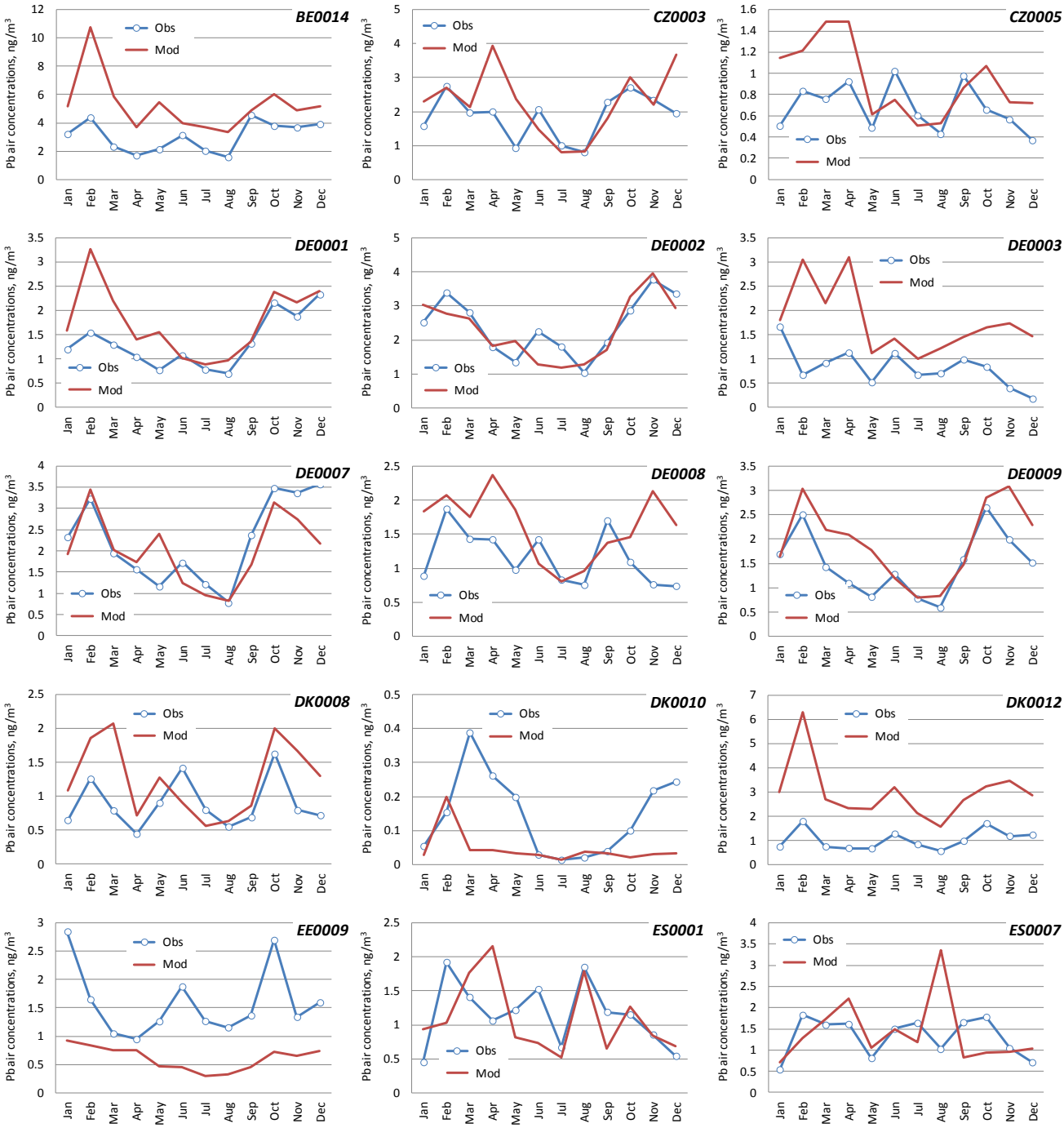

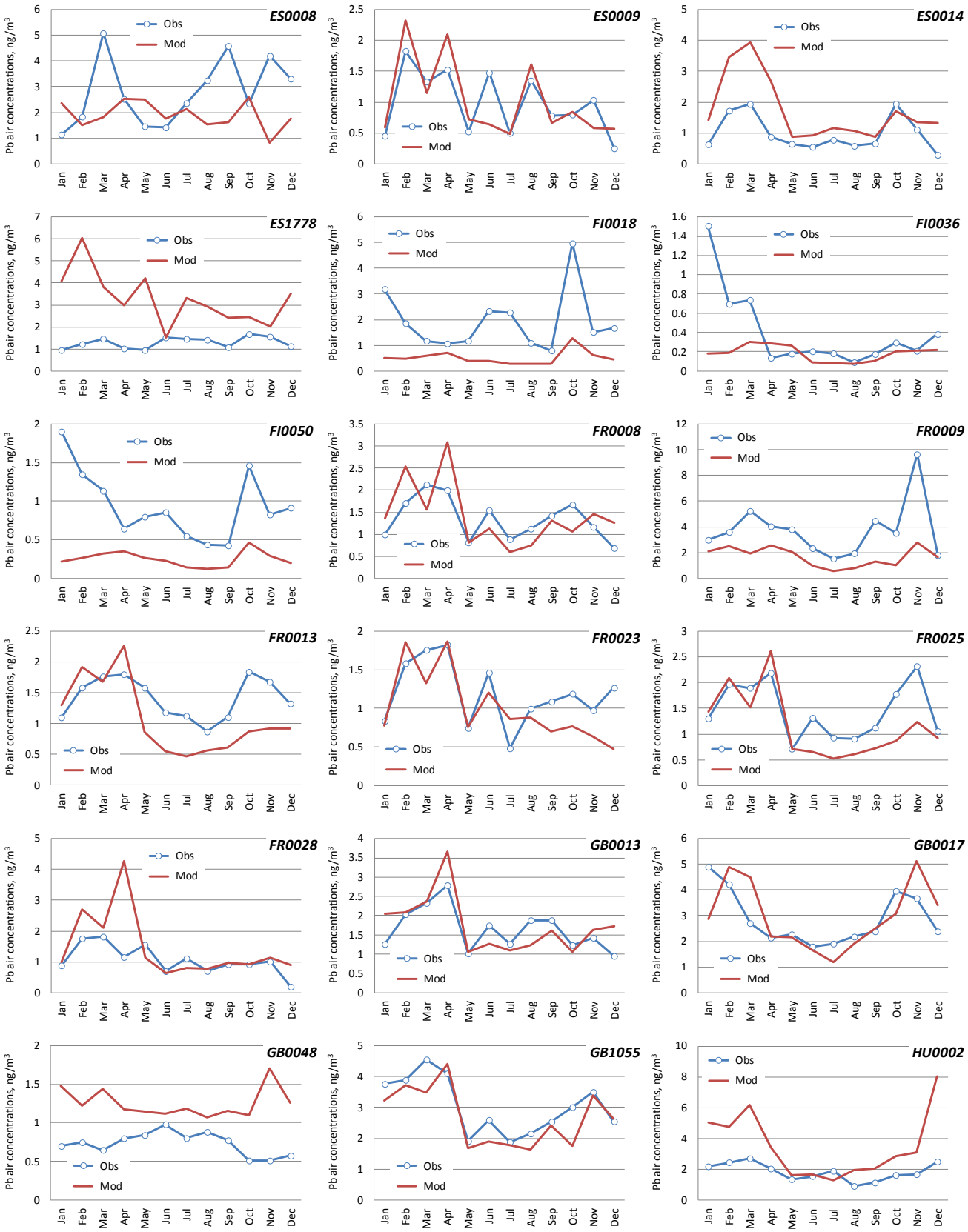
ES0008
ES0009
ES0014
ES1778
FI0018
FI0036
FI0050
FR0008
FR0009
FR0013
FR0023
FR0025
FR0028
GB0013
GB0017
GB0048
GB1055
HU0002
Obs
Mod
Pb air concentrations, ng/m³
Jan
Feb
Mar
Apr
May
Jun
Jul
Aug
Sep
Oct
Nov
Dec

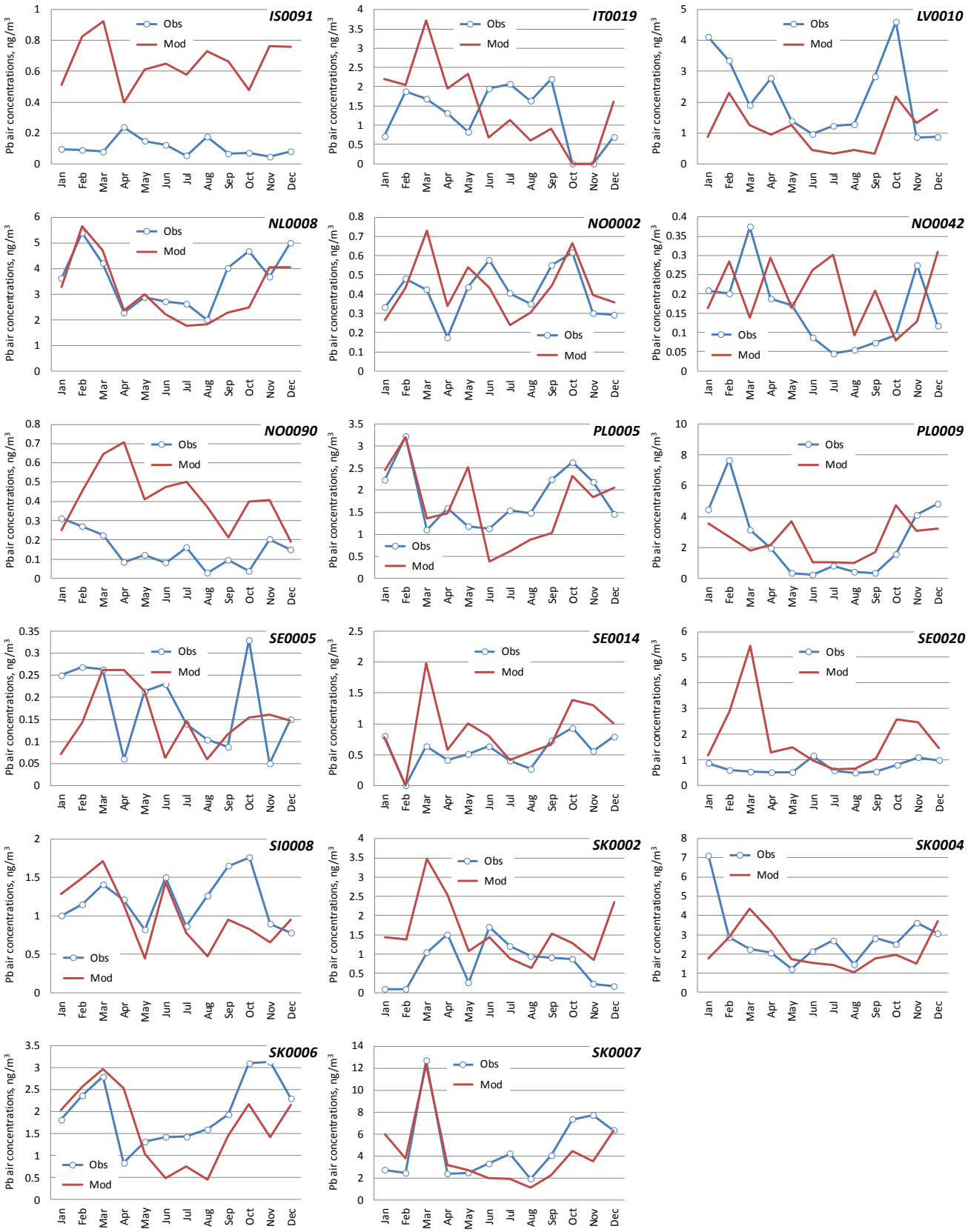

***Fig. A.2**. Modelled and observed monthly mean concentrations of Pb in air at the EMEP stations in 2021.*

Wet deposition

Table A.3. *Annual sums of modelled and observed Pb wet deposition fluxes, g/km²/y, temporal correlation coefficient (Rc) and relative bias (Bias) at EMEP stations in 2021.*

Station name	Code	Longit	Latit	Observed flux	Modelled flux	Rc	Bias
Koksijde	BE0014R	2.66	51.12	350.24	355.97	0.53	1.6
Kosetice (NOAK)	CZ0003R	15.08	49.57	520.18	189.58	0.75	-63.6
Westerland	DE0001R	8.31	54.93	195.53	274.63	0.86	40.5
Waldhof	DE0002R	10.76	52.80	177.76	196.87	0.34	10.7
Schauinsland	DE0003R	7.91	47.91	320.52	267.69	0.28	-16.5
Neuglobsow	DE0007R	13.03	53.17	269.62	280.66	0.63	4.1
Schmucke	DE0008R	10.77	50.65	481.58	299.52	0.11	-37.8
Zingst	DE0009R	12.72	54.44	176.23	215.28	0.57	22.2
Lahemaa	EE0009R	25.90	59.50	183.50	59.03	0.14	-67.8
Vilsandi	EE0011R	21.82	58.38	183.53	138.91	0.38	-24.3
Niembro	ES0008R	-4.85	43.44	6607.72	196.87	0.38	-97.0
Campisabalos	ES0009R	-3.14	41.27	1191.94	105.47	0.34	-91.2
Virolahti III	FI0018R	27.67	60.53	373.35	138.74	0.50	-62.8
Pallas (Matorova)	FI0036R	24.24	68.00	95.64	52.20	0.74	-45.4
Hyytiälä	FI0050R	24.28	61.85	250.10	91.68	0.39	-63.3
Hailuoto II	FI0053R	24.69	65.00	187.47	90.55	0.68	-51.7
Hietajärvi	FI0092R	30.72	63.17	197.08	70.91	0.78	-64.0
Kotinen	FI0093R	25.07	61.23	234.97	122.89	0.57	-47.7
Donon	FR0008R	7.13	48.50	944.10	180.86	-0.07	-80.8
Revin	FR0009R	4.63	49.90	713.92	270.47	0.76	-62.1
Peyrusse Vieille	FR0013R	0.18	43.62	273.43	122.60	0.09	-55.2
Saint-Nazaire-le-Desert	FR0023R	5.28	44.57	653.40	354.75	0.24	-45.7
Vemeuil	FR0025R	2.61	46.81	436.70	189.06	0.22	-56.7
Kergoff	FR0028R	-2.94	48.26	275.65	105.15	0.68	-61.9
Porspoder	FR0090R	-4.75	48.52	456.29	216.14	0.79	-52.6
LoughNavar	GB0006R	-7.87	54.44	42.22	124.80	0.48	195.6
Yamer Wood	GB0013R	-3.71	50.60	45.39	118.34	0.92	160.7
Heigham Holmes	GB0017R	1.62	52.72	52.06	127.59	-0.05	145.1
Auchencorth Moss	GB0048R	-3.24	55.79	23.03	95.25	0.42	313.5
Chilbolton Observatory	GB1055R	-1.44	51.15	12.79	102.28	0.77	699.9
K-puszta	HU0002R	19.58	46.97	687.60	235.14	0.51	-65.8
Vestmannaeyjar	IS0091R	-20.29	63.40	363.52	196.52	-0.32	-45.9
Rucava	LV0010R	21.17	56.16	468.00	235.81	0.67	-49.6
Vredepeel	NL0010R	5.85	51.54	660.53	226.81	0.15	-65.7
De Zilk	NL0091R	4.50	52.30	352.06	288.07	0.39	-18.2
Birkenes	NO0001R	8.25	58.38	462.44	264.88	0.91	-42.7
Kårvatn	NO0039R	8.88	62.78	430.83	143.13	0.05	-66.8
Hurdal	NO0056R	11.08	60.37	542.47	147.81	0.68	-72.8
Leba	PL0004R	17.53	54.75	185.75	167.14	0.22	-10.0
Diabla Gora	PL0005R	22.07	54.15	276.94	246.40	0.22	-11.0
Bredkälen	SE0005R	15.33	63.85	155.50	82.33	0.45	-47.1
Råö	SE0014R	11.91	57.39	334.32	295.07	0.93	-11.7
Hallahus	SE0020R	13.15	56.04	234.40	287.98	0.80	22.9
Iskrba	SI0008R	14.87	45.57	597.73	347.76	0.28	-41.8
Chopok	SK0002R	19.58	48.93	1597.38	335.49	0.56	-79.0
Stara Lesna	SK0004R	20.28	49.15	610.17	467.68	0.22	-23.4
Starina	SK0006R	22.27	49.05	676.85	382.28	0.65	-43.5
Topolniky	SK0007R	17.86	47.96	585.12	282.53	-0.06	-51.7

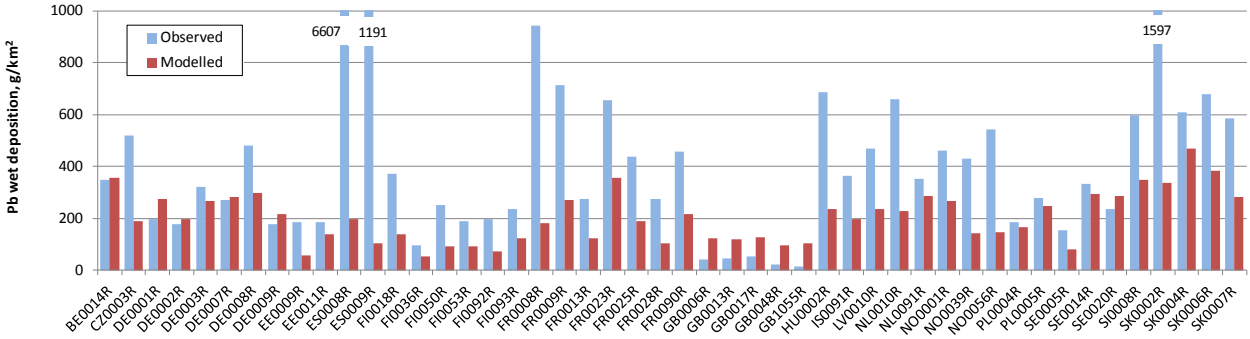

Fig. A.3. *Modelled and observed annual wet deposition fluxes of Pb at the EMEP stations in 2021.*

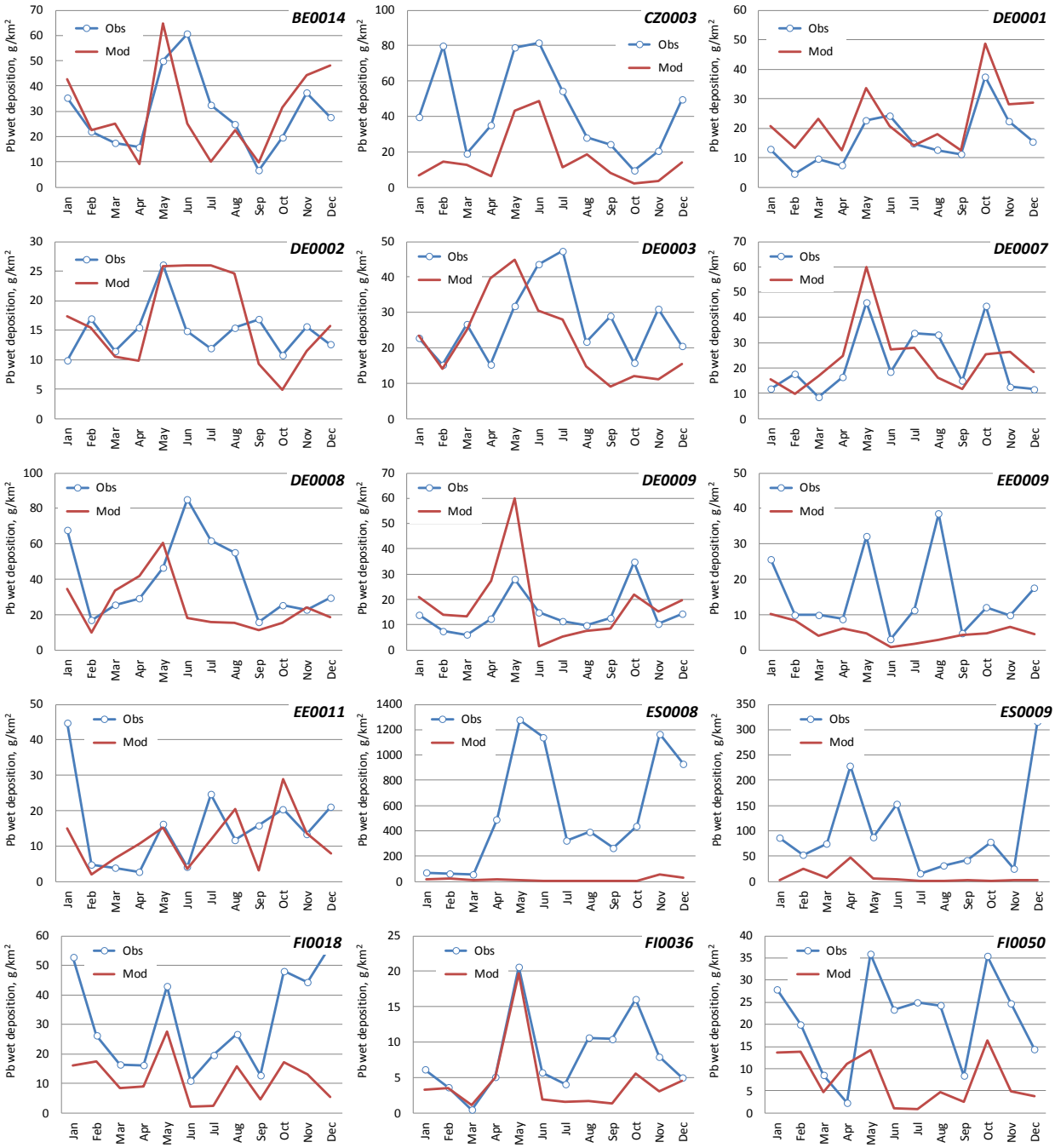

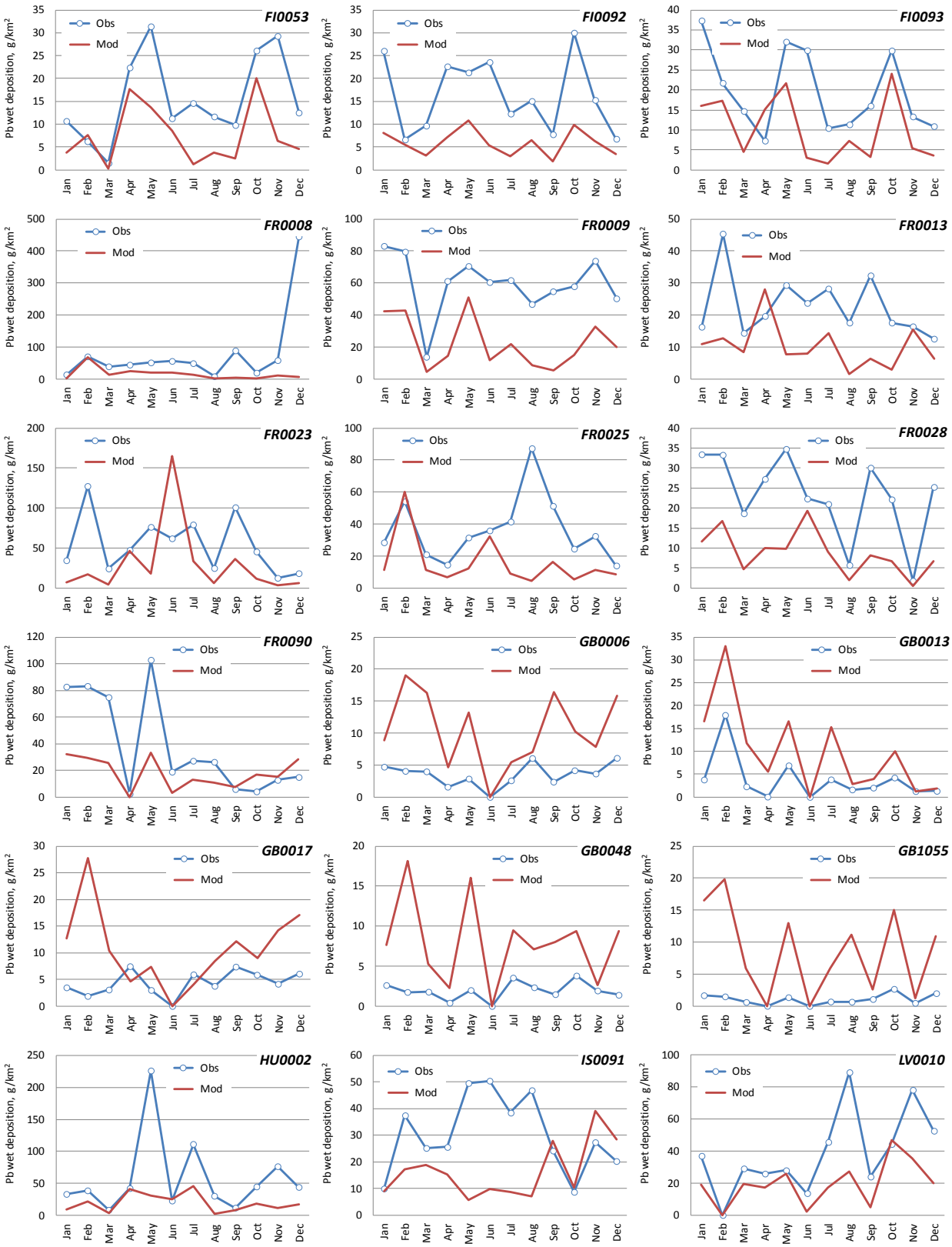
FI0053
FI0092
FI0093
FR0008
FR0009
FR0013
FR0023
FR0025
FR0028
FR0090
GB0006
GB0013
GB0017
GB0048
GB1055
HU0002
IS0091
LV0010
Obs
Mod
Pb wet deposition, g/km²
Jan
Feb
Mar
Apr
May
Jun
Jul
Aug
Sep
Oct
Nov
Dec

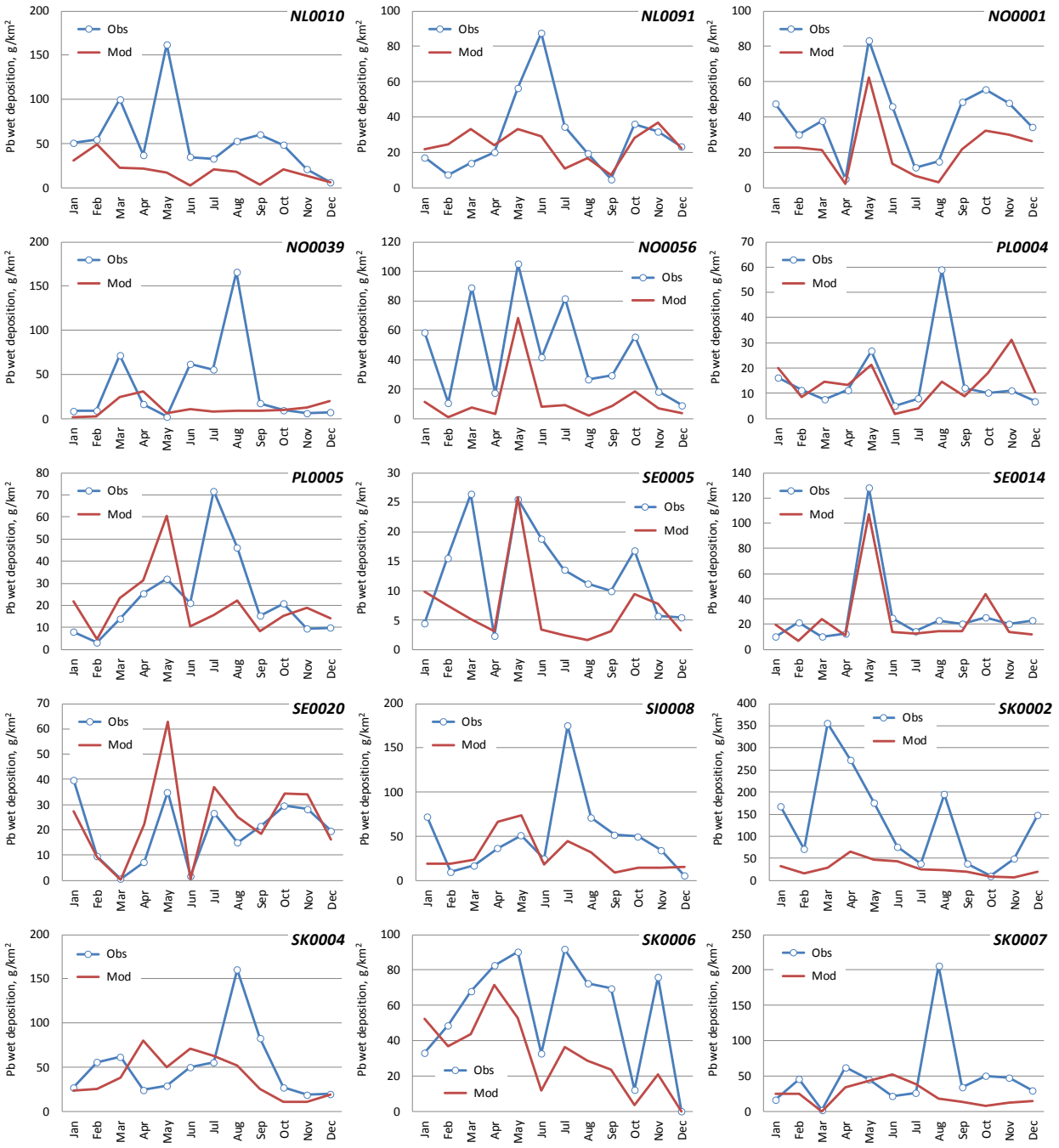

Fig. A.4. *Modelled and observed monthly wet deposition fluxes of Pb at the EMEP stations in 2021.*

A.1.2. Cadmium

Air concentrations

Table A.4. *Annual mean modelled and observed Cd air concentrations, ng/m³, temporal correlation coefficient (Rc) and relative bias (Bias) at EMEP stations in 2021.*

Station name	Code	Longit	Latid	Observed	Modelled	Rc	Bias
Koksijde	BE0014R	2.66	51.12	0.08	0.19	0.69	143.56
Kosetice (NOAK)	CZ0003R	15.08	49.57	0.07	0.09	0.49	26.95
Churanov	CZ0005R	13.6	49.07	0.02	0.05	0.37	117.20
Westerland	DE0001R	8.31	54.93	0.04	0.08	0.94	85.66
Waldhof	DE0002R	10.76	52.8	0.07	0.11	0.75	42.15
Schauinsland	DE0003R	7.91	47.91	0.02	0.07	0.36	280.66
Neuglobsow	DE0007R	13.03	53.17	0.07	0.07	0.77	-3.25
Schmucke	DE0008R	10.77	50.65	0.03	0.07	0.64	142.66
Zingst	DE0009R	12.72	54.44	0.05	0.07	0.71	43.90
Anholt	DK0008R	11.52	56.72	0.03	0.05	0.59	97.43
Station-Nord	DK0010G	-16.67	81.6	0.00	0.00	0.36	-51.21
Riscoe	DK0012R	12.09	55.69	0.03	0.12	0.84	272.34
Lahemaa	EE0009R	25.9	59.5	0.05	0.03	0.22	-32.15
San Pablo de los Montes	ES0001R	-4.35	39.55	0.02	0.05	0.79	94.28
Viznar	ES0007R	-3.53	37.24	0.03	0.05	-0.13	96.75
Niembro	ES0008R	-4.85	43.44	0.07	0.06	0.16	-4.23
Campisabalos	ES0009R	-3.14	41.27	0.02	0.04	0.69	83.16
ElTorms	ES0014R	0.73	41.39	0.03	0.07	0.75	136.64
Montseny	ES1778R	2.35	41.77	0.04	0.14	0.50	298.77
Virolahti III	FI0018R	27.67	60.53	0.05	0.02	0.77	-59.89
Pallas (Matorova)	FI0036R	24.24	68	0.01	0.01	0.43	-34.96
Hyytiälä	FI0050R	24.28	61.85	0.04	0.01	0.64	-73.07
Donon	FR0008R	7.13	48.5	0.03	0.05	0.82	57.70
Revin	FR0009R	4.63	49.9	0.10	0.08	0.59	-19.45
Peyrusse Vieille	FR0013R	0.18	43.62	0.04	0.04	0.58	-19.99
Saint-Nazaire-le-Desert	FR0023R	5.28	44.57	0.03	0.03	0.66	-11.16
Verneuil	FR0025R	2.61	46.81	0.05	0.04	0.66	-32.21
Kergoff	FR0028R	-2.94	48.26	0.04	0.04	0.64	0.18
Yarner Wood	GB0013R	-3.71	50.6	0.06	0.07	0.42	22.72
Heigham Holmes	GB0017R	1.62	52.72	0.08	0.11	0.58	28.03
Auchencorth Moss	GB0048R	-3.24	55.79	0.02	0.05	0.10	145.42
Chilbolton Observatory	GB1055R	-1.44	51.15	0.08	0.11	0.60	26.48
K-puszta	HU0002R	19.58	46.97	0.04	0.18	0.32	336.55
Vestmannaeyjar	IS0091R	-20.29	63.4	0.02	0.02	-0.40	15.85
Monte-Martano	IT0019R	12.57	42.81	0.03	0.05	0.60	66.98
Rucava	LV0010R	21.17	56.16	0.07	0.05	0.41	-33.86
Bilthoven	NL0008R	5.2	52.12	0.08	0.18	0.86	120.88
Birkenes II	NO0002R	8.25	58.39	0.02	0.02	0.57	6.15
Zeppelin mountain (Ny-Alesund)	NO0042G	11.89	78.91	0.02	0.01	-0.18	-55.04
Alomar	NO0090R	16.01	69.28	0.01	0.02	-0.09	153.88
Diabla Gora	PL0005R	22.07	54.15	0.04	0.05	0.63	43.58
Zielonka	PL0009R	17.93	53.66	0.12	0.08	0.49	-39.55
Bredkälen	SE0005R	15.33	63.85	0.01	0.01	-0.12	-15.48
Råö	SE0014R	11.91	57.39	0.02	0.04	0.65	57.17
Hallahus	SE0020R	13.15	56.04	0.02	0.05	0.04	132.68
Iskrba	SI0008R	14.87	45.57	0.05	0.09	0.31	63.47
Chopok	SK0002R	19.58	48.93	0.02	0.08	-0.29	249.59
Stara Lesna	SK0004R	20.28	49.15	0.07	0.09	-0.28	28.08
Starina	SK0006R	22.27	49.05	0.07	0.07	-0.03	9.49
Topolniky	SK0007R	17.86	47.96	0.08	0.14	0.34	75.36

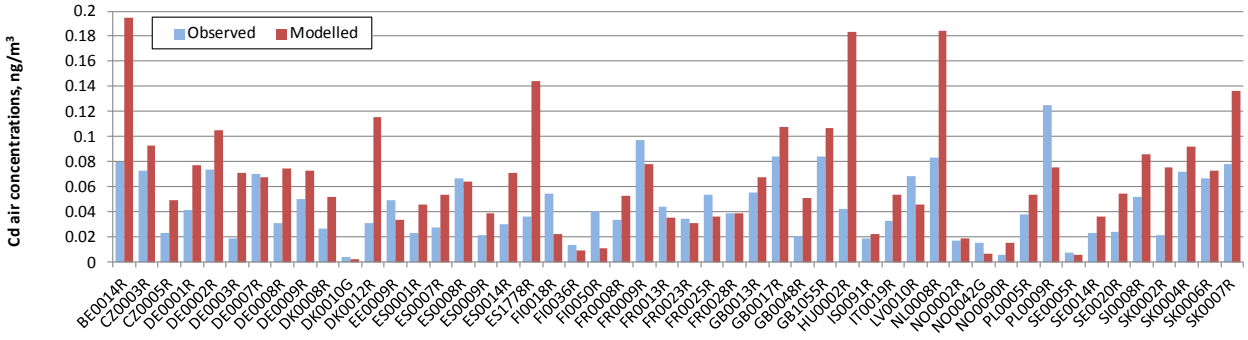

***Fig. A.5**. Modelled and observed annual mean concentrations of Cd in air at the EMEP stations in 2021.*

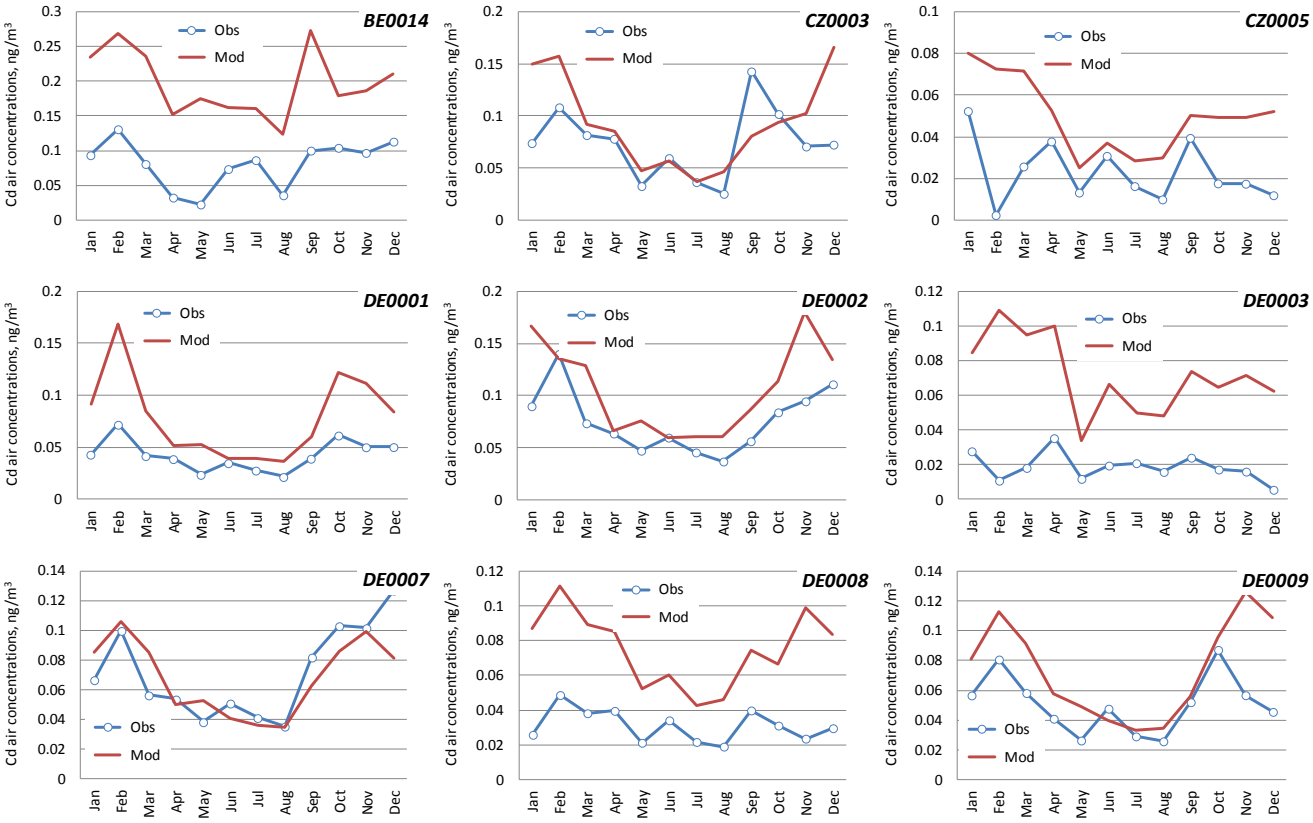

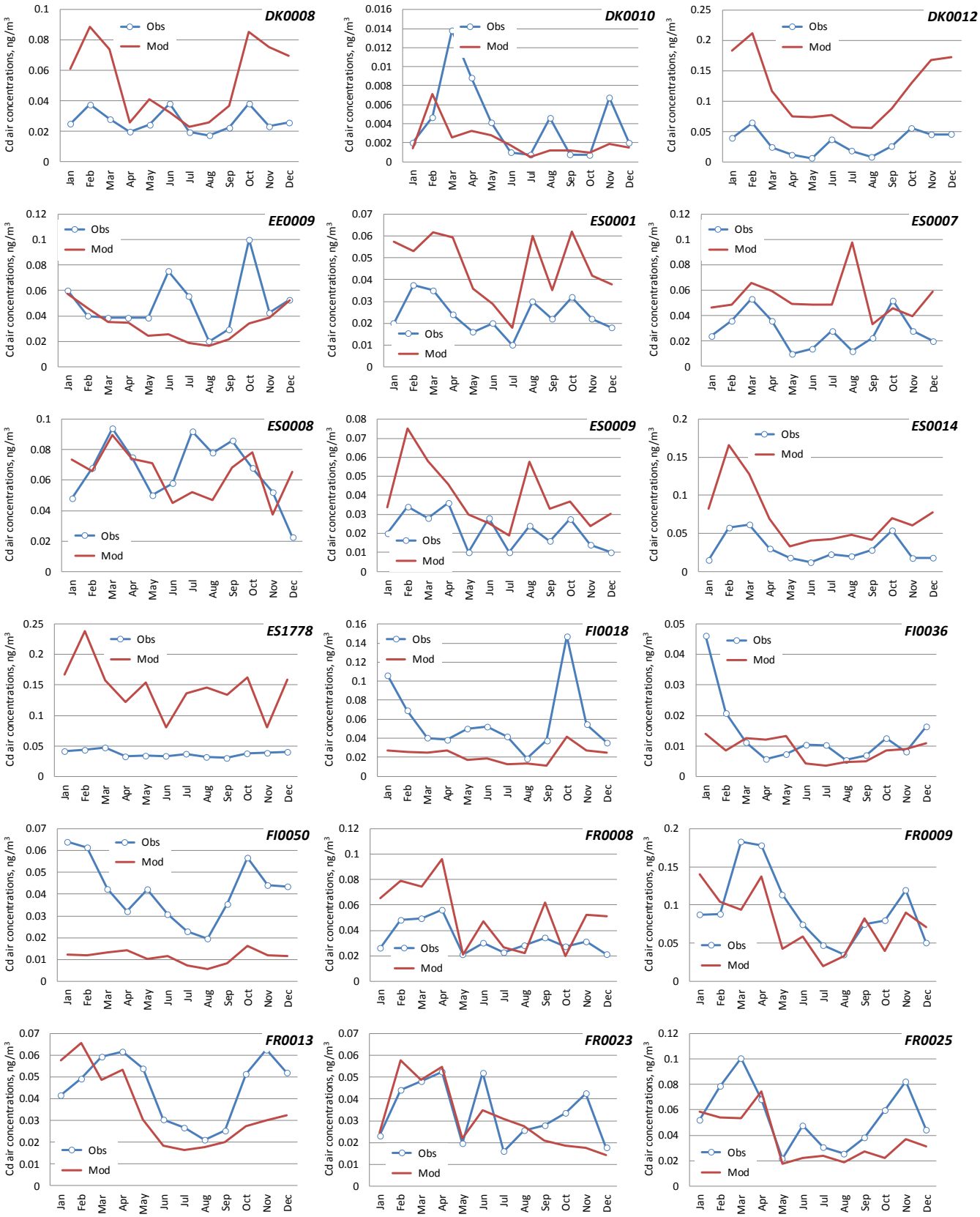
DK0008
DK0010
DK0012
EE0009
ES0001
ES0007
ES0008
ES0009
ES0014
ES1778
FI0018
FI0036
FI0050
FR0008
FR0009
FR0013
FR0023
FR0025
Obs
Mod
Cd air concentrations, ng/m³
Jan
Feb
Mar
Apr
May
Jun
Jul
Aug
Sep
Oct
Nov
Dec

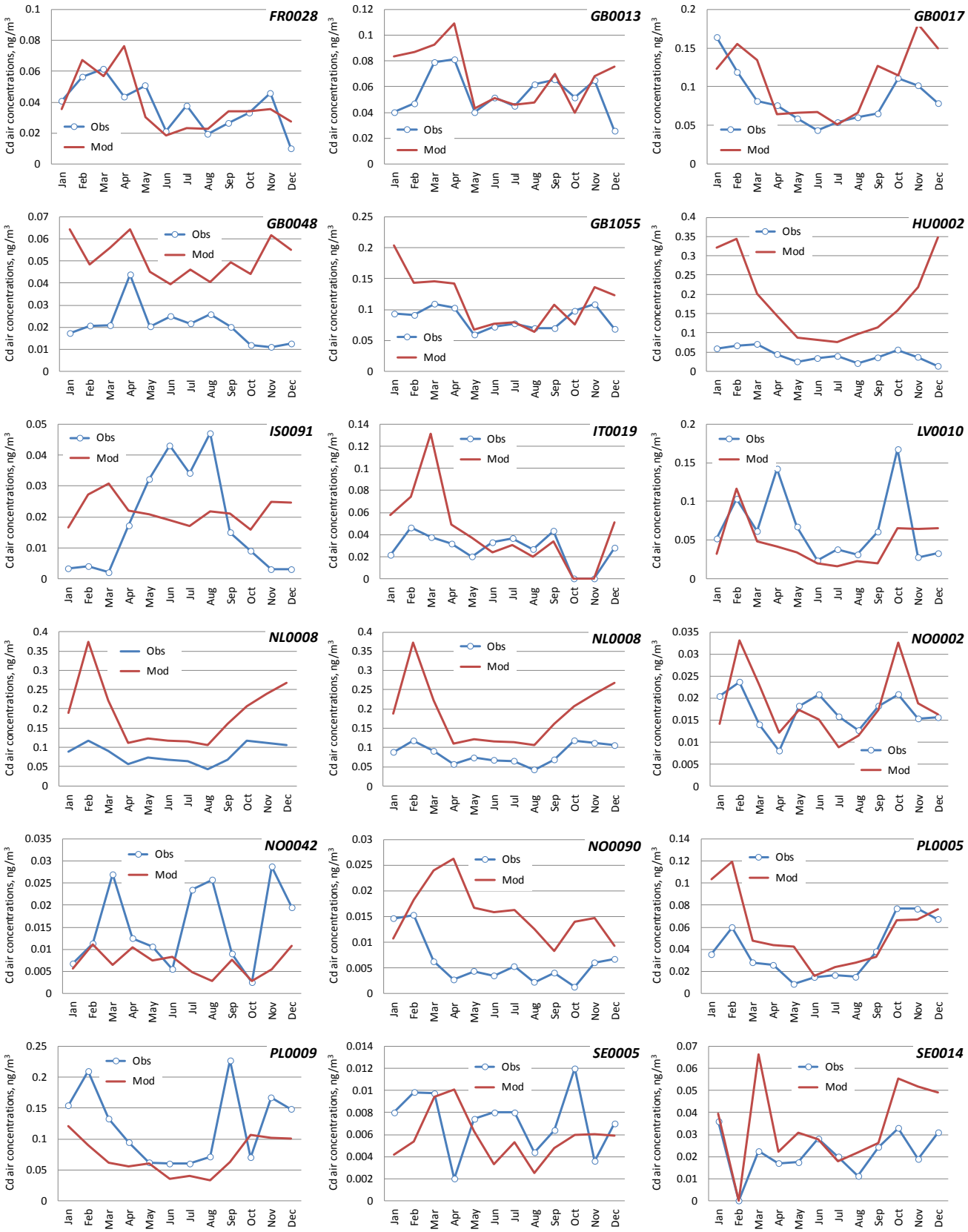
FR0028
GB0013
GB0017
GB0048
GB1055
HU0002
IS0091
IT0019
LV0010
NL0008
NL0008
NO0002
NO0042
NO0090
PL0005
PL0009
SE0005
SE0014
Obs
Mod
Cd air concentrations, ng/m³
Jan
Feb
Mar
Apr
May
Jun
Jul
Aug
Sep
Oct
Nov
Dec

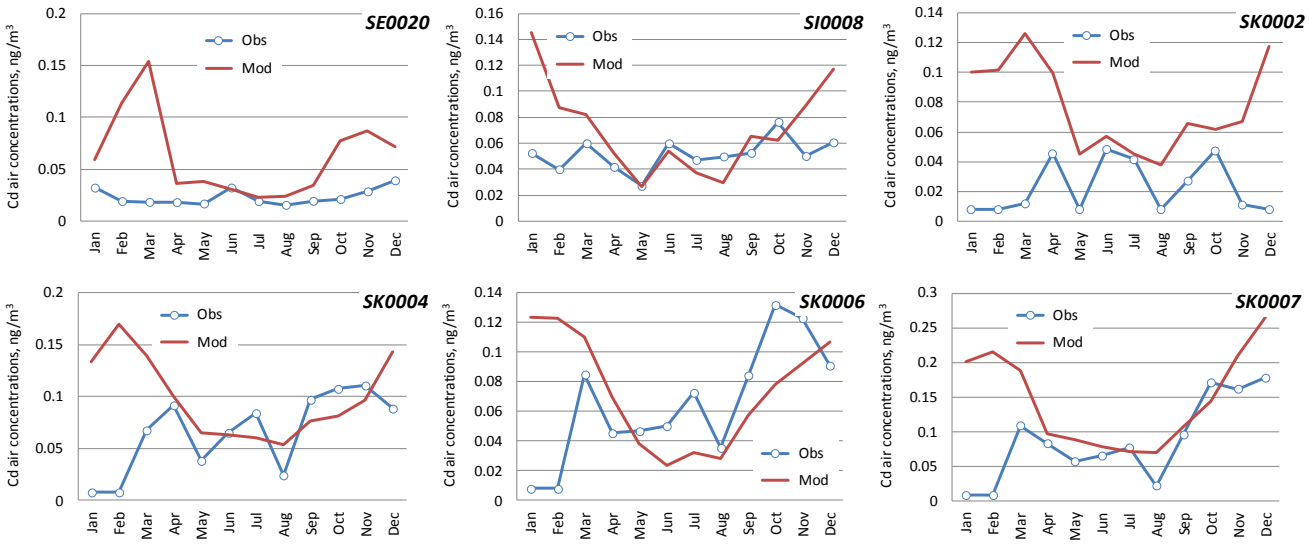

Fig. A.6. *Modelled and observed annual mean concentrations of Cd in air at the EMEP stations in 2021.*

Cadmium wet deposition

Table A.5. *Annual sums of modelled and observed Cd wet deposition fluxes, g/km²/y, temporal correlation coefficient (Rc) and relative bias (Bias) at EMEP stations in 2021.*

Station name	Code	Longit	Latit	Observed flux	Modelled flux	Rc	Bias
Koksijde	BE0014R	2.66	51.12	14.26	12.82	0.55	-10.1
Kosetice (NOAK)	CZ0003R	15.08	49.57	17.69	7.23	0.71	-59.1
Westerland	DE0001R	8.31	54.93	7.08	10.86	0.82	53.4
Waldhof	DE0002R	10.76	52.8	8.04	9.98	0.60	24.2
Schauinsland	DE0003R	7.91	47.91	10.72	9.97	0.69	-7.0
Neuglobsow	DE0007R	13.03	53.17	8.54	9.88	0.34	15.6
Schmucke	DE0008R	10.77	50.65	16.03	15.87	0.08	-1.0
Zingst	DE0009R	12.72	54.44	7.60	7.12	0.65	-6.3
Keldsnor	DK0005R	10.74	54.75	41.31	7.61	0.09	-81.6
Anholt	DK0008R	11.52	56.72	10.02	6.46	0.85	-35.5
Riscoe	DK0012R	12.09	55.69	21.33	10.37	0.93	-51.4
Sepstrup Sande	DK0022R	9.42	56.08	14.18	9.95	0.84	-29.8
Ulborg	DK0031R	8.43	56.29	13.08	9.99	0.57	-23.6
Lahemaa	EE0009R	25.9	59.5	17.17	2.74	0.11	-84.0
Vilsandi	EE0011R	21.82	58.38	15.61	4.76	0.79	-69.5
Niembro	ES0008R	-4.85	43.44	86.08	6.12	0.54	-92.9
Campisabalos	ES0009R	-3.14	41.27	174.77	3.94	-0.10	-97.7
Virolahti III	FI0018R	27.67	60.53	12.21	6.12	0.64	-49.9
Pallas (Matorova)	FI0036R	24.24	68	2.86	2.18	0.75	-23.8
Hyytiälä	FI0050R	24.28	61.85	10.45	3.65	0.28	-65.0
Hailuoto II	FI0053R	24.69	65	6.62	3.59	0.73	-45.8
Hietajärvi	FI0092R	30.72	63.17	8.58	3.28	0.45	-61.8
Kotinen	FI0093R	25.07	61.23	8.61	4.84	0.56	-43.7
Donon	FR0008R	7.13	48.5	46.76	6.44	-0.22	-86.2
Revin	FR0009R	4.63	49.9	44.70	8.56	-0.09	-80.8
Peyrusse Vieille	FR0013R	0.18	43.62	12.39	4.42	0.10	-64.4
Saint-Nazaire-le-Desert	FR0023R	5.28	44.57	30.47	10.23	0.11	-66.4
Verneuil	FR0025R	2.61	46.81	16.68	6.86	-0.20	-58.9
Kergoff	FR0028R	-2.94	48.26	14.42	4.44	-0.15	-69.2
Porspoder	FR0090R	-4.75	48.52	28.82	7.98	0.70	-72.3
LoughNavar	GB0006R	-7.87	54.44	3.40	5.15	0.42	51.6
Yarner Wood	GB0013R	-3.71	50.6	5.89	5.69	0.65	-3.4
Heigham Holmes	GB0017R	1.62	52.72	3.50	5.18	0.39	48.1
Auchencorth Moss	GB0048R	-3.24	55.79	0.70	2.88	0.52	308.9
Chilbolton Observatory	GB1055R	-1.44	51.15	0.38	2.89	0.75	658.3
K-puszta	HU0002R	19.58	46.97	72.35	11.08	0.47	-84.7
Vestmannaeyjar	IS0091R	-20.29	63.4	19.51	6.79	-0.30	-65.2
Rucava	LV0010R	21.17	56.16	23.29	8.19	0.77	-64.8
Vredepeel	NL0010R	5.85	51.54	27.07	21.16	0.51	-21.8
De Zilk	NL0091R	4.5	52.3	9.84	10.04	0.52	2.0
Birkenes	NO0001R	8.25	58.38	15.91	11.02	0.74	-30.7
Kårvatn	NO0039R	8.88	62.78	10.80	5.33	0.12	-50.6
Hurdal	NO0056R	11.08	60.37	12.60	4.64	0.84	-63.2
Leba	PL0004R	17.53	54.75	7.25	5.78	0.33	-20.3
Diabla Gora	PL0005R	22.07	54.15	21.27	7.64	0.75	-64.1
Bredkälen	SE0005R	15.33	63.85	6.50	2.61	-0.05	-59.8
Råö	SE0014R	11.91	57.39	12.36	7.51	0.15	-39.2
Hallahus	SE0020R	13.15	56.04	22.17	11.78	0.50	-46.9
Iskrba	SI0008R	14.87	45.57	15.19	13.66	0.42	-10.1
Chopok	SK0002R	19.58	48.93	157.73	11.61	0.19	-92.6
Stara Lesna	SK0004R	20.28	49.15	54.34	16.69	0.60	-69.3
Starina	SK0006R	22.27	49.05	110.88	16.08	0.16	-85.5
Topolniky	SK0007R	17.86	47.96	39.75	12.34	0.42	-69.0

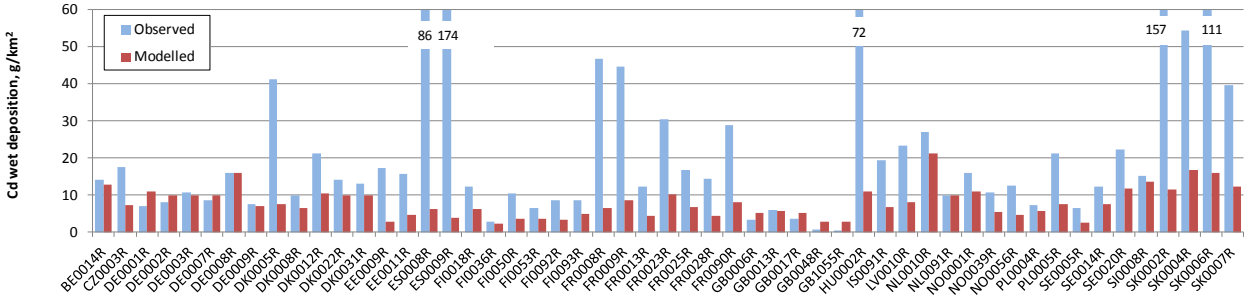

Fig. A.7. *Modelled and observed annual wet deposition fluxes of Cd at the EMEP stations in 2021.*

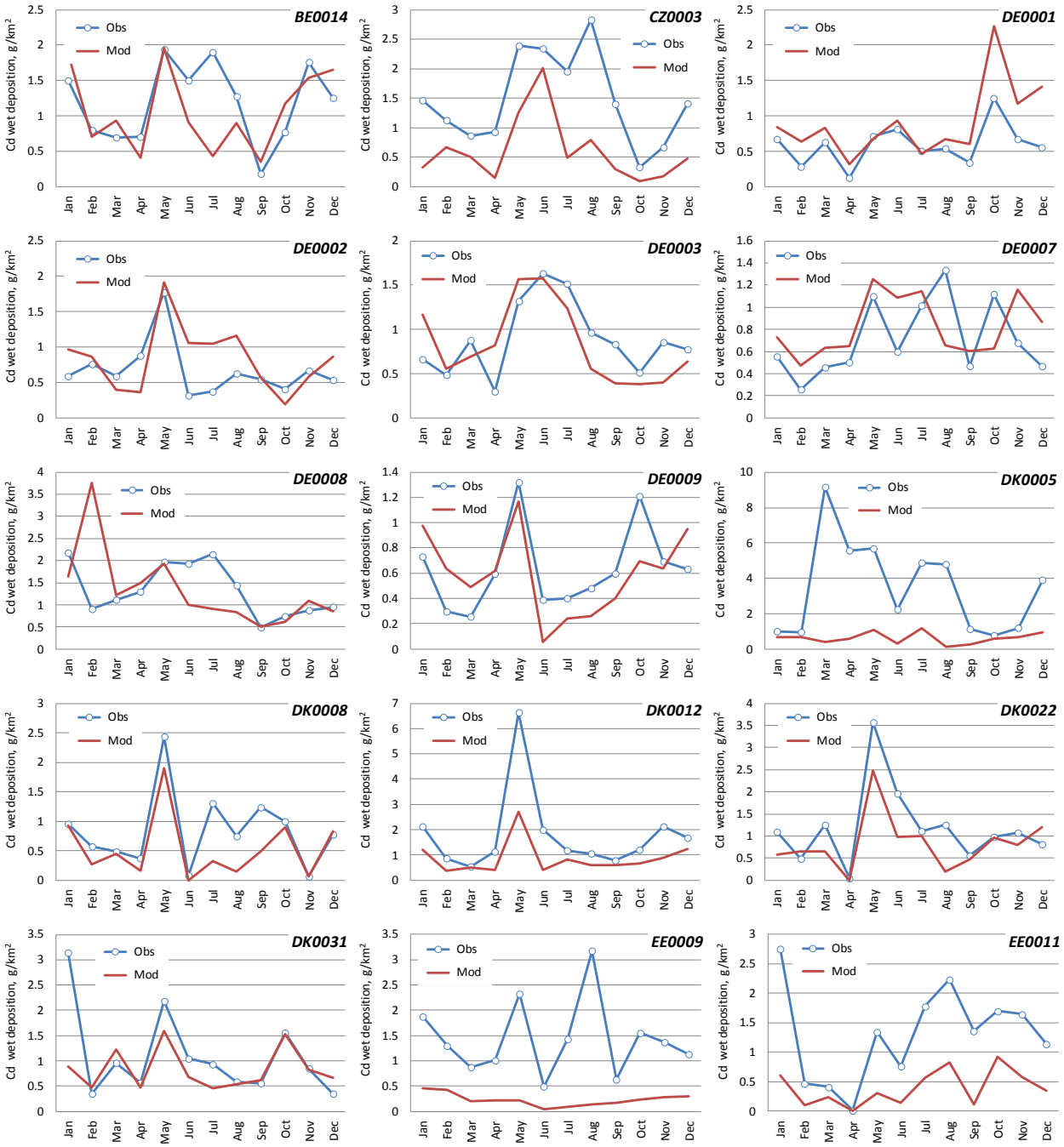

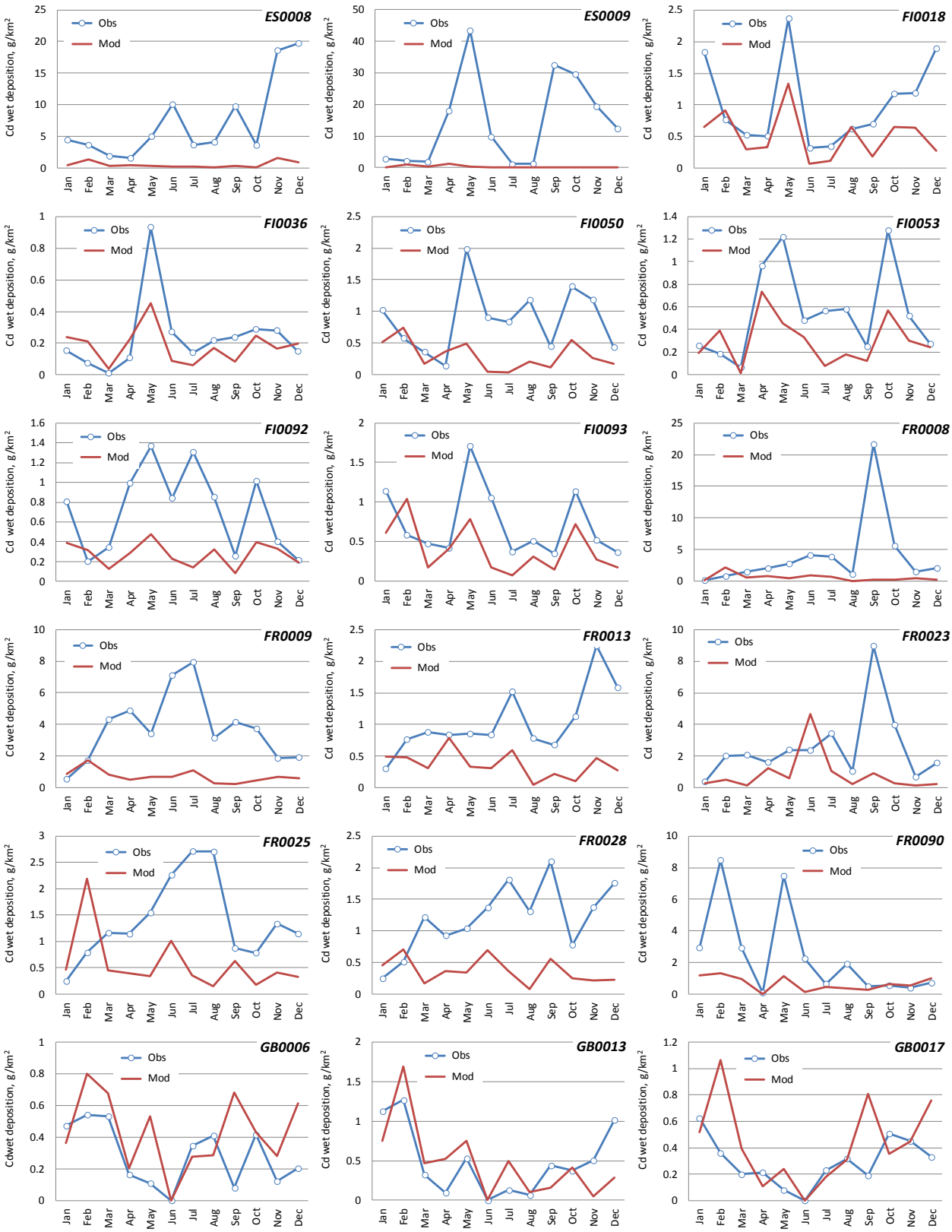
ES0008
ES0009
FI0018
FI0036
FI0050
FI0053
FI0092
FI0093
FR0008
FR0009
FR0013
FR0023
FR0025
FR0028
FR0090
GB0006
GB0013
GB0017
Obs
Mod
Cd wet deposition, g/km²
Jan
Feb
Mar
Apr
May
Jun
Jul
Aug
Sep
Oct
Nov
Dec

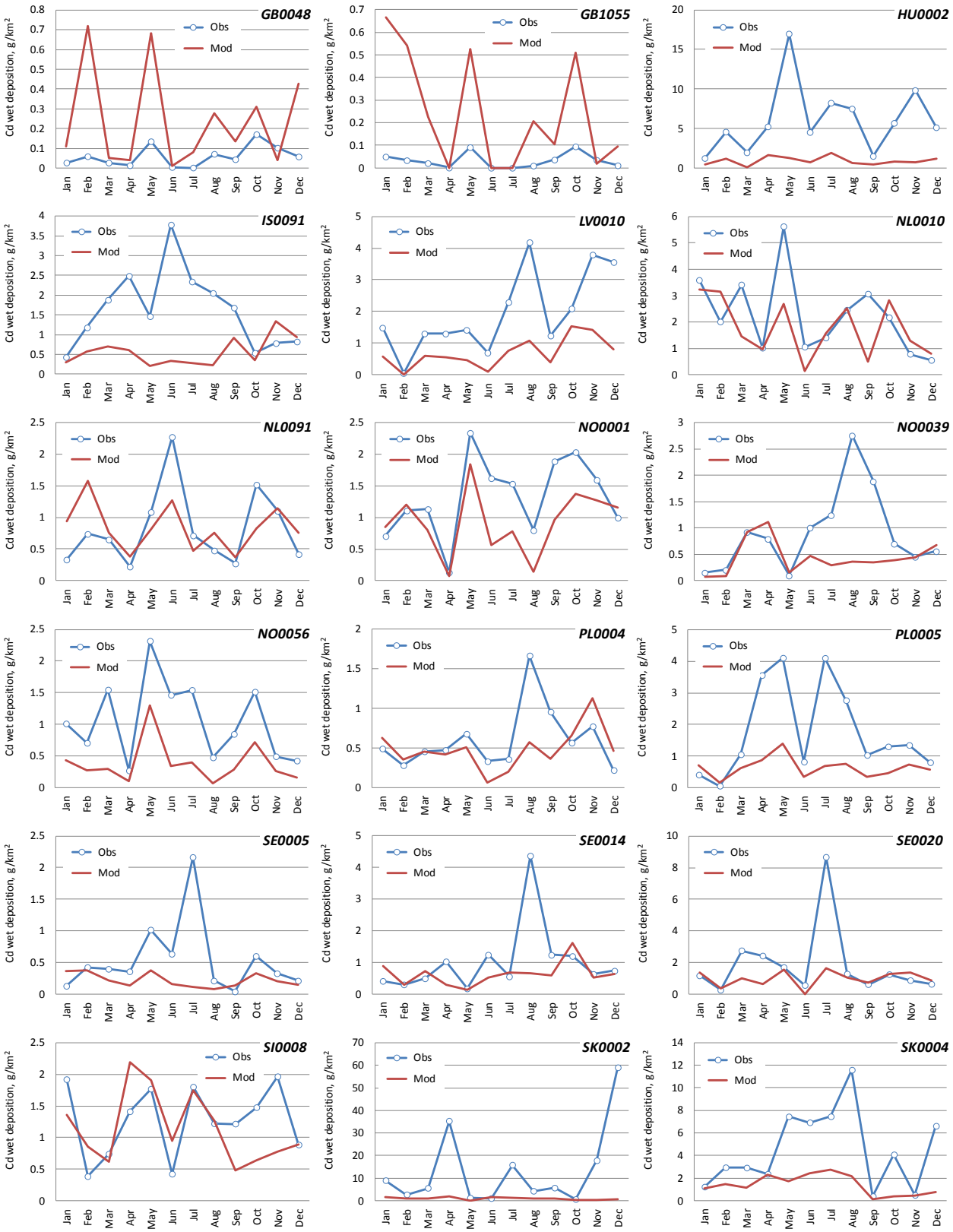
GB0048
GB1055
HU0002
IS0091
LV0010
NL0010
NL0091
NO0001
NO0039
NO0056
PL0004
PL0005
SE0005
SE0014
SE0020
SI0008
SK0002
SK0004
Obs
Mod
Cd wet deposition, g/km²
Jan
Feb
Mar
Apr
May
Jun
Jul
Aug
Sep
Oct
Nov
Dec

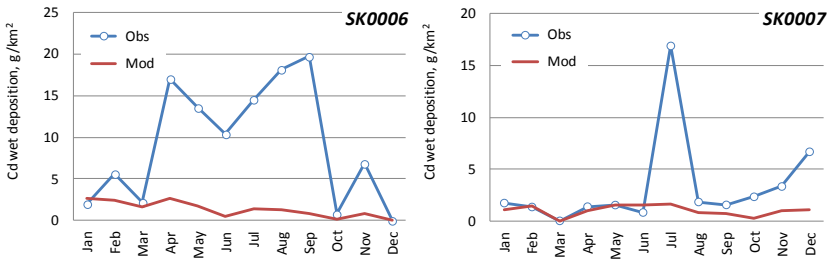

Fig. A.8. *Modelled and observed monthly wet deposition fluxes of Cd at the EMEP stations in 2021.*

A.1.3. Mercury

Air concentrations

Table A.6. *Annual mean modelled and observed Hg air concentrations, ng/m³, temporal correlation coefficient (Rc) and relative bias (Bias) at EMEP stations in 2021.*

Station Name	Code	Longitude	Latitude	Observed	Modelled	Rc	Bias
Waldhof	DE0002R	10.76	52.8	1.52	1.50	0.99	-1.51
Schauinsland	DE0003R	7.91	47.91	1.15	1.40	0.95	21.14
Schmucke	DE0008R	10.77	50.65	1.34	1.43	-0.67	6.52
Zingst	DE0009R	12.72	54.44	1.29	1.47	-0.40	13.90
Lahemaa	EE0009R	25.9	59.5	1.29	1.42	-0.48	10.12
Pallas (Matorova)	FI0036R	24.24	68	1.25	1.35	0.34	8.03
Auchencorth Moss	GB0048R	-3.24	55.79	1.68	1.31	0.92	-22.45
Bredkälen	SE0005R	15.33	63.85	1.21	1.35	0.25	11.53
Hallahus	SE0020R	13.15	56.04	1.18	1.45	0.19	23.03
Iskrba	SI0008R	14.87	45.57	1.46	1.44	1.00	-1.52

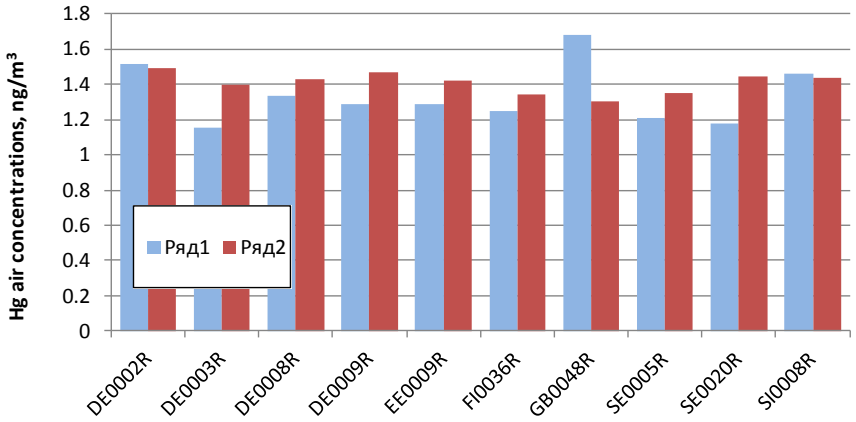

Fig. 4.9. *Modelled and observed annual mean concentrations of Hg in air at the EMEP stations in 2021.*

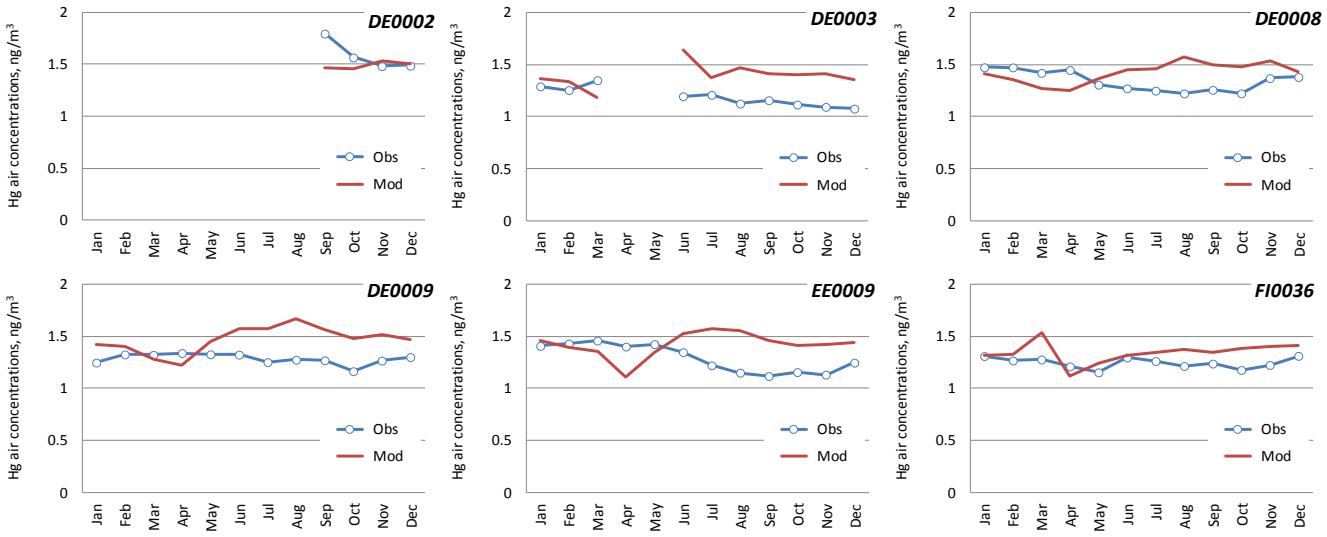

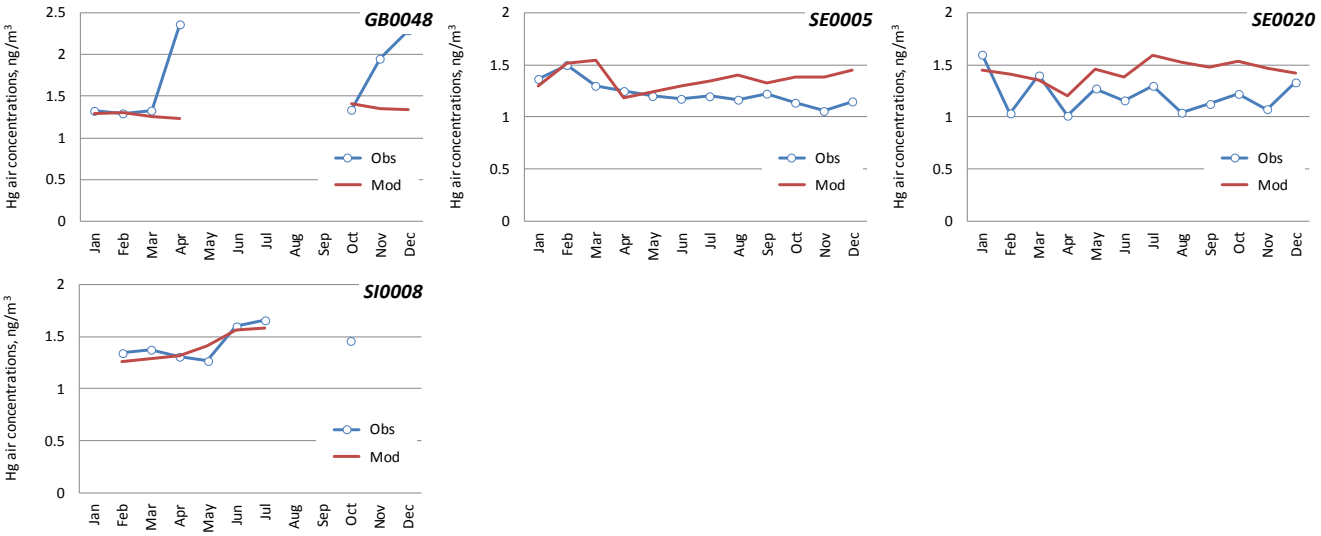

Fig. A.10. *Modelled and observed monthly mean concentrations of Hg in air at the EMEP stations in 2021.*

Wet deposition

Table A.7. *Annual sums of modelled and observed Hg wet deposition fluxes, g/km²/y, temporal correlation coefficient (Rc) and relative bias (Bias) at EMEP stations in 2021.*

Station name	Code	Longit	Latit	Observed flux	Modelled flux	Rc	Bias
Kosetice (NOAK)	CZ0003R	15.08	49.57	3.58	8.92	0.35	149.31
Westerland	DE0001R	8.31	54.93	3.06	6.18	0.83	101.71
Waldhof	DE0002R	10.76	52.8	3.09	6.04	0.87	95.33
Schauinsland	DE0003R	7.91	47.91	8.22	11.56	0.92	40.59
Schmucke	DE0008R	10.77	50.65	6.06	9.66	0.75	59.39
Zingst	DE0009R	12.72	54.44	2.82	3.96	0.48	40.32
Niembro	ES0008R	-4.85	43.44	3.79	2.98	0.80	-21.42
Pallas (Matorova)	FI0036R	24.24	68	1.61	6.34	-0.14	294.36
Kotinen	FI0093R	25.07	61.23	2.17	7.47	0.05	244.64
Yamer Wood	GB0013R	-3.71	50.6	3.57	4.41	0.74	23.59
Heigham Holmes	GB0017R	1.62	52.72	2.25	3.30	0.72	46.84
Auchencorth Moss	GB0048R	-3.24	55.79	1.92	3.93	0.69	104.77
Chilbolton Observatory	GB1055R	-1.44	51.15	1.96	4.86	0.76	148.55
De Zilk	NL0091R	4.5	52.3	7.62	5.55	0.82	-27.15
Birkenes	NO0001R	8.25	58.38	5.78	7.49	0.52	29.43
Kårvatn	NO0039R	8.88	62.78	4.83	11.34	0.59	134.85
Hurdal	NO0056R	11.08	60.37	9.11	4.03	0.88	-55.74
Diabla Gora	PL0005R	22.07	54.15	2.86	7.30	0.06	154.85
Bredkälen	SE0005R	15.33	63.85	2.62	4.21	0.25	61.12
Råö	SE0014R	11.91	57.39	2.87	6.01	0.70	109.13
Hallahus	SE0020R	13.15	56.04	3.88	6.53	0.86	68.21
Iskrba	SI0008R	14.87	45.57	5.85	9.61	0.62	64.22

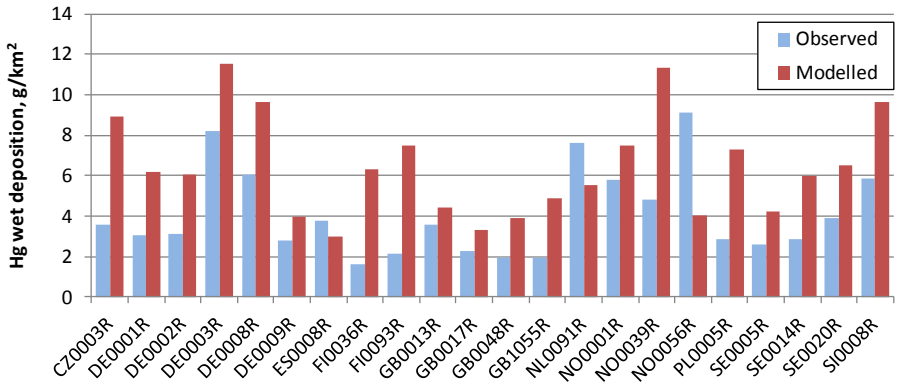

Fig. A.11. *Modelled and observed annual wet deposition fluxes of Hg at the EMEP stations in 2021.*

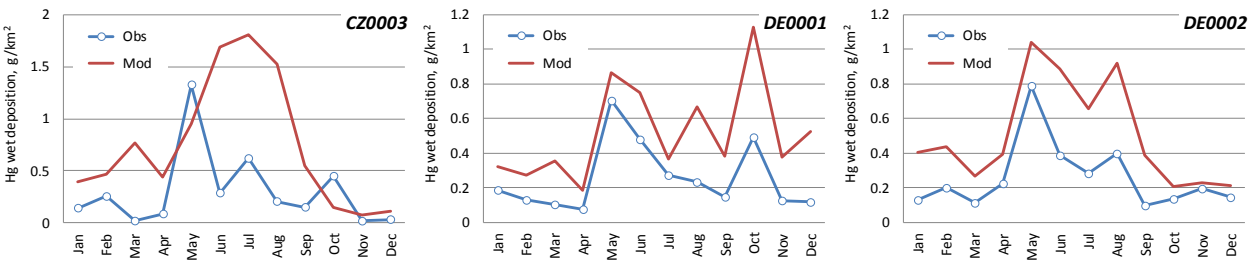

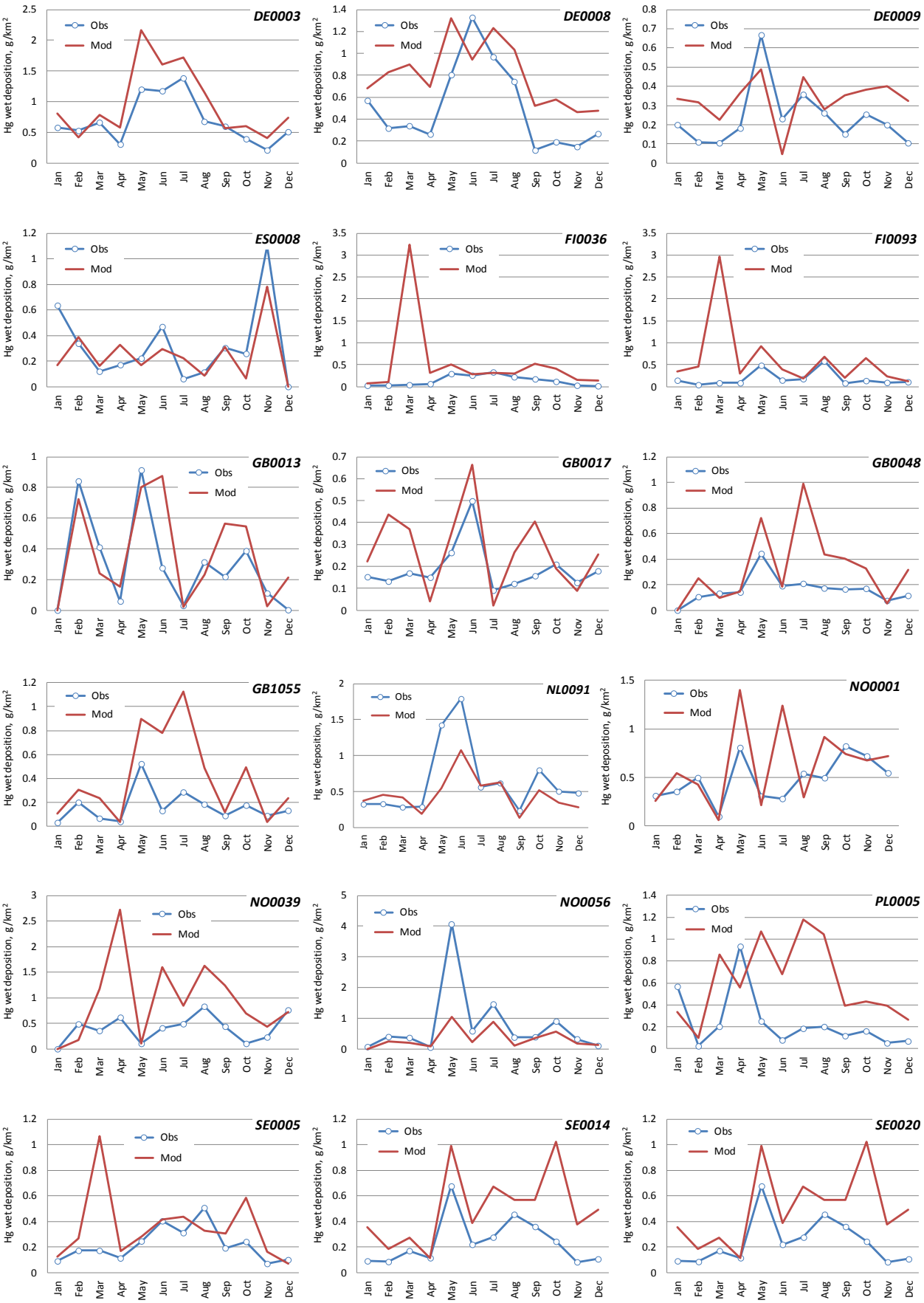
DE0003
DE0008
DE0009
ES0008
FI0036
FI0093
GB0013
GB0017
GB0048
GB1055
NL0091
NO0001
NO0039
NO0056
PL0005
SE0005
SE0014
SE0020
Obs
Mod
Hg wet deposition, g/km²
Jan
Feb
Mar
Apr
May
Jun
Jul
Aug
Sep
Oct
Nov
Dec

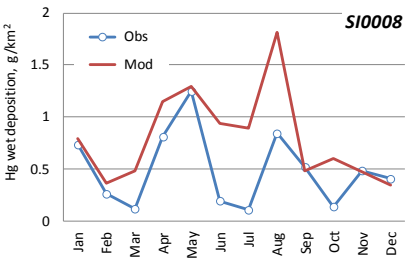

Fig. A.14. *Modelled and observed monthly wet deposition fluxes of Hg at the EMEP stations in 2021.*

A.2. EVALUATION OF MODELLING RESULTS VS. OBSERVATIONS FOR POPs

Verification of modelled concentrations was carried out via comparison with measurements of the EMEP monitoring network. Data of some of the EMEP stations were not taken into account in the comparison, in particular, of high-altitude stations (DE0003R, DE0008R, ES0007R, and HR0002R) due to specific meteorological conditions not captured well by the model, and of some Spanish stations (ES0001R, ES0012R) due to many values below detection limit. Overall statistics of the comparison are summarized in Table A.8. Modelled and measured annual mean air concentrations of selected POPs, namely, B(a)P, B(b)F, B(k)F, I(cd)P, PCB-153, HCB, PCDD/Fs, are summarized in Tables A.9 – A.15 for each station. Time series of modelled and observed monthly mean concentrations are demonstrated in Fig. A.15 - A.28.

Model estimates of B(a)P and I(cd)P air concentrations for 2021 were compared with measurements of 30 and 26 EMEP monitoring stations, respectively. Mean relative bias of modelled B(a)P concentrations in comparison to measurement data is -26%, and spatial correlation coefficient is 0.91. For 19 station the difference between the modelled and observed B(a)P concentrations does not exceed a factor of 2, and for 25 ones a factor of 3. Comparison of I(cd)P modelled and measured values showed quite similar bias -34% and spatial correlation 0.86. Differences between the modelled and observed I(cd)P concentrations do not exceed a factor of 2 for 19 stations, and a factor of 3 for 24 stations.

Model performance for B(b)F and B(k)F was analyzed using the measurements of 19 EMEP stations. For the whole set of the stations the model demonstrates some underestimation of observed B(b)F and B(k)F air concentrations. In particular, mean relative bias for B(b)F is -5% and for B(k)F is -22%. The spatial correlation coefficient for B(b)F and B(k)F is estimated to 0.94 and 0.87, respectively. For 12 stations the difference between the modelled and observed B(b)F concentrations does not exceed a factor of 2, and for 16 ones a factor of 3. Differences between the modelled and observed B(k)F concentrations do not exceed a factor of 2 for 15 stations, and a factor of 3 for 16 stations.

Comparison of modelled HCB air concentrations for 2021 was carried out for the measurements of 11 EMEP monitoring stations. Mean relative bias of HCB modelling results comparing to measurements is about 7%, and spatial correlation is 0.15. Discrepancies between the modelled and observed HCB concentrations do not exceed a factor of 2 for 8 stations, and a factor of 3 for all the stations. Model estimates tend to underpredict HCB concentrations observed at CZ0003R, NO0002R, NO0042R, and NO0090R. At the same time, measurements of DE0001R, DE0002R, DE0009R, IS0091R, SE0014R, and SE0022R were overpredicted. The highest differences were found for IS0091R and NO0042R stations.

Model performance for PCB-153 was tested using measurements of air concentrations of 10 EMEP monitoring stations for 2021. Mean relative bias of PCB-153 modelling results comparing to measurements is about -48%, and spatial correlation is 0.68. Differences between the modelled and observed HCB concentrations do not exceed a factor of 2 for 4 stations, and a factor of 3 for 8 stations. The highest difference, more than a factor of 3, was found for IS0091R and CZ0003R stations.

Modelled air concentrations of PCDD/Fs for 2021 were compared with measurements of two EMEP stations in Sweden, namely, SE0014R and SE0022R. Monitoring of PCDD/F at these stations was carried out for several months of the year, namely, for April, June, September, and December. Mean relative bias of modelling results for the data of two stations is about -20%. For the particular stations, good agreement was found for SE0014R (bias -3%), whereas for SE0022R the difference was higher (bias -38%).

Table A.8. *Statistical indices of comparison of modelled and observed mean annual concentrations in air in 2021 (N – number of stations, MRB – mean relative bias, R – spatial correlation coefficient, F2 – number of stations, for which the difference between the modelled and measured values is within a factor of 2).*

Pollutant	N	MRB, %	R	F2, %
B(a)P	30	-26	0.91	63
B(b)F	19	-5	0.94	63
B(k)F	19	-22	0.87	79
IcdP	26	-34	0.86	73
HCB	11	7	0.15	73
PCB-153	10	-48	0.68	40
PCDD/Fs	2	-20		100

A.2.1. Polycyclic aromatic hydrocarbons (PAHs)

Benzo(a)pyrene (B(a)P)

Table A.9. *Annual mean modelled and observed B(a)P air concentrations, ng/m³, and relative bias (Bias) at EMEP stations in 2021.*

Station name	Code	Type	Alt	Longitude	Latitude	Observed	Modelled	Bias
Houtem	BE0013R	pm10	2	2.582	51.016	0.061	0.066	7.5
Kosetice (NAOK)	CZ0003R	air+aerosol	535	15.08	49.573	0.250	0.500	99.7
Westerland	DE0001R	air+pm10	12	8.31	54.926	0.074	0.029	-60.6
Waldhof	DE0002R	air+pm10	74	10.759	52.802	0.157	0.097	-38.4
Zingst	DE0009R	air+pm10	1	12.725	54.437	0.113	0.065	-42.6
Lahemaa	EE0009R	pm10	32	25.9	59.5	0.098	0.054	-44.7
Niembro	ES0008R	pm10	134	-4.85	43.439	0.035	0.028	-21.1
Els Torms	ES0014R	pm10	470	0.735	41.394	0.035	0.014	-61.0
Virolahti III	FI0018R	pm10	4	27.668	60.53	0.153	0.057	-62.9
Pallas (Matorova)	FI0036R	air+aerosol	340	24.237	68	0.006	0.011	79.9
Hyytiälä	FI0050R	pm10	181	24.283	61.85	0.119	0.045	-62.0
Donon	FR0008R	pm10	775	7.133	48.5	0.039	0.074	90.0
Revin	FR0009R	pm10	390	4.633	49.9	0.041	0.058	40.6
Peyrusse Vieille	FR0013R	pm10	200	0.183	43.617	0.026	0.021	-20.3
Saint-Nazaire-le-Désert	FR0023R	pm10	605	5.279	44.569	0.079	0.018	-76.6
Vemeuil	FR0025R	pm10	182	2.61	46.815	0.092	0.030	-67.1
Kergoff	FR0028R	pm10	307	-2.944	48.262	0.014	0.014	-1.2
High Muffles	GB0014R	aerosol	267	-0.807	54.334	0.022	0.011	-50.2
Auchencorth Moss	GB0048R	pm10	260	-3.243	55.792	0.028	0.009	-66.9
Chilbolton Observatory	GB1055R	pm10	78	-1.438	51.15	0.075	0.031	-59.0
Rucava	LV0010R	pm10	18	21.173	56.162	0.431	0.089	-79.4
De Zilk	NL0091R	pm10	4	4.5	52.3	0.025	0.096	291.0
Birkenes II	NO0002R	air+aerosol	219	8.252	58.389	0.019	0.011	-41.3
Zeppelin mountain (Ny-Ålesund)	NO0042G	air+aerosol	474	11.887	78.907	0.002	0.000	-99.6
Diabla Gora	PL0005R	pm10	157	22.067	54.15	0.568	0.375	-34.0
Zielonka	PL0009R	pm10	121	17.934	53.662	0.899	0.631	-29.9
Råö	SE0014R	air+aerosol	5	11.914	57.394	0.015	0.026	79.5
Hallahus	SE0020R	air+aerosol	190	13.148	56.043	0.033	0.054	65.3
Norunda Stenen	SE0022R	air+aerosol	45	17.505	60.086	0.016	0.021	33.7
Iskrba	SI0008R	pm10	520	14.867	45.567	0.169	0.143	-15.2

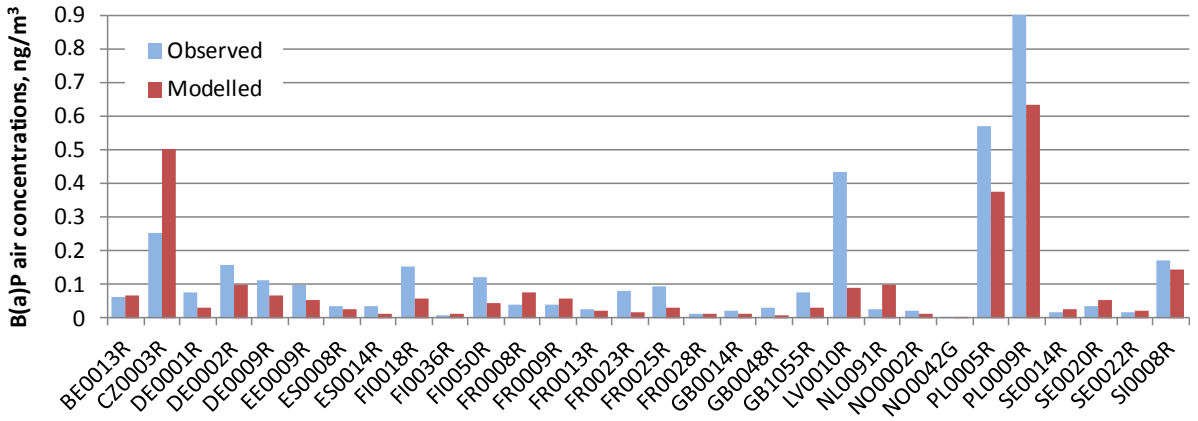

Fig. A.15. *Modelled and observed annual mean concentrations of B(a)P in air at the EMEP stations in 2021.*

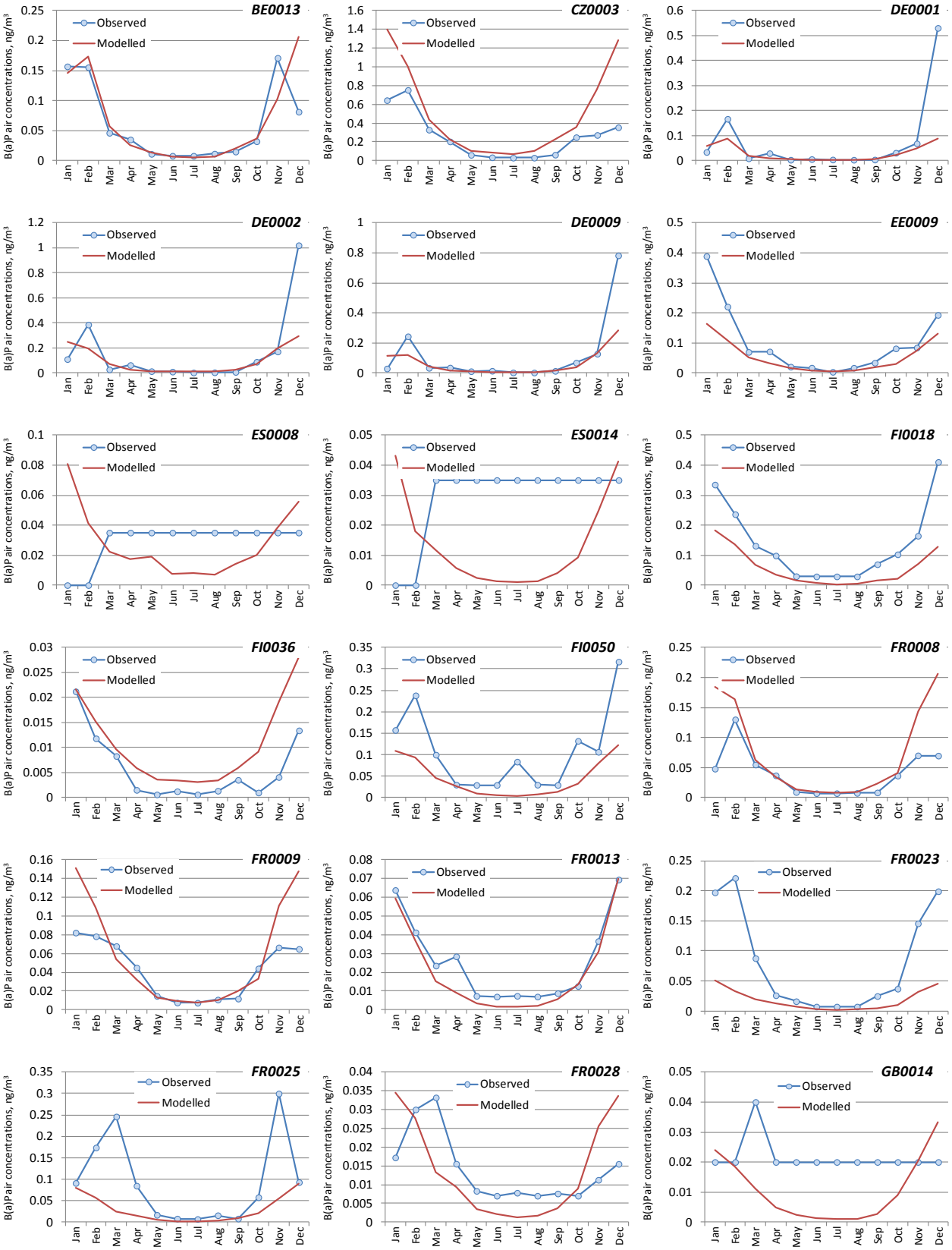
BE0013
CZ0003
DE0001
DE0002
DE0009
EE0009
ES0008
ES0014
FI0018
FI0036
FI0050
FR0008
FR0009
FR0013
FR0023
FR0025
FR0028
GB0014
Observed
Modelled
B(a)P air concentrations, ng/m³
Jan
Feb
Mar
Apr
May
Jun
Jul
Aug
Sep
Oct
Nov
Dec

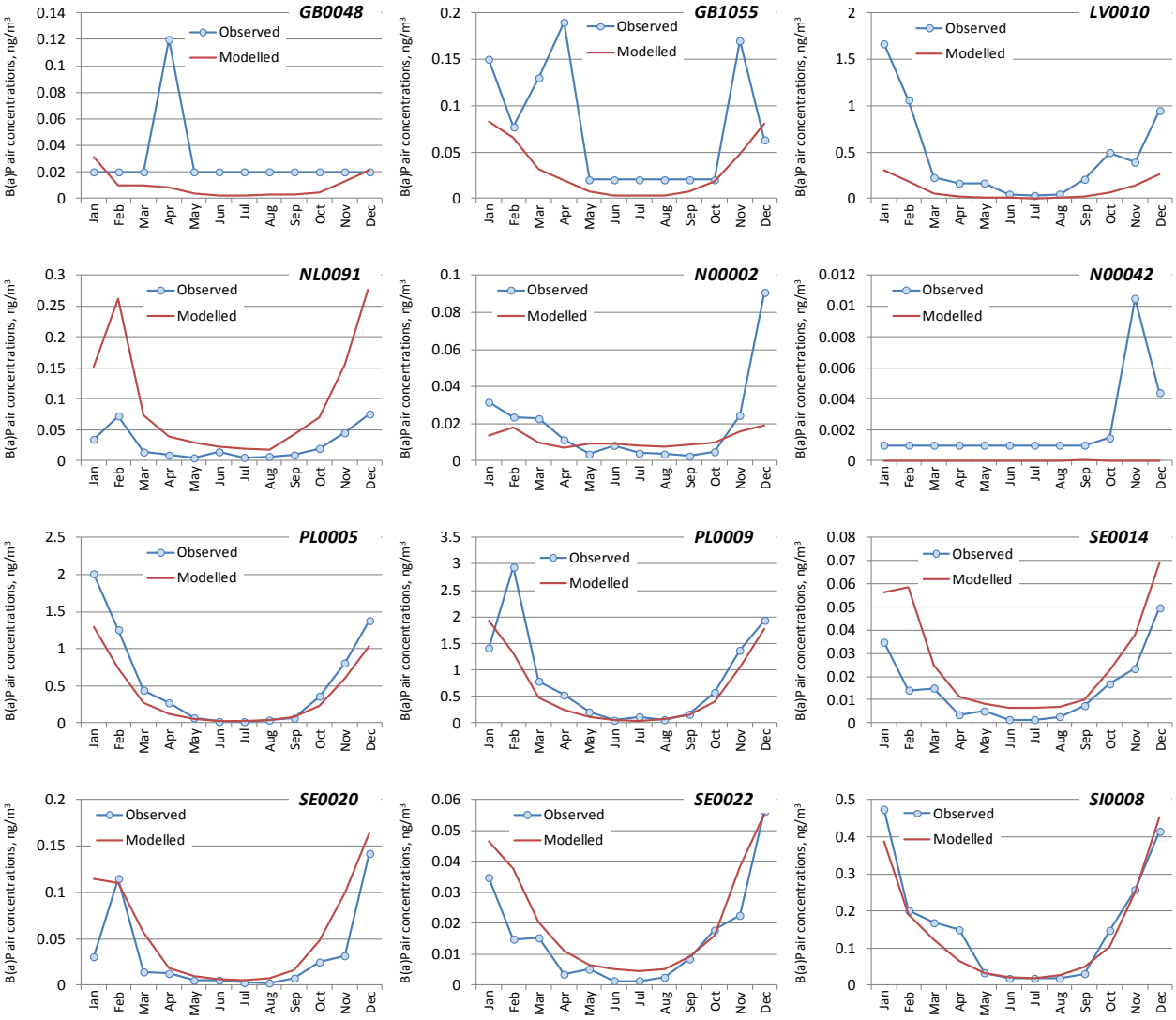

Fig. A.16. *Modelled and observed monthly mean concentrations of B(a)P in air at the EMEP stations in 2021.*

A.2.2. Benzo(b)fluoranthene (B(b)F)

Table A.10. *Annual mean modelled and observed B(b)F air concentrations, ng/m³, and relative bias (Bias) at EMEP stations in 2021.*

Station name	Code	Type	Alt	Longitude	Latitude	Observed	Modelled	Bias
Kosetice (NAOK)	CZ0003R	air+aerosol	535	15.08	49.573	0.397	0.561	41.4
Pallas (Matorova)	FI0036R	air+aerosol	340	24.237	68	0.013	0.014	5.1
Donon	FR0008R	pm10	775	7.133	48.5	0.063	0.165	162.8
Revin	FR0009R	pm10	390	4.633	49.9	0.076	0.122	60.1
Peyrusse Vieille	FR0013R	pm10	200	0.183	43.617	0.053	0.053	0.2
Saint-Nazaire-le-Désert	FR0023R	pm10	605	5.279	44.569	0.105	0.046	-56.8
Verneuil	FR0025R	pm10	182	2.61	46.815	0.155	0.073	-52.9
Kergoff	FR0028R	pm10	307	-2.944	48.262	0.031	0.036	15.9
High Muffles	GB0014R	aerosol	267	-0.807	54.334	0.044	0.025	-43.6
Auchencorth Moss	GB0048R	pm10	260	-3.243	55.792	0.046	0.018	-61.4
Chilbolton Observatory	GB1055R	pm10	78	-1.438	51.15	0.117	0.055	-52.6
Rucava	LV0010R	pm10	18	21.173	56.162	0.623	0.206	-67.0
Birkenes II	NO0002R	air+aerosol	219	8.252	58.389	0.055	0.037	-33.0
Zeppelin mountain (Ny-Ålesund)	NO0042G	air+aerosol	474	11.887	78.907	0.005	0.000	-98.8
Diabla Gora	PL0005R	pm10	157	22.067	54.15	0.799	0.649	-18.7
Zielonka	PL0009R	pm10	121	17.934	53.662	1.075	0.973	-9.4
Råö	SE0014R	air+aerosol	5	11.914	57.394	0.019	0.058	206.8
Hallahus	SE0020R	air+aerosol	190	13.148	56.043	0.032	0.109	235.0
Norunda Stenen	SE0022R	air+aerosol	45	17.505	60.086	0.018	0.043	146.3

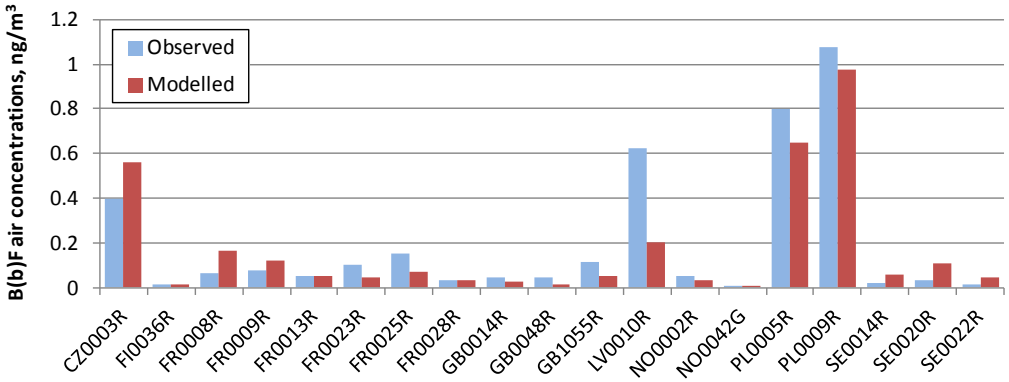

Fig. A.17. *Modelled and observed annual mean concentrations of B(b)F in air at the EMEP stations in 2021.*

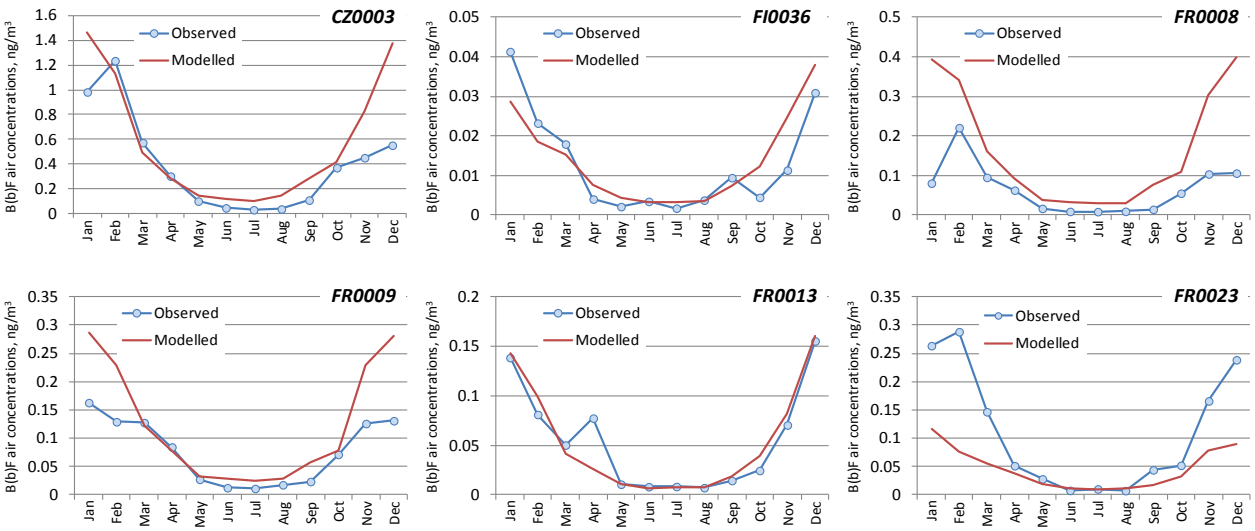

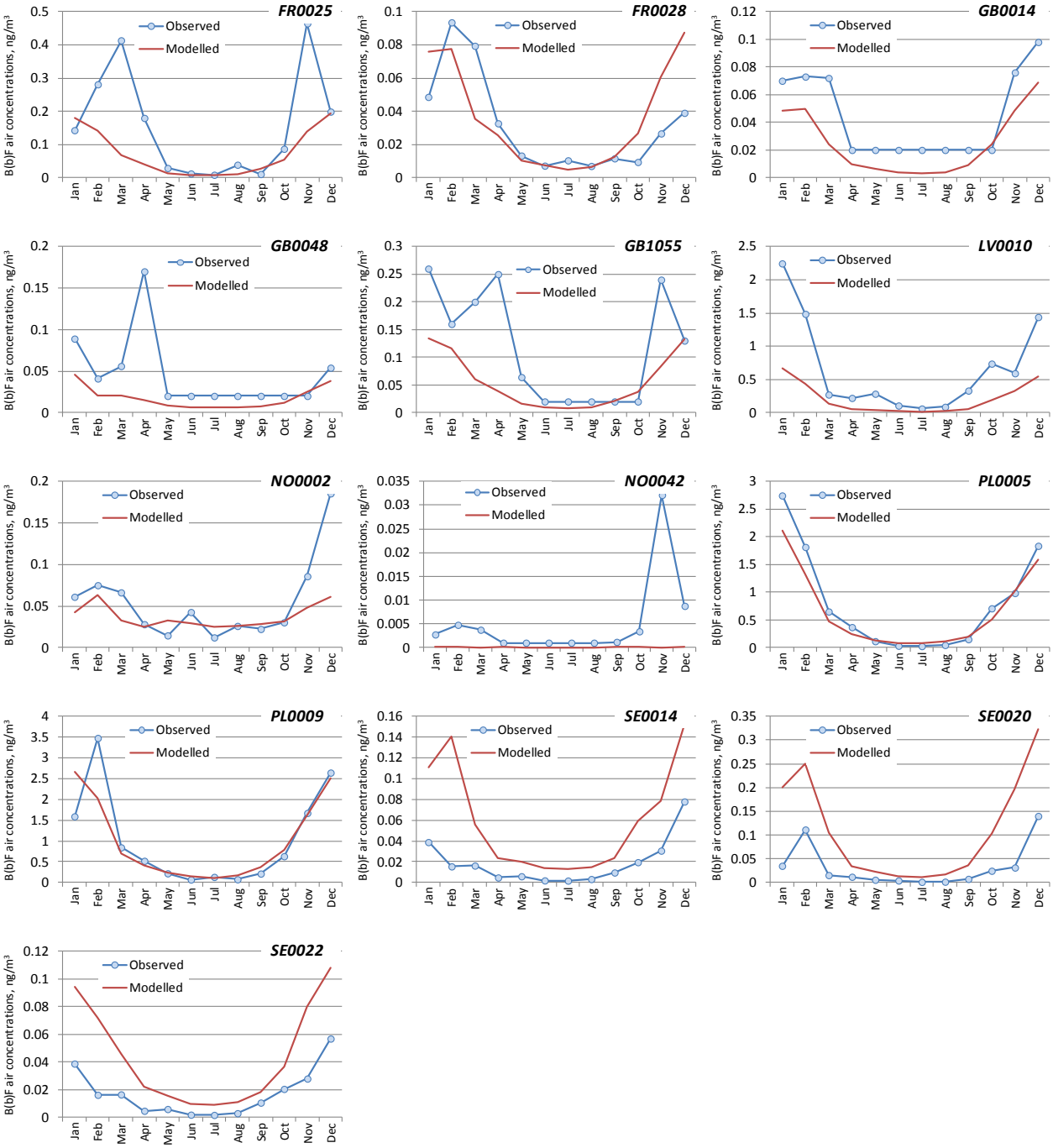

Fig. A.18. *Modelled and observed monthly mean concentrations of B(b)F in air at the EMEP stations in 2021.*

A.2.3. Benzo(k)fluoranthene (B(k)F)

***Table A.11**. Annual mean modelled and observed B(k)F air concentrations, ng/m³, and relative bias (Bias) at EMEP stations in 2021.*

Station name	Code	Type	R	Longitude	Latitude	Observed	Modelled	Bias
Kosetice (NAOK)	CZ0003R	air+aerosol	535	15.08	49.573	0.201	0.313	55.6
Pallas (Matorova)	FI0036R	air+aerosol	340	24.237	68	0.005	0.008	56.7
Donon	FR0008R	pm10	775	7.133	48.5	0.026	0.072	171.7
Revin	FR0009R	pm10	390	4.633	49.9	0.029	0.050	71.7
Peyrusse Vieille	FR0013R	pm10	200	0.183	43.617	0.021	0.020	-7.8
Saint-Nazaire-le-Désert	FR0023R	pm10	605	5.279	44.569	0.046	0.018	-60.0
Verneuil	FR0025R	pm10	182	2.61	46.815	0.063	0.031	-51.2
Kergoff	FR0028R	pm10	307	-2.944	48.262	0.013	0.013	-1.4
High Muffles	GB0014R	aerosol	267	-0.807	54.334	0.020	0.007	-65.0
Auchencorth Moss	GB0048R	pm10	260	-3.243	55.792	0.025	0.005	-80.1
Chilbolton Observatory	GB1055R	pm10	78	-1.438	51.15	0.054	0.016	-70.7
Rucava	LV0010R	pm10	18	21.173	56.162	0.370	0.064	-82.6
Birkenes II	NO0002R	air+aerosol	219	8.252	58.389	0.018	0.011	-38.4
Zeppelin mountain (Ny-Ålesund)	NO0042G	air+aerosol	474	11.887	78.907	0.002	0.000	-98.6
Diabla Gora	PL0005R	pm10	157	22.067	54.15	0.320	0.232	-27.3
Zielonka	PL0009R	pm10	121	17.934	53.662	0.545	0.357	-34.5
Råö	SE0014R	air+aerosol	5	11.914	57.394	0.012	0.020	61.7
Hallahus	SE0020R	air+aerosol	190	13.148	56.043	0.026	0.043	66.1
Norunda Stenen	SE0022R	air+aerosol	45	17.505	60.086	0.013	0.013	-2.9

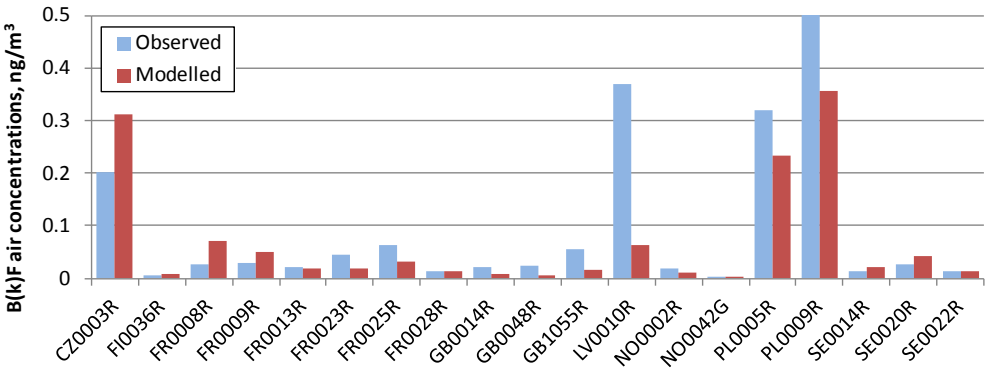

***Fig. A.19**. Modelled and observed annual mean concentrations of B(k)F in air at the EMEP stations in 2021.*

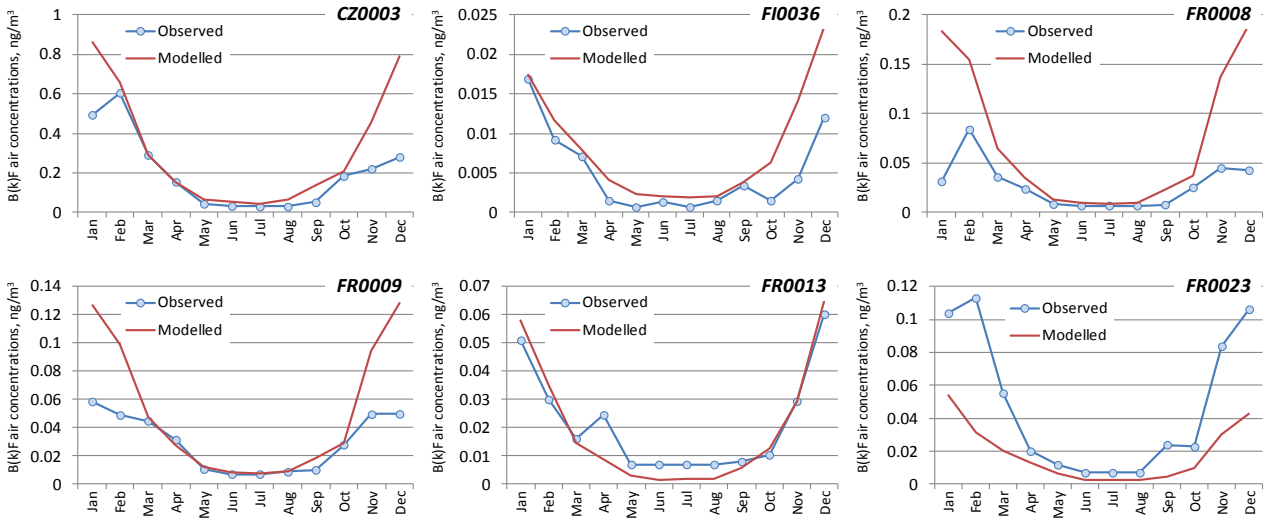

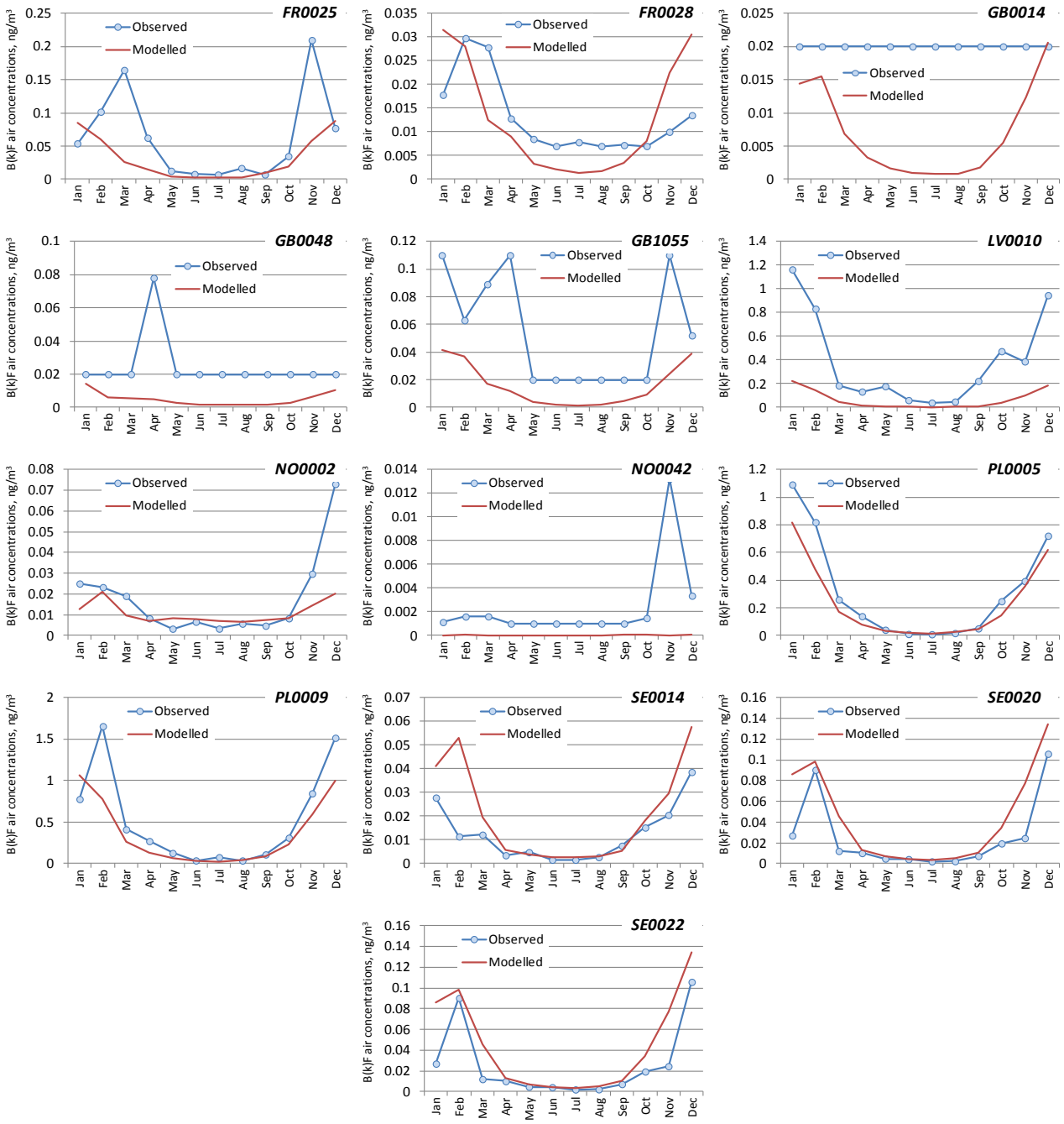

Fig. A.20. *Modelled and observed monthly mean concentrations of B(k)F in air at the EMEP stations in 2021.*

A.2.4. Indeno(1,2,3-cd)pyrene (I(cd)P)

Table A.12. *Annual mean modelled and observed I(cd)P air concentrations, ng/m³, and relative bias (Bias) at EMEP stations in 2021.*

Station name	Code	Type	Alt	Longitude	Latitude	Observed	Modelled	Bias
Houtem	BE0013R	pm10	2	2.582	51.016	0.084	0.082	-1.8
Kosetice (NAOK)	CZ0003R	air+aerosol	535	15.08	49.573	0.350	0.513	46.7
Westerland	DE0001R	air+pm10	12	8.31	54.926	0.086	0.050	-42.2
Waldhof	DE0002R	air+pm10	74	10.759	52.802	0.201	0.147	-26.6
Zingst	DE0009R	air+pm10	1	12.725	54.437	0.144	0.095	-34.0
Virolahti III	FI0018R	pm10	4	27.668	60.53	0.118	0.080	-32.6
Pallas (Matorova)	FI0036R	air+aerosol	340	24.237	68	0.009	0.013	49.9
Hyytiälä	FI0050R	pm10	181	24.283	61.85	0.086	0.064	-25.4
Donon	FR0008R	pm10	775	7.133	48.5	0.047	0.101	114.9
Revin	FR0009R	pm10	390	4.633	49.9	0.054	0.071	31.2
Peyrusse Vieille	FR0013R	pm10	200	0.183	43.617	0.042	0.035	-15.8
Saint-Nazaire-le-Désert	FR0023R	pm10	605	5.279	44.569	0.083	0.027	-67.0
Verneuil	FR0025R	pm10	182	2.61	46.815	0.115	0.046	-60.1
Kergoff	FR0028R	pm10	307	-2.944	48.262	0.021	0.024	16.9
High Muffles	GB0014R	aerosol	267	-0.807	54.334	0.035	0.019	-45.1
Auchencorth Moss	GB0048R	pm10	260	-3.243	55.792	0.038	0.015	-61.9
Chilbolton Observatory	GB1055R	pm10	78	-1.438	51.15	0.084	0.045	-47.0
Rucava	LV0010R	pm10	18	21.173	56.162	0.527	0.111	-79.0
Birkenes II	NO0002R	air+aerosol	219	8.252	58.389	0.033	0.014	-57.9
Zeppelin mountain (Ny-Ålesund)	NO0042G	air+aerosol	474	11.887	78.907	0.003	0.000	-98.8
Diabla Gora	PL0005R	pm10	157	22.067	54.15	0.748	0.276	-63.1
Zielonka	PL0009R	pm10	121	17.934	53.662	0.742	0.404	-45.5
Råö ¶	SE0014R	air+aerosol	5	11.914	57.394	0.022	0.031	42.8
Hallahus	SE0020R	air+aerosol	190	13.148	56.043	0.047	0.061	29.8
Norunda Stenen	SE0022R	air+aerosol	45	17.505	60.086	0.022	0.025	10.7
Iskrba	SI0008R	pm10	520	14.867	45.567	0.187	0.115	-38.4

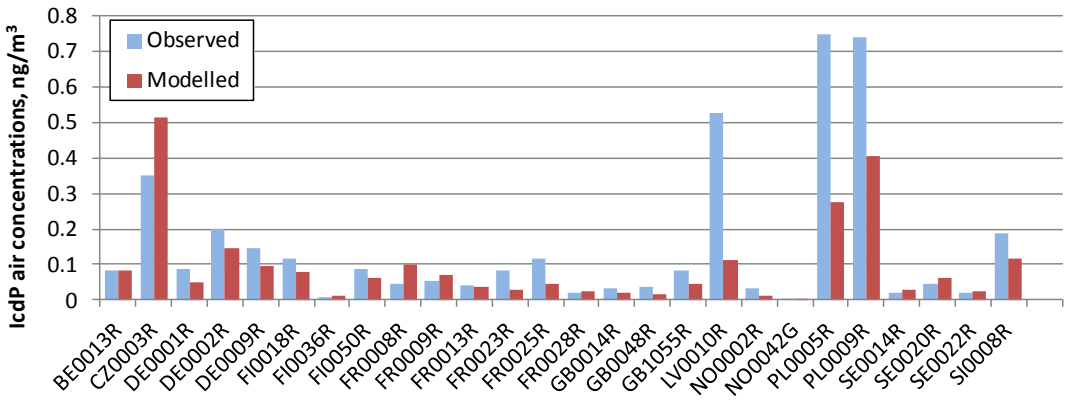

Fig. A.21. *Modelled and observed annual mean concentrations of I(cd)P in air at the EMEP stations in 2021.*

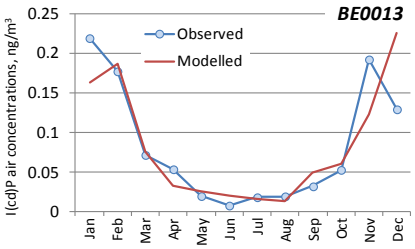
BE0013
Observed
Modelled
I(cd)P air concentrations, ng/m³
0.25
0.2
0.15
0.1
0.05
0
Jan Feb Mar Apr May Jun Jul Aug Sep Oct Nov Dec

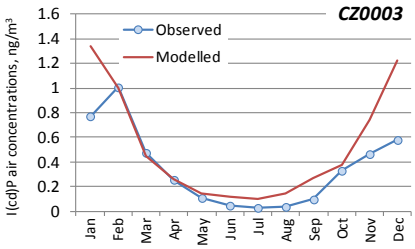
CZ0003
Observed
Modelled
I(cd)P air concentrations, ng/m³
1.6
1.4
1.2
1
0.8
0.6
0.4
0.2
0
Jan Feb Mar Apr May Jun Jul Aug Sep Oct Nov Dec

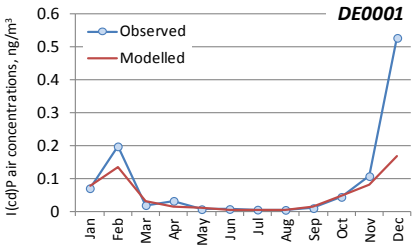
DE0001
Observed
Modelled
I(cd)P air concentrations, ng/m³
0.6
0.5
0.4
0.3
0.2
0.1
0
Jan Feb Mar Apr May Jun Jul Aug Sep Oct Nov Dec

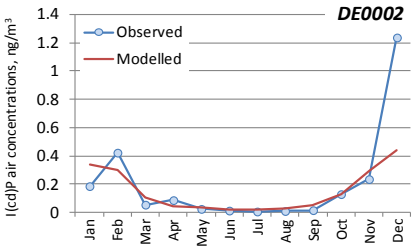
DE0002
Observed
Modelled
I(cd)P air concentrations, ng/m³
1.4
1.2
1
0.8
0.6
0.4
0.2
0
Jan Feb Mar Apr May Jun Jul Aug Sep Oct Nov Dec

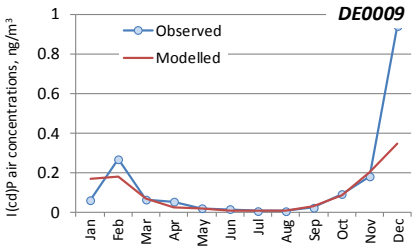
DE0009
Observed
Modelled
I(cd)P air concentrations, ng/m³
1
0.8
0.6
0.4
0.2
0
Jan Feb Mar Apr May Jun Jul Aug Sep Oct Nov Dec

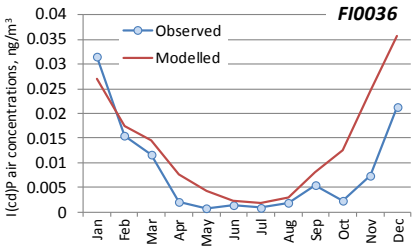
FI0036
Observed
Modelled
I(cd)P air concentrations, ng/m³
0.04
0.035
0.03
0.025
0.02
0.015
0.01
0.005
0
Jan Feb Mar Apr May Jun Jul Aug Sep Oct Nov Dec

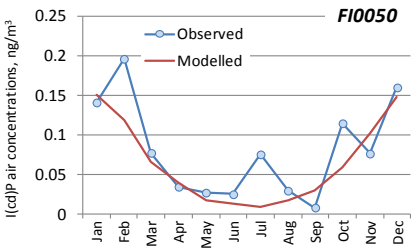
FI0050
Observed
Modelled
I(cd)P air concentrations, ng/m³
0.25
0.2
0.15
0.1
0.05
0
Jan Feb Mar Apr May Jun Jul Aug Sep Oct Nov Dec

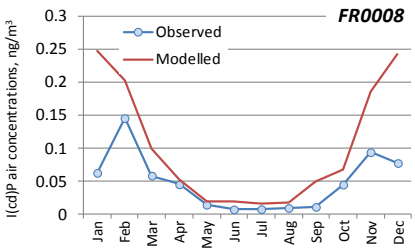
FR0008
Observed
Modelled
I(cd)P air concentrations, ng/m³
0.3
0.25
0.2
0.15
0.1
0.05
0
Jan Feb Mar Apr May Jun Jul Aug Sep Oct Nov Dec

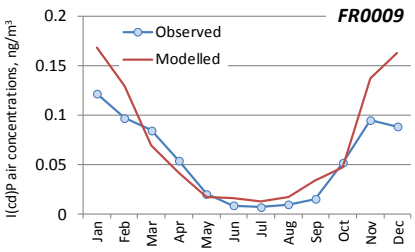
FR0009
Observed
Modelled
I(cd)P air concentrations, ng/m³
0.2
0.15
0.1
0.05
0
Jan Feb Mar Apr May Jun Jul Aug Sep Oct Nov Dec

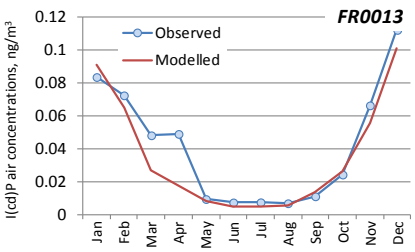
FR0013
Observed
Modelled
I(cd)P air concentrations, ng/m³
0.12
0.1
0.08
0.06
0.04
0.02
0
Jan Feb Mar Apr May Jun Jul Aug Sep Oct Nov Dec

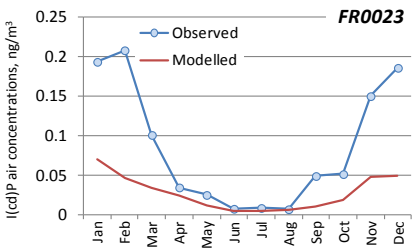
FR0023
Observed
Modelled
I(cd)P air concentrations, ng/m³
0.25
0.2
0.15
0.1
0.05
0
Jan Feb Mar Apr May Jun Jul Aug Sep Oct Nov Dec

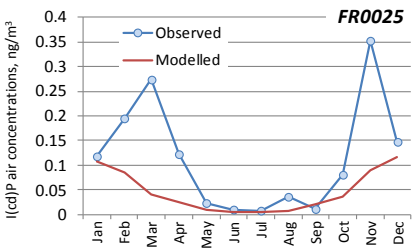
FR0025
Observed
Modelled
I(cd)P air concentrations, ng/m³
0.4
0.35
0.3
0.25
0.2
0.15
0.1
0.05
0
Jan Feb Mar Apr May Jun Jul Aug Sep Oct Nov Dec

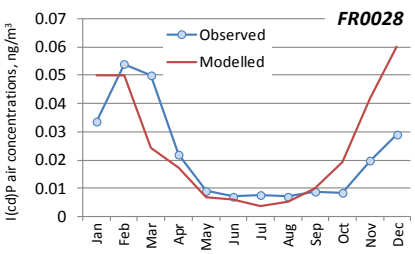
FR0028
Observed
Modelled
I(cd)P air concentrations, ng/m³
0.07
0.06
0.05
0.04
0.03
0.02
0.01
0
Jan Feb Mar Apr May Jun Jul Aug Sep Oct Nov Dec

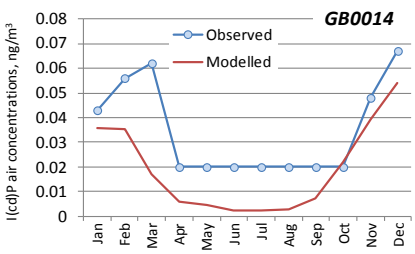
GB0014
Observed
Modelled
I(cd)P air concentrations, ng/m³
0.08
0.07
0.06
0.05
0.04
0.03
0.02
0.01
0
Jan Feb Mar Apr May Jun Jul Aug Sep Oct Nov Dec

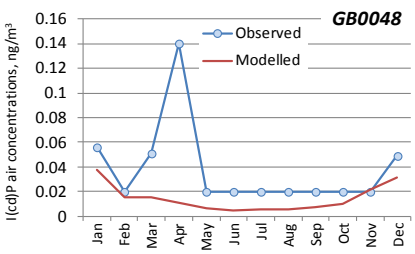
GB0048
Observed
Modelled
I(cd)P air concentrations, ng/m³
0.16
0.14
0.12
0.1
0.08
0.06
0.04
0.02
0
Jan Feb Mar Apr May Jun Jul Aug Sep Oct Nov Dec

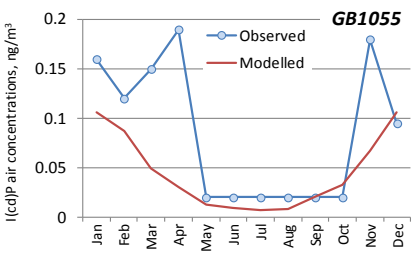
GB1055
Observed
Modelled
I(cd)P air concentrations, ng/m³
0.2
0.15
0.1
0.05
0
Jan Feb Mar Apr May Jun Jul Aug Sep Oct Nov Dec

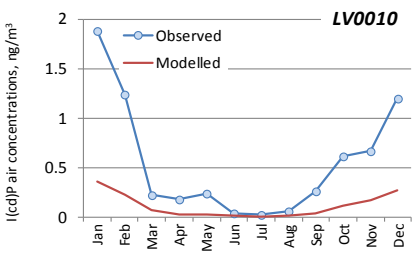
LV0010
Observed
Modelled
I(cd)P air concentrations, ng/m³
2
1.5
1
0.5
0
Jan Feb Mar Apr May Jun Jul Aug Sep Oct Nov Dec

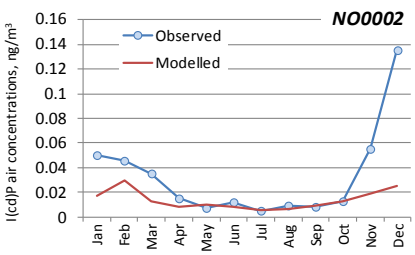
NO0002
Observed
Modelled
I(cd)P air concentrations, ng/m³
0.16
0.14
0.12
0.1
0.08
0.06
0.04
0.02
0
Jan Feb Mar Apr May Jun Jul Aug Sep Oct Nov Dec

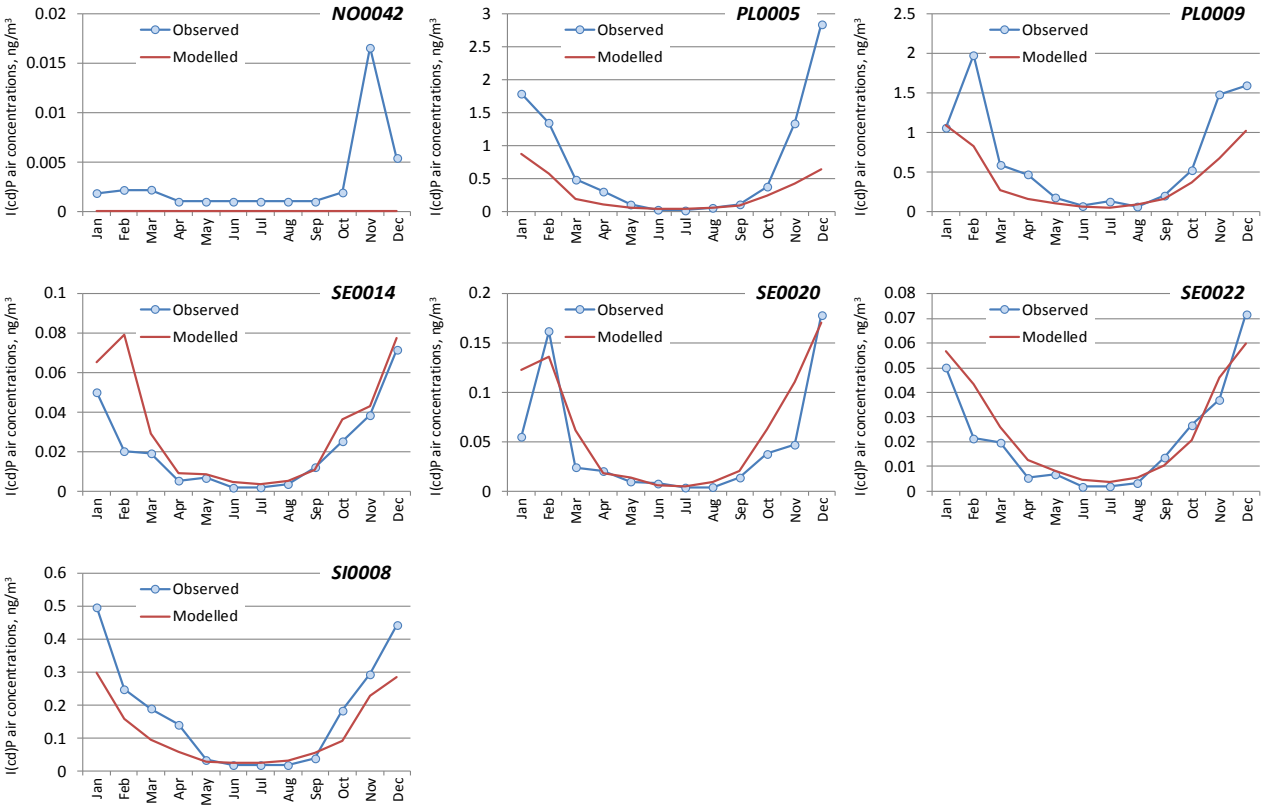

Fig. A.22. *Modelled and observed monthly mean concentrations of I(cd)P in air at the EMEP stations in 2021.*

A.2.5. Hexachlorobenzene (HCB)

Table A.13. *Annual mean modelled and observed HCB air concentrations, pg/m³, and relative bias (Bias) at EMEP stations in 2021.*

Station name	Code	Type	Alt	Longitude	Latitude	Observed	Modelled	Bias
Kosetice (NAOK)	CZ0003R	air+pm10	535	15.08	49.573	59.550	37.509	-37.01
Westerland	DE0001R	air+pm10	12	8.31	54.926	17.410	31.455	80.67
Waldhof	DE0002R	air+pm10	74	10.759	52.802	21.800	41.216	89.06
Zingst	DE0009R	air+pm10	1	12.725	54.437	17.890	38.843	117.12
Pallas (Matorova)	FI0036R	air+aerosol	340	24.237	68	20.000	20.087	0.43
Storhofdi	IS0091R	air+aerosol	118	-20.288	63.4	5.287	15.671	196.40
Birkenes II	NO0002R	air+aerosol	219	8.252	58.389	39.260	30.233	-22.99
Zeppelin mountain (Ny-Ålesund)	NO0042G	air+aerosol	474	11.887	78.907	44.530	15.845	-64.42
Andoya	NO0090R	air+aerosol	380	16.012	69.278	27.490	23.205	-15.59
Råö	SE0014R	air+aerosol	5	11.914	57.394	20.000	33.118	65.59
Norunda Stenen	SE0022R	air+aerosol	45	17.505	60.086	20.000	28.469	42.35

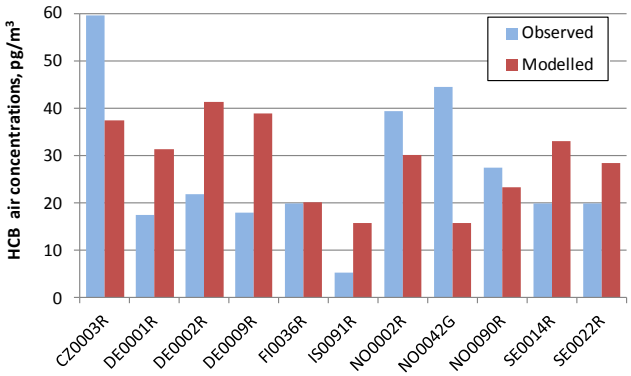

Fig. A.23. *Modelled and observed annual mean concentrations of HCB in air at the EMEP stations in 2021.*

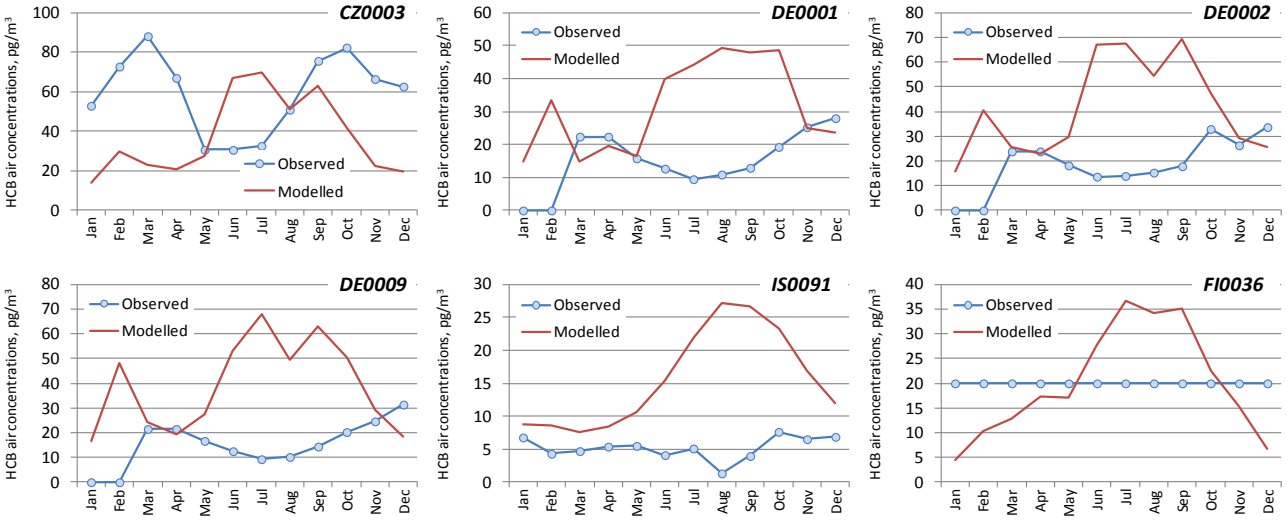

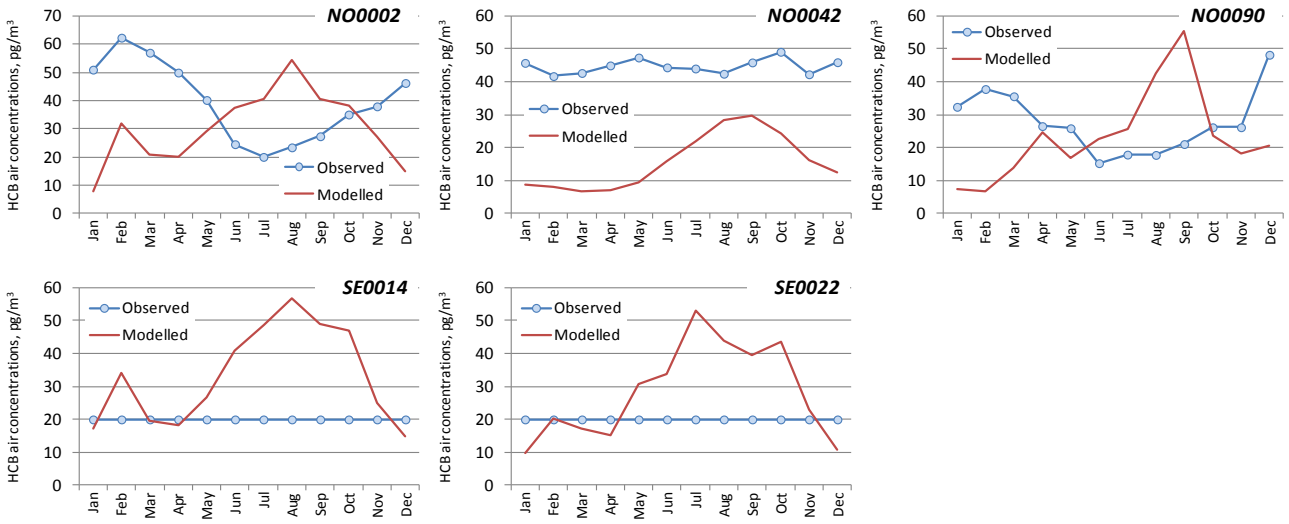

Fig. A.24. *Modelled and observed monthly mean concentrations of HCB in air at the EMEP stations in 2021.*

A.2.6. Polychlorinated biphenyls (PCB-153)

Table A.14. *Annual mean modelled and observed PCB-153 air concentrations, pg/m³, and relative bias (Bias) at EMEP stations in 2021.*

Station name	Code	Type	Alt	Longitude	Latitude	Observed	Modelled	Bias
Kosetice (NAOK)	CZ0003R	air+pm10	535	15.08	49.573	13.600	2.497	-81.6
Westerland	DE0001R	air+pm10	12	8.31	54.926	0.992	1.096	10.5
Waldhof	DE0002R	air+pm10	74	10.759	52.802	0.992	2.257	127.5
Zingst	DE0009R	air+pm10	1	12.725	54.437	0.453	1.307	188.8
Pallas (Matorova)	FI0036R	air+aerosol	340	24.237	68	0.107	0.191	79.1
Storhofdi	IS0091R	air+aerosol	118	-20.288	63.4	0.526	0.123	-76.5
Birkenes II	NO0002R	air+aerosol	219	8.252	58.389	0.237	0.342	44.4
Zeppelin mountain (Ny-Ålesund)	NO0042G	air+aerosol	474	11.887	78.907	0.090	0.038	-57.5
Råö ¶	SE0014R	air+aerosol	5	11.914	57.394	0.625	0.727	16.4
Norunda Stenen	SE0022R	air+aerosol	45	17.505	60.086	0.267	0.606	127.0

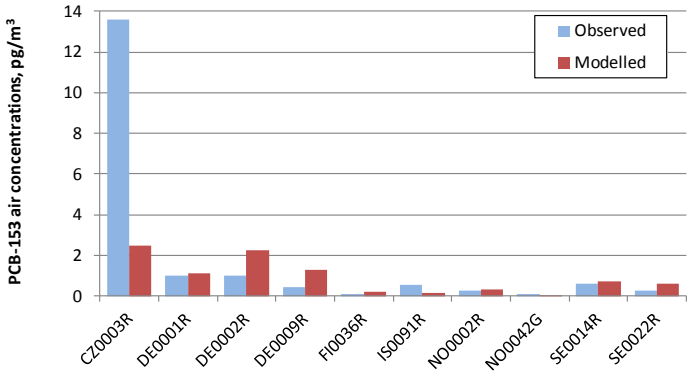

Fig. A.25. *Modelled and observed annual mean concentrations of PCB-153 in air at the EMEP stations in 2021.*

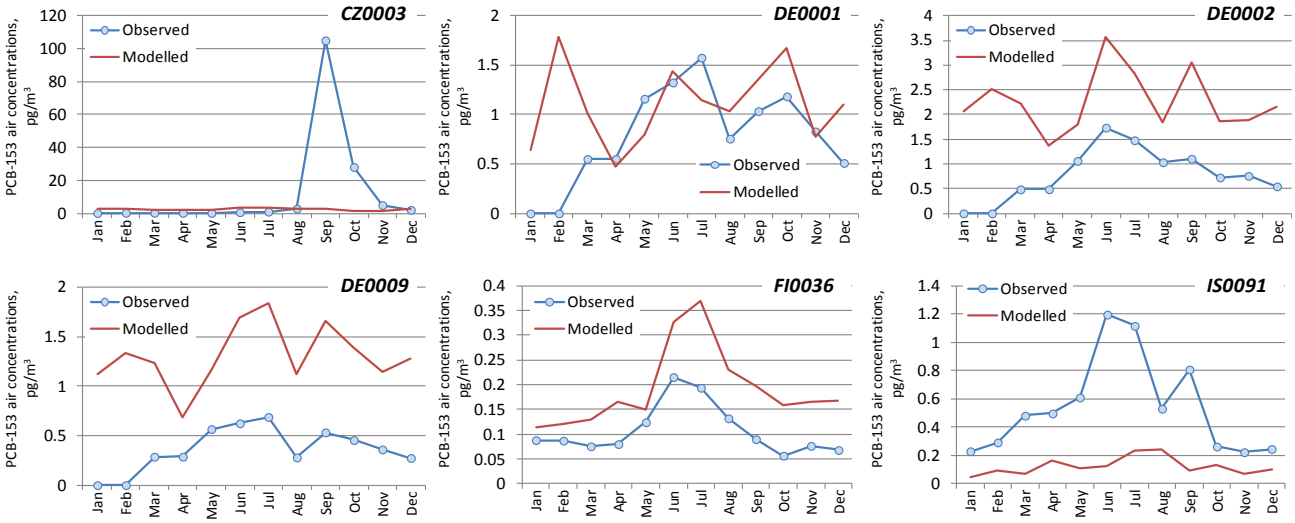

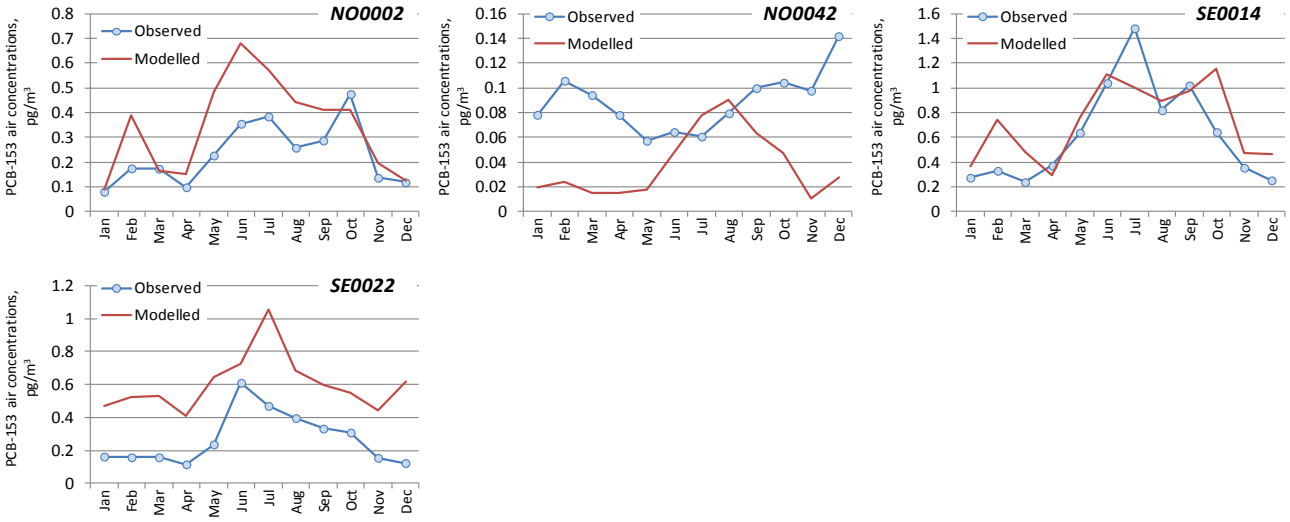

***Fig. A.26**. Modelled and observed monthly mean concentrations of PCB-153 in air at the EMEP stations in 2021.*

A.2.7. Polychlorinated dibenzo(p)dioxins and dibenzofurans (PCDD/Fs)

Table A.15. *Annual mean modelled and observed PCDD/F air concentrations, fg TEQ/m³, and relative bias (Bias) at EMEP stations in 2021.*

Station name	Code	Type	Alt	Longitude	Latitude	Observed	Modelled	Bias
Råö	SE0014R	air+aerosol	5	11.91	57.39	1.301	1.286	-1.17
Norunda Stenen	SE0022R	air+aerosol	45	17.51	60.09	1.005	0.638	-36.55

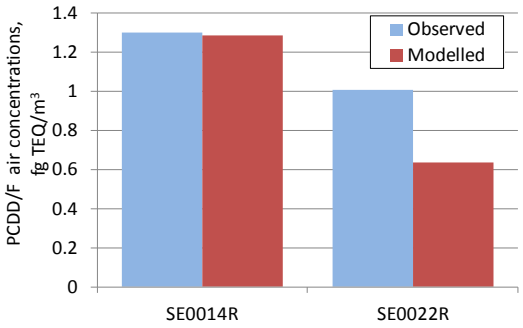

Fig. A.27. *Modelled and observed annual mean concentrations of PCDD/F in air at the EMEP stations in 2021.*

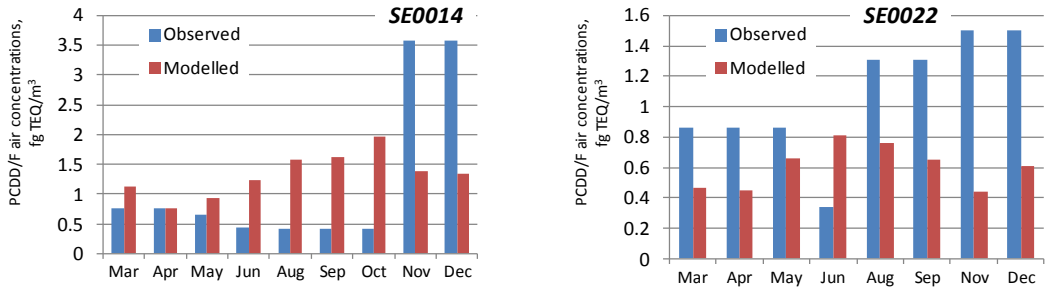

Fig. A.28. *Modelled and observed monthly mean concentrations of PCDD/F in air at the EMEP stations in 2021, fg TEQ/m³.*

Annex B

UPDATE OF THE ASSESSMENT RESULTS WITH THE NEW EMISSION REPORTING DATA

For model assessment of heavy metal and POP pollution levels for 2021 emission data for previous (2020) year were used. In summer of 2023 emission data for modelling for 2021 became available. Emission data of 2021 were derived from CEIP online data base (https://www.ceip.at/webdab-emission-database). This annex provides a brief overview of emission data and modelling results for 2021. In particular, it includes national total emissions in the EMEP countries, spatial distributions of air concentrations, total and wet deposition fluxes based on emission data for 2021. Besides, evaluation of the updated modelling results against measurements is demonstrated.

Lead (Pb)

Table B.1. *Emissions of Pb in 2021 in the EMEP countries, tonnes*

Country	Emissions	Country	Emissions	Country	Emissions
Albania	6.13	Greece	11.39	Poland	279.90
Armenia	0.80	Hungary	14.60	Portugal	23.71
Austria	12.53	Iceland	0.49	Moldova	1.69
Azerbaijan	2.10	Ireland	7.63	Romania	46.41
Belarus	7.70	Italy	210.08	Russia	235.75
Belgium	15.69	Kazakhstan	696.03	Serbia	38.26
Bosnia&Herzegovina	35.53	Kyrgyzstan	12.22	Slovakia	8.15
Bulgaria	14.95	Latvia	3.85	Slovenia	5.63
Croatia	6.30	Liechtenstein	0.05	Spain	100.70
Cyprus	1.09	Lithuania	3.72	Sweden	6.85
Czechia	14.68	Luxembourg	1.24	Switzerland	13.55
Denmark	14.55	Malta	0.50	Tajikistan	63.72
Estonia	4.95	Monaco	0.01	Türkiye	94.78
Finland	13.00	Montenegro	0.44	Turkmenistan	39.00
France	84.90	Netherlands	4.91	Ukraine	48.36
Georgia	2.72	North Macedonia	2.64	United Kingdom	114.91
Germany	154.45	Norway	5.45	Uzbekistan	184.82

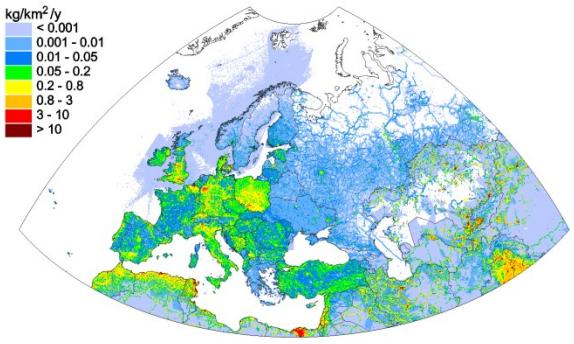

Fig. B.1. *Spatial distribution of Pb emissions in the EMEP region in 2021.*

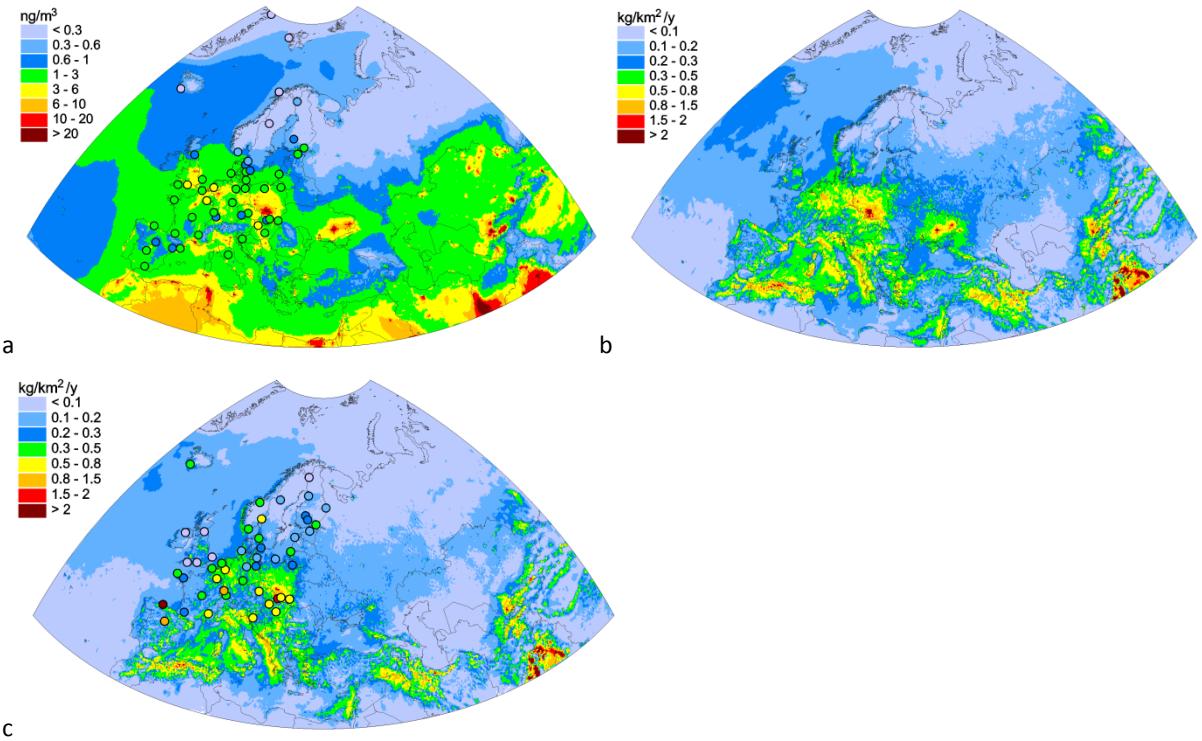

Fig. B.2. *Annual mean modelled air concentrations (a), total deposition fluxes (b) and wet deposition fluxes (c) of Pb based on the emissions data for 2021.*

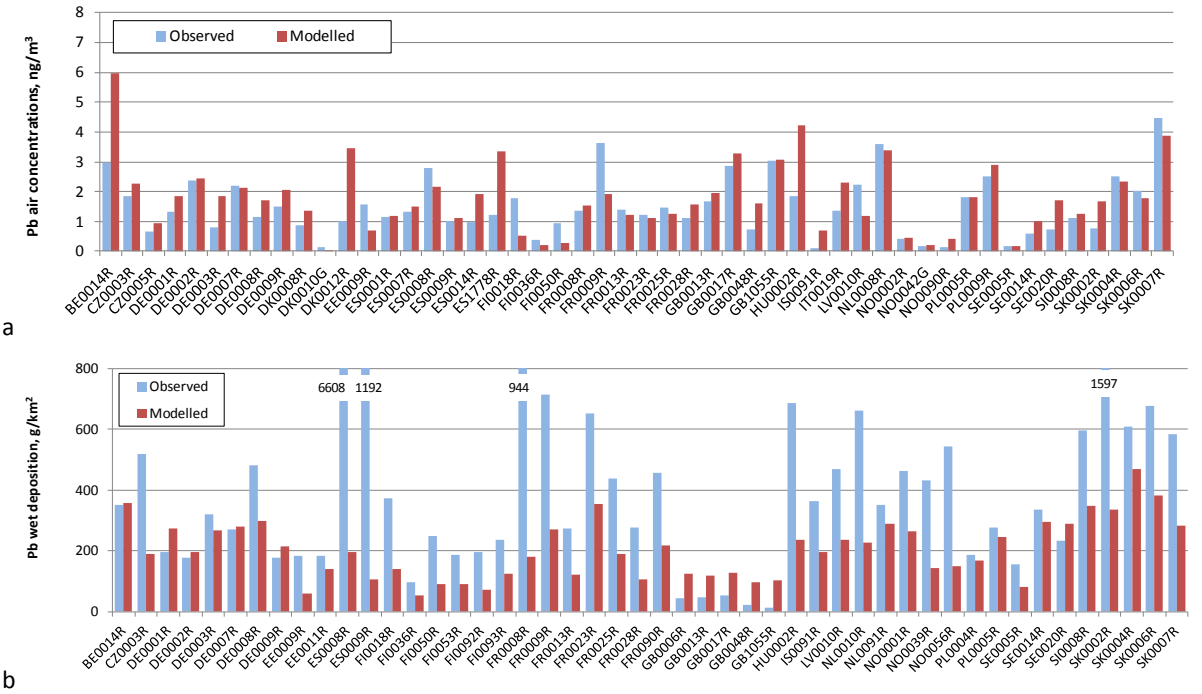

Fig. B.3. *Modelled and observed annual mean concentrations of Pb in air (a) and wet deposition fluxes (b) at the EMEP stations in 2021.*

Cadmium (Cd)

Table B.2. *Emissions of Cd in 2021 in the EMEP countries, tonnes*

Country	Emissions	Country	Emissions	Country	Emissions
Albania	0.19	Greece	1.52	Poland	10.96
Armenia	0.04	Hungary	1.38	Portugal	1.77
Austria	0.92	Iceland	0.01	Moldova	0.40
Azerbaijan	0.10	Ireland	0.27	Romania	3.14
Belarus	0.73	Italy	4.39	Russia	39.70
Belgium	1.15	Kazakhstan	11.06	Serbia	2.57
Bosnia&Herzegovina	1.49	Kyrgyzstan	0.50	Slovakia	0.62
Bulgaria	1.43	Latvia	0.55	Slovenia	0.58
Croatia	0.79	Liechtenstein	3.7E-03	Spain	6.84
Cyprus	0.03	Lithuania	0.26	Sweden	0.48
Czechia	1.27	Luxembourg	0.06	Switzerland	0.63
Denmark	0.67	Malta	0.01	Tajikistan	0.31
Estonia	0.46	Monaco	3.0E-04	Türkiye	3.97
Finland	0.85	Montenegro	0.11	Turkmenistan	0.27
France	2.59	Netherlands	0.87	Ukraine	2.45
Georgia	0.18	North Macedonia	0.23	United Kingdom	4.99
Germany	10.87	Norway	0.48	Uzbekistan	3.28

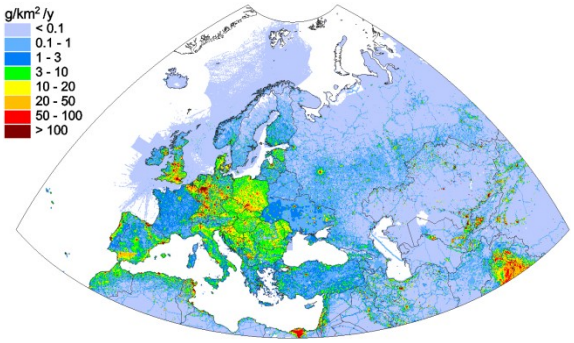

Fig. B.4. *Spatial distribution of Cd emissions in the EMEP region in 2021.*

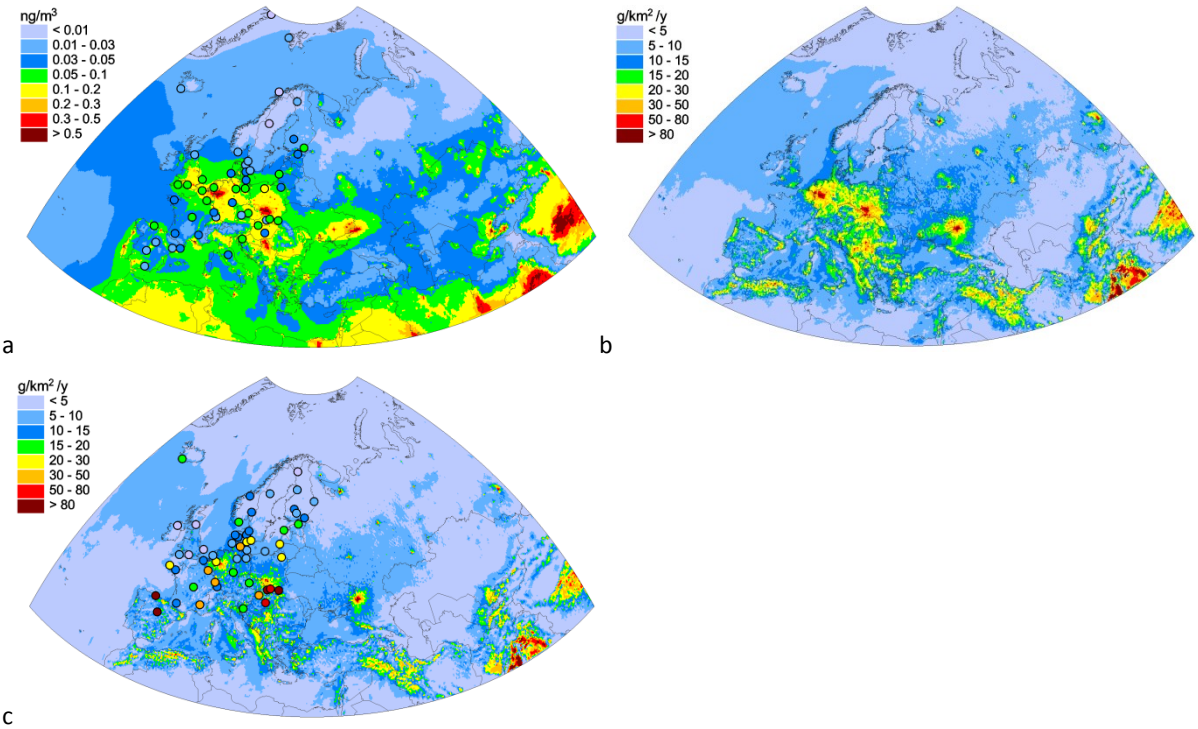

Fig. B.5. *Annual mean modelled air concentrations (a), total deposition fluxes (b) and wet deposition fluxes (c) of Cd based on the emissions data for 2021.*

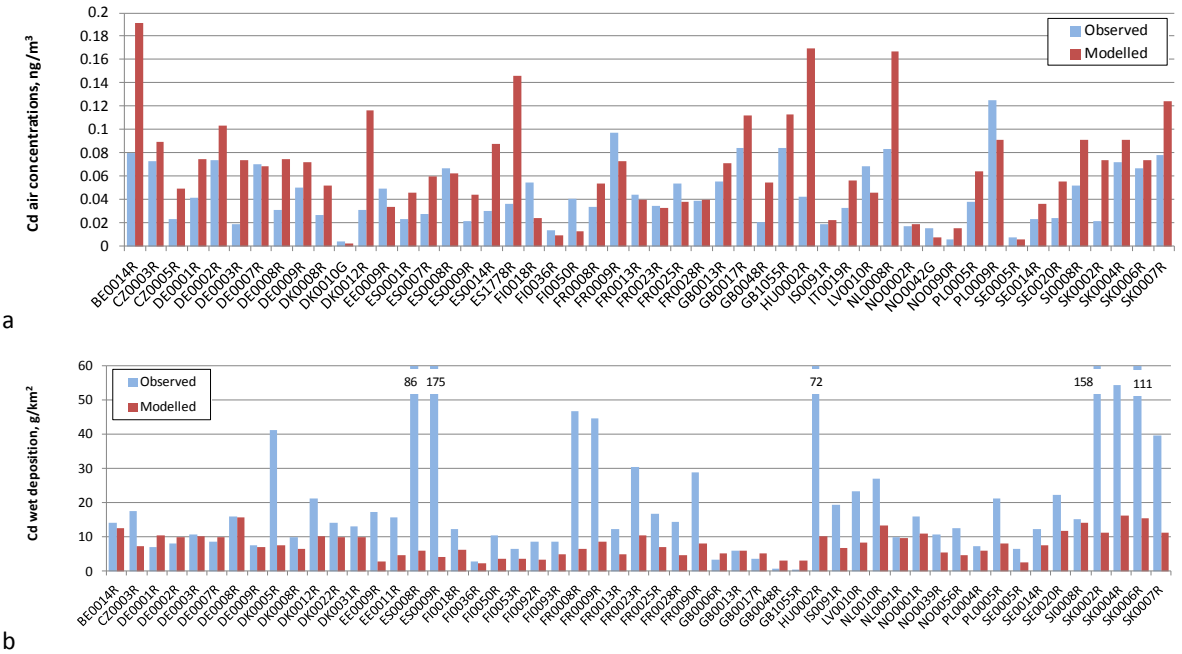

Fig. B.6. *Modelled and observed annual mean concentrations of Cd in air (a) and wet deposition fluxes (b) at the EMEP stations in 2021.*

Mercury (Hg)

Table B.3. *Emissions of Hg in 2021 in the EMEP countries, tonnes*

Country	Emissions	Country	Emissions	Country	Emissions
Albania	0.19	Greece	0.85	Poland	8.49
Armenia	0.04	Hungary	0.81	Portugal	1.23
Austria	1.04	Iceland	0.01	Moldova	0.10
Azerbaijan	0.27	Ireland	0.34	Romania	1.71
Belarus	0.27	Italy	6.33	Russia	13.76
Belgium	0.92	Kazakhstan	24.55	Serbia	1.45
Bosnia&Herzegovina	1.73	Kyrgyzstan	0.85	Slovakia	0.53
Bulgaria	0.97	Latvia	0.09	Slovenia	0.19
Croatia	0.38	Liechtenstein	5.3E-04	Spain	2.95
Cyprus	0.03	Lithuania	0.21	Sweden	0.41
Czechia	2.07	Luxembourg	0.08	Switzerland	0.68
Denmark	0.24	Malta	2.8E-03	Tajikistan	0.56
Estonia	0.22	Monaco	7.1E-04	Türkiye	10.73
Finland	0.52	Montenegro	0.05	Turkmenistan	0.48
France	2.59	Netherlands	0.47	Ukraine	4.33
Georgia	0.24	North Macedonia	0.21	United Kingdom	3.73
Germany	6.66	Norway	0.22	Uzbekistan	5.85

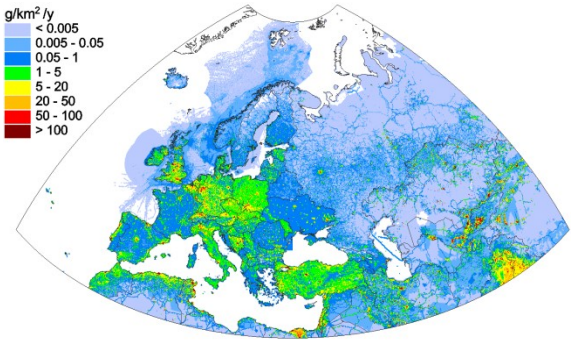

Fig. B.7. *Spatial distribution of Hg emissions in the EMEP region in 2021.*

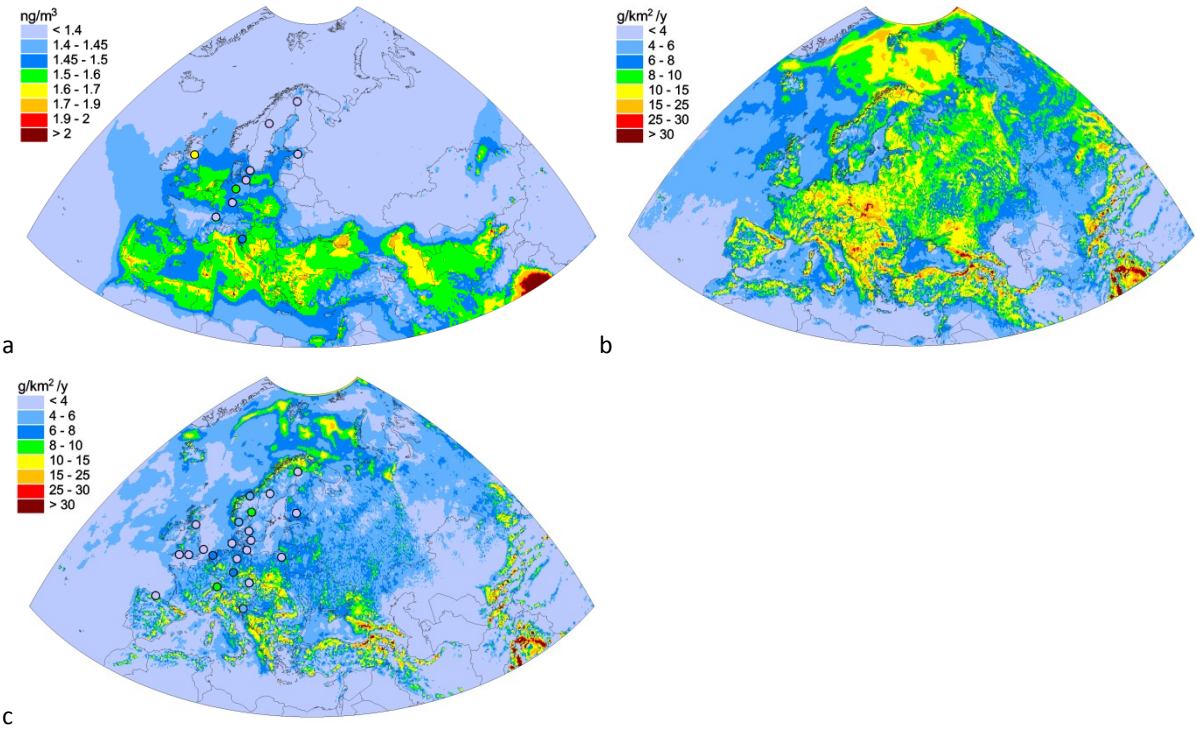

Fig. B.8. *Annual mean modelled air concentrations (a), total deposition fluxes (b) and wet deposition fluxes (c) of Hg based on the emissions data for 2021.*

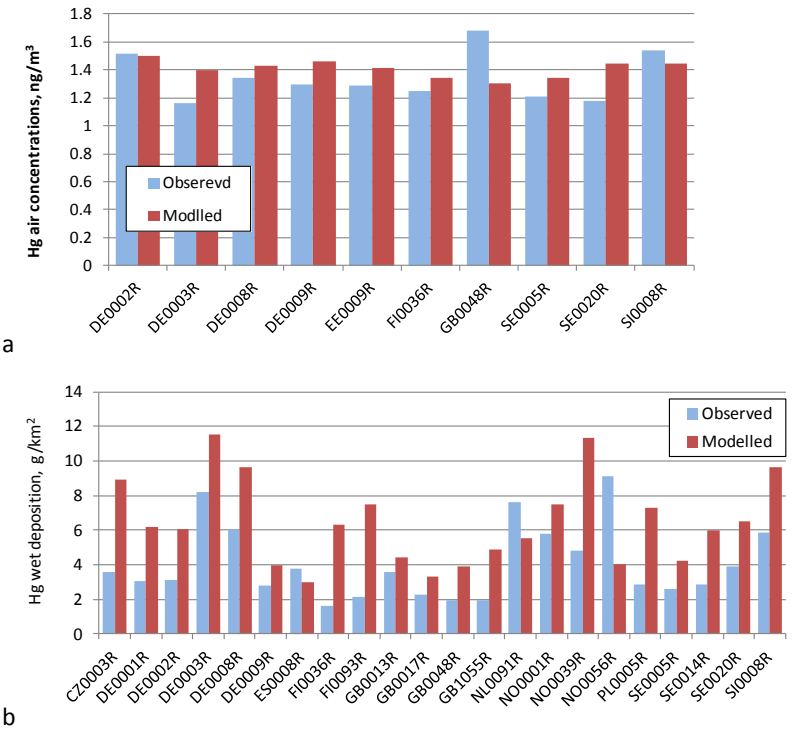

Fig. B.9. *Modelled and observed annual mean concentrations of Hg in air (a) and wet deposition fluxes (b) at the EMEP stations in 2021.*

Polycyclic Aromatic Hydrocarbons (PAHs)

Table B.4. *Emissions of PAHs in 2021 in the EMEP countries, tonnes*

Country	Emissions	Country	Emissions	Country	Emissions
Albania	2.25	Greece	16.95	Poland	260.50
Armenia	1.21	Hungary	21.40	Portugal	16.71
Austria	7.20	Iceland	0.07	Moldova	13.81
Azerbaijan	1.25	Ireland	12.00	Romania	59.49
Belarus	29.68	Italy	66.51	Russia	363.58
Belgium	6.78	Kazakhstan	198.52	Serbia	30.69
Bosnia&Herzegovina	11.55	Kyrgyzstan	14.23	Slovakia	25.58
Bulgaria	15.50	Latvia	7.07	Slovenia	4.50
Croatia	13.48	Liechtenstein	9.0E-03	Spain	30.92
Cyprus	0.72	Lithuania	9.46	Sweden	7.06
Czechia	29.99	Luxembourg	0.53	Switzerland	2.57
Denmark	4.40	Malta	0.06	Tajikistan	10.71
Estonia	2.96	Monaco	8.1E-04	Türkiye	150.87
Finland	20.09	Montenegro	0.30	Turkmenistan	6.03
France	37.20	Netherlands	4.32	Ukraine	196.28
Georgia	5.38	North Macedonia	4.02	United Kingdom	21.14
Germany	74.21	Norway	4.84	Uzbekistan	13.79

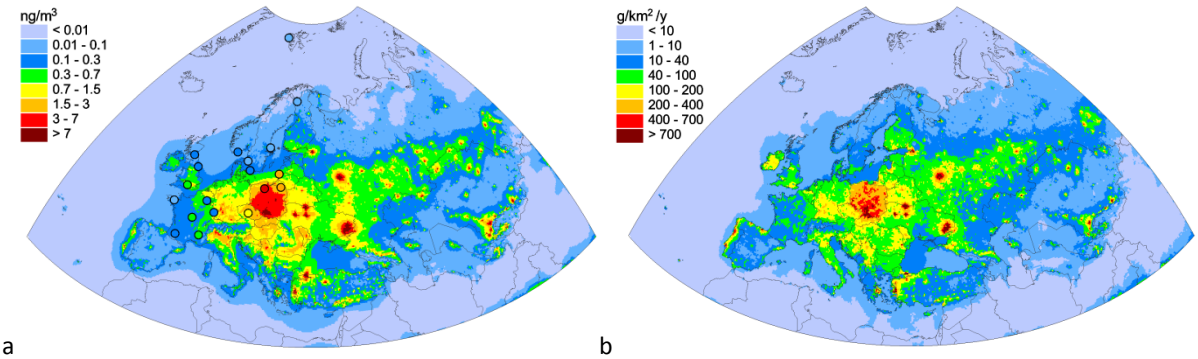

a b

Fig. B.10. *Annual mean modelled air concentrations (a) and total deposition fluxes (b) of the sum of 4 PAHs based on the emissions data for 2021.*

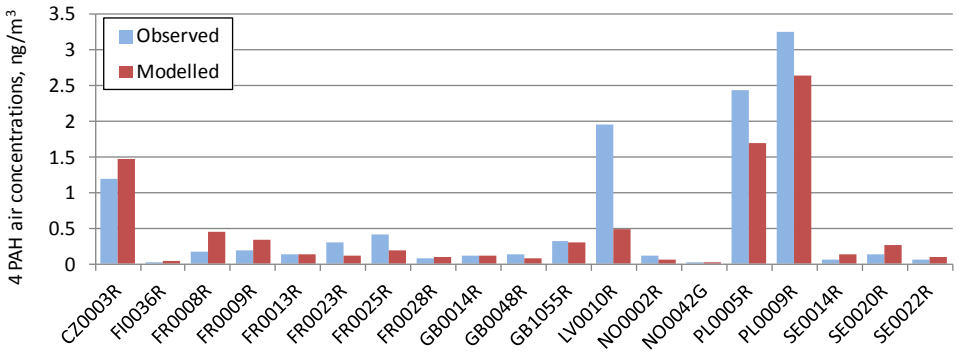

Fig. B.11. *Modelled and observed annual mean concentrations of the sum of 4 PAHs in air at the EMEP stations in 2021.*

Benzo(a)pyrene (B(a)P)

Table B.5. *Emissions of B(a)P in 2021 in the EMEP countries, tonnes*

Country	Emissions	Country	Emissions	Country	Emissions
Albania	0.68	Greece	5.44	Poland	89.12
Armenia	0.42	Hungary	7.33	Portugal	5.83
Austria	2.28	Iceland	0.01	Moldova	4.42
Azerbaijan	0.40	Ireland	3.00	Romania	20.32
Belarus	7.27	Italy	19.80	Russia	110.00
Belgium	2.14	Kazakhstan	59.28	Serbia	10.07
Bosnia&Herzegovina	3.06	Kyrgyzstan	4.11	Slovakia	8.44
Bulgaria	5.36	Latvia	2.51	Slovenia	1.92
Croatia	4.72	Liechtenstein	1.7E-03	Spain	10.21
Cyprus	0.12	Lithuania	2.97	Sweden	2.34
Czechia	10.08	Luxembourg	0.12	Switzerland	0.77
Denmark	1.29	Malta	0.02	Tajikistan	4.01
Estonia	0.82	Monaco	1.8E-04	Türkiye	42.62
Finland	6.58	Montenegro	0.07	Turkmenistan	1.19
France	10.76	Netherlands	1.51	Ukraine	51.95
Georgia	1.63	North Macedonia	1.29	United Kingdom	6.34
Germany	18.39	Norway	0.95	Uzbekistan	2.8

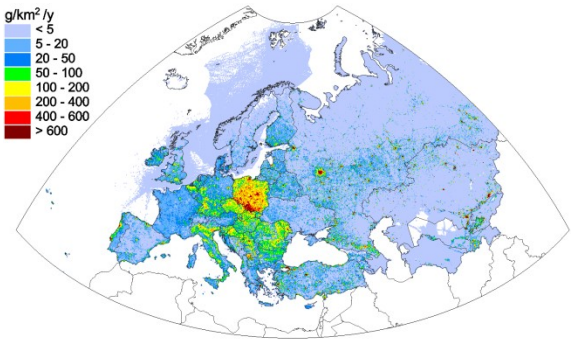

Fig. B.12. *Spatial distribution of B(a)P emissions in the EMEP region in 2021.*

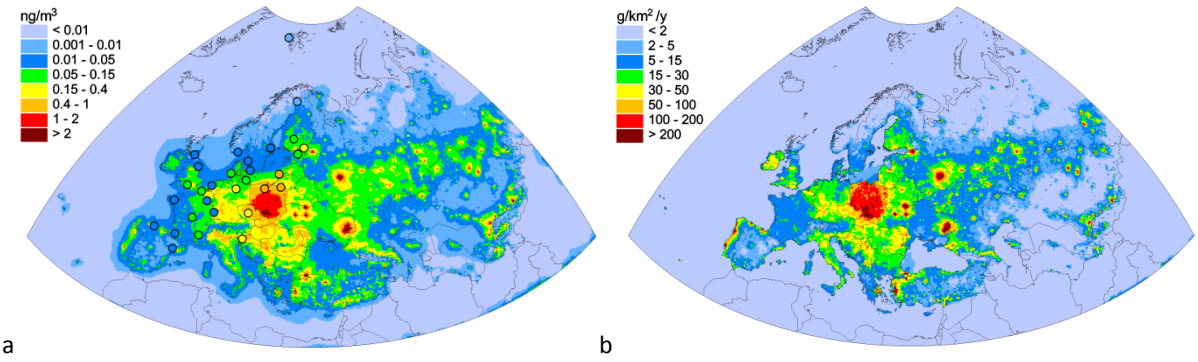

Fig. B.13. *Annual mean modelled air concentrations (a) and total deposition fluxes (b) of B(a)P based on the emissions data for 2021.*

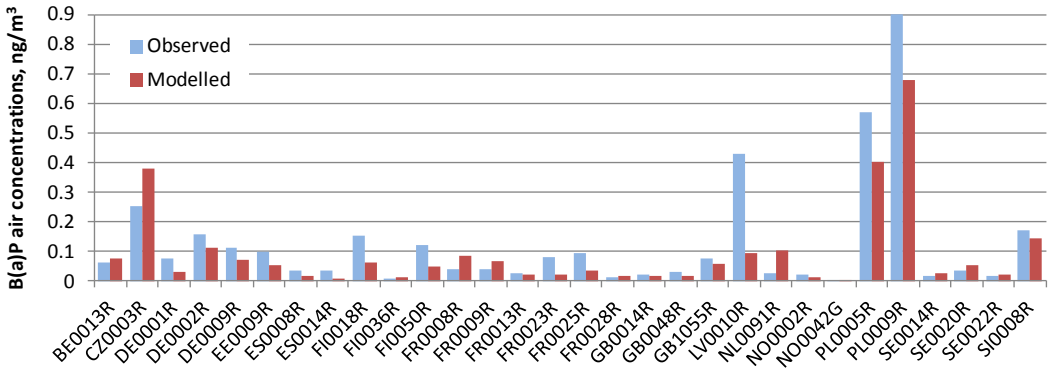

Fig. B.14. *Modelled and observed annual mean concentrations of B(a)P in air at the EMEP stations in 2021.*

Benzo(b)fluoranthene (B(b)F)

Table B.6. *Emissions of B(b)F in 2021 in the EMEP countries, tonnes*

Country	Emissions	Country	Emissions	Country	Emissions
Albania	0.68	Greece	5.90	Poland	91.71
Armenia	0.39	Hungary	7.15	Portugal	4.95
Austria	2.58	Iceland	0.03	Moldova	4.76
Azerbaijan	0.42	Ireland	5.05	Romania	19.44
Belarus	14.29	Italy	23.02	Russia	123.05
Belgium	2.41	Kazakhstan	77.37	Serbia	10.49
Bosnia&Herzegovina	4.07	Kyrgyzstan	5.86	Slovakia	8.09
Bulgaria	5.27	Latvia	2.32	Slovenia	1.10
Croatia	4.39	Liechtenstein	1.8E-03	Spain	10.59
Cyprus	0.34	Lithuania	3.36	Sweden	2.48
Czechia	7.79	Luxembourg	0.22	Switzerland	0.82
Denmark	1.41	Malta	0.02	Tajikistan	3.30
Estonia	0.81	Monaco	2.3E-04	Türkiye	53.56
Finland	5.19	Montenegro	0.15	Turkmenistan	2.63
France	12.21	Netherlands	1.39	Ukraine	83.56
Georgia	1.82	North Macedonia	1.46	United Kingdom	7.54
Germany	26.43	Norway	2.28	Uzbekistan	5.48

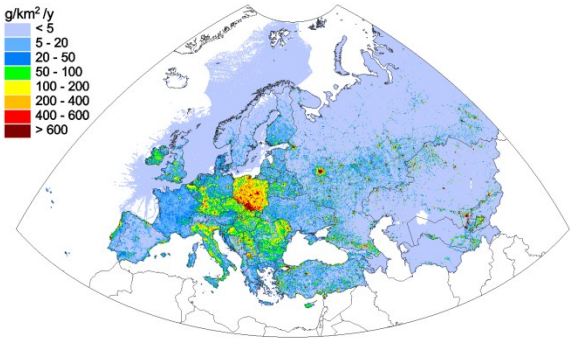

Fig. B.15. *Spatial distribution of B(b)F emissions in the EMEP region in 2021.*

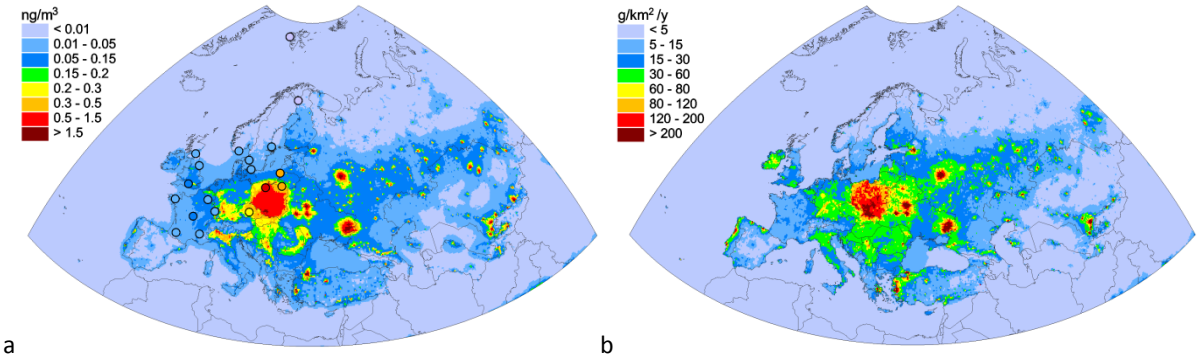

Fig. B.16. *Annual mean modelled air concentrations (a) and total deposition fluxes (b) of B(b)F based on the emissions data for 2021.*

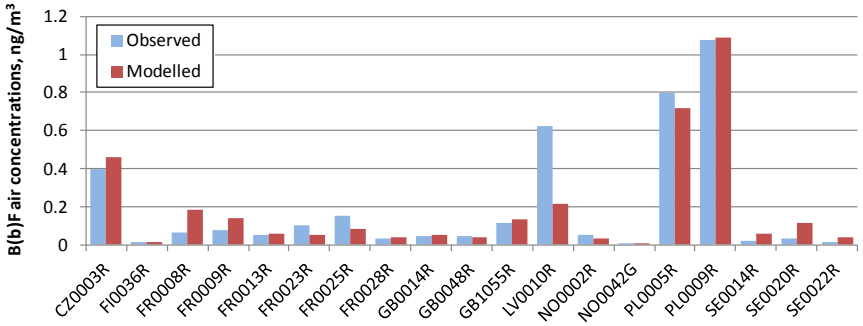

Fig. B.17. *Modelled and observed annual mean concentrations of B(b)F in air at the EMEP stations in 2021.*

Benzo(k)fluoranthene (B(k)F)

Table B.7. *Emissions of B(k)F in 2021 in the EMEP countries, tonnes*

Country	Emissions	Country	Emissions	Country	Emissions
Albania	0.31	Greece	3.23	Poland	43.90
Armenia	0.15	Hungary	2.75	Portugal	2.64
Austria	1.04	Iceland	0.01	Moldova	2.24
Azerbaijan	0.35	Ireland	2.16	Romania	7.95
Belarus	3.99	Italy	10.79	Russia	64.33
Belgium	1.03	Kazakhstan	38.92	Serbia	4.30
Bosnia&Herzegovina	1.63	Kyrgyzstan	2.31	Slovakia	4.20
Bulgaria	2.11	Latvia	0.89	Slovenia	1.06
Croatia	1.69	Liechtenstein	2.7E-03	Spain	4.75
Cyprus	0.15	Lithuania	1.54	Sweden	0.93
Czechia	5.54	Luxembourg	0.11	Switzerland	0.52
Denmark	0.85	Malta	0.01	Tajikistan	2.29
Estonia	0.54	Monaco	2.1E-04	Türkiye	20.37
Finland	3.82	Montenegro	0.04	Turkmenistan	1.82
France	7.46	Netherlands	0.70	Ukraine	30.61
Georgia	0.91	North Macedonia	0.57	United Kingdom	3.84
Germany	11.96	Norway	0.85	Uzbekistan	4.26

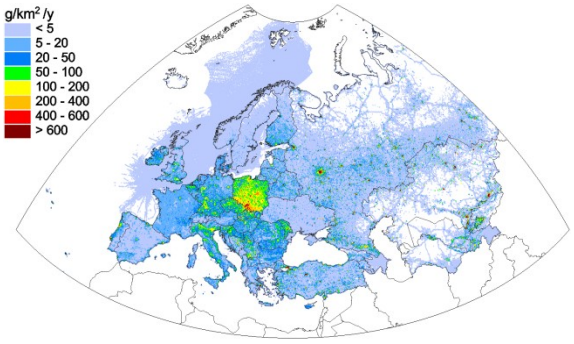

Fig. B.18. *Spatial distribution of B(k)F emissions in the EMEP region in 2021.*

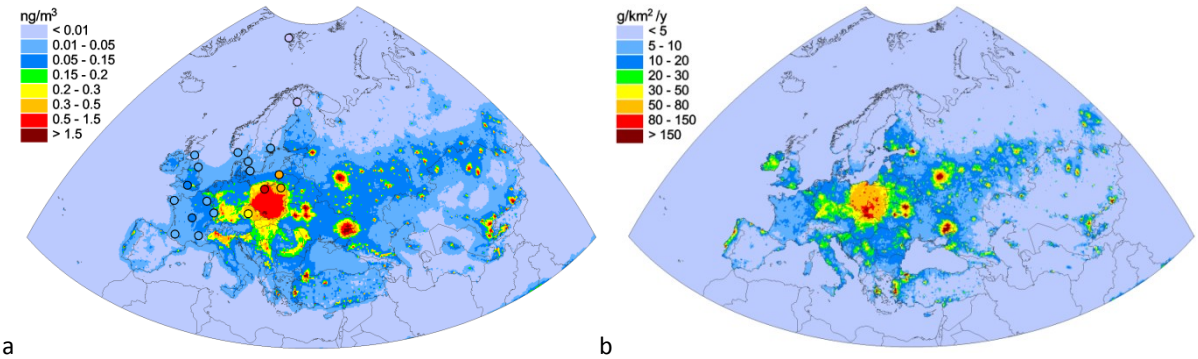

a b

Fig. B.19. *Annual mean modelled air concentrations (a) and total deposition fluxes (b) of B(k)F based on the emissions data for 2021.*

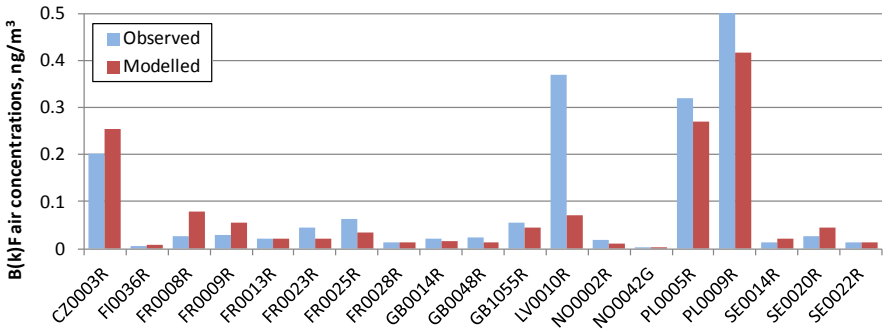

Fig. B.20. *Modelled and observed annual mean concentrations of B(k)F in air at the EMEP stations in 2021.*

Indeno(1,2,3-cd)pyrene (IcdP)

Table B.8. *Emissions of IcdP in 2021 in the EMEP countries, tonnes*

Country	Emissions	Country	Emissions	Country	Emissions
Albania	0.57	Greece	2.38	Poland	35.77
Armenia	0.25	Hungary	4.16	Portugal	3.29
Austria	1.30	Iceland	0.01	Moldova	2.39
Azerbaijan	0.08	Ireland	1.78	Romania	11.78
Belarus	4.14	Italy	12.90	Russia	66.20
Belgium	1.21	Kazakhstan	22.94	Serbia	5.83
Bosnia&Herzegovina	2.79	Kyrgyzstan	1.94	Slovakia	4.86
Bulgaria	2.76	Latvia	1.34	Slovenia	0.42
Croatia	2.68	Liechtenstein	2.7E-03	Spain	5.36
Cyprus	0.11	Lithuania	1.59	Sweden	1.31
Czechia	6.58	Luxembourg	0.08	Switzerland	0.45
Denmark	0.84	Malta	0.01	Tajikistan	1.10
Estonia	0.80	Monaco	1.8E-04	Türkiye	34.33
Finland	4.50	Montenegro	0.03	Turkmenistan	0.39
France	6.77	Netherlands	0.73	Ukraine	30.16
Georgia	1.03	North Macedonia	0.70	United Kingdom	3.41
Germany	17.44	Norway	0.76	Uzbekistan	1.25

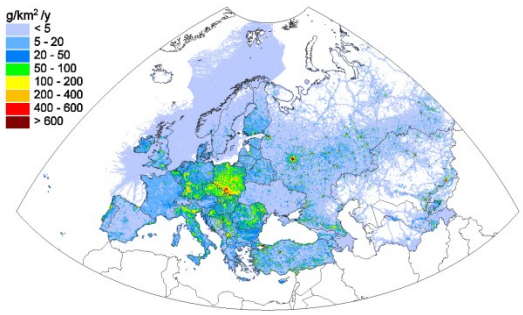

Fig. B.21. *Spatial distribution of I(cd)P emissions in the EMEP region in 2021.*

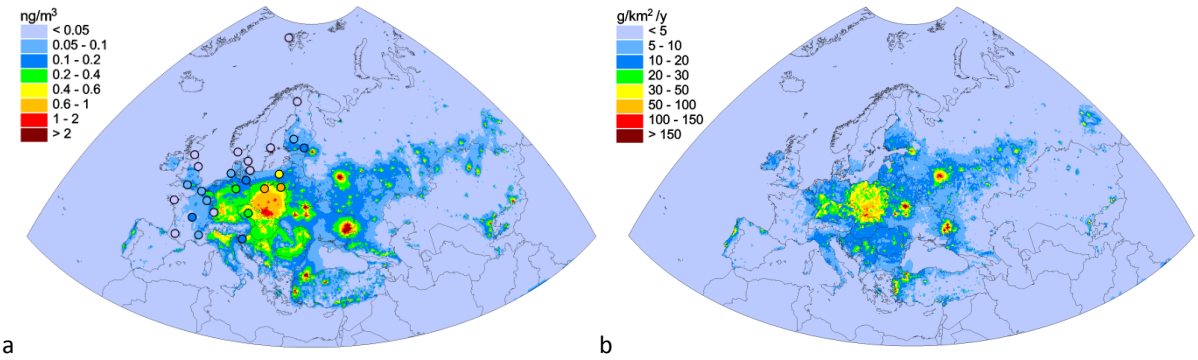

Fig. B.22. Annual mean modelled air concentrations (a) and total deposition fluxes (b) of IcdP based on the emissions data for 2021.

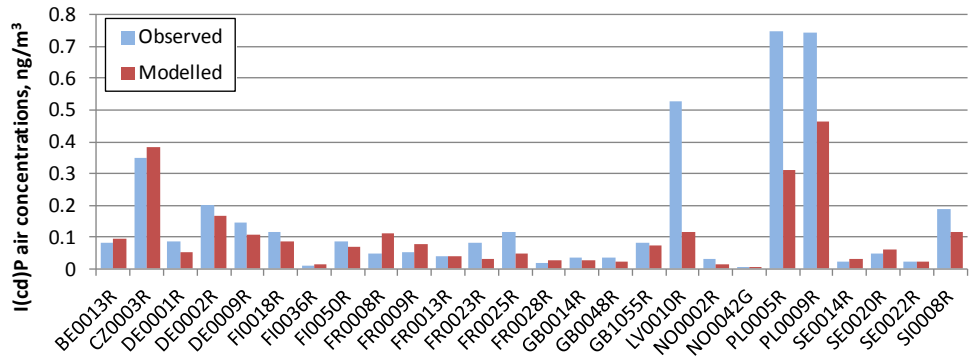

Fig. B.23. Modelled and observed annual mean concentrations of IcdP in air at the EMEP stations in 2021.

Hexachlorobenzene (HCB)

Table B.9. Emissions of HCB in 2021 in the EMEP countries, kg

Country	Emissions	Country	Emissions	Country	Emissions
Albania	0.13	Greece	1.96	Poland	3.81
Armenia	0.02	Hungary	1.64	Portugal	1.27
Austria	15.92	Iceland	0.10	Moldova	0.19
Azerbaijan	0.04	Ireland	2.53	Romania	3.59
Belarus	0.92	Italy	12.90	Russia	5.65
Belgium	3.12	Kazakhstan	18.38	Serbia	2.16
Bosnia&Herzegovina	50.00	Kyrgyzstan	0.67	Slovakia	3.05
Bulgaria	1.82	Latvia	0.52	Slovenia	0.46
Croatia	0.51	Liechtenstein	4.9E-04	Spain	2.05
Cyprus	0.01	Lithuania	0.58	Sweden	3.05
Czechia	11.09	Luxembourg	0.71	Switzerland	0.37
Denmark	2.28	Malta	0.06	Tajikistan	0.84
Estonia	0.47	Monaco	0.01	Türkiye	4.25
Finland	23.05	Montenegro	0.13	Turkmenistan	1.06
France	17.17	Netherlands	3.47	Ukraine	165.95
Georgia	29.01	North Macedonia	0.16	United Kingdom	38.14
Germany	4.58	Norway	1.33	Uzbekistan	1.03

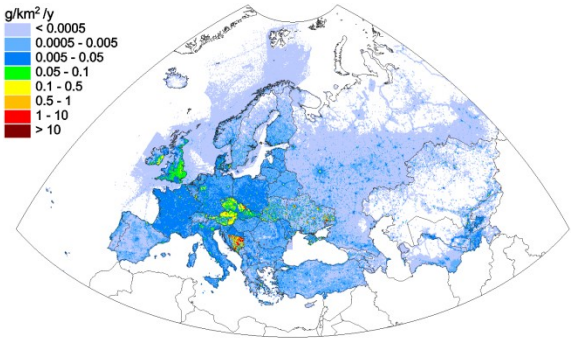

Fig. B.24. *Spatial distribution of HCB emissions in the EMEP region in 2021.*

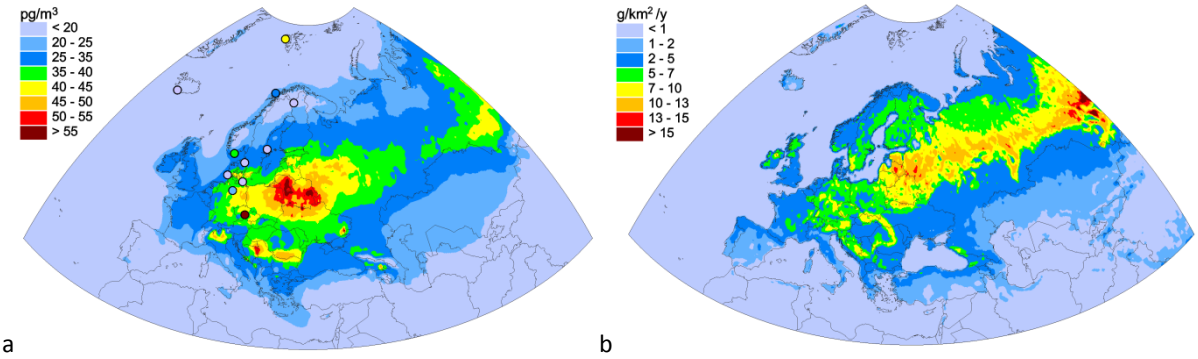

Fig. B.25. *Annual mean modelled air concentrations (a) and total deposition fluxes (b) of HCB based on the emissions data for 2021.*

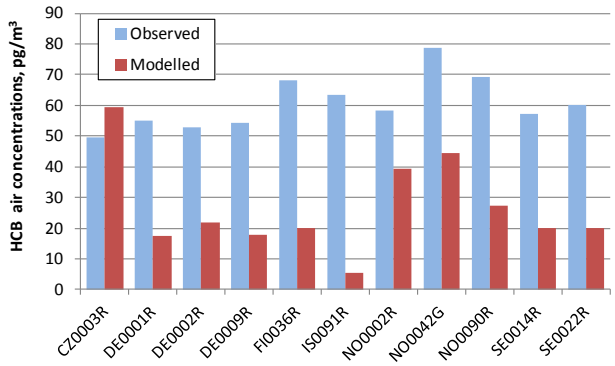

Fig. B.26. *Modelled and observed annual mean concentrations of HCB in air at the EMEP stations in 2021.*

Dibenzo(p)dioxins and dibenzofurans (PCDD/Fs)

Table B.10. *Emissions of PCDD/Fs in 2021 in the EMEP countries, g-TEQ*

Country	Emissions	Country	Emissions	Country	Emissions
Albania	9.18	Greece	25.68	Poland	316.39
Armenia	2.80	Hungary	57.75	Portugal	59.74
Austria	37.28	Iceland	0.98	Moldova	47.32
Azerbaijan	5.18	Ireland	16.91	Romania	210.69
Belarus	30.21	Italy	314.50	Russia	1784.4
Belgium	29.08	Kazakhstan	3070.47	Serbia	73.06
Bosnia&Herzegovina	48.00	Kyrgyzstan	14.60	Slovakia	39.53
Bulgaria	42.50	Latvia	15.13	Slovenia	14.26
Croatia	26.26	Liechtenstein	0.06	Spain	477.03
Cyprus	0.51	Lithuania	18.06	Sweden	17.04
Czechia	22.17	Luxembourg	1.91	Switzerland	15.13
Denmark	30.53	Malta	0.18	Tajikistan	69.08
Estonia	3.77	Monaco	0.92	Türkiye	1269.38
Finland	10.78	Montenegro	0.19	Turkmenistan	44.81
France	125.24	Netherlands	30.21	Ukraine	235.83
Georgia	10.16	North Macedonia	9.42	United Kingdom	115.75
Germany	116.04	Norway	22.02	Uzbekistan	173.99

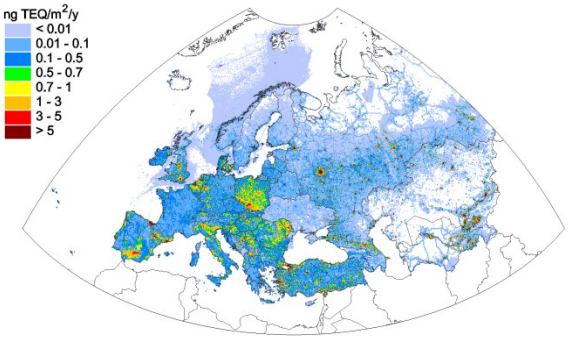

Fig. B.27. *Spatial distribution of PCDD/F emissions in the EMEP region in 2021.*

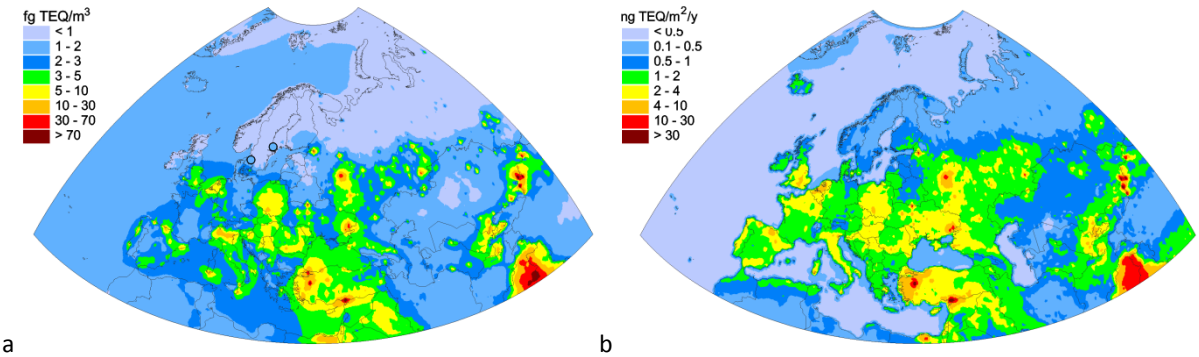

a b

Fig. B.28. *Annual mean modelled air concentrations (a) and total deposition fluxes (b) of PCDD/Fs based on the emissions data for 2021.*

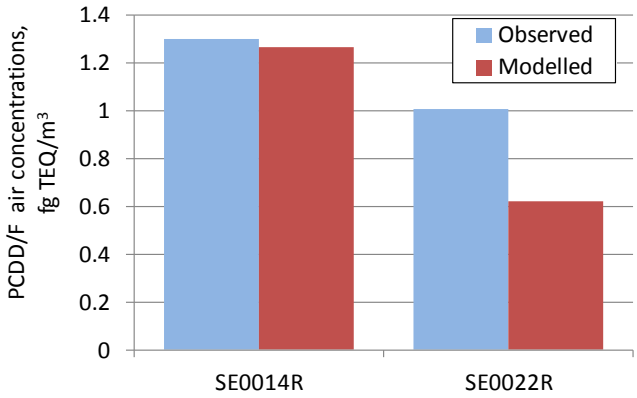

Fig. B.29. *Modelled and observed annual mean concentrations of PCDD/Fs in air at the EMEP stations in 2021.*